

Drivers of plant nutrient acquisition and allocation strategies and their influence  
on plant responses to environmental change

by

Evan A. Perkowski, B.S.

A Dissertation

In

Biological Sciences

Submitted to the Graduate Faculty  
of Texas Tech University in  
Partial Fulfillment of  
the Requirements for  
the Degree of

Doctor of Philosophy

Approved

Nicholas G. Smith, Ph.D.  
Chair of Committee

Aimée T. Classen, Ph.D.

Natasja van Gestel, Ph.D.

Lindsey C. Slaughter, Ph.D.

Dylan W. Schwilk, Ph.D.

Mark Sheridan, Ph.D.  
Dean of the Graduate School

May 2023

Copyright 2023, Evan A. Perkowski

## Acknowledgements

This dissertation was made possible by the mentorship, collaboration, and friendship of many people. I am so thankful to be surrounded by such supportive and helpful mentors, peers, and friends that have made navigating through graduate school and finishing this dissertation an enjoyable experience. Specifically, I am thankful for the incredible mentorship of my advisor and committee chair, Dr. Nick Smith, and my committee members, Drs. Aimée Classen, Natasja van Gestel, Dylan Schwilk, and Lindsey Slaughter, for useful feedback and invaluable support as I planned and implemented experiments. I am very fortunate to have such a strong team of positive and supportive mentors guide me along the start of my academic journey.

I am also thankful for past and present members of the EcoHealth lab for encouragement, support, and extracurricular activities that made time inside and outside the lab enjoyable and memorable. Particular thanks go to the friendship of Dr. Lizz Waring, Dr. Xiulin Gao, Helen Scott, and Risa McNellis, all of whom were invaluable to helping me navigate my first year. I am especially thankful for the mentorship of Dr. Lizz Waring, as our weekly coffee chats were instrumental for helping me feel welcome in Lubbock and acclimate to life as a graduate student. I am also thankful for the friendship of Billi Jean Petermann and the late Dr. Kris Petterson for their encouragement and willingness to discuss microbial symbioses over coffee on random Saturday mornings.

Additional thanks must go out to Risa McNellis, Jorge Ochoa, Peter Eludini, Jose Villeda, Avery Schoenherr, Zinny Ezekannagha, Brad Posch, Jeff Chidini,

eppa, Snehanjana Chatterjee, Monika Kelley, Eve Gray, Isa Beltran and Azaj Mahmud for help with experiment setup, experiment processing, or for lending an ear over puzzling results. I am also thankful for collaborators Dr. Christy Goodale and Dave Frey, who provided invaluable insight for the second experimental chapter.

I would like to thank my undergraduate advisor, Dr. Janice Krumm, for continued mentorship and friendship and for insightful advice about navigating graduate school, but most of all for helping me realize my career aspirations and pushing me to pursue this endeavor. I would also like to thank my family, particularly my parents, partner, and dog for continued support and distractions outside the lab. The experiments included here would not have been possible without their emotional and monetary support.

This work was made possible from funding by the NSF, USDA, Braun and Gresham, PLLC., and was a contribution to the LEMONTREE (Land Ecosystem Models based On New Theory, obseRvations and ExperimEnts) project. The LEMONTREE project is an international coalition of researchers funded through the generosity of Eric and Wendy Schmidt by recommendation of the Schmidt Futures programme and the Imperial College initiative on Grand Challenges in Ecosystems and the Environment. This work was also funded by graduate student research awards from Texas Tech University and the Botanical Society of America.

I have inevitably missed mentioning folks that were instrumental to the completion of these experiments and contributed to my development as a plant physiological ecologist. Please know that I am grateful and appreciative of our interactions.

## Table of Contents

<b>Acknowledgements . . . . .</b>	ii
<b>Abstract . . . . .</b>	ix
<b>List of Tables . . . . .</b>	xii
<b>List of Figures . . . . .</b>	xvi
<b>1. Introduction . . . . .</b>	1
<b>2. Structural carbon costs to acquire nitrogen are determined by nitrogen and light availability in two species with different nitrogen acquisition strategies . . . . .</b>	8
2.1    Introduction . . . . .	8
2.2    Methods . . . . .	12
2.2.1 <i>Experiment setup</i> . . . . .	12
2.2.2 <i>Plant measurements and calculations</i> . . . . .	13
2.2.3 <i>Statistical analyses</i> . . . . .	14
2.3    Results . . . . .	16
2.3.1 <i>Carbon costs to acquire nitrogen</i> . . . . .	16
2.3.2 <i>Whole plant nitrogen biomass</i> . . . . .	19
2.3.3 <i>Root carbon biomass</i> . . . . .	21
2.3.4 <i>Root nodule biomass</i> . . . . .	23
2.4    Discussion . . . . .	27
2.4.1 <i>Carbon costs to acquire nitrogen increase with light availability and decrease with fertilization</i> . . . . .	27
2.4.2 <i>Modeling implications</i> . . . . .	29
2.4.3 <i>Study limitations</i> . . . . .	31
2.4.4 <i>Conclusions</i> . . . . .	33
<b>3. Soil nitrogen availability modifies leaf nitrogen economies in mature temperate deciduous forests: a direct test of photosynthetic least-cost theory . . . . .</b>	35
3.1    Introduction . . . . .	35

3.2 Methods . . . . .	39
3.2.1 <i>Study site description</i> . . . . .	39
3.2.2 <i>Experimental design</i> . . . . .	40
3.2.3 <i>Leaf gas exchange and trait measurements</i> . . . . .	40
3.2.4 $A_{net}/C_i$ curve-fitting and parameter estimation . . . . .	43
3.2.5 Proportion of leaf nitrogen allocated to photosynthesis and structure . . . . .	45
3.2.6 Tradeoffs between nitrogen and water use . . . . .	46
3.2.7 Soil nitrogen availability and pH . . . . .	47
3.2.8 Statistical analyses . . . . .	49
3.3 Results . . . . .	51
3.3.1 Leaf N content . . . . .	51
3.3.2 Net photosynthesis and leaf biochemistry . . . . .	54
3.3.3 Leaf N allocation . . . . .	57
3.3.4 Tradeoffs between nitrogen and water use . . . . .	60
3.4 Discussion . . . . .	63
3.4.1 Soil nitrogen availability modifies tradeoffs between nitrogen and water use . . . . .	64
3.4.2 Soil pH did not modify tradeoffs between nitrogen and water usage . . . . .	66
3.4.3 Species identity explains a large amount of variation in leaf and whole plant traits . . . . .	67
3.4.4 Implications for photosynthetic least-cost theory model development . . . . .	68
3.4.5 Conclusions . . . . .	70
4. The relative cost of resource use for photosynthesis drives variance in leaf nitrogen content across a climate and soil resource availability gradient . . . . .	71
4.1 Introduction . . . . .	71
4.2 Methods . . . . .	77
4.2.1 Site descriptions and sampling methodology . . . . .	77

4.2.2	<i>Leaf trait measurements</i>	77
4.2.3	<i>Site climate data</i>	83
4.2.4	<i>Site edaphic characteristics</i>	83
4.2.5	<i>Plant functional group assignments</i>	85
4.2.6	<i>Data analysis</i>	86
4.3	Results	88
4.3.1	<i>Cost to acquire nitrogen relative to water</i>	88
4.3.2	$C_i:C_a$	92
4.3.3	<i>Leaf nitrogen content</i>	95
4.3.4	<i>Structural equation model</i>	99
4.4	Discussion	102
4.4.1	<i>Negative effects of leaf <math>C_i:C_a</math> on <math>N_{\text{area}}</math> are driven by reductions in <math>M_{\text{area}}</math>, not <math>N_{\text{mass}}</math></i>	102
4.4.2	<i>Soil nitrogen availability increases <math>N_{\text{area}}</math> through changes in the cost to acquire nitrogen</i>	104
4.4.3	<i>Soil moisture increases <math>N_{\text{area}}</math> by facilitating increases in soil nitrogen availability</i>	105
4.4.4	<i>Indirect effects of climate on <math>N_{\text{area}}</math> are mediated through changes in leaf <math>C_i:C_a</math> and <math>\beta</math></i>	106
4.4.5	<i>Species identity traits modify effects of the environment on <math>\beta</math>, leaf <math>C_i:C_a</math>, and <math>N_{\text{area}}</math></i>	106
4.4.6	<i>Next steps for optimality model development</i>	108
4.4.7	<i>Conclusions</i>	109
5.	<b>Optimal resource investment to photosynthetic capacity maximizes nutrient allocation to whole plant growth under elevated CO<sub>2</sub></b>	110
5.1	Introduction	110
5.2	Methods	115
5.2.1	<i>Seed treatments and experimental design</i>	115
5.2.2	<i>Growth chamber conditions</i>	116
5.2.3	<i>Leaf gas exchange measurements</i>	118

5.2.4 <i>Leaf trait measurements</i> . . . . .	119
5.2.5 <i>A/C<sub>i</sub> curve fitting and parameter estimation</i> . . . . .	121
5.2.6 Stomatal limitation . . . . .	121
5.2.7 <i>Proportion of leaf nitrogen allocated to photosynthesis and structure</i> . . . . .	122
5.2.8 <i>Whole plant traits</i> . . . . .	124
5.2.9 <i>Statistical analyses</i> . . . . .	126
5.3 Results . . . . .	128
5.3.1 <i>Leaf nitrogen and chlorophyll content</i> . . . . .	128
5.3.2 <i>Leaf biochemistry and stomatal conductance</i> . . . . .	132
5.3.3 <i>Leaf nitrogen allocation</i> . . . . .	136
5.3.4 <i>Whole plant traits</i> . . . . .	140
5.3.5 <i>Nitrogen fixation</i> . . . . .	144
5.4 Discussion . . . . .	148
5.4.1 <i>Soil nitrogen fertilization has divergent effects on leaf and whole plant acclimation responses to CO<sub>2</sub></i> . . . . .	149
5.4.2 <i>Implications for future model development</i> . . . . .	153
5.4.3 <i>Study limitations and future directions</i> . . . . .	154
5.4.4 <i>Conclusions</i> . . . . .	156
6. Conclusions . . . . .	158
References . . . . .	169
Appendix A: Supplemental material for "Structural carbon costs to acquire nitrogen are determined by nitrogen and light availability in two species with different nitrogen acquisition strategies" . . . . .	206
Appendix B: Supplemental material for "Soil nitrogen availability modifies leaf nitrogen economies in mature temperate deciduous forests: a direct test of photosynthetic least-cost theory" . . . . .	210

<b>Appendix C: Supplemental material for "The relative cost of resource use for photosynthesis drives variance in leaf nitrogen content across a climate and soil resource availability gradient" . . . . .</b>	<b>215</b>
<b>Appendix D: Supplemental material for "Optimal resource investment to photosynthetic capacity maximizes nutrient allocation to whole plant growth under elevated CO<sub>2</sub>" . . .</b>	<b>222</b>

## Abstract

Photosynthesis is the largest carbon flux between the atmosphere and is constrained by ecosystem carbon and nutrient cycle dynamics. Terrestrial biosphere models are therefore sensitive to the formulation of photosynthesis, and uncertainty in the acclimation response of photosynthetic processes to environmental change likely contributes to widespread divergence of terrestrial biosphere model predictions. Photosynthetic least-cost theory provides a promising framework for understanding effects of climatic and edaphic factors on photosynthetic acclimation responses to changing environments. Yet, empirical tests of the theory are rare, which limits our ability to assess whether the theory is suitable for implementation in next-generation terrestrial biosphere models.

Here, I present four experiments designed to test assumptions of photosynthetic least-cost theory using a combination of greenhouse, growth chamber, field manipulation, and field gradient experiments. Experiment chapters are flanked by a general introduction chapter and conclusions chapter. The first experimental chapter, which reports work published in *Journal of Experimental Botany*, I quantify structural carbon costs to acquire nitrogen in *Glycine max* and *Gossypium hirsutum* grown under four nitrogen fertilization levels and four light availability levels in a full factorial greenhouse experiment. I find that carbon costs to acquire nitrogen in both species generally increase with increasing light availability and decrease with increasing fertilization, though responses to fertilization in *G. max* were markedly less than *G. hirsutum*. The second experimental chapter, which reports work currently in review, quantifies leaf nitrogen and photosynthetic traits

in upper canopy leaves of deciduous trees growing in a 9-year nitrogen-by-sulfur field manipulation experiment. I find strong evidence for nitrogen-water use trade-offs with increasing soil nitrogen availability, evidenced through a strong negative relationship between leaf nitrogen content and leaf  $C_i:C_a$  and stronger increase in leaf nitrogen content with increasing soil nitrogen availability than leaf  $C_i:C_a$ . The third experiment, which reports work that is currently in preparation for journal submission, investigates variance in leaf nitrogen content across a climate and soil resource availability gradient in Texan grasslands, showing that effects of soil resource availability and climate on leaf nitrogen content are driven by changes in leaf  $C_i:C_a$ . Finally, the fourth experiment, which reports work that is currently in preparation for journal submission, quantifies leaf and whole plant acclimation responses in *G. max* grown under two atmospheric CO<sub>2</sub> levels, with and without inoculation with *Bradyrhizobium japonicum*, and across nine nitrogen fertilization treatments in a full factorial growth chamber experiment. I find that leaf acclimation responses to CO<sub>2</sub> were independent of soil nitrogen fertilization or inoculation treatment, though stimulations in whole plant growth under elevated CO<sub>2</sub> were enhanced with increasing soil nitrogen fertilization and in inoculated pots under low nitrogen fertilization. Experimental chapters are presented either as copies

Experiments included in this dissertation provide consistent support for patterns expected from photosynthetic least-cost theory. The use of multiple experimental approaches allowed me to examine mechanisms driving patterns expected from the theory and investigate whether these patterns occur naturally across environmental gradients. Findings from these chapters challenge common paradigms in plant ecophysiology, providing evidence that including photosyn-

thetic least-cost frameworks in next-generation terrestrial biosphere models may improve the observed divergence in simulated outcomes across terrestrial biosphere model products. I look forward to continuing this work, collaborating with modelers to understand how results from these experiments compare to simulations from optimality models that leverage photosynthetic least-cost frameworks.

## List of Tables

2.1 Analysis of variance results exploring species-specific effects of light availability, nitrogen fertilization, and their interactions on carbon costs to acquire nitrogen ( $N_{\text{cost}}$ ), whole-plant nitrogen biomass ( $N_{\text{wp}}$ ), and root carbon biomass ( $C_{\text{bg}}$ ) . . . . .	17
2.2 Analysis of variance results exploring effects of light availability, nitrogen fertilization, and their interactions on <i>G. max</i> root nodule biomass and the ratio of root nodule biomass to root biomass* . . . . .	24
2.3 Slopes of the regression line describing the relationship between each dependent variable and nitrogen fertilization at each light level* . . . . .	25
3.1 Effects of soil N availability, soil pH, and species on leaf N content per unit leaf area ( $N_{\text{area}}$ ), leaf N content per unit leaf mass ( $N_{\text{mass}}$ ), and leaf mass per unit leaf area ( $M_{\text{area}}$ ) . . . . .	52
3.2 Effects of soil N availability, soil pH, species, and $N_{\text{area}}$ on leaf biochemistry . . . . .	55
3.3 Effects of soil N availability, soil pH, and species on the proportion of leaf nitrogen content allocated to photosynthesis, Rubisco, bioenergetics, and structure . . . . .	58
3.4 Effects of soil N availability, soil pH, species, and $N_{\text{area}}$ on tradeoffs between nitrogen and water use . . . . .	61

4.1	Site locality information, sampling year(s), 2006-2020 mean annual precipitation (MAP; mm), mean annual temperature (MAT; °C), and water holding capacity (WHC; mm)* . . . . .	81
4.2	Effects of soil moisture, soil nitrogen availability, and plant functional group on $\beta$ . . . . .	90
4.3	Effects of soil moisture, soil nitrogen availability, and plant functional group on leaf $C_i:C_a^*$ . . . . .	93
4.4	Effects of soil nitrogen fertilization, inoculation, and CO <sub>2</sub> treatments on $N_{\text{area}}$ , $N_{\text{mass}}$ , and $M_{\text{area}}$ . . . . .	97
4.5	Structural equation model results investigating direct effects of climatic and soil resource availability on $N_{\text{area}}$ , $N_{\text{mass}}$ , $M_{\text{area}}$ , leaf $C_i:C_a$ , and $\beta$ . . . . .	100
5.1	Effects of soil nitrogen fertilization, inoculation, and CO <sub>2</sub> treatments on $N_{\text{area}}$ , $N_{\text{mass}}$ , $M_{\text{area}}$ , and $Chl_{\text{area}}$ . . . . .	130
5.2	Effects of soil nitrogen fertilization, inoculation, and CO <sub>2</sub> on leaf biochemistry . . . . .	134
5.3	Effects of soil N availability, soil pH, species, and $N_{\text{area}}$ on leaf nitrogen allocation . . . . .	138
5.4	Effects of soil N availability, soil pH, species, and $N_{\text{area}}$ on total leaf area, whole plant biomass, and carbon costs to acquire nitrogen . .	142
5.5	Effects of soil N availability, soil pH, species, and $N_{\text{area}}$ on root nodule biomass and plant investments in symbiotic nitrogen fixation	146

A1	Summary table containing volumes of compounds used to create modified Hoagland's solutions for each soil nitrogen fertilization treatment. All volumes are expressed as milliliters per liter (mL/L)	206
A2	Analysis of variance results exploring species-specific effects of light availability, nitrogen fertilization, and their interactions on the ratio of whole plant biomass to pot volume . . . . .	207
A3	Slopes of the regression line describing the relationship between each dependent variable and nitrogen fertilization at each light level* <sup>*</sup>	208
B1	Sample sizes of each species, abbreviated by their USDA NRCS PLANTS database code, within each plot at each site . . . . .	210
B2	Analysis of variance results exploring the linear effect of leaf temperature on net photosynthesis rate and stomatal conductance measured at 400 $\mu\text{mol mol}^{-1}$ CO <sub>2</sub> . . . . .	211
B3	Second order log-polynomial regression coefficients that described the effect of leaf temperature on net photosynthesis and stomatal conductance measured at 400 $\mu\text{mol mol}^{-1}$ CO <sub>2</sub> . . . . .	212
B4	Mean, standard error, and 95% confidence interval ranges of soil nitrogen availability estimates across all measured plots. All units are expressed as $\mu\text{g N g}^{-1}$ resin d <sup>-1</sup> . . . . .	213
C1	List of sampled species and their plant functional group assignment	217
C2	List of sampled species and their plant functional group assignment (cont.) . . . . .	218

C3	List of sampled species and their plant functional group assignment (cont.)	219
C4	Model selection results for soil moisture, air temperature, and vapor pressure deficit. Soil moisture was used in a bivariate regression against $\beta$ , while vapor pressure deficit was used in bivariate regressions against leaf $C_i:C_a^*$	220
D1	Summary table containing volumes of compounds used to create modified Hoagland's solutions for each soil nitrogen fertilization treatment. All volumes are expressed as milliliters per liter (mL/L)	222
D2	Summary of the daily growth chamber growing condition program	223

## List of Figures

2.1 Relationships between soil nitrogen fertilization and light availability on carbon costs to acquire nitrogen in <i>G. hirsutum</i> and <i>G. max</i> . . . . .	18
2.2 Relationships between soil nitrogen fertilization and light availability on whole-plant nitrogen biomass in <i>G. hirsutum</i> and <i>G. max</i> . . . . .	20
2.3 Relationships between soil nitrogen fertilization and light availability on root carbon biomass in <i>G. hirsutum</i> and <i>G. max</i> . . . . .	22
2.4 Effects of shade cover and nitrogen fertilization on root nodule biomass and the ratio of root nodule biomass to root biomass in <i>G. max</i> . . . . .	26
3.1 Effects of soil N availability and species on leaf N content per unit leaf area, leaf nitrogen content per unit leaf biomass, and leaf mass per leaf area . . . . .	53
3.2 Effects of soil N availability, species, and leaf N content leaf biochemistry . . . . .	56
3.3 Effects of soil N availability, species, and leaf N content on the fraction of leaf nitrogen allocated to photosynthesis and structure	59
3.4 Effects of soil N availability, species, and leaf N content on tradeoffs between nitrogen and water use . . . . .	62
4.1 Maps that detail site locations along 2006-2020 mean annual precipitation and mean annual temperature gradients in Texas, USA.	82

4.2 Effects of soil nitrogen availability and soil moisture on the unit cost ratio $\beta$	91
4.3 Effects of 4-day mean vapor pressure deficit, 2-day soil moisture (per water holding capacity), and soil nitrogen availability on leaf $C_i:C_a$	94
4.4 Effects of leaf $C_i:C_a$ , soil nitrogen availability, and soil moisture on leaf nitrogen content per unit leaf area, leaf nitrogen content per unit leaf biomass, and leaf mass per area	98
4.5 Structural equation model results exploring drivers of $N_{\text{area}}$	101
5.1 Effects of $\text{CO}_2$ , fertilization, and inoculation on leaf nitrogen per unit leaf area, leaf nitrogen content, leaf mass per unit leaf area, and chlorophyll content per unit leaf area	131
5.2 Effects of $\text{CO}_2$ , fertilization, and inoculation on maximum rate of Rubisco carboxylation, the maximum rate of RuBP regeneration, and the ratio of the maximum rate of RuBP regeneration to the maximum rate of Rubisco carboxylation leaf mass per unit leaf area, dark respiration, stomatal conductance, and stomatal limitation	135
5.3 Effects of $\text{CO}_2$ , fertilization, and inoculation on the relative fraction of leaf nitrogen allocated to photosynthesis and the fraction of leaf nitrogen allocated to structure	139
5.4 Effects of $\text{CO}_2$ , fertilization, and inoculation on total leaf area, total biomass, and structural carbon costs to acquire nitrogen	143

5.5 Effects of CO <sub>2</sub> , fertilization, and inoculation on nodule biomass, nodule: root biomass, and percent nitrogen fixed from the atmosphere. . . . .	147
A1 Effects of shade cover and nitrogen fertilization on the ratio of plant biomass to rooting volume in <i>G. hirsutum</i> and <i>G. max</i> . . . . .	209
B1 Effects of leaf temperature on net photosynthesis rate and stomatal conductance values when measured at 400 μmol mol <sup>-1</sup> CO <sub>2</sub> . . . . .	214
C2 Model selection results exploring relevant timescales for soil moisture and vapor pressure deficit . . . . .	221
D1 Relationships between area-based leaf nitrogen content, mass-based leaf nitrogen content, and leaf mass per unit leaf area measured on the focal leaf used to generate $A_{\text{net}}/C_i$ curves and leaf nitrogen content measured on the leaf used for chlorophyll extractions . . . . .	224
D2 Effects of CO <sub>2</sub> , fertilization, and inoculation on the ratio of whole plant biomass to pot volume . . . . .	225

# 1 Chapter 1

## 2 Introduction

3 Photosynthesis represents the largest carbon flux between the atmosphere  
4 and biosphere, and is regulated by complex ecosystem carbon and nutrient cy-  
5 cles (Hungate et al. 2003; IPCC 2021). As a result, the inclusion of robust,  
6 empirically tested representations of photosynthetic processes is critical in order  
7 for terrestrial biosphere models to accurately and reliably simulate carbon and  
8 nutrient fluxes between the atmosphere and terrestrial biosphere (Wieder et al.  
9 2015; Smith and Dukes 2013; Prentice et al. 2015; Oreskes et al. 1994). Despite  
10 evidence that the inclusion of coupled carbon and nutrient cycles can improve  
11 model uncertainty, widespread divergence in predicted carbon and nutrient fluxes  
12 is still apparent across model products (Arora et al. 2020; Friedlingstein et al.  
13 2014; Davies-Barnard et al. 2020). Divergence in predicted carbon and nutrient  
14 fluxes across terrestrial biosphere models may be due to an incomplete under-  
15 standing of how plants acclimate to changing environments (Smith and Dukes  
16 2013; Davies-Barnard et al. 2020), as terrestrial biosphere models are sensitive to  
17 the formulation of photosynthetic processes (Ziehn et al. 2011; Bonan et al. 2011;  
18 Booth et al. 2012; Smith et al. 2016; Smith et al. 2017; Rogers et al. 2017).

Many terrestrial biosphere models predict leaf-level photosynthesis through linear relationships between area-based leaf nitrogen content and the maximum rate of Ribulose-1,5-bisphosphate carboxylase/oxygenase ("Rubisco"), following from the idea that large fractions of leaf nitrogen content are allocated to the construction and maintenance of Rubisco and other photosynthetic enzymes (Evans

24 1989). The inclusion of coupled carbon and nutrient cycles in terrestrial biosphere  
25 models (Shi et al. 2016; Braghieri et al. 2022) allows for the prediction of leaf ni-  
26 trogen content through soil nitrogen availability, which causes models to indirectly  
27 predict photosynthetic processes through shifts in soil nitrogen availability (Smith  
28 et al. 2014; Lawrence et al. 2019). While these patterns are commonly observed  
29 in ecosystems globally (Brix 1971; Evans 1989; Liang et al. 2020; Firn et al. 2019),  
30 this formulation of photosynthetic processes does not allow for the prediction of  
31 leaf and whole plant acclimation responses to changing environments (Smith and  
32 Dukes 2013; Rogers et al. 2017; Harrison et al. 2021), and suggests that con-  
33 stant leaf nitrogen-photosynthesis relationships are ubiquitous across ecosystems.  
34 Incorporating leaf and whole plant acclimation schemes in terrestrial biosphere  
35 models is important (Smith and Dukes 2013), particularly because recent work  
36 indicates that variance in leaf nitrogen content and leaf photosynthesis across en-  
37 vironmental gradients may be better explained as an integrated product of leaf  
38 acclimation responses to changing climates and soil nitrogen availability than soil  
39 nitrogen availability alone (Dong et al. 2017; Dong et al. 2020; Smith et al. 2019;  
40 Querejeta et al. 2022; Dong et al. 2022; Westerband et al. 2023).

41 Photosynthetic least-cost theory (Prentice et al. 2014; Wang et al. 2017;  
42 Smith et al. 2019; Scott and Smith 2022; Harrison et al. 2021) provides a con-  
43 temporary framework for predicting leaf and whole plant acclimation responses  
44 to environmental change. The theory, which unifies photosynthetic optimal coor-  
45 dination (Chen et al. 1993; Maire et al. 2012) and least-cost (Wright et al. 2003)  
46 theories, posits that plants optimize photosynthetic processes by minimizing the  
47 summed cost of nitrogen and water use (referred to here and in the rest of this

48 dissertation as  $\beta$ ). The summed cost of nitrogen and water use is predicted to  
49 be positively correlated with the ratio of intercellular CO<sub>2</sub> to atmospheric CO<sub>2</sub>  
50 (referred to here and in the rest of this dissertation as leaf  $C_i:C_a$ , which is deter-  
51 mined by factors that influence leaf nitrogen demand, such as CO<sub>2</sub>, temperature,  
52 vapor pressure deficit, and light availability (Prentice et al. 2014; Smith et al.  
53 2019; Stocker et al. 2020; Wang et al. 2017). Photosynthetic processes are opti-  
54 mized such that nitrogen is allocated to photosynthetic enzymes in to allow net  
55 photosynthesis rates to be equally co-limited by the maximum rate of Rubisco  
56 carboxylation and the maximum rate of Ribulose-1,5-bisphosphate (RuBP) re-  
57 generation (Chen et al. 1993; Maire et al. 2012). The theory indicates that costs  
58 of nitrogen and water use are substitutable such that, in a given environment,  
59 optimal photosynthesis rates can be achieved by sacrificing inefficient use of a  
60 relatively more abundant (and less costly to acquire) resource for more efficient  
61 use of a relatively less abundant (and more costly to acquire) resource. These  
62 predictions imply that acclimation responses to changing environments may be  
63 partially driven by trade-offs between nitrogen and water use, though empirical  
64 tests of the theory are sparse.

65 Optimality models leveraging patterns expected from photosynthetic least-  
66 cost theory have been developed for both C<sub>3</sub> (Wang et al. 2017; Smith et al. 2019;  
67 Stocker et al. 2020) and more recently for C<sub>4</sub> species (Scott and Smith 2022). Such  
68 models show broad agreement with patterns observed across environmental gradi-  
69 ents (Paillassa et al. 2020; Querejeta et al. 2022; Smith et al. 2019; Westerband  
70 et al. 2023), and are capable of reconciling dynamic leaf nitrogen-photosynthesis  
71 relationships and acclimation responses to elevated CO<sub>2</sub>, temperature, light avail-

72 ability, and vapor pressure deficit (Dong et al. 2017; Dong et al. 2020; Dong et al.  
73 2022; Dong et al. 2022; Smith and Keenan 2020; Luo et al. 2021; Peng et al. 2021;  
74 Querejeta et al. 2022; Westerband et al. 2023). Current versions of optimality  
75 models that invoke patterns expected from photosynthetic least-cost theory hold  
76  $\beta$  constant across growing environments. As growing evidence suggests that costs  
77 of nitrogen use change across resource availability and climatic gradients in species  
78 with different nutrient acquisition strategies (Fisher et al. 2010; Brzostek et al.  
79 2014; Allen et al. 2020; Terrer et al. 2018), one might expect that  $\beta$  should  
80 dynamically change across environments and in species with different acquisition  
81 strategies. However, manipulative experiments that test mechanisms underlying  
82 nitrogen-water use trade-offs and leaf nitrogen-photosynthesis relationships pre-  
83 dicted from theory across soil resource availability and climatic gradients are rare.  
84 Furthermore, no study has related shifts in  $\beta$  to nitrogen-water use trade-offs or  
85 leaf nitrogen-photosynthesis relationships. Understanding the dynamic nature of  
86  $\beta$  across different environmental contexts and impacts of  $\beta$  on patterns expected  
87 from theory are critical for further optimality model development, and is the cen-  
88 tral motivation for the experiments presented in this dissertation.

89 In this dissertation, I use four experiments to quantify nutrient acquisition  
90 and allocation responses under different environmental conditions and in species  
91 with different nutrient acquisition strategies. These experiments provide impor-  
92 tant empirical data needed to evaluate patterns expected from photosynthetic  
93 least-cost theory and test mechanisms that drive such patterns. In the first ex-  
94 perimental chapter, I re-analyze data from a greenhouse experiment that grew  
95 *Glycine max* L. (Merr) and *Gossypium hirsutum* seedlings under full-factorial

96 combinations of four light treatments and four fertilization treatments. This re-  
97 analysis examined the effect of soil nitrogen availability and light availability on  
98 structural carbon costs to acquire nitrogen in a species capable of forming associ-  
99 ations with symbiotic nitrogen-fixing bacteria (*G. max*) and a species not capable  
100 of forming such associations (*G. hirsutum*). I find strong evidence suggesting that  
101 increasing light availability increases structural carbon costs to acquire nitrogen  
102 and that increasing soil nitrogen fertilization decreases structural carbon costs to  
103 acquire nitrogen.

104 In the second experimental chapter, I measure leaf physiological traits in  
105 the upper canopy of mature trees growing in a 9-year nitrogen-by-pH field manip-  
106 ulation experiment to assess whether changes in soil nitrogen availability or soil  
107 pH modify nitrogen-water use trade-offs expected from photosynthetic least-cost  
108 theory. I find strong nitrogen-water use trade-offs in response to increasing soil ni-  
109 trogen availability, indicated by a strong negative relationship between leaf  $C_i:C_a$   
110 (referred to here and in the rest of this dissertation as  $\chi$ ) and leaf nitrogen content,  
111 as well as a strong increase in leaf nitrogen content per unit leaf  $\chi$  with increas-  
112 ing soil nitrogen availability. Interestingly, I also find a null effect of soil pH on  
113 nitrogen-water use trade-offs. These patterns provide strong support for patterns  
114 expected from photosynthetic least-cost theory across soil nitrogen availability  
115 gradients, and indicate that previous studies which note strong nitrogen-water  
116 use trade-offs in response to soil pH may be driven by covariation between soil  
117 nitrogen availability and soil pH (Paillassa et al. 2020; Westerband et al. 2023).

118 In the third experimental chapter, I leverage a broad precipitation and soil  
119 nutrient availability gradient in Texan grasslands to investigate primary drivers of

120 leaf nitrogen content. In this chapter, I directly quantify  $\beta$  and  $\chi$  using leaf  $\delta^{13}\text{C}$  to  
121 examine primary drivers of leaf nitrogen content and find that leaf nitrogen content  
122 is driven through a negative relationship with  $\chi$ . I also show that soil nitrogen  
123 availability is negatively associated with  $\beta$ , and that  $\beta$  is positively associated  
124 with  $\chi$ . I show strong support for patterns expected from theory, showing for  
125 the first time that positive effects of increasing soil nitrogen availability on leaf  
126 nitrogen content are mediated by changes in  $\beta$ .

127 In the fourth experimental chapter, I use reach-in growth chambers to  
128 quantify leaf and whole plant acclimation responses to  $\text{CO}_2$  across a soil nitro-  
129 gen fertilization gradient, while also manipulating nutrient acquisition strategy  
130 by controlling whether seedlings were able to form associations with symbiotic  
131 nitrogen-fixing bacteria. Specifically, I measure leaf physiological and whole plant  
132 growth responses of 7-week *G. max* seedlings grown under one of two  $\text{CO}_2$  treat-  
133 ments, one of nine fertilization treatments, and one of two inoculation treatments  
134 in a full factorial design. I find a down-regulation in leaf nitrogen content and  
135 leaf photosynthesis under elevated  $\text{CO}_2$ , a pattern that is not modified across  
136 the fertilization gradient or between inoculation treatments. However, I also find  
137 strong stimulation in total leaf area and whole plant growth under elevated  $\text{CO}_2$   
138 that are enhanced with increasing fertilization. There was no observable effect of  
139 inoculation in modifying whole plant growth responses to  $\text{CO}_2$ , which I speculate  
140 is the result of a down-regulation in plant investments to nitrogen fixation with  
141 increasing fertilization. Results from this experiment provide strong evidence sug-  
142 gesting that leaf acclimation responses to  $\text{CO}_2$  were controlled by optimal resource  
143 investment to photosynthetic capacity, following patterns expected from photo-

144 synthetic least-cost theory, and suggest divergent roles of soil nitrogen fertilization  
145 in modifying leaf and whole plant acclimation responses to CO<sub>2</sub>.

146 Throughout the four experimental chapters, I find strong and consistent  
147 patterns supportive of patterns expected from photosynthetic least-cost theory.  
148 Specifically, I find strong nitrogen-water use trade-offs in response to changing  
149 climates and soil resources, that shifts in soil nitrogen availability have strong  
150 negative impacts on costs of nitrogen acquisition, and therefore tend to increase  
151  $\beta$ , and that constant leaf nitrogen-photosynthesis relationships only occur in sys-  
152 tems where nitrogen is limiting. In a final conclusion chapter, I summarize ma-  
153 jor findings from each of the four experimental chapters and synthesize common  
154 mechanisms that drive leaf and whole plant responses to changing environmen-  
155 tal conditions. I conclude this dissertation with brief dialogue on lessons learned  
156 throughout experimental chapters, and propose future experiments that will tar-  
157 get additional uncertainties in photosynthetic least-cost theory responses across  
158 environmental gradients.

159

## Chapter 2

160

Structural carbon costs to acquire nitrogen are determined by  
161 nitrogen and light availability in two species with different nitrogen  
162 acquisition strategies

163 2.1 Introduction

164

Carbon and nitrogen cycles are tightly coupled in terrestrial ecosystems.

165

This tight coupling influences photosynthesis (Walker et al. 2014; Rogers et al.

166

2017), net primary productivity (LeBauer and Treseder 2008; Thomas et al. 2013),

167

decomposition (Cornwell et al. 2008; Bonan et al. 2013; Sulman et al. 2019), and

168

plant resource competition (Gill and Finzi 2016; Xu-Ri and Prentice 2017). Ter-

169

restrial biosphere models are beginning to include connected carbon and nitrogen

170

cycles to improve the realism of their simulations (Fisher et al. 2010; Brzostek

171

et al. 2014; Wieder et al. 2015; Shi et al. 2016; Zhu et al. 2019). Simula-

172

tions from these models indicate that coupling carbon and nitrogen cycles can

173

drastically influence future biosphere-atmosphere feedbacks under global change,

174

such as elevated carbon dioxide or nitrogen deposition (Thornton et al. 2007;

175

Goll et al. 2012; Wieder et al. 2015; Wieder et al. 2019). Nonetheless, there

176

are still limitations in our quantitative understanding of connected carbon and

177

nitrogen dynamics (Thomas et al. 2015; Meyerholt et al. 2016; Rogers et al.

178

2017; Exbrayat et al. 2018; Shi et al. 2019), forcing models to make potentially

179

unreliable assumptions.

180

Plant nitrogen acquisition is a process in terrestrial ecosystems by which

181

carbon and nitrogen are tightly coupled (Vitousek and Howarth 1991; Delaire

182

et al. 2005; Brzostek et al. 2014). Plants must allocate photosynthetically de-

183 rived carbon belowground to produce and maintain root systems or exchange with  
184 symbiotic soil microbes in order to acquire nitrogen (Högberg et al. 2008; Hög-  
185 berg et al. 2010). Thus, plants have an inherent carbon cost associated with  
186 acquiring nitrogen, which can include both direct energetic costs associated with  
187 nitrogen acquisition and indirect costs associated with building structures that  
188 support nitrogen acquisition (Gutschick 1981; Rastetter et al. 2001; Vitousek  
189 et al. 2002; Menge et al. 2008). Model simulations (Fisher et al. 2010; Brzostek  
190 et al. 2014; Shi et al. 2016; Allen et al. 2020) and meta-analyses (Terrer et al.  
191 2018) suggest that these carbon costs vary between species, particularly those  
192 with different nitrogen acquisition strategies. For example, simulations using iter-  
193 ations of the Fixation and Uptake of Nitrogen (FUN) model indicate that species  
194 that acquire nitrogen from non-symbiotic active uptake pathways (e.g. mass flow)  
195 generally have larger carbon costs to acquire nitrogen than species that acquire  
196 nitrogen through symbiotic associations with nitrogen-fixing bacteria (Brzostek  
197 et al. 2014; Allen et al. 2020).

198 Carbon costs to acquire nitrogen likely vary in response to changes in soil  
199 nitrogen availability. For example, if the primary mode of nitrogen acquisition  
200 is through non-symbiotic active uptake, then nitrogen availability could decrease  
201 carbon costs to acquire nitrogen as a result of increased per-root nitrogen up-  
202 take (Franklin et al. 2009; Wang et al. 2018). However, if the primary mode of  
203 nitrogen acquisition is through symbiotic active uptake, then nitrogen availabil-  
204 ity may incur additional carbon costs to acquire nitrogen if it causes microbial  
205 symbionts to shift toward parasitism along the parasitism–mutualism continuum  
206 (Johnson et al. 1997; Hoek et al. 2016; Friel and Friesen 2019) or if it reduces

207 the nitrogen acquisition capacity of a microbial symbiont (van Diepen et al. 2007;  
208 Soudzilovskaia et al. 2015; Muñoz et al. 2016). Species may respond to shifts in  
209 soil nitrogen availability by switching their primary mode of nitrogen acquisition  
210 to a strategy with lower carbon costs to acquire nitrogen in order to maximize  
211 the magnitude of nitrogen acquired from a belowground carbon investment and  
212 outcompete other individuals for soil resources (Rastetter et al. 2001; Menge et al.  
213 2008).

214 Environmental conditions that affect demand to acquire nitrogen to sup-  
215 port new and existing tissues could also be a source of variance in plant carbon  
216 costs to acquire nitrogen. For example, an increase in plant nitrogen demand could  
217 increase carbon costs to acquire nitrogen if this increases the carbon that must be  
218 allocated belowground to acquire a proportional amount of nitrogen (Kulmatiski  
219 et al. 2017; Noyce et al. 2019). This could be driven by a temporary state of  
220 diminishing return associated with investing carbon toward building and main-  
221 taining structures that are necessary to support enhanced nitrogen uptake, such  
222 as fine roots (Matamala and Schlesinger 2000; Norby et al. 2004; Arndal et al.  
223 2018), mycorrhizal hyphae (Saleh et al. 2020), or root nodules (Parvin et al. 2020).  
224 Alternatively, if the environmental factor that increases plant nitrogen demand  
225 causes nitrogen to become more limiting in the system (e.g. atmospheric CO<sub>2</sub>;  
226 Luo et al. (2004), LeBauer and Treseder (2008), Vitousek et al. (2010), Liang  
227 et al. (2016)), species might switch their primary mode of nitrogen acquisition to  
228 a strategy with lower relative carbon costs to acquire nitrogen in order to gain a  
229 competitive advantage over species with either different or more limited modes of  
230 nitrogen acquisition (Ainsworth and Long 2005; Taylor and Menge 2018).

231        Using a plant economics approach, I examined the influence of plant ni-  
232      trogen demand and soil nitrogen availability on plant carbon costs to acquire  
233      nitrogen. This was done by growing a species capable of forming associations  
234      with nitrogen-fixing bacteria (*Glycine max* L. (Merr)) and a species not capable  
235      of forming these associations (*Gossypium hirsutum* L.) under four levels of light  
236      availability (plant nitrogen demand proxy) and four levels of soil nitrogen fertil-  
237      ization (soil nitrogen availability proxy) in a full-factorial, controlled greenhouse  
238      experiment. I used this experimental set-up to test the following hypotheses:

- 239      1. An increase in plant nitrogen demand due to increasing light availability will  
240        increase carbon costs to acquire nitrogen through a proportionally larger  
241        increase in belowground carbon than whole-plant nitrogen acquisition. This  
242        will be the result of an increased investment of carbon toward belowground  
243        structures that support enhanced nitrogen uptake, but at a lower nitrogen  
244        return.
- 245      2. An increase in soil nitrogen availability will decrease carbon costs to acquire  
246        nitrogen as a result of increased per root nitrogen uptake in *G. hirsutum*.  
247        However, soil nitrogen availability will not affect carbon costs to acquire  
248        nitrogen in *G. max* because of the already high return of nitrogen supplied  
249        through nitrogen fixation.

**250** 2.2 Methods

**251** 2.2.1 *Experiment setup*

**252** *Gossypium hirsutum* and *G. max* were planted in individual 3 liter pots  
**253** (NS-300; Nursery Supplies, Orange, CA, USA) containing a 3:1 mix of unfertil-  
**254** ized potting mix (Sungro Sunshine Mix #2, Agawam, MA, USA) to native soil  
**255** extracted from an agricultural field most recently planted with *G. max* at the  
**256** USDA-ARS Laboratory in Lubbock, TX, USA (33.59°N, -101.90°W). The field  
**257** soil was classified as Amarillo fine sandy loam (75% sand, 10% silt, 15% clay).  
**258** Upon planting, all *G. max* pots were inoculated with *Bradyrhizobium japonicum*  
**259** (Verdesian N-Dure™ Soybean, Cary, NC, USA) to stimulate root nodulation. In-  
**260** dividuals of both species were grown under similar, unshaded, ambient greenhouse  
**261** conditions for 2 weeks to germinate and begin vegetative growth. Three blocks  
**262** were set up in the greenhouse, each containing four light treatments created us-  
**263** ing shade cloth that reduced incoming radiation by either 0 (full sun), 30, 50,  
**264** or 80%. Two weeks post-germination, individuals were randomly placed in the  
**265** four light treatments in each block. Individuals received one of four nitrogen fer-  
**266** tilization doses as 100ml of a modified Hoagland solution (Hoagland and Arnon  
**267** 1950) equivalent to either 0, 70, 210, or 630 ppm N twice per week within each  
**268** light treatment. Nitrogen fertilization doses were received as topical agents to  
**269** the soil surface. Each Hoagland solution was modified to keep concentrations of  
**270** other macro- and micronutrients equivalent (Supplementary Table S1). Plants  
**271** were routinely well watered to eliminate water stress.

**272** 2.2.2 *Plant measurements and calculations*

**273** Each individual was harvested after 5 weeks of treatment, and biomass  
**274** was separated by organ type (leaves, stems, and roots). Nodules on *G. max*  
**275** roots were also harvested. Except for the 0% shade cover and 630 ppm N treat-  
**276** ment combination, all treatment combinations in both species had lower average  
**277** dry biomass:pot volume ratios than the 1:1 ratio recommended by Poorter et al.  
**278** (2012) to minimize the likelihood of pot volume-induced growth limitation (Sup-  
**279** plementary Tables S2, S3; Supplementary Fig. S1). All harvested material was  
**280** dried, weighed, and ground by organ type. Carbon and nitrogen content ( $\text{g g}^{-1}$ )  
**281** was determined by subsampling from ground and homogenized biomass of each  
**282** organ type using an elemental analyzer (Costech 4010; Costech, Inc., Valencia,  
**283** CA, USA). We scaled these values to total leaf, stem, and root carbon and ni-  
**284** trogen biomass (g) by multiplying dry biomass of each organ type by carbon or  
**285** nitrogen content of each corresponding organ type. Whole-plant nitrogen biomass  
**286** (g) was calculated as the sum of total leaf (g), stem (g), and root (g) nitrogen  
**287** biomass. Root nodule carbon biomass was not included in the calculation of root  
**288** carbon biomass; however, relative plant investment toward root or root nodule  
**289** standing stock was estimated as the ratio of root biomass to root nodule biomass  
**290** ( $\text{g g}^{-1}$ ), following similar metrics to those adopted by Dovrat et al. (2018) and  
**291** Dovrat et al. (2020).

**292** Carbon costs to acquire nitrogen ( $N_{\text{cost}}$ ;  $\text{gC gN}^{-1}$ ) were estimated as the  
**293** ratio of total root carbon biomass ( $C_{\text{bg}}$ ;  $\text{gC}$ ) to whole-plant nitrogen biomass  
**294** ( $N_{\text{wp}}$ ;  $\text{gN}$ ). This calculation quantifies the relationship between carbon spent on  
**295** nitrogen acquisition and whole-plant nitrogen acquisition by using root carbon

296 biomass as a proxy for estimating the magnitude of carbon allocated toward ni-  
297 trogen acquisition. This calculation therefore assumes that the magnitude of root  
298 carbon standing stock is proportional to carbon transferred to root nodules or my-  
299 corrhizae, or lost through root exudation or turnover. The assumption has been  
300 supported in species that associate with ectomycorrhizal fungi (Hobbie 2006; Hob-  
301 bie and Hobbie 2008), but is less clear in species that acquire nitrogen through  
302 non-symbiotic active uptake or symbiotic nitrogen fixation. It is also unclear  
303 whether relationships between root carbon standing stock and carbon transfer to  
304 root nodules are similar in magnitude to carbon lost through exudation or when  
305 allocated toward other active uptake pathways. Thus, because of the way mea-  
306 surements were calculated, proximal values of carbon costs to acquire nitrogen are  
307 underestimates.

308 2.2.3 *Statistical analyses*

309 I explored the effects of light and nitrogen availability on carbon costs to ac-  
310 quire nitrogen using separate linear mixed-effects models for each species. Models  
311 included shade cover, nitrogen fertilization, and interactions between shade cover  
312 and nitrogen fertilization as continuous fixed effects, and also included block as a  
313 random intercept term. Three separate models for each species were built with  
314 this independent variable structure for three different dependent variables: (i)  
315 carbon costs to acquire nitrogen ( $\text{gC gN}^{-1}$ ); (ii) whole plant nitrogen biomass (de-  
316 nominator of carbon cost to acquire nitrogen;  $\text{gN}$ ); and (iii) belowground carbon  
317 biomass (numerator of carbon cost to acquire nitrogen;  $\text{gC}$ ). I constructed two  
318 additional models for *G. max* with the same model structure described above to

319 investigate the effects of light availability and nitrogen fertilization on root nodule  
320 biomass (g) and the ratio of root nodule biomass to root biomass (unitless).

321 I used Shapiro–Wilk tests of normality to determine whether species spe-  
322 cific linear mixed-effects model residuals followed a normal distribution. None of  
323 our models satisfied residual normality assumptions when models were fit using  
324 untransformed data (Shapiro–Wilk:  $p < 0.05$  in all cases). I attempted to satisfy  
325 residual normality assumptions by first fitting models using dependent variables  
326 that were natural-log transformed. If residual normality assumptions were still  
327 not met (Shapiro–Wilk:  $p < 0.05$ ), then models were fit using dependent variables  
328 that were square root transformed. All residual normality assumptions were satis-  
329 fied when models were fit with either a natural-log or square root transformation  
330 (Shapiro–Wilk:  $p > 0.05$  in all cases). Specifically, I natural-log transformed *G.*  
331 *hirsutum* carbon costs to acquire nitrogen and *G. hirsutum* whole-plant nitrogen  
332 biomass. I also square root transformed *G. max* carbon costs to acquire nitrogen,  
333 *G. max* whole-plant nitrogen biomass, root carbon biomass in both species, *G.*  
334 *max* root nodule biomass, and the *G. max* ratio of root nodule biomass to root  
335 biomass. I used the ‘lmer’ function in the ‘lme4’ R package (Bates et al. 2015) to  
336 fit each model and the ‘Anova’ function in the ‘car’ R package (Fox and Weisberg  
337 2019) to calculate Wald’s  $\chi^2$  to determine the significance ( $\alpha = 0.05$ ) of each fixed  
338 effect coefficient. Finally, I used the ‘emmeans’ R package (Lenth 2019) to conduct  
339 post-hoc comparisons of our treatment combinations using Tukey’s tests. Degrees  
340 of freedom for all Tukey’s tests were approximated using the Kenward–Roger ap-  
341 proach (Kenward and Roger 1997). All analyses and plots were conducted in R  
342 version 4.0.1 (R Core Team 2021).

**343** 2.3 Results

**344** 2.3.1 *Carbon costs to acquire nitrogen*

**345** Carbon costs to acquire nitrogen in *G. hirsutum* increased with increasing  
**346** light availability ( $p < 0.001$ ; Table 2.1; Fig. 2.1) and decreased with increasing  
**347** nitrogen fertilization ( $p < 0.001$ ; Table 2.1; Fig. 2.1). There was no interaction  
**348** between light availability and nitrogen fertilization ( $p = 0.486$ , Table 2.1; Fig.  
**349** 2.1).

**350** Carbon costs to acquire nitrogen in *G. max* also increased with increasing  
**351** light availability ( $p < 0.001$ , Table 2.1; Fig. 2.1) and decreased with increasing  
**352** nitrogen fertilization ( $p < 0.001$ ; Table 2.1; Fig. 2.1). There was no interaction  
**353** between light availability and nitrogen fertilization ( $p = 0.261$ , Table 2.1; Fig.  
**354** 2.1).

**Table 2.1.** Analysis of variance results exploring species-specific effects of light availability, nitrogen fertilization, and their interactions on carbon costs to acquire nitrogen ( $N_{\text{cost}}$ ), whole-plant nitrogen biomass ( $N_{\text{wp}}$ ), and root carbon biomass ( $C_{\text{bg}}$ )

	df	$N_{\text{cost}}$			$N_{\text{wp}}$			$C_{\text{bg}}$		
		Coefficient	$\chi^2$	p	Coefficient	$\chi^2$	p	Coefficient	$\chi^2$	p
<i>G. hirsutum</i>										
Intercept		1.594	-	-	-3.232	-	-	0.432	-	-
Light (L)	1	-1.09E-02	56.494	<0.001	-6.41E-03	91.275	<0.001	-2.62E-03	169.608	<0.001
Nitrogen (N)	1	-1.34E-03	54.925	<0.001	1.83E-03	118.784	<0.001	1.15E-04	2.901	0.089
L*N	1	3.88E-06	0.485	0.486	-1.34E-05	10.721	0.001	-1.67E-06	3.140	0.076
<i>G. max</i>										
Intercept		1.877	-	-	0.239	-	-	0.438	-	-
Light (L)	1	-7.67E-03	174.156	<0.001	-6.72E-04	39.799	<0.001	-2.55E-03	194.548	<0.001
Nitrogen (N)	1	-2.35E-04	21.948	<0.001	1.55E-04	70.771	<0.001	2.52E-04	19.458	<0.001
L*N	1	-2.89E-06	1.262	0.261	-6.32E-07	1.435	0.231	-3.16E-06	10.803	0.001

355 \*Significance determined using Wald's  $\chi^2$  tests ( $P = 0.05$ ).  $P$ -values  $< 0.05$  are in bold and  $p$ -values between 0.05 and

356 0.1 are italicized. Negative coefficients for light treatments indicate a positive effect of increasing light availability

357 on all response variables, as light availability is treated as percent shade cover in all linear mixed-effects models.

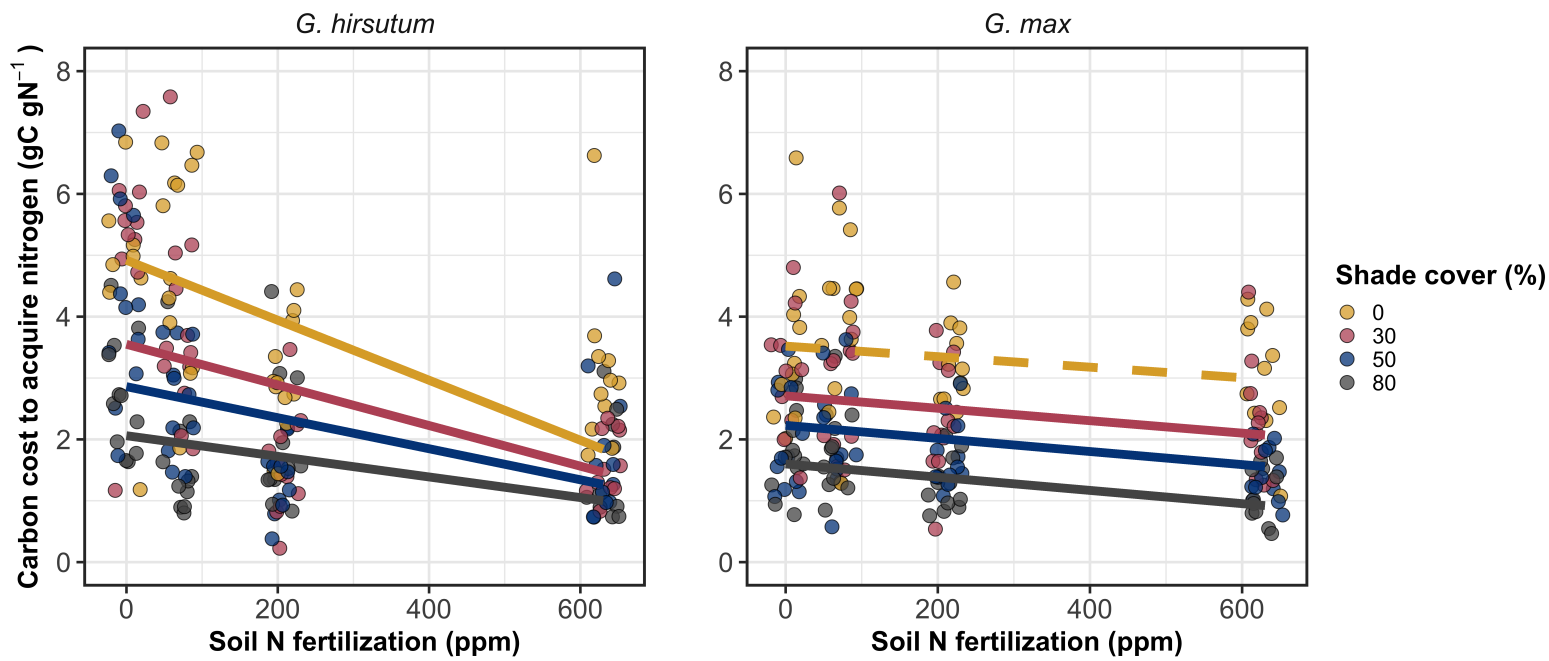


**Figure 2.1.** Relationships between soil nutrient fertilization and light availability on carbon costs to acquire nitrogen in *G. hirsutum* and *G. max*. Nitrogen fertilization treatments are represented on the x-axis. Shade cover treatments are represented through colored points and trendlines. Trendlines were created by back-transforming marginal mean slopes and intercepts from species-specific linear mixed-effects models. These values were calculated using the ‘emtrends’ and ‘emmeans’ functions in the ‘emmeans’ R package (Lenth, 2019). Yellow points and trendlines represent the 0% shade cover treatment, red points and trendlines represent the 30% shade cover treatment, blue points and trendlines represent the 50% shade cover treatment, and gray points and trendlines represent the 80% shade cover treatment. Solid trendlines indicate slopes that are significantly different from zero (Tukey:  $p < 0.05$ ), while dashed trendlines indicate slopes that are not statistically different from zero.

**358** 2.3.2 *Whole plant nitrogen biomass*

**359** Whole-plant nitrogen biomass in *G. hirsutum* was driven by an interaction  
**360** between light availability and nitrogen fertilization ( $p = 0.001$ ; Table 2.1; Fig.  
**361** 2.2). This interaction indicated a greater stimulation of whole-plant nitrogen  
**362** biomass by nitrogen fertilization as light levels increased (Table 2.1; Fig. 2.2).

**363** Whole-plant nitrogen biomass in *G. max* increased with increasing light  
**364** availability ( $p < 0.001$ ) and nitrogen fertilization ( $p < 0.001$ ), with no interaction  
**365** between light availability and nitrogen fertilization ( $p = 0.231$ ; Table 2.1; Fig.  
**366** 2.2).

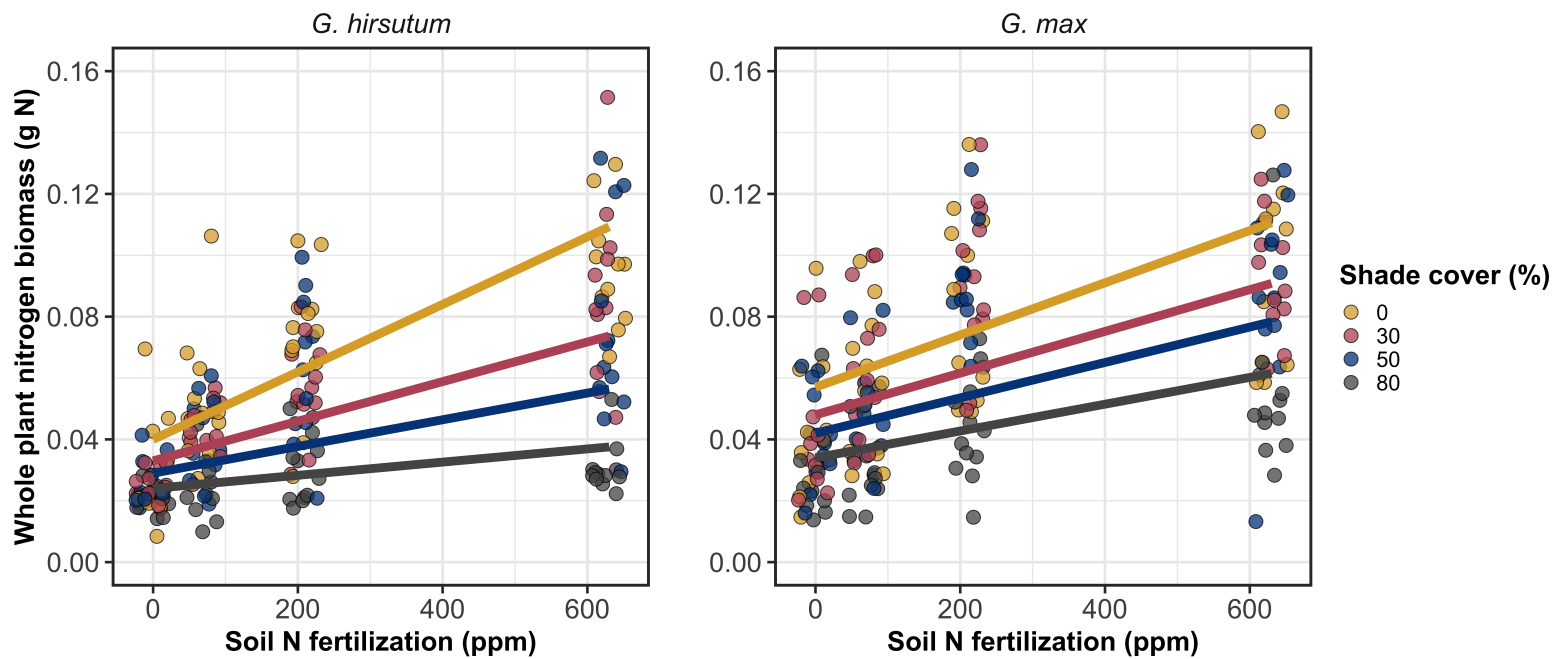


**Figure 2.2.** Relationships between soil nutrient fertilization and light availability on whole-plant nitrogen biomass in *G. hirsutum* and *G. max*. Whole-plant nitrogen biomass is the denominator of the carbon cost to acquire nitrogen calculation. Nitrogen fertilization treatments are represented on the x-axis. Shade cover treatments are represented through colored points and trendlines. Trendlines were created by back-transforming marginal mean slopes and intercepts from species-specific linear mixed-effects models. These values were calculated using the ‘emtrends’ and ‘emmeans’ functions in the ‘emmeans’ R package (Lenth 2019). Points are jittered for visibility. Colored points and trendlines are as explained in Fig. 2.1. Solid trendlines indicate slopes that are significantly different from zero (Tukey:  $p < 0.05$ ), while dashed trendlines indicate slopes that are not statistically different from zero.

**367** 2.3.3 *Root carbon biomass*

**368** Root carbon biomass in *G. hirsutum* significantly increased with increasing  
**369** light availability ( $p < 0.001$ ; Table 2.1; Fig. 2.3) and marginally increased with  
**370** nitrogen fertilization ( $p = 0.089$ ; Table 2.1; Fig. 2.3). There was also a marginal  
**371** interaction between light availability and nitrogen fertilization ( $p = 0.076$ ; Table  
**372** 2.1), driven by an increase in the positive response of root carbon biomass to  
**373** increasing nitrogen fertilization as light availability increased. This resulted in  
**374** significantly positive trends between root carbon biomass and nitrogen fertilization  
**375** in the two highest light treatments (Tukey:  $p < 0.05$  in both cases; Table 2.3;  
**376** Fig. 2.3) and no effect of nitrogen fertilization in the two lowest light treatments  
**377** (Tukey:  $p > 0.05$  in both cases; Table 2.3; Fig. 2.3).

**378** There was an interaction between light availability and nitrogen fertiliza-  
**379** tion on root carbon biomass in *G. max* ( $p = 0.001$ ; Table 2.1; Fig. 2.3). Post-hoc  
**380** analyses indicated that the positive effects of nitrogen fertilization on *G. max* root  
**381** carbon biomass increased with increasing light availability (Table 2.3; Fig. 2.3).  
**382** There were also positive individual effects of increasing nitrogen fertilization ( $p <$   
**383**  $0.001$ ) and light availability ( $p < 0.001$ ) on *G. max* root carbon biomass (Table  
**384** 2.1; Fig. 2.3).

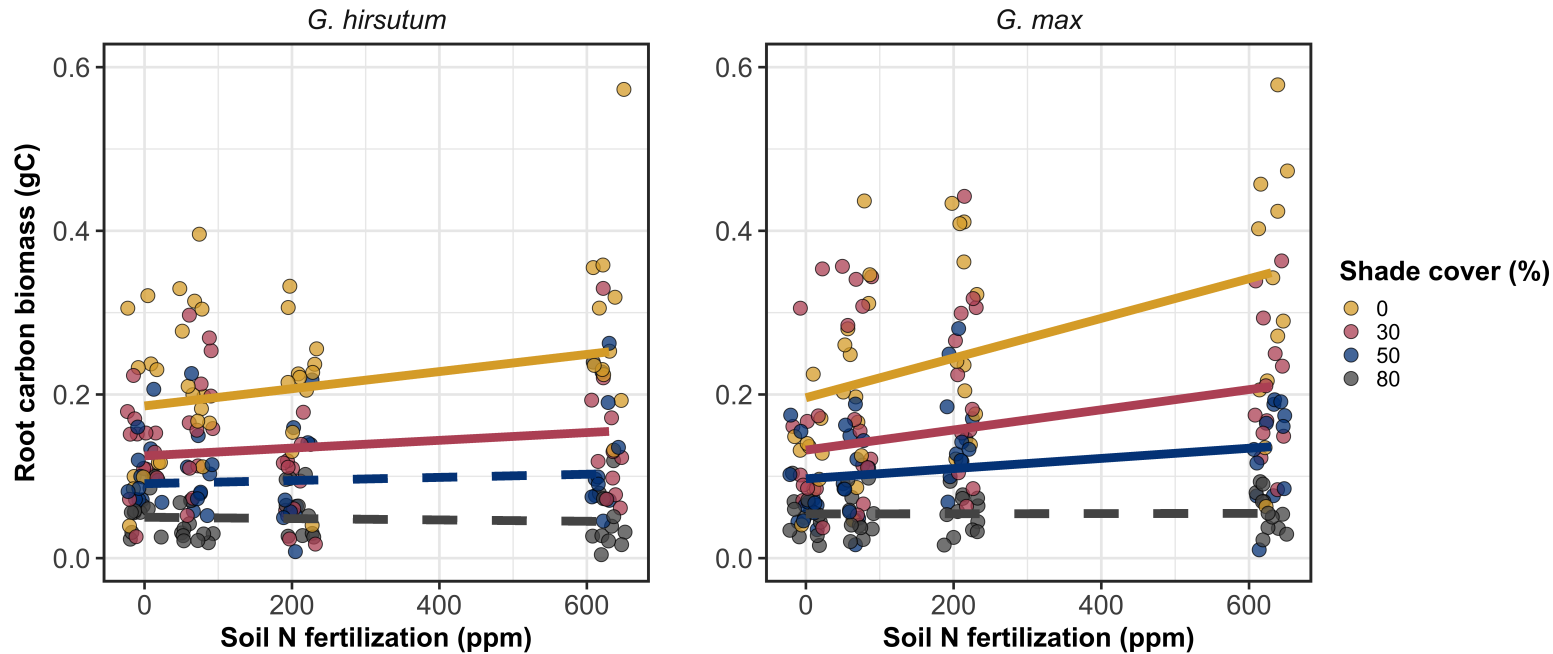


**Figure 2.3.** Relationships between soil nutrient fertilization and light availability on root carbon biomass in *G. hirsutum* and *G. max*. Root carbon biomass is the numerator of the carbon cost to acquire nitrogen calculation. Nitrogen fertilization treatments are represented on the x-axis. Shade cover treatments are represented through colored points and trendlines. Trendlines were created by back-transforming marginal mean slopes and intercepts from species-specific linear mixed-effects models. These values were calculated using the ‘emtrends’ and ‘emmmeans’ functions in the ‘emmeans’ R package (Lenth 2019). Points are jittered for visibility. Colored points and trendlines are as explained in Fig. 2.1.

Yellow points and trendlines represent the 0% shade cover treatment, blue points and trendlines represent the 30% shade cover treatment, green points and trendlines represent the 50% shade cover treatment, and purple points and trendlines represent the 80% shade cover treatment. Solid trendlines indicate slopes that are significantly different from zero (Tukey:  $p < 0.05$ ), while dashed trendlines indicate slopes that are not statistically different from zero.

**385** 2.3.4 *Root nodule biomass*

**386** Root nodule biomass in *G. max* increased with increasing light availability  
**387** ( $p < 0.001$ ; Table 2.2; Fig. 2.4A) and decreased with increasing nitrogen fertiliza-  
**388** tion ( $p < 0.001$ ; Table 2.2; Fig. 2.4A). There was no interaction between nitrogen  
**389** fertilization and light availability ( $p = 0.133$ ; Table 2.2; Fig. 2.4A). The ratio of  
**390** root nodule biomass to root biomass did not change in response to light avail-  
**391** ability ( $p = 0.481$ ; Table 2.2; Fig. 2.4B) but decreased with increasing nitrogen  
**392** fertilization ( $p < 0.001$ ; Table 2.2; Fig. 2.4B). There was no interaction between  
**393** nitrogen fertilization and light availability on the ratio of root nodule biomass to  
**394** root biomass ( $p = 0.621$ ; Table 2.2; Fig. 2.4B).

**Table 2.2.** Analysis of variance results exploring effects of light availability, nitrogen fertilization, and their interactions on *G. max* root nodule biomass and the ratio of root nodule biomass to root biomass\*

	Nodule biomass			Nodule biomass: root biomass			<i>p</i>
	df	Coefficient	$\chi^2$	<i>p</i>	Coefficient	$\chi^2$	
(Intercept)		0.302	-	-	0.448	-	-
Light (L)	1	-1.81E-03	72.964	<b>&lt;0.001</b>	-8.76E-05	0.496	0.481
Nitrogen (N)	1	-2.83E-04	115.377	<b>&lt;0.001</b>	-5.09E-04	156.476	<b>&lt;0.001</b>
L*N	1	1.14E-06	2.226	0.133	-7.30E-07	0.244	0.621

395 \*Significance determined using Wald's  $\chi^2$  tests ( $\alpha = 0.05$ ). *P*-values less than 0.05 are in bold. Negative coefficients  
 396 for light treatments indicate a positive effect of increasing light availability on all response variables, as light avail-  
 397 ability is treated as percent shade cover in all linear mixed-effects models. Root nodule biomass and nodule biomass:  
 398 root biomass models were only constructed for *G. max* because *G. hirsutum* was not inoculated with *B. japonicum*  
 399 and is not capable of forming root nodules.

**Table 2.3.** Slopes of the regression line describing the relationship between each dependent variable and nitrogen fertilization at each light level\*

Shade cover	Carbon cost to acquire nitrogen	Whole plant N biomass	Belowground C biomass	Root nodule biomass	Nodule biomass: root biomass
<i>G. hirsutum</i>					
0%	<b>-1.34E-03<sup>a</sup></b>	<b>1.83E-03<sup>a</sup></b>	<b>1.15E-04<sup>b</sup></b>	-	-
30%	<b>-1.22E-03<sup>a</sup></b>	<b>1.43E-03<sup>a</sup></b>	<b>1.17E-04<sup>b</sup></b>	-	-
50%	<b>-1.14E-03<sup>a</sup></b>	<b>1.17E-03<sup>a</sup></b>	3.12E-05 <sup>b</sup>	-	-
80%	<b>-1.02E-03<sup>a</sup></b>	<b>7.66E-04<sup>a</sup></b>	-1.89E-06 <sup>b</sup>	-	-
<i>G. max</i>					
0%	-2.35E-04 <sup>b</sup>	<b>1.55E-05<sup>b</sup></b>	<b>2.51E-04<sup>b</sup></b>	<b>-2.83E-04<sup>b</sup></b>	<b>-5.09E-04<sup>b</sup></b>
30%	<b>-3.22E-04<sup>b</sup></b>	<b>1.35E-05<sup>b</sup></b>	<b>1.57E-04<sup>b</sup></b>	<b>-2.49E-04<sup>b</sup></b>	<b>-5.31E-04<sup>b</sup></b>
50%	<b>-3.80E-04<sup>b</sup></b>	<b>1.23E-05<sup>b</sup></b>	<b>9.37E-05<sup>b</sup></b>	<b>-2.26E-04<sup>b</sup></b>	<b>-5.45E-04<sup>b</sup></b>
80%	<b>-4.66E-04<sup>b</sup></b>	<b>1.04E-05<sup>b</sup></b>	-9.95E-07 <sup>b</sup>	<b>-1.92E-04<sup>b</sup></b>	<b>-5.67E-04<sup>b</sup></b>

25

400 \*Slopes represent estimated marginal mean slopes from linear mixed-effects models described in the Methods. Slopes  
 401 were calculated using the ‘emmeans’ R package (Lenth 2019). Superscripts indicate slopes fit to natural-log<sup>(a)</sup> or  
 402 square root<sup>(b)</sup> transformed data. Slopes statistically different from zero (Tukey:  $p < 0.05$ ) are indicated in bold.  
 403 Marginally significant slopes (Tukey:  $0.05 < p < 0.1$ ) are italicized.

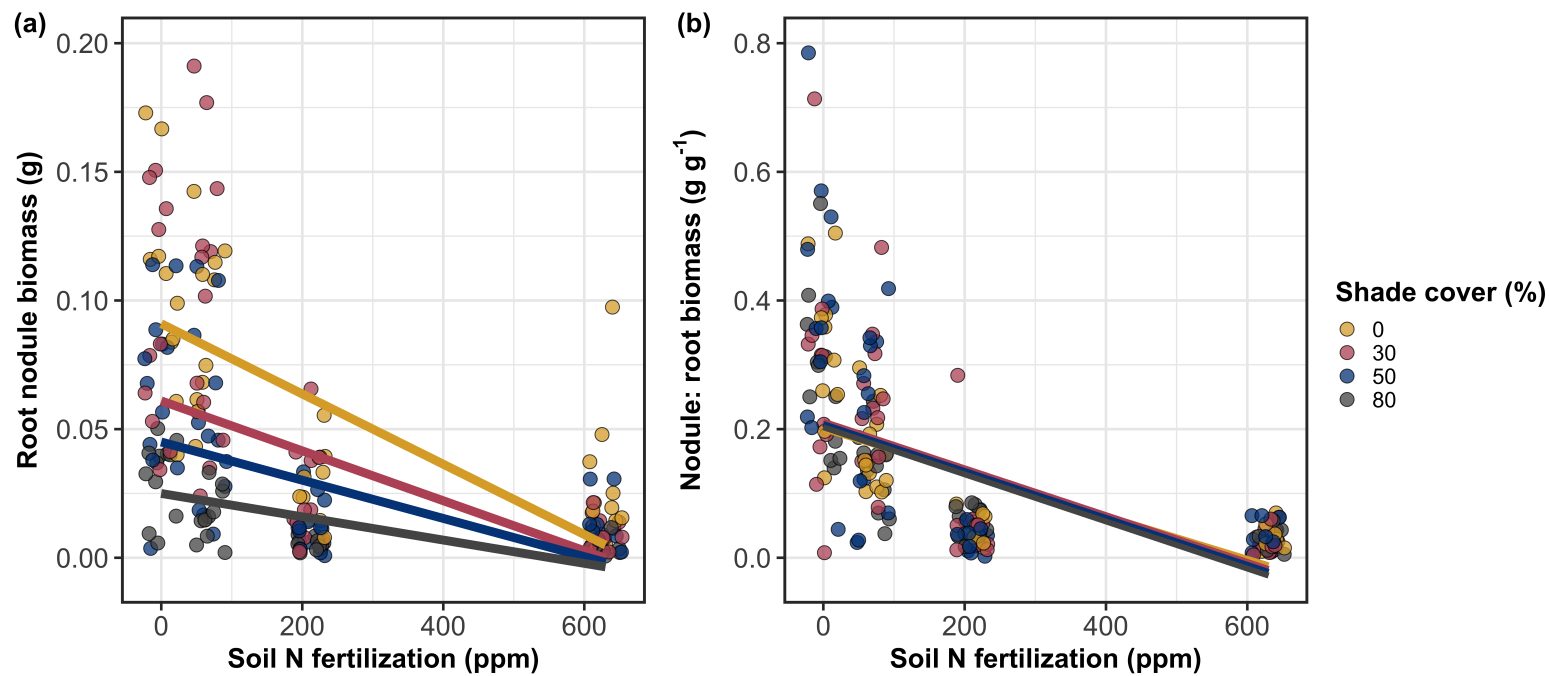


**Figure 2.4.** Effects of shade cover and nitrogen fertilization on root nodule biomass (A) and the ratio of root nodule biomass to root biomass (B) in *G. max*. Nitrogen fertilization treatments are represented on the x-axis. Shade cover treatments are represented through colored points and trendlines. Trendlines were created by back-transforming marginal mean slopes and intercepts from species-specific linear mixed-effects models. These values were calculated using the ‘emtrends’ and ‘emmeans’ functions in the ‘emmeans’ R package (Lenth 2019). Points are jittered for visibility. Yellow points and trendlines represent the 0% shade cover treatment, blue points and trendlines represent the 30% shade cover treatment, green points and trendlines represent the 50% shade cover treatment, and purple points and trendlines represent the 80% shade cover treatment. Solid trendlines indicate slopes that are significantly different from zero (Tukey:  $p < 0.05$ ), while dashed trendlines indicate slopes that are not statistically different from zero.

**404** 2.4 Discussion

**405** In this chapter, I determined the effects of light availability and soil ni-  
**406** trogen fertilization on root mass carbon costs to acquire nitrogen in *G. hirsutum*  
**407** and *G. max*. In support of my hypotheses, I found that carbon costs to acquire  
**408** nitrogen generally increased with increasing light availability and decreased with  
**409** increasing soil nitrogen fertilization in both species. These findings suggest that  
**410** carbon costs to acquire nitrogen are determined by factors that influence plant  
**411** nitrogen demand and soil nitrogen availability. In contrast to my second hypothe-  
**412** sis, root nodulation data suggested that *G. max* and *G. hirsutum* achieved similar  
**413** directional carbon cost responses to nitrogen fertilization despite a likely shift in  
**414** *G. max* allocation from nodulation to root biomass along the nitrogen fertilization  
**415** gradient (Fig. 2.4B).

**416** 2.4.1 *Carbon costs to acquire nitrogen increase with light availability and*  
**417** *decrease with fertilization*

**418** Both *G. max* and *G. hirsutum* experienced an increase in carbon costs to  
**419** acquire nitrogen due to increasing light availability. These patterns were driven by  
**420** a larger increase in root carbon biomass than whole-plant nitrogen biomass. In-  
**421** creases in root carbon biomass due to factors that increase plant nitrogen demand  
**422** are a commonly observed pattern, as carbon allocated belowground provides sub-  
**423** strate needed to produce and maintain structures that satisfy aboveground plant  
**424** nitrogen demand (Nadelhoffer and Raich 1992; Giardina et al. 2005; Raich et al.  
**425** 2014). Findings suggest that plants allocate relatively more carbon for acquiring  
**426** nitrogen when demand increases over short temporal scales, which may cause a

427 temporary state of diminishing return due to asynchrony between belowground  
428 carbon and whole-plant nitrogen responses to plant nitrogen demand (Kulmatiski  
429 et al. 2017; Noyce et al. 2019). These responses might be attributed to a temporal  
430 lag associated with producing structures that enhance nitrogen acquisition. For  
431 example, fine roots (Matamala and Schlesinger 2000; Norby et al. 2004; Arndal  
432 et al. 2018) and root nodules (Parvin et al. 2020) take time to build and first  
433 require the construction of coarse roots. Thus, full nitrogen returns from these  
434 investments may not occur immediately (Kayler et al. 2010; Kayler et al. 2017),  
435 and may vary by species acquisition strategy. I speculate that increases in ni-  
436 trogen acquisition from a given carbon investment may occur beyond the 5-week  
437 scope of this experiment. A similar study conducted over a longer temporal scale  
438 would address this.

439 Increasing soil nitrogen fertilization generally decreased carbon costs to  
440 acquire nitrogen in both species. These patterns were driven by a larger increase  
441 in whole-plant nitrogen biomass than root carbon biomass. In *G. hirsutum*, re-  
442 ductions in carbon costs to acquire nitrogen may have been due to an increase in  
443 per-root nitrogen uptake, allowing individuals to maximize the amount of nitro-  
444 gen acquired from a belowground carbon investment. Interestingly, increased soil  
445 nitrogen fertilization increased whole-plant nitrogen biomass in *G. max* despite  
446 reductions in root nodule biomass that likely reduced the nitrogen-fixing capac-  
447 ity of *G. max* (Andersen et al. 2005; Muñoz et al. 2016). While reductions in  
448 root nodulation due to increased soil nitrogen availability are commonly observed  
449 (Gibson and Harper 1985; Fujikake et al. 2003), root nodulation responses were  
450 observed in tandem with increased root carbon biomass, implying that *G. max*

451 shifted relative carbon allocation from nitrogen fixation to soil nitrogen acquisition  
452 (Markham and Zekveld 2007; Dovrat et al. 2020). This was likely because  
453 there was a reduction in the carbon cost advantage of acquiring fixed nitrogen  
454 relative to soil nitrogen, and suggests that species capable of associating with  
455 symbiotic nitrogen-fixing bacteria shift their relative nitrogen acquisition path-  
456 way to optimize nitrogen uptake (Rastetter et al. 2001). Future studies should  
457 further investigate these patterns with a larger quantity of phylogenetically re-  
458 lated species, or different varieties of a single species that differ in their ability to  
459 form associations with symbiotic nitrogen-fixing bacteria to more directly test the  
460 impact of nitrogen fixation on the patterns observed in this study.

461 2.4.2 *Modeling implications*

462 Carbon costs to acquire nitrogen are subsumed in the general discussion of  
463 economic analogies to plant resource uptake (Bloom et al. 1985; Rastetter et al.  
464 2001; Vitousek et al. 2002; Phillips et al. 2013; Terrer et al. 2018; Henneron et al.  
465 2020). Despite this, terrestrial biosphere models rarely include costs of nitrogen  
466 acquisition within their framework for predicting plant nitrogen uptake. There  
467 is currently one plant resource uptake model, FUN, that quantitatively predicts  
468 carbon costs to acquire nitrogen within a framework for predicting plant nitrogen  
469 uptake for different nitrogen acquisition strategies (Fisher et al. 2010; Brzostek  
470 et al. 2014). Iterations of FUN are currently coupled to two terrestrial biosphere  
471 models: the Community Land Model 5.0 and the Joint UK Land Environment  
472 Simulator (Shi et al. 2016; Lawrence et al. 2019; Clark et al. 2011). Recent work  
473 suggests that coupling FUN to CLM 5.0 caused a large overprediction of plant

474 nitrogen uptake associated with nitrogen fixation (Davies-Barnard et al. 2020)  
475 compared to other terrestrial biosphere model products. Thus, empirical data  
476 from manipulative experiments that explicitly quantify carbon costs to acquire  
477 nitrogen in species capable of associating with nitrogen-fixing bacteria across dif-  
478 ferent environmental contexts is an important step toward identifying potential  
479 biases in models such as FUN.

480 My findings broadly support the FUN formulation of carbon costs to ac-  
481 quire nitrogen in response to soil nitrogen availability. FUN calculates carbon  
482 costs to acquire nitrogen based on the sum of carbon costs to acquire nitrogen  
483 via nitrogen fixation, mycorrhizal active uptake, non-mycorrhizal active uptake,  
484 and retranslocation (Fisher et al. 2010; Brzostek et al. 2014). Carbon costs to  
485 acquire nitrogen via mycorrhizal or non-mycorrhizal active uptake pathways are  
486 derived as a function of nitrogen availability, root biomass, and two parameterized  
487 values based on nitrogen acquisition strategy (Brzostek et al. 2014). Due to this,  
488 FUN simulates a net decrease in carbon costs to acquire nitrogen with increasing  
489 nitrogen availability for mycorrhizal and non-mycorrhizal active uptake pathways,  
490 assuming constant root biomass. This was a pattern I observed in *G. hirsutum*  
491 regardless of light availability. In contrast, FUN would not simulate a net change  
492 in carbon costs to acquire nitrogen via nitrogen fixation due to nitrogen avail-  
493 ability. This is because carbon costs to acquire nitrogen via nitrogen fixation are  
494 derived from a well established function of soil temperature, which is independent  
495 of soil nitrogen availability (Houlton et al. 2008; Fisher et al. 2010). I observed  
496 a net reduction in carbon costs to acquire nitrogen in *G. max*, except when in-  
497 dividuals were grown under 0% shade cover (Fig. 2.1). While a net reduction of

498 carbon costs in response to nitrogen fertilization runs counter to nitrogen fixa-  
499 tion carbon costs simulated by FUN, these patterns were likely because *G. max*  
500 individuals switched their primary mode of nitrogen acquisition from symbiotic  
501 nitrogen fixation to a non-symbiotic active uptake pathway (Fig. 2.4B).

502 2.4.3 *Study limitations*

503 It should be noted that the metric used in this study to determine carbon  
504 costs to acquire nitrogen has several limitations. Most notably, this metric uses  
505 root carbon biomass as a proxy for estimating the amount of carbon spent on  
506 nitrogen acquisition. While it is true that most carbon allocated belowground has  
507 at least an indirect structural role in acquiring soil resources, it remains unclear  
508 whether this assumption holds true for species that acquire nitrogen via symbi-  
509 otic nitrogen fixation. I also cannot quantify carbon lost through root exudates  
510 or root turnover, which may increase due to factors that increase plant nitrogen  
511 demand (Tingey et al. 2000; Phillips et al. 2011), and can increase the magni-  
512 tude of available nitrogen from soil organic matter through priming effects on soil  
513 microbial communities (Uselman et al. 2000; Bengtson et al. 2012). It is also not  
514 clear whether these assumptions hold under all environmental conditions, such  
515 as those that shift belowground carbon allocation toward a different mode of ni-  
516 trogen acquisition (Taylor and Menge 2018; Friel and Friesen 2019) or between  
517 species with different acquisition strategies. In this study, increasing soil nitrogen  
518 fertilization increased carbon investment to roots relative to carbon transferred  
519 to root nodules (Fig. 2.4B). By assuming that carbon allocated to root carbon  
520 was proportional to carbon allocated to root nodules across all treatment com-

521 binations, these observed responses to soil nitrogen fertilization were likely to be  
522 overestimated in *G. max*. I encourage future research to quantify these carbon  
523 fates independently.

524 Researchers conducting pot experiments must carefully choose pot volume  
525 to minimize the likelihood of growth limitations induced by pot volume (Poorter  
526 et al. 2012). Poorter et al. (2012) indicate that researchers are likely to avoid  
527 growth limitations associated with pot volume if measurements are collected when  
528 the plant biomass:pot volume ratio is less than 1 g L<sup>-1</sup>. In this experiment, all  
529 treatment combinations in both species had biomass:pot volume ratios less than  
530 1 g L<sup>-1</sup> except for *G. max* and *G. hirsutum* that were grown under 0% shade  
531 cover and had received 630 ppm N. Specifically, *G. max* and *G. hirsutum* had  
532 average respective biomass:pot volume ratios of 1.24±0.07 g L<sup>-1</sup> and 1.34±0.13 g  
533 L<sup>-1</sup>, when grown under 0% shade cover and received 630 ppm N (Supplementary  
534 Tables S2, S3; Supplementary Fig. S1). If growth in this treatment combination  
535 was limited by pot volume, then individuals may have had larger carbon costs  
536 to acquire nitrogen than would be expected if they were grown in larger pots.  
537 This pot volume induced growth limitation could cause a reduction in per-root  
538 nitrogen uptake associated with more densely packed roots, which could reduce  
539 the positive effect of nitrogen fertilization on whole-plant nitrogen biomass relative  
540 to root carbon biomass (Poorter et al. 2012).

541 Growth limitation associated with pot volume provides a possible explana-  
542 tion for the marginally insignificant effect of increasing nitrogen fertilization on *G.*  
543 *max* carbon costs to acquire nitrogen when grown under 0% shade cover (Table  
544 2.3; Fig. 2.1). This is because the regression line describing the relationship be-

545 tween carbon costs to acquire nitrogen and nitrogen fertilization in *G. max* grown  
546 under 0% shade cover would have flattened if growth limitation had caused larger  
547 than expected carbon costs to acquire nitrogen in the 0% shade cover, 630 ppm  
548 N treatment combination. This may have been exacerbated by the fact that *G.*  
549 *max* likely shifted relative carbon allocation from nitrogen fixation to soil nitrogen  
550 acquisition, which could have increased the negative effect of more densely packed  
551 roots on nitrogen uptake. These patterns could have also occurred in *G. hirsutum*  
552 grown under 0% shade cover; however, there was no change in the effect of nitro-  
553 gen fertilization on *G. hirsutum* carbon costs to acquire nitrogen grown under 0%  
554 shade cover relative to other shade cover treatments. Regardless, the possibility  
555 of growth limitation due to pot volume suggests that effects of increasing nitro-  
556 gen fertilization on carbon costs to acquire nitrogen in both species grown under  
557 0% shade cover could have been underestimated. Follow-up studies using a simi-  
558 lar experimental design with a larger pot volume would be necessary in order to  
559 determine whether these patterns were impacted by pot volume-induced growth  
560 limitation.

#### 561 2.4.4 *Conclusions*

562 In conclusion, this chapter provides empirical evidence that carbon costs to  
563 acquire nitrogen are influenced by light availability and soil nitrogen fertilization  
564 in a species capable of acquiring nitrogen via symbiotic nitrogen fixation and a  
565 species not capable of forming such associations. We show that carbon costs to  
566 acquire nitrogen generally increase with increasing light availability and decrease  
567 with increasing nitrogen fertilization. This chapter provides important empirical

568 data needed to evaluate the formulation of carbon costs to acquire nitrogen in  
569 terrestrial biosphere models, particularly carbon costs to acquire nitrogen that  
570 are associated with symbiotic nitrogen fixation. My findings broadly support the  
571 general formulation of these carbon costs in the FUN biogeochemical model in  
572 response to shifts in nitrogen availability. However, there is a need for future  
573 studies to explicitly quantify carbon costs to acquire nitrogen under different en-  
574 vironmental contexts, over longer temporal scales, and using larger selections of  
575 phylogenetically related species. In addition, I suggest that future studies mini-  
576 mize the limitations associated with the metric used here by explicitly measuring  
577 belowground carbon fates independently.

578

## Chapter 3

579     Soil nitrogen availability modifies leaf nitrogen economies in mature  
580     temperate deciduous forests: a direct test of photosynthetic least-cost  
581     theory

582     3.1     Introduction

583             Photosynthesis represents the largest carbon flux between the atmosphere  
584     and land surface (IPCC 2021), and plays a central role in biogeochemical cycling  
585     at multiple spatial and temporal scales (Vitousek and Howarth 1991; LeBauer and  
586     Treseder 2008; Kaiser et al. 2015; Wieder et al. 2015). Therefore, carbon and  
587     energy fluxes simulated by terrestrial biosphere models are sensitive to the formu-  
588     lation of photosynthetic processes (Ziehn et al. 2011; Bonan et al. 2011; Booth  
589     et al. 2012; Smith et al. 2016; Smith et al. 2017) and must be represented using  
590     robust, empirically tested processes (Prentice et al. 2015; Wieder et al. 2019).  
591             Current formulations of photosynthesis vary across terrestrial biosphere models  
592     (Smith and Dukes 2013; Rogers et al. 2017), which causes variation in modeled  
593     ecosystem processes (Knorr 2000; Knorr and Heimann 2001; Bonan et al. 2011;  
594     Friedlingstein et al. 2014) and casts uncertainty on the ability of these models to  
595     accurately predict terrestrial ecosystem responses and feedbacks to global change  
596     (Zaehle et al. 2005; Schaefer et al. 2012; Davies-Barnard et al. 2020).

597             Terrestrial biosphere models commonly represent C<sub>3</sub> photosynthesis th-  
598     rough variants of the Farquhar et al. (1980) biochemical model (Smith and Dukes  
599     2013; Rogers 2014; Rogers et al. 2017). This well-tested photosynthesis model  
600     estimates leaf-level carbon assimilation, or photosynthetic capacity, as a function  
601     of the maximum rate of Ribulose-1,5-bisphosphate carboxylase-oxygenase (Ru-

602 bisco) carboxylation ( $V_{cmax}$ ) and the maximum rate of Ribulose-1,5-bisphosphate  
603 (RuBP) regeneration ( $J_{max}$ ) (Farquhar et al. 1980). Many terrestrial biosphere  
604 models predict these model inputs based on plant functional group specific linear  
605 relationships between leaf nutrient content and  $V_{cmax}$  (Smith and Dukes 2013;  
606 Rogers 2014; Rogers et al. 2017) under the tenet that a large fraction of leaf  
607 nutrients, and nitrogen (N) in particular, are partitioned toward building and  
608 maintaining enzymes that support photosynthetic capacity, such as Rubisco (Brix  
609 1971; Gulmon and Chu 1981; Evans 1989; Kattge et al. 2009; Walker et al. 2014).  
610 Terrestrial biosphere models also predict leaf nutrient content from soil nutrient  
611 availability based on the assumption that increasing soil nutrients generally in-  
612 creases leaf nutrients (Firn et al. 2019; Li et al. 2020; Liang et al. 2020) which, in  
613 the case of N, generally corresponds with an increase in photosynthetic processes  
614 (Li et al. 2020; Liang et al. 2020).

615       Recent work calls the generality of relationships between soil nutrient avail-  
616 ability, leaf nutrient content, and photosynthetic capacity into question, suggest-  
617 ing instead that leaf nutrients and photosynthetic capacity are better predicted as  
618 an integrated product of aboveground climate, leaf traits, and soil nutrient avail-  
619 ability, rather than soil nutrient availability alone (Dong et al. 2017; Dong et al.  
620 2020; Dong et al. 2022; Firn et al. 2019; Smith et al. 2019; Peng et al. 2021).  
621 It has been reasoned that this result is because plants allocate added nutrients to  
622 growth and storage rather than alterations in leaf chemistry (Smith et al. 2019),  
623 perhaps as a result of nutrient limitation of primary productivity (LeBauer and  
624 Treseder 2008; Fay et al. 2015). Additionally, recent work suggests that relation-  
625 ships between leaf nutrient content and photosynthesis vary across environments,

626 and that the proportion of leaf nutrient content allocated to photosynthetic tis-  
627 sue varies over space and time with plant acclimation and adaptation responses  
628 to light availability, vapor pressure deficit, soil pH, soil nutrient availability, and  
629 environmental factors that influence leaf mass per area (Pons and Pearcy 1994;  
630 Niinemets and Tenhunen 1997; Evans and Poorter 2001; Hikosaka and Shigeno  
631 2009; Ghimire et al. 2017; Onoda et al. 2017; Luo et al. 2021). The use of linear  
632 relationships between leaf nutrient content and Vcmax to predict photosynthetic  
633 capacity, as commonly used in terrestrial biosphere models (Rogers 2014), is not  
634 capable of detecting such responses.

635 Photosynthetic least-cost theory provides an alternative framework for un-  
636 derstanding relationships between soil nutrient availability, leaf nutrient content,  
637 and photosynthetic capacity (Harrison et al. 2021). Leveraging a two-input mi-  
638 croeconomics approach (Wright et al. 2003), the theory posits that plants accli-  
639 mate to a given environment by optimizing leaf photosynthesis rates at the lowest  
640 summed cost of using nutrients and water (Prentice et al. 2014; Wang et al. 2017;  
641 Smith et al. 2019; Paillassa et al. 2020). Across resource availability gradients,  
642 the theory predicts that optimal photosynthetic rates can be achieved by trading  
643 less efficient use of a resource that is less costly to acquire (or more abundant)  
644 for more efficient use of a resource more costly to acquire (or less abundant). For  
645 example, an increase in soil nutrient availability should reduce the cost of acquir-  
646 ing and using nutrients (Bae et al. 2015; Eastman et al. 2021; Perkowski et al.  
647 2021), which could increase leaf nutrient investments in photosynthetic proteins to  
648 allow similar photosynthetic rates to be achieved with higher nutrient use (lower  
649 nutrient use efficiency) but lower water use (greater water use efficiency). The

650 theory suggests similar tradeoffs in response to increasing soil pH (Paillassa et al.  
651 2020), specifically, that increasing soil pH should reduce the cost of acquiring soil  
652 nutrients due to an increase in plant-available nutrient concentration (Paillassa  
653 et al. 2020; Dong et al. 2022). The theory is also capable of reconciling dynamic  
654 leaf nutrient-photosynthesis relationships at global scales (Luo et al. 2021).

655 Patterns expected from photosynthetic least-cost theory have recently re-  
656 ceived empirical support both in global environmental gradient (Smith et al.  
657 2019; Paillassa et al. 2020; Luo et al. 2021; Querejeta et al. 2022; Wester-  
658 band et al. 2023) and local manipulative invasion (Bialic-Murphy et al. 2021)  
659 studies. However, nutrient addition experiments that directly examine nutrient-  
660 water use tradeoffs expected from the theory are rare (Guerrieri et al. 2011), and  
661 only global gradient studies testing the theory have considered soil pH in their  
662 analyses. As a result, there is a need to use nutrient addition and soil pH manu-  
663 lation experiments to test mechanisms driving responses predicted by the theory.  
664 Such experiments would also be useful to detect whether patterns expected from  
665 theory translate to finer spatial scales.

666 In this study, we measured leaf responses to soil N availability in five decid-  
667 uous tree species growing in the upper canopy of mature closed canopy temperate  
668 forests in the northeastern United States. Soil N availability and pH were manipu-  
669 lated through an N-by-pH field manipulation experiment with treatments applied  
670 since 2011, eight years prior to measurement. Two different soil N treatments  
671 were applied to increase N availability with opposing effects on soil pH. An addi-  
672 tional N-free acidifying treatment was expected to decrease soil pH. I hypothesized  
673 that increased soil N availability would enable plants to increase nutrient uptake

**674** and create more photosynthetic enzymes per leaf, allowing similar photosynthetic  
**675** rates achieved with lower leaf C<sub>i</sub>:C<sub>a</sub> and increased leaf N content allocated to  
**676** photosynthetic leaf tissue. I expected that this response would be driven by a  
**677** reduction in the cost of acquiring N, which would cause trees to sacrifice efficient  
**678** N use to enable more efficient use of other limiting resources (i.e., water). Finally,  
**679** I hypothesized similar leaf responses to increasing soil pH.

**680** 3.2 Methods

**681** 3.2.1 *Study site description*

**682** We conducted this study in summer 2019 at three stands located within  
**683** a 20-km radius of Ithaca, NY, USA (42.444 °N, 76.502 °W). All stands contain  
**684** mature, closed-canopy forests dominated by deciduous tree species. Stands con-  
**685** tained abundant sugar maple (*Acer saccharum* Marshall), American beech (*Fagus*  
**686** *grandifolia* Ehrh.), and white ash (*Fraxinus americana* L.), accounting for 43%,  
**687** 15%, and 17% of the total aboveground biomass across the three stands, respec-  
**688** tively, with less frequent red maple (*Acer rubrum* L.; 9% of total aboveground  
**689** biomass) and red oak occurrences (*Quercus rubra* L.; 10% of total aboveground  
**690** biomass). Soils at each site were broadly classified as a channery silt loam Incep-  
**691** tisols using the USDA NRCS Web Soil Survey data product (Soil Survey Staff  
**692** 2022). Between 2006 and 2020, study sites averaged 972 mm of precipitation per  
**693** year and had an average temperature of 7.9 °C per a weather station located near  
**694** the Cornell University campus (42.449 °N, 76.449 °W) part of the NOAA NCEI  
**695** Global Historical Climatology Network (Menne et al. 2012).

**696** 3.2.2 *Experimental design*

**697** Four 40 m x 40 m plots were set up at each site in 2009, each with an  
**698** additional 10 m buffer along plot perimeters (60 m x 60 m total). The plots  
**699** were set up as a nitrogen-by-pH field manipulation experiment, with one each of  
**700** four treatments at each site. Two nitrogen treatments were applied, both at 50  
**701** kg N ha<sup>-1</sup> yr<sup>-1</sup>, as either sodium nitrate (NaNO<sub>3</sub>) to raise soil pH, or ammonium  
**702** sulfate ((NH<sub>4</sub>)<sub>2</sub>SO<sub>4</sub>) to acidify; an elemental sulfur treatment was selected to acid-  
**703** ify without N, applied at the same rate of S addition (57 kg S ha<sup>-1</sup> yr<sup>-1</sup>); and  
**704** control plots received no additions. All amendments were added in pelletized form  
**705** using hand-held fertilizer spreaders to both the main plots and buffers. Amend-  
**706** ments were divided into three equal doses distributed across the growing season  
**707** from 2011-2017 and added as a single dose from 2018 onward. During 2019, plots  
**708** were fertilized during the week of May 20.

**709** 3.2.3 *Leaf gas exchange and trait measurements*

**710** We sampled one leaf each from 6 to 10 individuals per plot between June  
**711** 25 and July 12, 2019 for gas exchange measurements (Table S1). Leaves were  
**712** collected from deciduous broadleaf trees represented across all sites and plots  
**713** and were replicated in efforts to mimic the species abundance of each plot at  
**714** each site. We also attempted to collect leaves from the upper canopy to reduce  
**715** differential shading effects on leaf physiology. Leaves were accessed by pulling  
**716** down small branches using an arborist's slingshot and weighted beanbag attached  
**717** to a throw line. Branches were immediately recut under deionized water and  
**718** remained submerged to reduce stomatal closure and avoid xylem embolism (as in

719 Smith & Dukes, 2018) until gas exchange data were collected.

720 Randomly selected leaves with little to no visible external damage were  
721 attached to a Li-COR LI-6800 (Li-COR Bioscience, Lincoln, Nebraska, USA)  
722 portable photosynthesis machine to measure net photosynthesis ( $A_{\text{net}}$ ;  $\mu\text{mol m}^{-2}$   
723  $\text{s}^{-1}$ ), stomatal conductance ( $g_{\text{sw}}$ ;  $\text{mol m}^{-2} \text{s}^{-1}$ ), and intercellular  $\text{CO}_2$  concentra-  
724 tion ( $C_i$ ;  $\mu\text{mol mol}^{-1}$ ) at different reference  $\text{CO}_2$  concentrations ( $C_a$ ;  $\mu\text{mol mol}^{-1}$ )  
725 concentrations (i.e., an  $A_{\text{net}}/C_i$  curve) under saturating light conditions (2,000  
726  $\mu\text{mol m}^{-2} \text{s}^{-1}$ ). Reference  $\text{CO}_2$  concentrations followed the sequence: 400, 300,  
727 200, 100, 50, 400, 400, 600, 800, 1000, 1200, 1500, and 2000  $\mu\text{mol mol}^{-1} \text{CO}_2$ . Leaf  
728 temperatures were not controlled in the cuvette and ranged from 21.8 °C to 31.7  
729 °C (mean±SD:  $27.2 \pm 2.2$  °C). A linear and second order log-polynomial nonlinear  
730 regression suggested no effect of temperature on stomatal conductance measured  
731 at 400  $\mu\text{mol mol}^{-1} \text{CO}_2$  or net photosynthesis measured at  $\mu\text{mol mol}^{-1} \text{CO}_2$  (Ta-  
732 ble S2-3; Fig. S1). All  $A_{\text{net}}/C_i$  curves were generated within one hour of branch  
733 severance.

734 Leaf morphological and chemical traits were collected on the same leaf used  
735 to generate each  $A_{\text{net}}/C_i$  curve. Images of each leaf were taken using a flat-bed  
736 scanner to determine fresh leaf area using the ‘LeafArea’ R package (Katabuchi  
737 2015), which automates leaf area calculations using ImageJ software (Schneider  
738 et al. 2012). Each leaf was dried at 65°C for at least 48 hours, weighed, and  
739 ground using a Retsch MM200 ball mill grinder (Verder Scientific, Inc., Newtown,  
740 PA, USA) until homogenized. Leaf mass per area ( $M_{\text{area}}$ ,  $\text{g m}^{-2}$ ) was calculated  
741 as the ratio of dry leaf biomass to fresh leaf area. Using a subsample of ground and  
742 homogenized leaf biomass, leaf N content ( $N_{\text{mass}}$ ;  $\text{gN g}^{-1}$ ) and leaf  $\delta^{13}\text{C}$  (‰, rela-

743 tive to VPDB) were measured at the Cornell Stable Isotope Lab with an elemental  
 744 analyzer (NC 2500, CE Instruments, Wigan, UK) interfaced to an isotope ratio  
 745 mass spectrometer (Delta V Isotope Ratio Mass Spectrometer, ThermoFisher Sci-  
 746 entific, Waltham, MA, USA). Leaf N content per unit leaf area ( $N_{\text{area}}$ ; gN m<sup>-2</sup>)  
 747 was calculated by multiplying  $N_{\text{mass}}$  by  $M_{\text{area}}$ .

748 We used leaf  $\delta^{13}\text{C}$  values to estimate  $\chi$  (unitless), which is an isotope-  
 749 derived estimate of the leaf  $C_i:C_a$  ratio. While intercellular and atmospheric CO<sub>2</sub>  
 750 concentrations were directly measured during each  $A_{\text{net}}/C_i$  curve, deriving  $\chi$  from  
 751  $\delta^{13}\text{C}$  provides a more integrative estimate of the  $C_i:C_a$  over an individual leaf's  
 752 lifespan. We derived  $\chi$  following the approach of Farquhar et al. (1989) described  
 753 in Cernusak et al. (2013):

$$\chi = \frac{\Delta^{13}C - a}{b - a} \quad (3.1)$$

754 where  $\Delta^{13}\text{C}$  represents the relative difference between leaf  $\delta^{13}\text{C}$  (‰) and air  $\delta^{13}\text{C}$   
 755 (‰), and is calculated from the following equation:

$$\Delta^{13}C = \frac{\delta^{13}C_{\text{air}} - \delta^{13}C_{\text{leaf}}}{1 + \delta^{13}C_{\text{leaf}}} \quad (3.2)$$

756 where  $\delta^{13}C_{\text{air}}$  is assumed to be -8‰ (Keeling et al. 1979; Farquhar et al. 1989), a  
 757 represents the fractionation between <sup>12</sup>C and <sup>13</sup>C due to diffusion in air, assumed  
 758 to be 4.4‰, and b represents the fractionation caused by Rubisco carboxylation,  
 759 assumed to be 27‰ (Farquhar et al. 1989).

**760** 3.2.4  $A_{\text{net}}/C_i$  curve-fitting and parameter estimation

**761** We fit  $A_{\text{net}}/C_i$  curves of each individual using the ‘fitaci’ function in the  
**762** ‘plantecophys’ R package (Duursma 2015). This function estimates the maxi-  
**763** mum rate of Rubisco carboxylation ( $V_{\text{cmax}}$ ;  $\mu\text{mol m}^{-2} \text{s}^{-1}$ ) and maximum rate  
**764** of electron transport for RuBP regeneration ( $J_{\text{max}}$ ;  $\mu\text{mol m}^{-2} \text{s}^{-1}$ ) based on the  
**765** Farquhar, von Caemmerer, and Berry biochemical model of C<sub>3</sub> photosynthesis  
**766** (Farquhar et al. 1980). For each curve fit, we included triose phosphate uti-  
**767** lization (TPU) limitation to avoid underestimating  $J_{\text{max}}$  (Gregory et al. 2021).  
**768** Curves were visually examined to confirm the likely presence of TPU limitation.

**769** We determined Michaelis-Menten coefficients for Rubisco affinity to CO<sub>2</sub>  
**770** ( $K_c$ ;  $\mu\text{mol mol}^{-1}$ ) and O<sub>2</sub> ( $K_o$ ;  $\mu\text{mol mol}^{-1}$ ), and the CO<sub>2</sub> compensation point  
**771** ( $\Gamma^*$ ;  $\mu\text{mol mol}^{-1}$ ) using leaf temperature and equations described in Medlyn et al.  
**772** (2002) and derived in Bernacchi et al. (2001). Specifically,  $K_c$  and  $K_o$  were  
**773** calculated as:

$$K_c = 404.9 * \exp^{\frac{79430(T_k - 298)}{298RT_k}} \quad (3.3)$$

**774** and

$$K_o = 278.4 * \exp^{\frac{36380(T_k - 298)}{298RT_k}} \quad (3.4)$$

**775** while  $\Gamma^*$  was calculated as:

$$\Gamma^* = 42.75 * \exp^{\frac{37830(T_k - 298)}{298RT_k}} \quad (3.5)$$

**776** In all three equations,  $T_k$  is the leaf temperature (in Kelvin) during each  $A_{\text{net}}/C_i$

**777** curve and R is the universal gas constant ( $8.314 \text{ J mol}^{-1} \text{ K}^{-1}$ ).

**778** We standardized  $V_{\text{cmax}}$  and  $J_{\text{max}}$  estimates to  $25^\circ\text{C}$  using a modified Ar-

**779** rhenius equation (Kattge and Knorr 2007):

$$k_{25} = \frac{k_{\text{obs}}}{e^{\frac{H_a(T_{\text{obs}} - T_{\text{ref}})}{T_{\text{ref}}RT_{\text{obs}}}} * \frac{1+e^{\frac{T_{\text{ref}}\Delta S - H_d}{T_{\text{obs}}}}}{1+e^{\frac{T_{\text{obs}}\Delta S - H_d}{T_{\text{obs}}}}}} \quad (3.6)$$

**780**  $k_{25}$  represents the standardized  $V_{\text{cmax}}$  or  $J_{\text{max}}$  rate at  $25^\circ\text{C}$ ,  $k_{\text{obs}}$  represents

**781** the  $V_{\text{cmax}}$  or  $J_{\text{max}}$  estimate at the average leaf temperature measured inside the

**782** cuvette during the  $A_{\text{net}}/C_i$  curve.  $H_a$  is the activation energy of  $V_{\text{cmax}}$  ( $71,513$

**783**  $\text{J mol}^{-1}$ ) Kattge and Knorr (2007) or  $J_{\text{max}}$  ( $49,884 \text{ J mol}^{-1}$ ) (Kattge and Knorr

**784** 2007).  $H_d$  represents the deactivation energy of both  $V_{\text{cmax}}$  and  $J_{\text{max}}$  ( $200,000 \text{ J}$

**785**  $\text{mol}^{-1}$ ) (Medlyn et al. 2002), and R represents the universal gas constant ( $8.314$

**786**  $\text{J mol}^{-1} \text{ K}^{-1}$ ).  $T_{\text{ref}}$  represents the standardized temperature of  $298.15 \text{ K}$  ( $25^\circ\text{C}$ )

**787** and  $T_{\text{obs}}$  represents the mean leaf temperature (in K) during each  $A_{\text{net}}/C_i$  curve.

**788**  $\Delta S$  is an entropy term that (Kattge and Knorr 2007) derived as a linear relation-

**789** ship with average growing season temperature ( $T_g$ ;  $^\circ\text{C}$ ), where:

$$\Delta S_{v_{\text{cmax}}} = -1.07 T_g + 668.39 \quad (3.7)$$

**790** and

$$\Delta S_{j_{\text{max}}} = -0.75 T_g + 659.70 \quad (3.8)$$

**791** We estimated  $T_g$  in Equations 3.7 and 3.8 based on mean daily (24-hour) air  
**792** temperature of the 30 days leading up to the day of each sample collection using  
**793** the same weather station reported in the site description. We then used  $V_{cmax25}$   
**794** and  $J_{max25}$  estimates to calculate the ratio of  $J_{max25}$  to  $V_{cmax25}$  ( $J_{max25}:V_{cmax25}$ ;  
**795** unitless).

**796** 3.2.5 *Proportion of leaf nitrogen allocated to photosynthesis and structure*

**797** We used equations from Niinemets and Tenhunen (1997) to estimate the  
**798** proportion of leaf N content allocated to Rubisco and bioenergetics. The propor-  
**799** tion of leaf N allocated to Rubisco ( $\rho_{rub}$ ; gN gN $^{-1}$ ) was calculated as a function  
**800** of  $V_{cmax25}$  and  $N_{area}$ :

$$\rho_{rubisco} = \frac{V_{cmax25} N_r}{V_{cr} N_{area}} \quad (3.9)$$

**801** where  $N_r$  is the amount of nitrogen in Rubisco, set to 0.16 gN (gN in Rubisco) $^{-1}$   
**802** and  $V_{cr}$  is the maximum rate of RuBP carboxylation per unit Rubisco protein,  
**803** set to 20.5  $\mu$ mol CO $_2$  (g Rubisco) $^{-1}$ . The proportion of leaf nitrogen allocated to  
**804** bioenergetics ( $\rho_{bioe}$ ; gN gN $^{-1}$ ) was similarly calculated as a function of  $J_{max25}$  and  
**805**  $N_{area}$ :

$$\rho_{bioe} = \frac{J_{max25} N_b}{J_{mc} N_{area}} \quad (3.10)$$

**806** where  $N_b$  is the amount of nitrogen in cytochrome f, set to 0.12407 gN ( $\mu$ mol  
**807** cytochrome f) $^{-1}$  assuming a constant 1: 1: 1.2 cytochrome f: ferredoxin NADP  
**808** reductase: coupling factor molar ratio (Evans and Seemann 1989; Niinemets and

809 Tenhunen 1997), and  $J_{mc}$  is the capacity of electron transport per cytochrome f,  
810 set to  $156 \mu\text{mol electron} (\mu\text{mol cytochrome f})^{-1}\text{s}^{-1}$ .

811 We estimated the proportion of leaf N content allocated to photosynthetic  
812 tissue ( $\rho_{photo}$ ;  $\text{gN gN}^{-1}$ ) as the sum of  $\rho_{rub}$  and  $\rho_{bioe}$ . This calculation is an un-  
813 derestimate of the proportion of leaf N allocated to photosynthetic tissue because  
814 it does not include N allocated to light harvesting proteins. This leaf N pool was  
815 not included because we did not perform chlorophyll extractions on focal leaves.  
816 However, the proportion of leaf N content allocated to light harvesting proteins  
817 tends to be small relative to  $\rho_{rub}$  and  $\rho_{bioe}$ , and may scale with changes in  $\rho_{rub}$   
818 and  $\rho_{bioe}$  (Niinemets and Tenhunen 1997).

819 Finally, we estimated the proportion of leaf N content allocated to struc-  
820 tural tissue ( $\rho_{str}$ ;  $\text{gN gN}^{-1}$ ) using an empirical equation from Onoda et al. (2017):

$$N_{cw} = 0.000355 * M_{area}^{1.39} \quad (3.11)$$

821 where  $N_{cw}$  is the leaf N content allocated to cell walls ( $\text{gN m}^{-2}$ ).  $\rho_{str}$  was estimated  
822 by dividing  $N_{cw}$  by  $N_{area}$ .

### 823 3.2.6 *Tradeoffs between nitrogen and water use*

824 Photosynthetic nitrogen use efficiency (PNUE;  $\mu\text{mol CO}_2 \text{ mol}^{-1} \text{ N s}^{-1}$ )  
825 was calculated by dividing  $A_{net}$  by  $N_{area}$ , first converting  $N_{area}$  to  $\text{mol N m}^{-2}$   
826 using the molar mass of N ( $14 \text{ g mol}^{-1}$ ). We used  $\chi$  as an indicator of water  
827 use efficiency, which exploratory analyses suggest had similar responses to soil N  
828 availability and pH as intrinsic water use efficiency measured from gas exchange

829 ( $A_{\text{net}}/g_s$ ). Tradeoffs between nitrogen and water use were determined by cal-  
830 culating the ratio of  $N_{\text{area}}$  to  $\chi$  ( $N_{\text{area}}:\chi$ ; g N m<sup>-2</sup>) and  $V_{\text{cmax25}}$  to  $\chi$  ( $V_{\text{cmax25}}:\chi$ ;  
831  $\mu\text{mol m}^{-2} \text{s}^{-1}$ ). This approach is similar to tradeoff calculations in which nitrogen-  
832 water use tradeoffs are measured as the ratio of  $N_{\text{area}}$  or  $V_{\text{cmax25}}$  to  $g_s$  (Paillassa  
833 et al. 2020; Bialic-Murphy et al. 2021). In this study, we quantify these re-  
834 lationships using  $\chi$  in lieu of  $g_s$  because  $g_s$  rapidly changes with environmental  
835 conditions and therefore may have been altered by recent tree branch severance  
836 and/or placement in the cuvette.

837 3.2.7 *Soil nitrogen availability and pH*

838 To characterize soil N availability at the time of our leaf gas exchange  
839 measurements, we used mixed bed resin bags to quantify mobile ammonium-N  
840 and nitrate-N concentrations in each plot. Lycra mesh bags were filled with 5 g  
841 of Dowex® Marathon MR-3 hydrogen and hydroxide form resin (MilliporeSigma,  
842 Burlington, MA USA) and sealed with a zip tie. Each bag was activated by  
843 soaking in 0.5 M HCl for 20 minutes, then in 2 M NaCl until pH of the saline  
844 solution stabilized, as described in Allison et al. (2008). Five resin bags were  
845 inserted about 10 cm below the soil surface at each plot on June 25, 2019: one  
846 near each of the four plot corners and one near the plot center. All resin bags  
847 were collected 24 days later on July 19, 2019 and were frozen until extracted.

848 Prior to anion and cation extraction, each resin bag was rinsed with ul-  
849 trapure water (MilliQ IQ 7000; Millipore Sigma, Burlington, MA) to remove any  
850 surface soil residues. Anions and cations were extracted from surface-cleaned resin  
851 bags by individually soaking and shaking each bag in 100 mL of a 0.1 M HCl/2.0

852 M NaCl matrix for one hour. Using a microplate reader (Biotek Synergy H1;  
853 Biotek Instruments, Winooski, VT USA), nitrate-N concentrations were quanti-  
854 fied spectrophotometrically at 540 nm with the end product of a single reagent  
855 vanadium (III) chloride reaction (Doane and Horwáth 2003), and ammonium-N  
856 concentrations quantified at 650 nm with the end product of a modified phenol-  
857 hypochlorite reaction (Weatherburn 1967; Rhine et al. 1998). Both the single  
858 reagent vanadium (III) chloride and modified phenol-hypochlorite methodologies  
859 have been well established for determining nitrate-N and ammonium-N concen-  
860 trations in resin bag extracts (Arnone 1997; Allison et al. 2008). We used a  
861 series of negative and positive controls throughout each well plate to verify the  
862 accuracy and precision of our measurements, assaying each resin bag extract and  
863 control in triplicate. Soil N availability was estimated as the sum of the nitrate-N  
864 and ammonium-N concentration in each resin bag, normalized per g of resin and  
865 duration in the field ( $\mu\text{g N g}^{-1} \text{ resin d}^{-1}$ ), then subsequently averaged across all  
866 resin bags in a plot for a plot-level mean.

867 Soil pH was measured on 0-10 cm mineral soil samples collected prior to  
868 fertilization in 2019. Near each of the four plot corners, three 5.5 cm diameter soil  
869 cores were collected after first removing the forest floor where present. Each set  
870 of three cores was placed in a plastic bag, and later composited by hand mixing  
871 and sieved to 4mm. Soil pH was determined for a 1:2 soil:water slurry (10 g field-  
872 moist soil to 20 mL DI water) of each sample using an Accumet AB15 pH meter  
873 with flushable junction probe (Fisher Scientific; Hampton, NH, USA), and was  
874 estimated at the plot level as the mean soil pH within each plot.

**875** 3.2.8 *Statistical analyses*

**876** We built two separate series of linear mixed-effects models to explore effects  
**877** of soil N availability, soil pH, species, and leaf N content on leaf physiological  
**878** traits. In the first series of linear mixed-effects models, we explored the effect  
**879** of soil N availability, soil pH, and species on leaf N content, leaf photosynthesis,  
**880** stomatal conductance, and nitrogen-water use tradeoffs. Models included plot-  
**881** level soil N availability and plot-level soil pH as continuous fixed effects, species  
**882** as a categorical fixed effect, and site as a categorical random intercept term.  
**883** Interaction terms between fixed effects were not included due to the small number  
**884** of experimental plots. We built a series of separate models with this independent  
**885** variable structure to quantify individual effects of soil N availability, soil pH,  
**886** and species on  $N_{\text{area}}$ ,  $M_{\text{area}}$ ,  $N_{\text{mass}}$ ,  $A_{\text{net}}$ ,  $V_{\text{cmax25}}$ ,  $J_{\text{max25}}$ ,  $J_{\text{max25}}:V_{\text{cmax25}}$ ,  $\rho_{\text{rubisco}}$ ,  
**887**  $\rho_{\text{bioenergetics}}$ ,  $\rho_{\text{photo}}$ ,  $\rho_{\text{structure}}$ ,  $\chi$ , PNUE,  $N_{\text{area}}:\chi$ , and  $V_{\text{cmax25}}:\chi$ .

**888** A second series of linear mixed-effects models were built to investigate  
**889** relationships between leaf N content and photosynthetic parameters. Statistical  
**890** models included  $N_{\text{area}}$  as a single continuous fixed effect with species and site des-  
**891** ignated as individual random intercept terms. We used this independent variable  
**892** structure to quantify individual effects of leaf N content on  $A_{\text{net}}$ ,  $V_{\text{cmax25}}$ ,  $J_{\text{max25}}$ ,  
**893**  $J_{\text{max25}}:V_{\text{cmax25}}$ , and  $\chi$ .

**894** For all linear mixed-effects models, we used Shapiro-Wilk tests of normal-  
**895** ity to determine whether linear mixed-effects models satisfied residual normality  
**896** assumptions. If residual normality assumptions were not met, then models were  
**897** fit using dependent variables that were natural log transformed. If residual nor-  
**898** mality assumptions were still not met (Shapiro-Wilk:  $p < 0.05$ ), then models were

899 fit using dependent variables that were square root transformed. All residual nor-  
900 mality assumptions for both sets of models that did not originally satisfy residual  
901 normality assumptions were met with either a natural log or square root data  
902 transformation (Shapiro-Wilk:  $p > 0.05$  in all cases).

903 In the first series of models, models for  $N_{\text{area}}$ ,  $M_{\text{area}}$ ,  $N_{\text{mass}}$ ,  $V_{\text{cmax25}}$ ,  $J_{\text{max25}}$ ,  
904  $\chi$ ,  $N_{\text{area}}:\chi$ , and  $V_{\text{cmax25}}:\chi$ ,  $\rho_{\text{rubisco}}$ ,  $\rho_{\text{bioenergetics}}$ ,  $\rho_{\text{photo}}$ ,  $\rho_{\text{structure}}$  satisfied residual  
905 normality assumptions without data transformations (Shapiro-Wilk:  $p > 0.05$  in  
906 all cases). The model for  $J_{\text{max25}}:V_{\text{cmax25}}$  satisfied residual normality assumptions  
907 with a natural log data transformation, while models for  $A_{\text{net}}$  and PNUE each  
908 satisfied residual normality assumptions with square root data transformations.  
909 In the second series of models, models for  $V_{\text{cmax25}}$ ,  $J_{\text{max25}}$ ,  $\chi$ , and  $V_{\text{cmax25}}:\chi$  satisfied  
910 residual normality assumptions without data transformations (Shapiro-Wilk:  $p$   
911  $> 0.05$  in all cases). The model for  $J_{\text{max25}}:V_{\text{cmax25}}$  required a natural log data  
912 transformation and the model for  $A_{\text{net}}$  required a square root data transformation  
913 (Shapiro-Wilk:  $p > 0.05$  in both cases).

914 In all models, we used the ‘lmer’ function in the ‘lme4’ R package (Bates  
915 et al. 2015) to fit each model and the ‘Anova’ function in the ‘car’ R package (Fox  
916 and Weisberg 2019) to calculate Type II Wald’s  $\chi^2$  and determine the significance  
917 level ( $\alpha = 0.05$ ) of each fixed effect coefficient. Finally, we used the ‘emmeans’  
918 R package (Lenth, 2019) to conduct post-hoc comparisons using Tukey’s tests,  
919 where degrees of freedom were approximated using the Kenward-Roger approach  
920 (Kenward and Roger 1997). All analyses and plots were conducted in R version  
921 4.1.1 (R Core Team 2021). All figure regression lines and associated 95% confi-  
922 dence interval error bars were plotted using predictions generated across the soil

**923** nitrogen availability gradient using the ‘emmeans’ R package (Lenth 2019).

**924** 3.3 Results

**925** 3.3.1 *Leaf N content*

**926** Increasing soil N availability generally increased  $N_{\text{area}}$  (Table 3.1; Fig.  
**927** 3.1a). This pattern was driven by an increase in  $N_{\text{mass}}$  (Table 3.1; Fig. 3.1c)  
**928** and a marginal increase in  $M_{\text{area}}$  (Table 3.1; Fig. 3.1e) with increasing soil N  
**929** availability. There was no effect of soil pH on  $N_{\text{area}}$ ,  $N_{\text{mass}}$ , or  $M_{\text{area}}$  (Table 3.1);  
**930** however, we did observe strong differences in  $N_{\text{area}}$  (Fig. 3.1b),  $N_{\text{mass}}$  (Fig. 3.1d),  
**931** and  $M_{\text{area}}$  (Fig. 3.1e) between species (Table 3.1).

**Table 3.1.** Effects of soil N availability, soil pH, and species on leaf N content per unit leaf area ( $N_{\text{area}}$ ), leaf N content per unit leaf mass ( $N_{\text{mass}}$ ), and leaf mass per unit leaf area ( $M_{\text{area}}$ )

	$N_{\text{area}}$			$N_{\text{mass}}$			$M_{\text{area}}$			
	df	Coefficient	$\chi^2$	p	Coefficient	$\chi^2$	p	Coefficient	$\chi^2$	p
Intercept	-	9.03E-01	-	-	1.68E+00	-	-	4.60E+01	-	-
Soil N	1	1.68E-02	11.990	<b>0.001</b>	1.25E-02	6.902	<b>0.009</b>	4.87E-01	4.143	<b>0.042</b>
Soil pH	1	9.28E-02	0.836	0.361	8.08E-02	0.663	0.415	4.05E+00	0.653	0.419
Species	4	-	72.128	<b>&lt;0.001</b>	-	35.074	<b>&lt;0.001</b>	-	29.869	<b>&lt;0.001</b>

932 \*Significance determined using Type II Wald  $\chi^2$  tests ( $\alpha = 0.05$ ). P-values  $< 0.05$  are in bold.

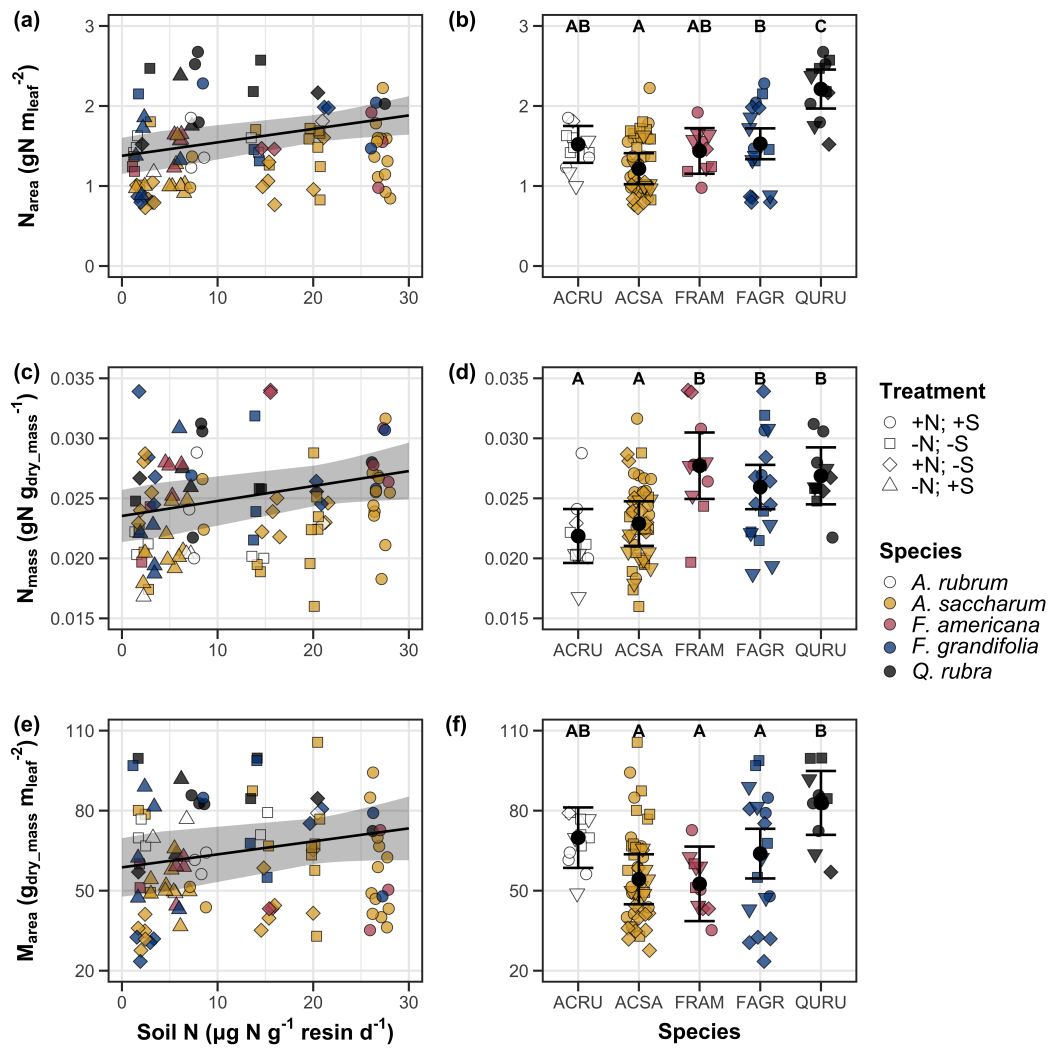


**Figure 3.1.** Effects of soil N availability and species on leaf N content per unit leaf area (a-b), leaf nitrogen content per unit leaf biomass (c-d), and leaf mass per leaf area (e-f). Soil N availability is represented on the x-axis in the left column of panels, while species is represented on the x-axis in the right column of panels. Tree species are represented as colored points and treatment plots are represented as shaped points, jittered for visibility. Species are abbreviated in the right column of panels through their assigned NRCS PLANTS Database symbol (USDA NRCS 2022), grouped along the x-axis per common mycorrhizal association, where the first three species commonly associate with arbuscular mycorrhizae (ACRU, ASCA, FAGR) and the second two species with ectomycorrhizae (FAGR, QURU). Trendlines are only included when the regression slope is statistically different from zero ( $p < 0.05$ ).

**933** 3.3.2 *Net photosynthesis and leaf biochemistry*

**934** Increasing soil N availability generally had no effect on  $A_{\text{net}}$ ,  $V_{\text{cmax25}}$ ,  $J_{\text{max25}}$ ,  
**935** or  $J_{\text{max25}}:V_{\text{cmax25}}$  (Table 3.2, Figs. 3.2a, 3.2d, 3.2g). We also observed strong  
**936** species effects on all measured leaf photosynthetic traits (Table 3.2; Figs. 3.2b,  
**937** 3.2e, 3.2h). Increasing soil pH had a marginal negative effect on  $A_{\text{net}}$ , but had no  
**938** effect on  $V_{\text{cmax25}}$ ,  $J_{\text{max25}}$ , or  $J_{\text{max25}}:V_{\text{cmax25}}$  (Table 3.2). There was a weak positive  
**939** effect of increasing  $N_{\text{area}}$  on  $A_{\text{net}}$  (Fig. 3.2c), but quite strong positive effects of  
**940** increasing  $N_{\text{area}}$  on  $V_{\text{cmax25}}$  and  $J_{\text{max25}}$  (Table 3.2; Fig. 3.2f and 3.2i).

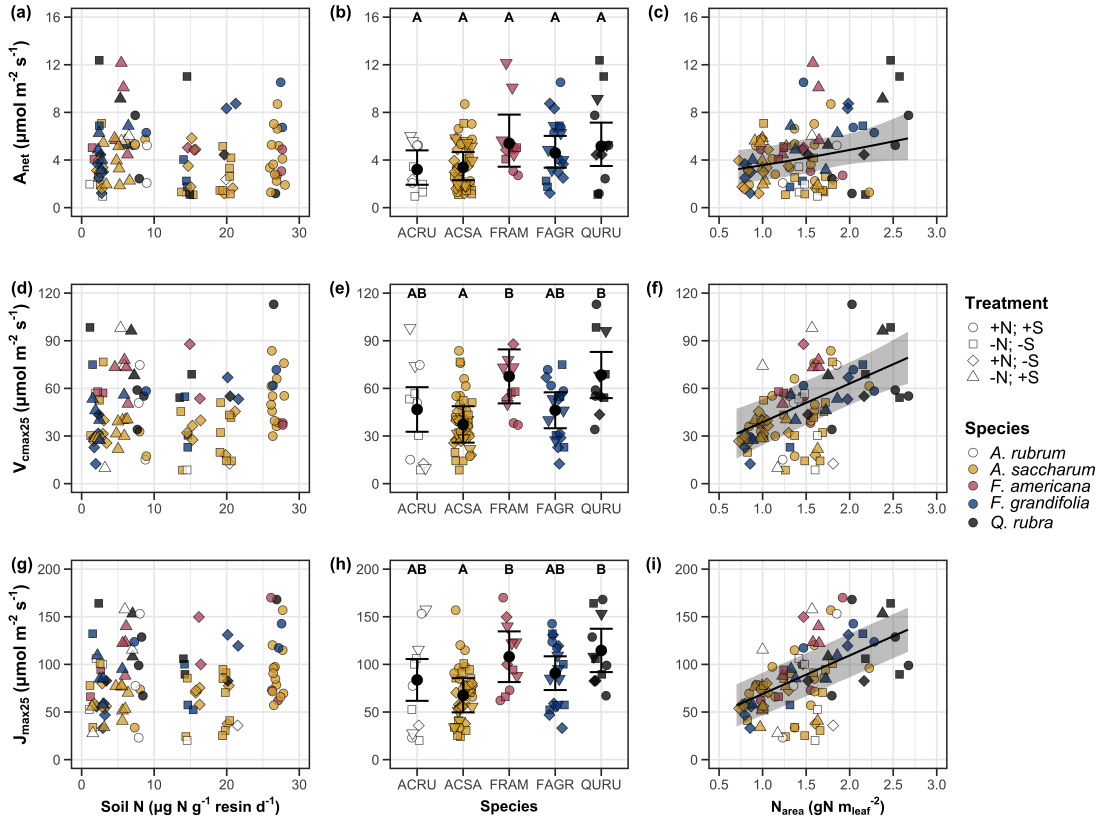
**Table 3.2.** Effects of soil N availability, soil pH, species, and  $N_{\text{area}}$  on leaf biochemistry

	$A_{\text{net}}$			$V_{\text{cmax25}}$			$J_{\text{max25}}$			
	df	Coefficient	$\chi^2$	p	Coefficient	$\chi^2$	p	Coefficient	$\chi^2$	p
(Intercept)	-	3.29E+00 <sup>b</sup>	-	-	6.38E+01	-	-	1.12E+02	-	-
Soil N	1	-1.23E-03 <sup>b</sup>	1.798	0.180	-3.84E-01	1.745	0.187	-6.70E-01	2.172	0.141
Soil pH	1	-3.09E-01 <sup>b</sup>	3.312	0.069	-4.91E+00	0.655	0.418	-8.18E+00	0.742	0.389
Species	4	-	11.838	<b>0.019</b>	-	31.748	<0.001	-	27.291	<0.001
( $N_{\text{area}}$ int.)	-	6.59E-01 <sup>b</sup>	-	-	1.45E-01	-	-	2.86E+01	-	-
$N_{\text{area}}$	4	3.13E-01 <sup>b</sup>	4.790	<b>0.029</b>	2.43E+01	22.616	<0.001	4.04E+01	28.259	<0.001

	$J_{\text{max25}}:V_{\text{cmax25}}$			
	df	Coefficient	$\chi^2$	p
(Intercept)	-	6.59E-01 <sup>a</sup>	-	-
Soil N	1	7.04E-04 <sup>a</sup>	0.088	0.767
Soil pH	1	-7.84E-03 <sup>a</sup>	0.025	0.874
Species	4	-	12.745	<b>0.013</b>
( $N_{\text{area}}$ int.)	-	6.69E-01 <sup>a</sup>	-	-
$N_{\text{area}}$	4	-4.69E-02 <sup>a</sup>	1.142	0.285

941 \*Significance determined using Type II Wald  $\chi^2$  tests ( $\alpha = 0.05$ ). P-values  $< 0.05$  are in bold, while p-values between  
 942 0.05 and 0.1 are italicized. Superscript letters indicate model coefficients fit to natural-log (<sup>a</sup>) or square-root (<sup>b</sup>)  
 943 transformed data. Relationships between  $N_{\text{area}}$  and each response variable were fit using the second series of bivariate  
 944 mixed-effects models, so model coefficients and results are independent of model coefficients and results reported  
 945 for relationships between soil N, soil pH, and species for each response variable. Key:  $A_{\text{net}}$  – light saturated net  
 946 photosynthesis rate;  $V_{\text{cmax25}}$  – maximum rate of Rubisco carboxylation at 25°C;  $J_{\text{max25}}$  – maximum rate of electron  
 947 transport for RuBP regeneration at 25°C,  $J_{\text{max25}}:V_{\text{cmax25}}$  – the ratio of  $J_{\text{max25}}$  to  $V_{\text{cmax25}}$ .



**Figure 3.2.** Effects of soil N availability (left column of panels), species (middle column of panels), and leaf N content per unit leaf area (right column of panels) on net photosynthesis (a-c), maximum Rubisco carboxylation rate (d-f), and maximum RuBP regeneration rate (g-i). Soil N availability is represented on the x-axis in the left column of panels, species is represented on the x-axis in the middle column of panels, and leaf N content per unit leaf area is represented continuously on the x-axis in the right column of panels. Species abbreviations and position along the x-axis in the middle column of panels, colored points, shapes, and trendlines are as explained in Figure 3.1.

**948** 3.3.3 *Leaf N allocation*

**949** Neither soil N availability nor soil pH affected the proportion of leaf N  
**950** allocated to Rubisco or bioenergetics (Table 3.3; Fig. 3.3a, Fig. 3.3c), nor was  
**951** there any subsequent effect on the proportion of leaf N allocated to photosynthesis  
**952** (Table 3.3; Fig. 3.3f). We also found no effect of soil N availability or soil pH on  
**953** the proportion of leaf N allocated to structure (Table 3.3; Fig 3.3g). Species varied  
**954** in the proportion of leaf N allocated to Rubisco, photosynthesis, and structure (Fig  
**955** 3.3b, Fig. 3.3d, Fig 3.3h), with no detectable species effect on the proportion of  
**956** leaf N allocated to bioenergetics (Table 3.3).

**Table 3.3.** Effects of soil N availability, soil pH, and species on the proportion of leaf nitrogen content allocated to photosynthesis, Rubisco, bioenergetics, and structure

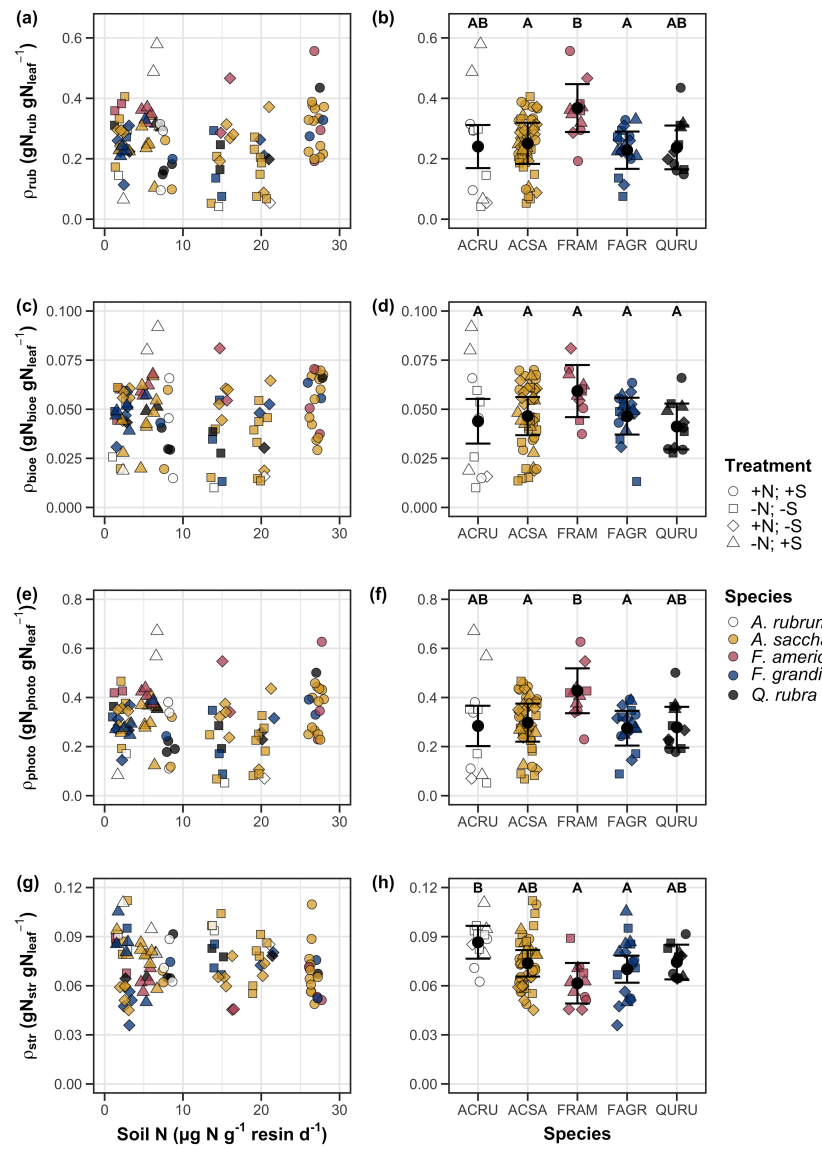
	$\rho_{\text{photo}}$			$\rho_{\text{rub}}$			$\rho_{\text{bioe}}$			
	df	Coefficient	$\chi^2$	p	Coefficient	$\chi^2$	p	Coefficient	$\chi^2$	p
Intercept	-	4.93E-01	-	-	4.17E-01	-	-	7.64E-02	-	-
Soil N	1	-1.23E-03	0.521	0.470	-1.04E-03	0.501	0.479	-1.77E-04	0.557	0.455
Soil pH	1	-4.37E-02	1.581	0.209	-3.70E-02	1.511	0.219	-6.84E-03	1.941	0.164
Species	4	-	13.106	<b>0.011</b>	-	14.152	<b>0.007</b>	-	7.300	0.121

	$\rho_{\text{str}}$			
	df	Coefficient	$\chi^2$	p
Intercept	-	9.77E-02	-	-
Soil N	1	-2.29E-04	1.165	0.280
Soil pH	1	-1.87E-03	0.179	0.672
Species	4	-	16.428	<b>0.002</b>

58

957 \*Significance determined using Type II Wald  $\chi^2$  tests ( $\alpha = 0.05$ ). P-values  $< 0.05$  are in bold. Key:  $\rho_{\text{photo}}$  -  
 958 proportion of leaf nitrogen content allocated to photosynthesis;  $\rho_{\text{rub}}$  - proportion of leaf nitrogen content allocated  
 959 to Rubisco;  $\rho_{\text{bioe}}$  - proportion of leaf nitrogen content allocated to bioenergetics;  $\rho_{\text{str}}$  - proportion of leaf nitrogen  
 960 content allocated to structure.



**Figure 3.3.** Effects of soil nitrogen availability and species on the proportion of leaf nitrogen content allocated to Rubisco (a-b), bioenergetics (c-d), photosynthesis (e-f), and structure (g-h). Soil nitrogen availability is represented on the x-axis in the left column of panels and species are represented on the x-axis in the right column of panels. Species abbreviations and position along the x-axis in the middle column of panels, colored points, shapes, trendlines, error bars, and compact lettering are as explained in Figure 3.1.

**961** 3.3.4 *Tradeoffs between nitrogen and water use*

**962** Although soil N availability did not affect  $\chi$  (Table 3.4; Fig. 3.4a), increasing  
**963** soil N availability decreased PNUE (Table 3.4; Fig. 3.4d) and increased the  
**964** ratio of  $N_{\text{area}}:\chi$  (Table 3.4; Fig. 3.4f). Specifically, this response yielded a 26%  
**965** reduction in PNUE and 37% stimulation in  $N_{\text{area}}:\chi$  across the soil nitrogen avail-  
**966** ability gradient. There was no apparent effect of soil N availability on  $V_{\text{cmax25}}:\chi$   
**967** (Table 3.4; Fig. 3.4h). Increasing soil pH had a weak marginal negative effect  
**968** on PNUE, but did not influence  $\chi$ ,  $N_{\text{area}}:\chi$ , or  $V_{\text{cmax25}}:\chi$  (Table 3.4). We also  
**969** observed differences in  $\chi$  (Fig. 3.4b), PNUE (Fig. 3.4e),  $N_{\text{area}}:\chi$  (Fig. 3.4g), and  
**970**  $V_{\text{cmax25}}:\chi$  (Fig. 3.4i) between species (Table 3.4). Finally, increasing  $N_{\text{area}}$  had a  
**971** strong negative effect on  $\chi$  (Table 3.4; Fig. 3.4c) and a strong positive effect on  
**972**  $V_{\text{cmax25}}:\chi$  (Table 3.4; Fig. 3.4j).

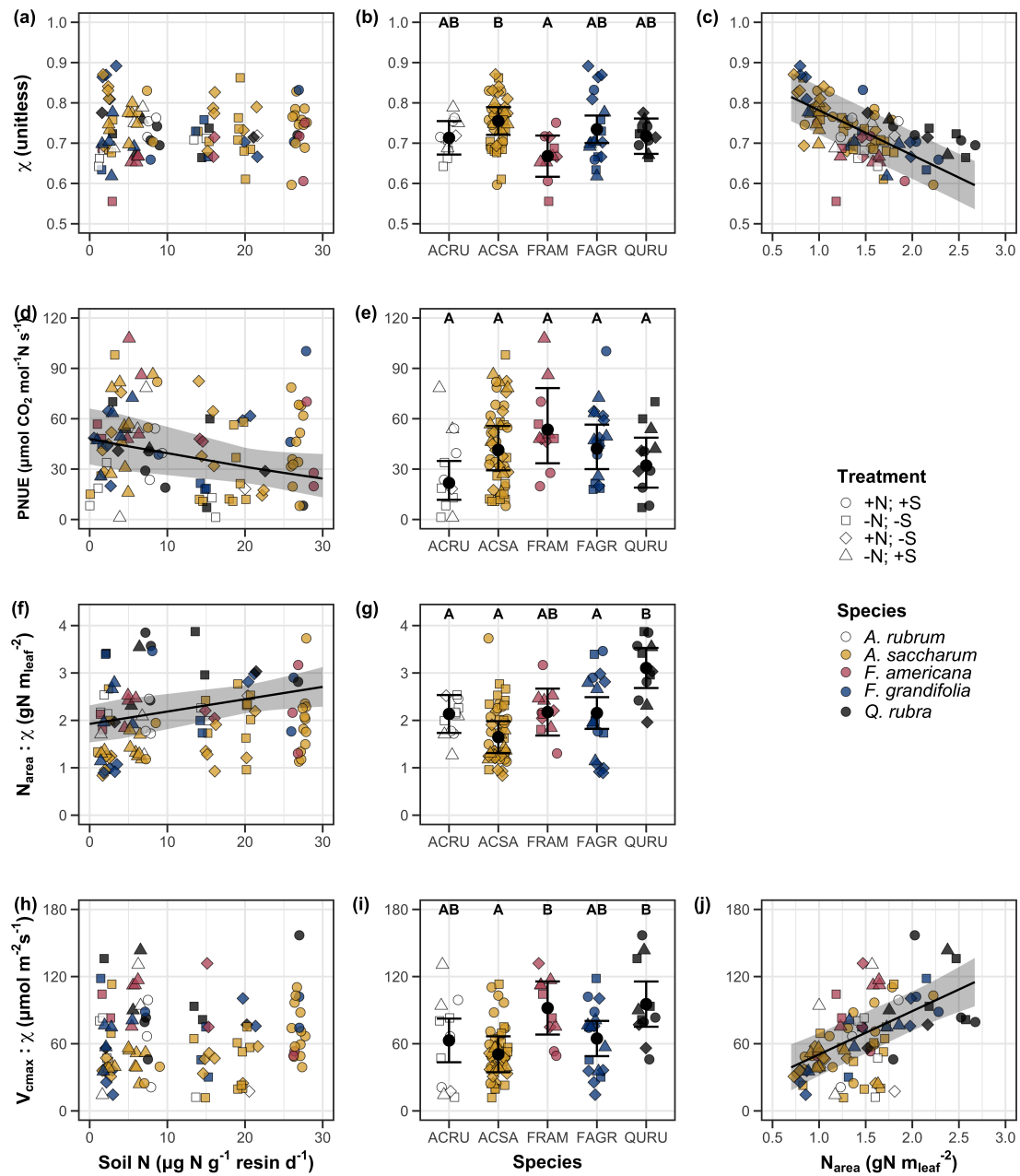
**Table 3.4.** Effects of soil N availability, soil pH, species, and  $N_{\text{area}}$  on tradeoffs between nitrogen and water use

	$\chi$			PNUE			$N_{\text{area}}:\chi$			
	df	Coefficient	$\chi^2$	p	Coefficient	$\chi^2$	p	Coefficient	$\chi^2$	p
(Intercept)	-	8.12E-01	-	-	9.57E+00	-	-	9.19E-01	-	-
Soil N	1	-1.14E-03	1.698	0.193	-6.63E-02	6.396	<b>0.011</b>	2.60E-02	9.533	<b>0.002</b>
Soil pH	1	-1.91E-02	1.087	0.297	-9.25E-01	2.843	<i>0.092</i>	2.03E-01	1.321	0.250
Species	4	-	18.843	<b>0.001</b>	-	13.454	<b>0.009</b>	-	52.983	<b>&lt;0.001</b>
$(N_{\text{area}} \text{ int.})$	-	8.93E-01	-	-	-	-	-	-	-	-
$N_{\text{area}}$	1	-1.11E-01	80.606	<b>&lt;0.001</b>	-	-	-	-	-	-

	$V_{\text{cmax25}}:\chi$			
	df	Coefficient	$\chi^2$	p
(Intercept)	-	7.20E+01	-	-
Soil N	1	3.99E-01	0.963	0.326
Soil pH	1	-3.12E+00	0.138	0.711
Species	4	-	31.450	<b>&lt;0.001</b>
$(N_{\text{area}} \text{ int.})$	-	1.18E+01	-	-
$N_{\text{area}}$	4	3.87E+01	32.797	<b>&lt;0.001</b>

973 \*Significance determined using Type II Wald  $\chi^2$  tests ( $\alpha = 0.05$ ). P-values  $< 0.05$  are in bold, while p-values  
 974 between 0.05 and 0.1 are italicized. Superscript letters indicate model coefficients fit to natural-log <sup>(a)</sup> or square-root  
 975 <sup>(b)</sup> transformed data. Relationships between  $N_{\text{area}}$  and each response variable were fit using the second series of  
 976 bivariate mixed-effects models, so model coefficients and results are independent of model coefficients and results  
 977 reported for relationships between soil N, soil pH, and species for each response variable. Key:  $\chi$  - isotope-derived  
 978 estimate of the  $C_i:C_a$ ; PNUE - photosynthetic N use efficiency, ratio of net photosynthesis to leaf N content per unit  
 979 leaf area;  $N_{\text{area}}:\chi$  - ratio of  $N_{\text{area}}$  to  $\chi$ ;  $V_{\text{cmax25}}:\chi$  - ratio of  $V_{\text{cmax25}}$  to  $\chi$ .



**Figure 3.4.** Effects of soil nitrogen availability and species on the proportion of leaf nitrogen content allocated to Rubisco (a-b), bioenergetics (c-d), photosynthesis (Rubisco + bioenergetics; e-f), and structure (g-h). Soil nitrogen availability is represented on the x-axis in the left column of panels and species are represented on the x-axis in the right column of panels. Species abbreviations and position along the x-axis in the middle column of panels, colored points, shapes, trendlines, error bars, and compact lettering are as explained in Figure 3.1.

**980** 3.4 Discussion

**981** Photosynthetic least-cost theory provides an explanation for understand-  
**982** ing relationships between soil nutrient availability, leaf nutrient allocation, and  
**983** photosynthetic capacity. The theory suggests that plants acclimate to a given  
**984** environment by optimizing leaf photosynthesis rates at the lowest summed cost  
**985** of using nutrients and water Prentice et al. (2014), Wang et al. (2017), Smith  
**986** et al. (2019), Paillassa et al. (2020). The theory predicts that an increase in  
**987** soil nutrient availability should allow similar photosynthesis rates to be achieved  
**988** with increased leaf nutrient content and photosynthetic capacity (i.e.,  $V_{cmax25}$  and  
**989**  $J_{max25}$ ) at lower leaf  $C_i:C_a$  ( $\chi$ ), resulting in an increase in water use efficiency,  
**990** decrease in nutrient use efficiency, and increase in both leaf nutrient content and  
**991** photosynthetic capacity per unit  $\chi$ . The theory predicts similar leaf responses to  
**992** increasing soil pH under acidic conditions, presumably due to generally faster nu-  
**993** trient cycle dynamics and consequent reductions in the cost of acquiring nutrients  
**994** relative to water with increasing soil pH (Wang et al. 2017; Paillassa et al. 2020;  
**995** Dong et al. 2020).

**996** Supporting the theory, we showed that increasing soil N availability was  
**997** associated with increased leaf N content (Fig 3.1a, 3.1c), a pattern that reduced  
**998** photosynthetic N use efficiency (Fig 3.4d) and increased leaf N content per unit  
**999**  $\chi$  (Fig 3.4f). Increasing soil N coincided with slight, but non-significant decreases  
**1000** in  $\chi$  and increases in  $V_{cmax25}$  and  $J_{max25}$  ( $p < 0.2$ , Table 3.2). The positive trend  
**1001** between soil N availability and photosynthetic capacity was supported by the con-  
**1002** current strong increase in leaf N content with increasing soil N availability, which  
**1003** resulted in no change in the proportion of leaf N content allocated to photosynthe-

1004 sis across the soil N availability gradient. Additionally, leaf N content exhibited a  
1005 strong negative correlation with  $\chi$ , indicative of strong nitrogen-water use trade-  
1006 offs at the leaf level. Responses tended to vary more due to soil N availability  
1007 than soil pH. Overall, these findings are consistent with the nutrient-water use  
1008 tradeoffs predicted from theory.

1009 3.4.1 *Soil nitrogen availability modifies tradeoffs between nitrogen and water use*

1010 In support of expected least-cost outcomes and past environmental gradient  
1011 studies (Dong et al. 2017; Paillassa et al. 2020), we found that increasing soil N  
1012 availability was associated with increased leaf N content. Soil N availability had  
1013 smaller impacts on measures of net photosynthesis and  $\chi$ , which led to reductions  
1014 in PNUE and increases in leaf N content per unit  $\chi$ , as expected from theory.  
1015 Photosynthetic least-cost theory suggests that reductions in PNUE should be  
1016 driven by an increase in the proportion of leaf N allocated to photosynthetic tissue,  
1017 a pattern that should allow plants to achieve optimal photosynthetic rates with  
1018 greater photosynthetic capacity to make better use of available light. Contrasting  
1019 theory predictions, we found no effect of soil N availability on photosynthetic  
1020 capacity. However, photosynthetic capacity did tend to increase with increasing  
1021 soil N availability ( $p < 0.20$ ; Table 3.2) resulting in no effect of soil N availability on  
1022 the relative fraction of leaf N allocated to photosynthesis, Rubisco, or bioenergetics  
1023 (Fig. 3.3). These lines of evidence support the idea that trees use additional N  
1024 to support increased leaf N allocation toward photosynthetic tissue and enhance  
1025 photosynthetic capacity (Wright et al. 2003).

1026 Soil N availability had a stronger effect on leaf N than photosynthetic ca-

1027 pacity. This pattern suggests that additional plant N uptake due to increased  
1028 soil N availability was also being used to support non-photosynthetic N pools,  
1029 possibly to structural tissue or stress-induced amino acid and polyamine synthe-  
1030 sis (Minocha et al. 2000; Onoda et al. 2004; Bubier et al. 2011). While we  
1031 found no change in the proportion of leaf N allocated to leaf structural tissue, the  
1032 overall stimulation in leaf N content with increasing soil N availability suggests an  
1033 increase in the net amount of N invested in leaf structural tissue along the N avail-  
1034 ability gradient. Importantly, leaf N allocated to structure was calculated using  
1035 an empirical relationship between  $M_{\text{area}}$  and the amount of leaf N allocated to cell  
1036 walls (Onoda et al. 2017). As the generality of relationships between  $M_{\text{area}}$  and  
1037 the amount of leaf N allocated to cell walls has been called into question (Harrison  
1038 et al. 2009), future work should consider explicitly measuring N allocation to cell  
1039 wall tissue and stress-induced amino acid synthesis to confirm these patterns.

1040 In opposition to patterns expected from least-cost theory, increasing soil  
1041 N availability had no apparent effect on  $\chi$  (Fig. 3.4a). Interestingly, despite  
1042 the null effect of soil N availability on  $\chi$ , we observed a strong negative effect of  
1043 increasing  $N_{\text{area}}$  on  $\chi$  (Fig. 3.4c), consistent with the nitrogen-water use tradeoffs  
1044 expected from theory. The null response of  $\chi$  to increasing soil N availability may  
1045 have been due to a lack of water limitation in the system, given that the area  
1046 received approximately 20% more precipitation (1167 mm) during the 12-month  
1047 period leading up to our measurement period than normally expected (972 mm).  
1048 However, droughts can and do occur in temperate forests of the northeastern  
1049 United States (Sweet et al. 2017), so the observed increase in leaf N content  
1050 with increasing soil N availability could be a strategy that allows trees to hedge

**1051** bets against drier than normal growing seasons (Onoda et al. 2004; Onoda et al.  
**1052** 2017; Hallik et al. 2009). As was suggested in Paillassa et al. (2020), and more  
**1053** recently by Querejeta et al. (2022), negative effects of soil N availability on  $\chi$  may  
**1054** increase with increasing aridity. This strategy would be especially advantageous if  
**1055** it allows individuals growing in arid regions to maintain carbon assimilation rates  
**1056** with reduced water loss. Future work should attempt to quantify interactive roles  
**1057** of climate and soil nitrogen availability on nitrogen-water use tradeoffs, which  
**1058** could be done by leveraging coordinated and multifactor nutrient (Borer et al.  
**1059** 2014) and water (Knapp et al. 2017) manipulation experiments across broad  
**1060** climatic gradients.

**1061** 3.4.2 *Soil pH did not modify tradeoffs between nitrogen and water usage*

**1062** While the primary purpose of this study was to examine the role of soil N  
**1063** availability on nitrogen-water use tradeoffs, our experimental design manipulated  
**1064** both soil N and pH, providing an opportunity to isolate the roles of these variables.  
**1065** Previous correlational studies along environmental gradients identified soil pH as  
**1066** a particularly important factor that can modify tradeoffs between nutrient and  
**1067** water use (Smith et al. 2019; Paillassa et al. 2020; Westerband et al. 2023)  
**1068** and the proportion of leaf nitrogen allocated to photosynthesis (Luo et al. 2021).  
**1069** Such studies implied that these patterns may be driven by reductions in the cost of  
**1070** acquiring nutrients relative to water with increasing pH, which may be exacerbated  
**1071** in acidic soils.

**1072** Consistent with theory (Wright et al. 2003; Prentice et al. 2014), our  
**1073** results indicate that increasing soil pH was negatively associated with PNUE.

1074 However, there was no effect of soil pH on leaf N content,  $\chi$ , or leaf N content per  
1075 unit  $\chi$ , most likely because the experimental N additions increased soil N sup-  
1076 ply while both increasing (sodium nitrate) and decreasing (ammonium sulfate)  
1077 soil pH. These results suggest that soil pH did not play a major role in modify-  
1078 ing expected photosynthetic least-cost theory patterns, contrasting findings from  
1079 Paillassa et al. (2020) and other gradient studies that note positive effects of in-  
1080 creasing soil pH on leaf N content, Rubisco carboxylation, and  $\chi$  (Viet et al. 2013;  
1081 Cornwell et al. 2018; Luo et al. 2021). Instead, null responses to soil pH show  
1082 that leaf photosynthetic parameters depend more on soil N availability than pH  
1083 per se, and that inferences from gradient studies might be confounding covariation  
1084 between N availability and soil acidity.

1085 3.4.3 *Species identity explains a large amount of variation in leaf and whole*  
1086 *plant traits*

1087 Species generally explained a larger amount of variation in measured leaf  
1088 traits than soil N availability or soil pH. Interspecies variation is an important  
1089 factor to consider when deducing mechanisms that drive photosynthetic least-  
1090 cost theory, particularly for species that form distinct mycorrhizal associations or  
1091 have different photosynthetic pathways, growth forms, or leaf habit (Espelta et al.  
1092 2005; Adams et al. 2016; Bialic-Murphy et al. 2021; Scott and Smith 2022). The  
1093 need to consider species may also be important when comparing nutrient-water  
1094 use tradeoffs in early and late successional species, or in species with different  
1095 resource economic strategies (Abrams and Mostoller 1995; Ellsworth and Reich  
1096 1996; Wright et al. 2004; Reich 2014; Onoda et al. 2017; Ziegler et al. 2020).

1097       A strength of the study design and sampling effort is that it controls for  
1098 many species differences that should modify nitrogen-water use tradeoffs expected  
1099 from theory. All tree species measured in this study shared the leaf habit of decid-  
1100 uous broadleaves, were growing in forests of similar successional stage, but differed  
1101 in mycorrhizal association and consequent resource economic strategies. As stands  
1102 tended to be dominated by trees that associate with arbuscular mycorrhizae (*Frax-*  
1103 *inus* and both *Acer* species made up 70% of total aboveground biomass across  
1104 stands), ecosystem biogeochemical cycle dynamics may be more closely aligned  
1105 to the inorganic nutrient economy proposed in Phillips et al. (2013), which may  
1106 promote stronger nitrogen-water use tradeoffs in tree species that associate with  
1107 arbuscular mycorrhizae. This result was not observed here, as photosynthetic  
1108 properties varied as much within as across the two mycorrhizal associations rep-  
1109 resented. Given the high variability in measured photosynthetic traits within  
1110 and across species, effects of mycorrhizal association likely require more intensive  
1111 sampling efforts to detect than were possible here.

1112 3.4.4 *Implications for photosynthetic least-cost theory model development*

1113       In the field, soil nutrient availability is heterogeneous across time and space  
1114 (Table S4). Unaccounted within-plot heterogeneity may have contributed to the  
1115 low amount of variation explained by soil N availability in our statistical mod-  
1116 els, as resin bags are a coarse surrogate for soil N availability. Despite this, we  
1117 still observed evidence for nutrient-water use tradeoffs, suggesting that observed  
1118 responses reported here may be an underestimate toward the net effect of soil  
1119 N availability on these tradeoffs. While we urge caution in the interpretation of

1120 these results, they do provide a promising baseline for future studies investigating  
1121 patterns expected from photosynthetic least-cost theory at finer spatiotemporal  
1122 resolutions.

1123 The general stronger relationship between leaf N content and photosyn-  
1124 thetic parameters versus between leaf N content and soil N availability suggests  
1125 that leaf N content is more directly tied to photosynthesis than soil N availabil-  
1126 ity. While this could be due to the high spatiotemporal heterogeneity of soil N  
1127 availability, principles from photosynthetic least-cost theory suggest that leaf N  
1128 content is the downstream product of leaf nutrient demand to build and maintain  
1129 photosynthetic machinery, which is set by aboveground environmental conditions  
1130 such as light availability, CO<sub>2</sub>, temperature, or vapor pressure deficit (Smith  
1131 et al. 2019; Paillassa et al. 2020; Peng et al. 2021; Westerband et al. 2023). The  
1132 stronger relationship between leaf N and photosynthetic parameters paired with  
1133 the strong negative relationship between leaf N and  $\chi$  could indicate a relatively  
1134 stronger effect of climate on leaf N-photosynthesis relationships than soil resource  
1135 availability. However, the short distance between plots and across sites limited  
1136 our ability to test this mechanism.

1137 Variation in soil pH affected least cost responses less than variations in  
1138 soil N availability, in part because experimental treatments directly increased soil  
1139 N and affected soil pH in opposite directions. While soil pH has been shown  
1140 to drive nitrogen-water tradeoffs in global gradient analyses (Viet et al. 2013;  
1141 Paillassa et al. 2020), these responses may be due to covariations between soil pH  
1142 and nutrient cycling rather than a role of pH per se. The direct manipulations  
1143 of soil pH and soil N availability in this study allowed us to partly disentangle

**1144** these factors and show that variation in N availability matters more for least-cost  
**1145** tradeoffs than pH alone.

**1146** 3.4.5 *Conclusions*

**1147** Increasing soil N availability generally increased leaf N content (both area-  
**1148** and mass-based), but did not significantly influence  $\chi$ . This shift in leaf N led  
**1149** to a reduction in PNUE, and an increase in leaf N per unit  $\chi$  with increasing  
**1150** soil N availability. Despite null effects of soil N availability on  $\chi$ , we observed a  
**1151** strong negative relationship between leaf N content and  $\chi$ . These results provide  
**1152** empirical support for the nutrient-water use tradeoffs expected from photosyn-  
**1153** thetic least-cost theory in response to soil nutrient availability, but suggest that  
**1154** all tenets of the theory may not hold in every environment. These results exper-  
**1155** imentially test previous work suggesting that leaf water-nitrogen economies vary  
**1156** across gradients of soil nutrient availability and pH, and show that variations in  
**1157** nutrient availability matter more for determining variation in leaf photosynthetic  
**1158** traits than soil pH.

1159

## Chapter 4

1160 The relative cost of resource use for photosynthesis drives variance in  
1161 leaf nitrogen content across a climate and soil resource availability  
1162 gradient

1163 4.1 Introduction

1164 Terrestrial biosphere models, which comprise the land surface component  
1165 of Earth system models, are sensitive to the formulation of photosynthetic pro-  
1166 cesses (Knorr and Heimann 2001; Ziehn et al. 2011; Booth et al. 2012; Walker  
1167 et al. 2021). This is because photosynthesis is the largest carbon flux between the  
1168 atmosphere and terrestrial biosphere (IPCC 2021), and is constrained by ecosys-  
1169 tem carbon and nutrient cycles (Hungate et al. 2003; LeBauer and Treseder  
1170 2008; Fay et al. 2015). Many terrestrial biosphere models formulate photosyn-  
1171 thesis by parameterizing photosynthetic capacity within plant functional groups  
1172 through empirical linear relationships between area-based leaf nitrogen content  
1173 ( $N_{\text{area}}$ ) and the maximum carboxylation rate of Ribulose-1,5-bisphosphate car-  
1174 boxylase/oxygenase (Kattge et al. 2009; Rogers 2014; Rogers et al. 2017). Models  
1175 are also beginning to include connected carbon-nitrogen cycles (Wieder et al. 2015;  
1176 Shi et al. 2016; Davies-Barnard et al. 2020; Braghieri et al. 2022), which allows  
1177 leaf photosynthesis to be predicted directly through changes in  $N_{\text{area}}$  and indirectly  
1178 through changes in soil nitrogen availability (e.g., LPJ-GUESS, CLM5.0) (Smith  
1179 et al. 2014; Lawrence et al. 2019). Despite recent model developments, open  
1180 questions remain regarding the generality of ecological relationships between soil  
1181 nitrogen availability, leaf nitrogen content, and leaf photosynthesis across edaphic  
1182 and climatic gradients.

**1183** Empirical support for positive relationships between soil nitrogen availabil-  
**1184** ity and  $N_{\text{area}}$  is abundant (Firn et al. 2019; Liang et al. 2020), and is a result  
**1185** often attributed to the high nitrogen cost of building and maintaining Rubisco  
**1186** (Evans 1989; Evans and Seemann 1989; Onoda et al. 2004; Onoda et al. 2017;  
**1187** Walker et al. 2014; Dong et al. 2020). Such patterns imply that positive rela-  
**1188** tionships between soil nitrogen availability and  $N_{\text{area}}$  should cause an increase in  
**1189** leaf photosynthesis and photosynthetic capacity by increasing the maximum rate  
**1190** of Rubisco carboxylation through increased investments to Rubisco construction  
**1191** and maintenance. This integrated  $N_{\text{area}}$ -photosynthesis response to soil nitrogen  
**1192** availability has been observed both in manipulative experiments and across envi-  
**1193** ronmental gradients (Field and Mooney 1986; Evans 1989; Walker et al. 2014; Li  
**1194** et al. 2020), and is thought to be driven by ecosystem nitrogen limitation, which  
**1195** limits primary productivity globally (LeBauer and Treseder 2008; Fay et al. 2015).  
**1196** However, this response is not consistently observed, as recent studies note variable  
**1197**  $N_{\text{area}}$ -photosynthesis relationships across soil nitrogen availability gradients (Liang  
**1198** et al. 2020; Luo et al. 2021) and that aboveground growing conditions (e.g., light  
**1199** availability, temperature, vapor pressure deficit) or species identity traits (e.g.,  
**1200** photosynthetic pathway, nitrogen acquisition strategy) may be more important  
**1201** for explaining variance in  $N_{\text{area}}$  and photosynthetic capacity across environmental  
**1202** gradients (Adams et al. 2016; Dong et al. 2017; Dong et al. 2020; Dong et al.  
**1203** 2022; Smith et al. 2019; Peng et al. 2021; Westerband et al. 2023).

**1204** One hypothesized mechanism to explain variance in  $N_{\text{area}}$  across environ-  
**1205** mental gradients has been proposed via photosynthetic least-cost theory (Wright  
**1206** et al. 2003; Prentice et al. 2014; Paillassa et al. 2020; Harrison et al. 2021).

**1207** The theory predicts that plants acclimate to environments by optimizing photo-  
**1208** synthetic assimilation rates at the lowest summed cost of nitrogen and water use  
**1209** (Wright et al. 2003; Prentice et al. 2014). In a given environment, the theory pro-  
**1210** poses that nitrogen and water use can be substituted for each other to maintain  
**1211** the lowest summed cost to satisfy leaf resource demand, such that optimal photo-  
**1212** synthetic rates are achieved with less efficient use of the more abundant and less  
**1213** costly resource to acquire in exchange for more efficient use of the less abundant  
**1214** and more costly resource to acquire. The theory predicts that, all else equal, an  
**1215** increase in soil nitrogen availability should decrease the cost of acquiring and us-  
**1216** ing nitrogen relative to water (a ratio referred to herein as  $\beta$ ), resulting in optimal  
**1217** photosynthetic rates achieved with greater  $N_{\text{area}}$  at lower stomatal conductance  
**1218** and lower leaf  $C_i:C_a$  (Wright et al. 2003; Prentice et al. 2014). Alternatively, an  
**1219** increase in soil moisture should reduce costs of water acquisition and use, increas-  
**1220** ing  $\beta$ , stomatal conductance, and leaf  $C_i:C_a$ , resulting in optimal photosynthetic  
**1221** rates achieved with decreased  $N_{\text{area}}$ . The theory also predicts variability in stom-  
**1222**atal conductance and  $N_{\text{area}}$  in response to climatic factors, suggesting that the  
**1223** optimal response to increased vapor pressure deficit (VPD) should be a reduction  
**1224** in stomatal conductance and leaf  $C_i:C_a$  that is counterbalanced by an increase  
**1225** in  $N_{\text{area}}$  to support the higher photosynthetic capacity needed to maintain high  
**1226** assimilation at lower conductance (Grossiord et al. 2020; Dong et al. 2020; López  
**1227** et al. 2021; Westerband et al. 2023).

**1228** Leaf nitrogen allocation responses to changing climates or soil resource  
**1229** availability may also depend on their mode of nutrient acquisition or photo-  
**1230** synthetic pathway. For example, species that form associations with symbiotic

**1231** nitrogen-fixing bacteria (referred as “N-fixing species” from this point forward)  
**1232** should, in theory, have access to a less finite nitrogen supply, which may result in  
**1233** lower  $\beta$  values than species not capable of forming such associations (referred as  
**1234** “non-fixing species” from this point forward). This result was previously shown in  
**1235** a greenhouse experiment, where a leguminous species generally had lower costs of  
**1236** nitrogen acquisition compared to a non-leguminous species, although these differ-  
**1237** ences were generally stronger under increased nitrogen limitation (Perkowski et al.  
**1238** 2021). Lower  $\beta$  values could be a possible explanation for why N-fixing species  
**1239** commonly have higher leaf nitrogen content than non-fixing species (Adams et al.  
**1240** 2016; Dong et al. 2017). Similarly, leaf nitrogen allocation patterns across en-  
**1241** vironmental gradients may be dependent on photosynthetic pathway. Lower leaf  
**1242**  $C_i:C_a$  values in C<sub>4</sub> species suggests that C<sub>4</sub> species should have lower  $\beta$  values  
**1243** than C<sub>3</sub> species (Scott and Smith 2022), a pattern that could be the result of  
**1244** increased costs associated with water acquisition and use or reduced costs of ni-  
**1245** trogen acquisition and use relative to C<sub>3</sub> species. No study to date has directly  
**1246** quantified  $\beta$  in C<sub>4</sub> species aside from the dataset used to initially parameterize  
**1247** an optimality model for C<sub>4</sub> species (Scott and Smith 2022).

**1248** While photosynthetic least-cost theory provides a unified hypothesis for un-  
**1249** derstanding effects of climate and soil resource availability on  $N_{area}$ , empirical tests  
**1250** of the theory are sparse. Increasing soil nitrogen availability has been previously  
**1251** shown to decrease the cost of acquiring nutrients (Bae et al. 2015; Perkowski et al.  
**1252** 2021; Lu et al. 2022), which can induce predictable nutrient-water use tradeoffs  
**1253** expected from the theory across broad environmental gradients (Paillassa et al.  
**1254** 2020; Querejeta et al. 2022; Westerband et al. 2023) and in manipulation experi-

1255 ments (Bialic-Murphy et al. 2021). Additionally, increasing VPD has been shown  
1256 to have a positive effect on  $N_{\text{area}}$  (Dong et al. 2017; Dong et al. 2020; Firn et al.  
1257 2019; López et al. 2021). However, studies have been restricted to exploring these  
1258 patterns with C3 species and, while previous studies have shown that variance  
1259 in  $N_{\text{area}}$  across environmental gradients is driven by strong negative relationships  
1260 with leaf  $C_i:C_a$  (3.4, (Dong et al. 2017; Paillassa et al. 2020; Westerband et al.  
1261 2023)), no study to date has explicitly investigated effects of soil resource avail-  
1262 ability or plant functional group on  $N_{\text{area}}$  using  $\beta$  as a direct predictor of leaf  
1263  $C_i:C_a$ . Additionally, as  $N_{\text{area}}$  can be broken down into structural (leaf mass per  
1264 area;  $M_{\text{area}}$ ; g m-2) and metabolic (mass-based leaf nitrogen content;  $N_{\text{mass}}$ ; gN  
1265 g-1) components (Dong et al. 2017), no study has investigated which component  
1266 of  $N_{\text{area}}$  drives the hypothesized response of  $N_{\text{area}}$  to leaf  $C_i:C_a$ . Understanding  
1267 whether changes in  $N_{\text{area}}$  due to leaf  $C_i:C_a$  are driven by changes in leaf morphol-  
1268 ogy or stoichiometry is important, especially because  $N_{\text{mass}}$  tends to covary with  
1269  $M_{\text{area}}$  due to tradeoffs between leaf longevity and leaf productivity (Wright et al.  
1270 2004; Reich 2014; Onoda et al. 2017; Wang et al. 2023).

1271 In this chapter, I measured  $N_{\text{area}}$ ,  $N_{\text{mass}}$ ,  $M_{\text{area}}$ , leaf  $\delta^{13}\text{C}$ -derived estimates  
1272 of leaf  $C_i:C_a$ , and leaf  $\delta^{13}\text{C}$ -derived estimates of  $\beta$  in 520 individuals spanning  
1273 57 species scattered across 24 grassland sites in Texas, USA (Table S1). Texas  
1274 contains a diverse climatic gradient, indicated by 2006-2020 mean annual precip-  
1275 itation totals ranging from 204 to 1803 mm and 2006-2020 mean annual temper-  
1276 ature ranging from 11.8° to 24.6°C. Variability in soil nitrogen availability and  
1277 soil moisture was expected across sites, owing to differences in soil texture and  
1278 aboveground climate that would drive differential rates of water retention and

1279 nitrogen transformations to plant-available substrate. I leveraged the expected  
1280 climatic and soil resource variability across sites to test the following hypotheses:

- 1281 1. Soil nitrogen availability will decrease  $\beta$  through a reduction in costs of  
1282 nitrogen acquisition and use, while soil moisture will increase  $\beta$  through a  
1283 reduction in costs of water acquisition and use. Following previous results,  
1284 we expected that N-fixing species would have lower  $\beta$  values and that C<sub>4</sub>  
1285 species would have lower  $\beta$  values.
- 1286 2. Leaf  $C_i:C_a$  will be positively related to  $\beta$ , a pattern that will result in a  
1287 negative indirect effect of increasing soil nitrogen availability on leaf  $C_i:C_a$ ,  
1288 a positive indirect effect of increasing soil moisture on leaf  $C_i:C_a$ , and lower  
1289 leaf  $C_i:C_a$  in both N-fixing species and C<sub>4</sub> species. We also expected that  
1290 leaf  $C_i:C_a$  would be negatively related to VPD, as increasing atmospheric  
1291 dryness should cause plants to close stomata to minimize water loss.
- 1292 3.  $N_{\text{area}}$  will be negatively related to leaf  $C_i:C_a$  and  $\beta$ . This response will result  
1293 in an indirect positive effect of increasing soil nitrogen availability, a negative  
1294 effect of increasing soil moisture on  $N_{\text{area}}$ , and generally larger  $N_{\text{area}}$  values  
1295 in both N-fixing species. While theory predicts that negative relationships  
1296 between  $N_{\text{area}}$  and leaf  $C_i:C_a$  should yield generally larger  $N_{\text{area}}$  in C<sub>4</sub> species,  
1297 we expected that C<sub>4</sub> species would have lower  $N_{\text{area}}$  due to generally greater  
1298 nitrogen use efficiency in C<sub>4</sub> species than C<sub>3</sub> species. Additionally, VPD  
1299 was expected to increase  $N_{\text{area}}$ , a pattern that would be directly mediated  
1300 through the reduction in leaf  $C_i:C_a$  with increasing VPD.

**1301** 4.2 Methods

**1302** 4.2.1 *Site descriptions and sampling methodology*

**1303** I collected leaf and soil samples from 24 open grassland sites across central and  
**1304** eastern Texas in summer 2020 and summer 2021 (Fig. 4.1). Twelve sites were vis-  
**1305** ited between June and July 2020 and 14 sites (11 unique from 2020) were visited  
**1306** between May and June 2021 (Table 4.1). I explicitly chose sites that maximized  
**1307** variability in precipitation and edaphic variability between sites while minimiz-  
**1308** ing temperature variability across the environmental gradient (Table 4.1). No  
**1309** site with personally communicated or anecdotal evidence of grazing or distur-  
**1310** bance (e.g., mowing, feral hog activity, etc.) were used. I collected leaf material  
**1311** from three individuals each of the five most abundant species at random locations  
**1312** at each site, only selecting species that were broadly classified as graminoid or  
**1313** forb/herb growth habits per the USDA PLANTS database (USDA NRCS 2022).  
**1314** All collected leaves were fully expanded with no visible herbivory or other external  
**1315** damage and also free from shading by nearby shrubs or trees. Five soil samples  
**1316** were collected from 0-15cm below the soil surface at each site near the leaf collec-  
**1317** tion sample locations. Soil samples were later mixed together by hand to create  
**1318** one composite soil sample per site.

**1319** 4.2.2 *Leaf trait measurements*

**1320** Images of each leaf were taken immediately following each site visit using a flat-  
**1321** bed scanner. Fresh leaf area was determined from each image using the 'LeafArea'  
**1322** R package (Katabuchi 2015), which automates leaf area calculations using ImageJ  
**1323** software (Schneider et al. 2012). Each leaf was dried at 65°C for at least 48 hours

**1324** to a constant mass, weighed, and manually ground in a mortar and pestle until  
**1325** homogenized. Leaf mass per area ( $M_{\text{area}}$ ; g m<sup>-2</sup>) was calculated as the ratio of  
**1326** dry leaf biomass to fresh leaf area. Subsamples of dried and homogenized leaf  
**1327** tissue were used to measure leaf nitrogen content ( $N_{\text{mass}}$ ; gN g<sup>-1</sup>) through ele-  
**1328** mental combustion analysis (Costech-4010, Costech Instruments, Valencia, CA).  
**1329** Leaf nitrogen content per unit leaf area ( $N_{\text{area}}$ ; gN m<sup>-2</sup>) was then calculated as  
**1330** the product of  $N_{\text{mass}}$  and  $M_{\text{area}}$ .

**1331** Subsamples of dried and homogenized leaf tissue were sent to the University  
**1332** of California-Davis Stable Isotope Facility to determine leaf  $\delta^{13}\text{C}$ . Leaf  $\delta^{13}\text{C}$  values  
**1333** were determined using an elemental analyzer (PDZ Europa ANCA-GSL; Sercon  
**1334** Ltd., Chestshire, UK) interfaced to an isotope ratio mass spectrometer (PDZ  
**1335** Europa 20-20 Isotope Ratio Mass Spectrometer, Sercon Ltd., Chestshire, UK).  
**1336** I used leaf  $\delta^{13}\text{C}$  values (‰; relative to Vienna Pee Dee Belemnite international  
**1337** reference standard) to estimate the ratio of intercellular ( $C_i$ ) to extracellular ( $C_a$ )  
**1338** CO<sub>2</sub> ratio (leaf  $C_i:C_a$ ; unitless) following the approach of Farquhar et al. (1989)  
**1339** described in Cernusak et al. (2013). Specifically, I derived leaf C<sub>i</sub>:C<sub>a</sub> as:

$$\text{Leaf } \frac{C_i}{C_a} = \frac{\Delta^{13}\text{C} - a}{b - a} \quad (4.1)$$

**1340** where  $\Delta^{13}\text{C}$  represents the relative difference between leaf  $\delta^{13}\text{C}$  (‰) and air  $\delta^{13}\text{C}$   
**1341** (‰), and is calculated as:

$$\Delta^{13}\text{C} = \frac{\delta^{13}\text{C}_{\text{air}} - \delta^{13}\text{C}_{\text{leaf}}}{1 + \delta^{13}\text{C}_{\text{leaf}}} \quad (4.2)$$

**1342**  $\delta^{13}\text{C}_{\text{air}}$ , traditionally assumed to be -8‰ (Keeling et al. 1979; Farquhar et al.

**1343** 1989), was calculated as a function of calendar year  $t$  using an empirical equation  
**1344** derived in Feng (1999):

$$\delta^{13}C_{air} = -6.429 - 0.006e^{0.0217(t-1740)} \quad (4.3)$$

**1345** This calculation resulted in  $\delta^{13}C_{air}$  values for 2020 and 2021 as -9.04‰ and -  
**1346** 9.09‰, respectively.  $a$  represents the fractionation between  $^{12}C$  and  $^{13}C$  due to  
**1347** diffusion in air, assumed to be 4.4‰, and  $b$  represents the fractionation caused  
**1348** by Rubisco carboxylation, assumed to be 27‰ (Farquhar et al. 1989). For  $C_4$   
**1349** species,  $b$  in Eqn. 4.1 was set to 6.3‰, and was derived from:

$$b = c + (d \cdot \phi) \quad (4.4)$$

**1350** Where  $c$  was set to -5.7‰ and  $d$  was set to 30‰ (Farquhar et al. 1989).  $\phi$ , which  
**1351** is the bundle sheath leakiness term, was set to 0.4. All leaf  $C_i:C_a$  values less than  
**1352** 0.1 and greater than 0.95 were assumed to be incorrect and removed.

**1353** I derived the unit cost of resource use ( $\beta$ ) using leaf  $C_i:C_a$  and site climate  
**1354** data with equations first described in Prentice et al. (2014) and simplified in  
**1355** Lavergne et al. (2020):

$$\beta = 1.6\eta^* D \frac{\chi - (\frac{\Gamma^*}{C_a})^2}{(1 - \chi)^2(K_m + \Gamma^*)} \quad (4.5)$$

**1356** where  $\eta^*$  is the viscosity of water relative to 25°C, calculated using elevation and  
**1357** mean air temperature of the seven days leading up to each site visit following  
**1358** equations in Huber et al. (2009).  $D$  represents vapor pressure deficit (Pa), set

**1359** to the mean vapor pressure deficit of the seven days leading up to each site visit,  
**1360**  $C_a$  represents atmospheric CO<sub>2</sub> concentration, arbitrarily set to 420  $\mu\text{mol mol}^{-1}$   
**1361** CO<sub>2</sub>.  $K_m$  (Pa) is the Michaelis-Menten coefficient for Rubisco affinity to CO<sub>2</sub> and  
**1362** O<sub>2</sub>, calculated as:

$$K_m = K_c \cdot \left(1 + \frac{O_i}{K_o}\right) \quad (4.6)$$

**1363** where  $K_c$  (Pa) and  $K_o$  (Pa) are the Michaelis-Menten coefficients for Rubisco  
**1364** affinity to CO<sub>2</sub> and O<sub>2</sub>, respectively, and  $O_i$  is the intercellular O<sub>2</sub> concentration.  
**1365**  $\Gamma^*$  (Pa) is the CO<sub>2</sub> compensation point in the absence of dark respiration.  $K_c$ ,  $K_o$ ,  
**1366** and  $\Gamma^*$  were determined using equations described in Medlyn et al. (2002) and  
**1367** derived in Bernacchi et al. (2001), invoking an elevation correction for atmospheric  
**1368** pressure as explained in Stocker et al. (2020).

**Table 4.1.** Site locality information, sampling year(s), 2006-2020 mean annual precipitation (MAP; mm), mean annual temperature (MAT; °C), and water holding capacity (WHC; mm)\*

Site	Latitude	Longitude	Sampling year	MAP	MAT	WHC
Edwards_2019_17	29.95	-100.36	2020	563.5	19.0	224.7
Uvalde_2020_02	29.59	-100.09	2020, 2021	648.5	19.5	224.7
Menard_2020_01	30.91	-99.59	2020	641.9	18.3	220.2
Kerr_2020_03	30.06	-99.34	2021	672.4	18.3	237.5
Bandera_2020_03	29.85	-99.30	2021	789.4	18.8	235.1
Sansaba_2020_01	31.29	-98.62	2020	733.0	18.8	234.3
Comal_2020_21	29.79	-98.43	2020	878.5	19.9	220.7
Blanco_2019_16	29.99	-98.43	2020	833.0	19.2	222.2
Bexar_2019_13	29.24	-98.43	2020	759.3	21.5	206.0
Burnet_2020_14	30.84	-98.34	2021	763.3	19.5	217.8
Comal_2020_19	30.01	-98.32	2021	845.0	19.3	220.4
Hays_2020_54	29.96	-98.17	2021	861.3	20.0	225.6
Burnet_2020_12	30.82	-98.06	2021	815.1	19.4	245.3
Williamson_2019_09	30.71	-97.86	2020	867.7	19.7	270.2
Williamson_2019_10	30.54	-97.77	2020	819.5	19.9	239.8
Bell_2021_08	31.06	-97.55	2021	937.3	19.6	232.3
Fayette_2021_12	29.86	-97.21	2021	985.7	20.4	165.6
Fayette_2019_04	30.09	-96.78	2020	1017.4	20.6	226.9
Fayette_2020_09	29.86	-96.71	2021	1002.7	20.8	187.6
Washington_2020_08	30.28	-96.41	2021	1077.4	20.4	203.9
Austin_2020_03	29.78	-96.24	2021	1108.7	20.6	253.0
Brazos_2020_16	30.93	-96.23	2021	1078.0	20.1	202.2
Brazos_2020_18	30.52	-96.21	2020, 2021	1099.4	20.4	233.5
Harris_2020_03	29.88	-95.31	2020, 2021	1492.0	21.6	265.6

**1369** \* Rows are arranged by longitude to visualize precipitation variability across sites

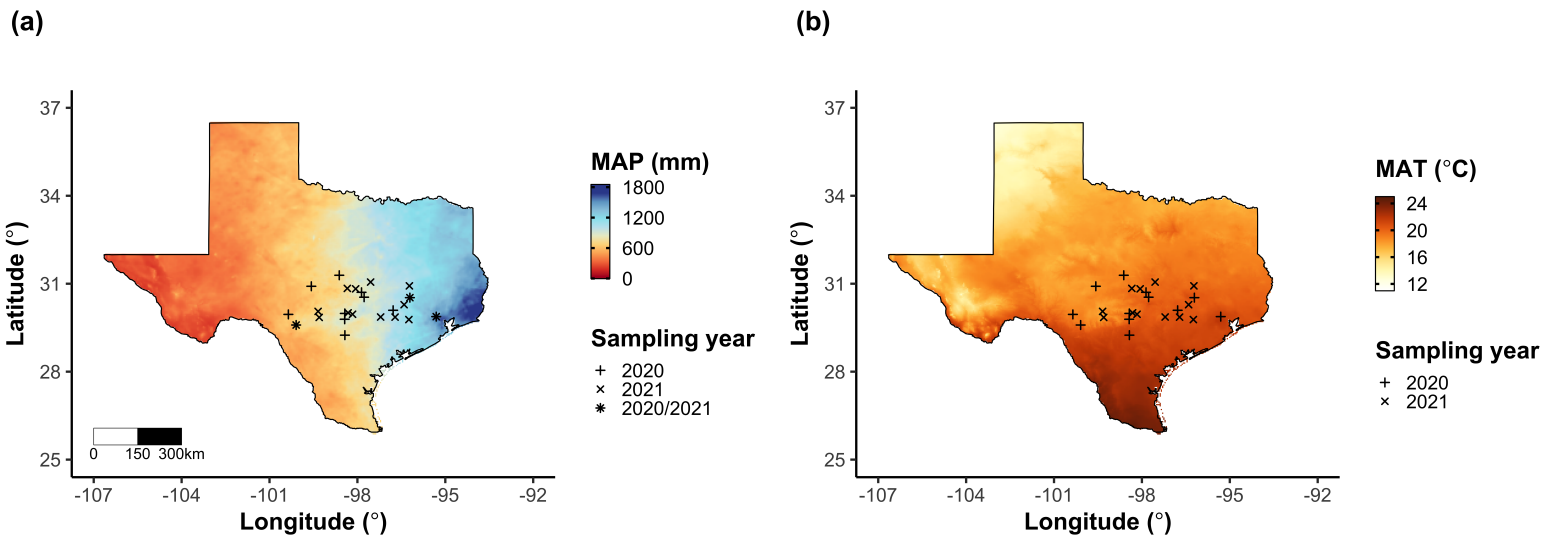


**Figure 4.1.** Maps that detail site locations along 2006-2020 mean annual precipitation (a) and mean annual temperature (b) gradients in Texas, USA. Precipitation and temperature data were plotted at a 4-km grid resolution and are masked to include only grid cells that occur in the Texas state boundary in the United States. In both panels, open circles refer to sites visited in 2020, open triangles to sites visited in 2021, and closed circles to sites visited in 2020 and 2021. The scale bar in (a) also applies to (b).

**1370** 4.2.3 *Site climate data*

**1371** I used the Parameter-elevation Regressions on Independent Slopes Model (PRISM)  
**1372** (Daly et al. 2008) climate product to access gridded daily temperature and precip-  
**1373** itation data for the coterminous United States at a 4-km grid resolution between  
**1374** January 1, 2006 and July 31, 2021 (PRISM Climate Group, Oregon State Uni-  
**1375** versity, <https://prism.oregonstate.edu>, data created 4 Feb 2014, accessed 24 Mar  
**1376** 2022). Daily mean air temperature, mean VPD, and total precipitation data were  
**1377** extracted from the grid cell that contained the latitude and longitude of each  
**1378** property using the ‘extract’ function in the ‘terra’ R package (Hijmans 2022).  
**1379** PRISM data were used in lieu of local weather station data because several rural  
**1380** sites did not have a local weather station present within a 20-km radius of the site.  
**1381** Daily site climate data were used to estimate mean annual precipitation and mean  
**1382** annual temperature for each site between 2006 and 2020 (Table 1). I calculated  
**1383** total precipitation and mean daily VPD for the prior 1, 2, 3, 4, 5, 6, 7, 8, 9, 10,  
**1384** 15, 20, 25, 30, 60, and 90 days leading up to each site visit.

**1385** 4.2.4 *Site edaphic characteristics*

**1386** Subsamples of composited soil samples were sent to the Texas A & M Soil, Water  
**1387** and Forage Laboratory to quantify soil nitrate concentration (NO<sub>3</sub>-N; ppm). Soil  
**1388** NO<sub>3</sub>-N was determined by extracting composite soil samples in 1 M KCl, measur-  
**1389** ing absorbance values of extracts at 520 nm using the end product of a NO<sub>3</sub>-N to  
**1390** NO<sub>2</sub>-N cadmium reduction reaction (Kachurina et al. 2000; Keeney and Nelson  
**1391** 1983). Soil texture data from 0-15cm below the soil surface were accessed using  
**1392** the SoilGrids2.0 data product (Poggio et al. 2021) through the ‘fetchSoilGrids’

**1393** function in the ‘soilDB’ R package (Beaudette et al. 2022). I used SoilGrids2.0  
**1394** to access soil texture data in lieu of analyses using the collected composite soil  
**1395** sample due to a lack of soil material from some sites after sending samples for soil  
**1396** NO<sub>3</sub>-N.

**1397** Soil moisture was not measured in the field, but was estimated using the  
**1398** ‘Simple Process-Led Algorithms for Simulating Habitats’ model (SPLASH) (Davis  
**1399** et al. 2017). This model, derived from the STASH model (Cramer and Prentice  
**1400** 1988), spins up a bucket model using Priestley-Taylor equations (Priestley and  
**1401** Taylor 1972) to calculate daily soil moisture ( $W_n$ ; mm) as a function of the previous  
**1402** day’s soil moisture ( $W_{n-1}$ ; mm), daily precipitation ( $P_n$ ; mm), condensation ( $C_n$ ;  
**1403** mm), actual evapotranspiration ( $E_n^a$ ; mm), and runoff (RO; mm):

$$W_n = W_{n-1} + P_n + C_n - E_n^a - RO \quad (4.7)$$

**1404** Models were spun up by equilibrating the previous day’s soil moisture using succes-  
**1405** sive model iterations with daily mean air temperature, daily precipitation total,  
**1406** the number of daily sunlight hours, and latitude as model inputs (Davis et al.  
**1407** 2017). Daily sunlight hours were estimated for each day at each site using the  
**1408** ‘getSunlightTimes’ function in the ‘suncalc’ R package, which estimated sunrise  
**1409** and sunset times of each property using date and site coordinates (Thieurmel and  
**1410** Elmarhraoui 2019). Water holding capacity (mm), or bucket size, was estimated  
**1411** as a function of soil texture using pedotransfer equations explained in Saxton and  
**1412** Rawls (2006), as done in Stocker et al. (2020) and Bloomfield et al. (2023). A  
**1413** summary of these equations is included in the Supplemental Information.

1414 Daily soil moisture outputs from the SPLASH model for each site were  
1415 used to calculate mean daily soil moisture for the prior 1, 2, 3, 4, 5, 6, 7, 8, 9,  
1416 10, 15, 20, 25, 30, 60, and 90 days leading up to each site visit. Mean daily  
1417 soil moisture values were then expressed as a fraction of water holding capacity  
1418 to normalize across sites with different bucket depths, as done in Stocker et al.  
1419 (2018).

1420 4.2.5 *Plant functional group assignments*

1421 Plant functional group was assigned to each species and used as the primary  
1422 descriptor of species identity. Specifically, I assigned plant functional groups  
1423 based on photosynthetic pathway ( $C_3$ ,  $C_4$ ) and ability to form associations with  
1424 symbiotic nitrogen-fixing bacteria. The ability to form associations with symbi-  
1425 otic nitrogen-fixing bacteria was assigned based on whether species were in the  
1426 *Fabaceae* family, and photosynthetic pathway of each species was determined from  
1427 past literature and confirmed through leaf  $\delta^{13}\text{C}$  values. We chose these plant func-  
1428 tional groups based on *a priori* hypotheses regarding the functional role of nitrogen  
1429 fixation and photosynthetic pathway on the sensitivity of plant nitrogen uptake  
1430 and leaf nitrogen allocation to soil nutrient availability and aboveground growing  
1431 conditions. These plant functional group classifications resulted in three distinct  
1432 plant functional groups within our dataset:  $C_3$  legumes ( $n = 53$ ),  $C_3$  non-legumes  
1433 ( $n = 350$ ), and  $C_4$  non-legumes ( $n = 117$ ).

**1434** 4.2.6 *Data analysis*

**1435** All analyses and plotting were conducted in R version 4.1.1 (R Core Team 2021).

**1436** I constructed a series of separate linear mixed-effects models to investigate en-

**1437** vironmental drivers of  $\beta$ , leaf  $C_i:C_a$ ,  $N_{\text{area}}$ ,  $N_{\text{mass}}$ , and  $M_{\text{area}}$ , followed by a path

**1438** analysis using a piecewise structural equation model to investigate direct and

**1439** indirect effects of climate and soil resource availability on  $N_{\text{area}}$ .

**1440** To explore environmental drivers of  $\beta$ , I built a linear mixed-effects model

**1441** that included soil moisture, soil nitrogen availability, and plant functional group

**1442** as fixed effect coefficients. Species were designated as a random intercept term.

**1443** Interaction coefficients between all possible combinations of the three fixed effect

**1444** coefficients were also included.  $\beta$  was natural log transformed to linearize data.

**1445** I used an information-theoretic model selection approach to determine whether

**1446** 90-, 60-, 30-, 20-, 15-, 10-, 9-, 8-, 7-, 6-, 5-, 4-, 3-, 2-, or 1-day mean daily soil

**1447** moisture conferred the best model fit for  $\beta$ . To do this, I constructed 16 separate

**1448** linear mixed-effects models where log-transformed  $\beta$  was included as the response

**1449** variable and each soil moisture time step was separately included as a single

**1450** continuous fixed effect. Species were included as a random intercept term for all

**1451** models. I used corrected Akaike Information Criterion (AICc) to select the soil

**1452** moisture timescale that conferred the best model fit, indicated by the model with

**1453** the lowest AICc score (Table S2; Fig. S2).

**1454** To explore environmental drivers of leaf  $C_i:C_a$ , I constructed a second linear

**1455** mixed effects model that included VPD, soil moisture, soil nitrogen availability,

**1456** and plant functional group as fixed effect coefficients. Two-way interactions be-

**1457** tween plant functional group and VPD, soil nitrogen availability, or soil moisture

1458 were also included as fixed effect coefficients, in addition to a three-way interaction  
1459 between soil moisture, soil nitrogen availability, and plant functional group.  
1460 Species were included as a random intercept term. I used an information-theoretic  
1461 model selection approach to determine whether 90-, 60-, 30-, 20-, 15-, 10-, 9-, 8-,  
1462 7-, 6-, 5-, 4-, 3-, 2-, or 1-day mean daily VPD conferred the best model fit for leaf  
1463  $C_i:C_a$  using the same approach explained above for the soil moisture effect on  $\beta$ .  
1464 The soil moisture timescale was set to the same timescale that conferred the best  
1465 fit for  $\beta$ .

1466 To explore environmental drivers of  $N_{\text{area}}$ ,  $N_{\text{mass}}$ , and  $M_{\text{area}}$ , I constructed  
1467 three separate linear mixed effects model that each included leaf  $C_i:C_a$ , soil ni-  
1468 trogen availability, soil moisture, and plant functional group as fixed effect coef-  
1469 ficients. Two-way interactions between plant functional group and  $\beta$ , leaf  $C_i:C_a$ ,  
1470 soil nitrogen availability, or soil moisture were included as additional fixed effect  
1471 coefficients, in addition to a three-way interaction between soil nitrogen availabil-  
1472 ity, soil moisture, and plant functional group. Species were included as a random  
1473 intercept term, with the soil moisture timescale set to the same timescale that  
1474 conferred the best fit for  $\beta$ .

1475 In all linear mixed-effects models explained above, including those to select  
1476 relevant timescales, I used the 'lmer' function in the 'lme4' R package (Bates et al.  
1477 2015) to fit each model and the 'Anova' function in the 'car' R package (Fox and  
1478 Weisberg 2019) to calculate Type II Wald's  $\chi^2$  and determine the significance  
1479 level ( $\alpha = 0.05$ ) of each fixed effect coefficient. I used the 'emmeans' R package  
1480 (Lenth 2019) to conduct post-hoc comparisons using Tukey's tests, where degrees  
1481 of freedom were approximated using the Kenward-Roger approach (Kenward and

**1482** Roger 1997). Trendlines and error ribbons for all plots were drawn using a series  
**1483** of ‘emmeans’ outputs across the range in plotted x-axis values.

**1484** Finally, I conducted a path analysis using a piecewise structural equation  
**1485** model to examine direct and indirect pathways that determined variance in  $N_{\text{area}}$ .  
**1486** Six separate linear mixed effects models were loaded into the piecewise structural  
**1487** equation model. Models were constructed per *a priori* hypotheses following pat-  
**1488** terns expected from photosynthetic least-cost theory. The first model regressed  
**1489**  $N_{\text{area}}$  against  $N_{\text{mass}}$  and  $M_{\text{area}}$ . The second model regressed  $M_{\text{area}}$  against leaf  
**1490**  $C_i:C_a$ . The third model regressed  $N_{\text{mass}}$  against leaf  $C_i:C_a$  and  $M_{\text{area}}$  (Dong et al.  
**1491** 2017; Dong et al. 2020). The fourth model regressed leaf  $C_i:C_a$  against  $\beta$  and  
**1492** VPD. The fifth model regressed  $\beta$  against soil nitrogen availability, soil moisture,  
**1493** ability to associate with symbiotic nitrogen-fixing bacteria, and photosynthetic  
**1494** pathway. The sixth model regressed soil nitrogen availability against soil mois-  
**1495** ture. All models included the relevant timescale selected in the individual linear  
**1496** mixed effect models explained above. Models included species as a random inter-  
**1497** cept term, were built using the ‘lme’ function in the ‘nlme’ R package (Pinheiro  
**1498** and Bates 2022), and subsequently loaded into the piecewise structural equation  
**1499** model using the ‘psem’ function in the ‘piecewiseSEM’ R package (Lefcheck 2016).

**1500** 4.3 Results

**1501** 4.3.1 *Cost to acquire nitrogen relative to water*

**1502** Model selection indicated that 90-day soil moisture conferred the best model fit  
**1503** for  $\beta$  ( $AICc=1429.14$ ; Table S2; Fig. S1).

**1504** Increasing soil nitrogen availability generally decreased  $\beta$  ( $p < 0.001$ ; Table

1505 4.2; Fig. 4.2a), a pattern driven by a negative effect of increasing soil nitrogen on  $\beta$   
1506 in C<sub>3</sub> nonlegumes (Tukey:  $p = 0.002$ ) and C<sub>3</sub> legumes (Tukey:  $p = 0.031$ ) despite  
1507 a null effect of soil nitrogen on  $\beta$  in C<sub>4</sub> nonlegumes (Tukey:  $p = 0.905$ ). There  
1508 was no effect of soil moisture on  $\beta$  ( $p = 0.902$ ; Table 4.2; Fig. 4.2b). A functional  
1509 group effect ( $p < 0.001$ ; Table 4.2) indicated that C<sub>4</sub> nonlegumes generally had  
1510 lower  $\beta$  values than both C<sub>3</sub> legumes and C<sub>3</sub> non-legumes (Tukey:  $p < 0.001$   
1511 in both cases), while  $\beta$  values in C<sub>3</sub> legumes did not differ from C<sub>3</sub> nonlegumes  
1512 (Tukey:  $p = 0.804$ ).

**Table 4.2.** Effects of soil moisture, soil nitrogen availability, and plant functional group on  $\beta$ 

	df	Coefficient	$\chi^2$	p
Intercept	-	3.39E+00	-	-
Soil moisture (SM <sub>90</sub> )	1	-2.03E-01	0.015	0.902
Soil N (N)	1	-1.49E-02	13.832	<b>&lt;0.001</b>
PFT	2	-	225.049	<b>&lt;0.001</b>
SM <sub>90</sub> *N	1	-8.86E-04	1.016	0.313
SM <sub>90</sub> *PFT	2	-	0.754	0.686
N*PFT	2	-	5.236	0.073
SM <sub>90</sub> *N*PFT	2	-	3.633	0.163

**1513** \*Significance determined using Type II Wald  $\chi^2$  tests ( $\alpha = 0.05$ ). P-values  $< 0.05$

**1514** are in bold. Model coefficients are expressed on the natural-log scale and are only

**1515** included for continuous fixed effects. Key: df = degrees of freedom,  $\chi^2$  = Wald

**1516** Type II chi-square test statistic

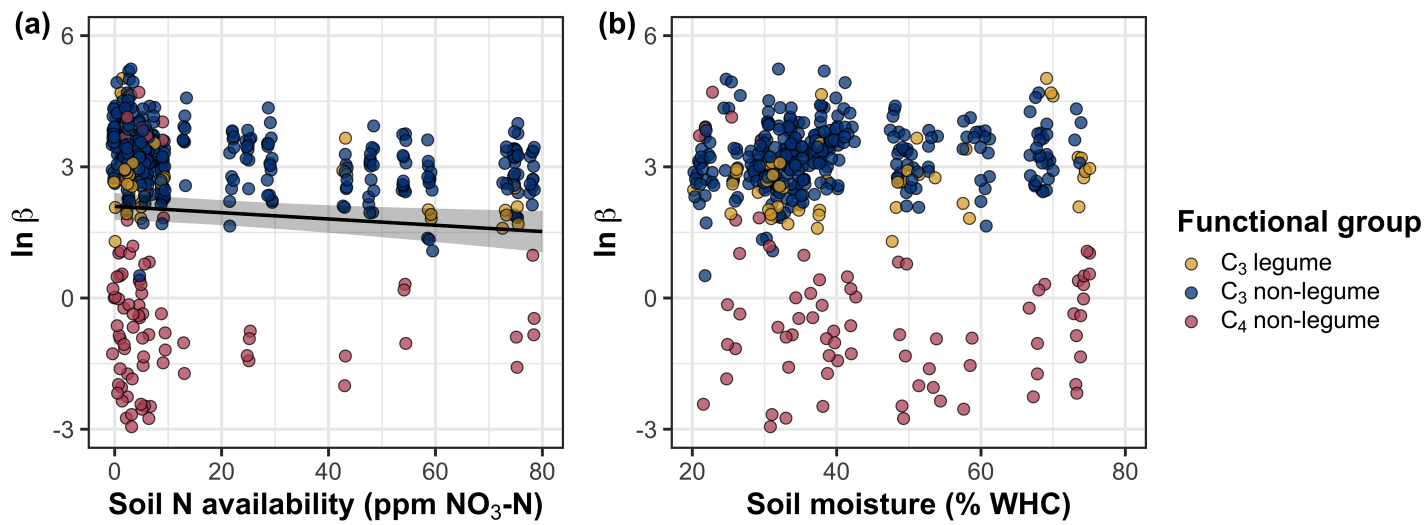


**Figure 4.2.** Effects of soil nitrogen availability (a) and 90-day soil moisture (b) on the unit cost ratio  $\beta$ . In (b), soil moisture is represented as a percent of site water holding capacity. Yellow shading and trendlines indicate C<sub>3</sub> legumes, blue shading and trendlines indicate C<sub>3</sub> non-legumes, and red shading and trendlines indicate C<sub>4</sub> non-legumes. Points are jittered for visibility. Variably colored trendlines are only included if there is an interaction between the x-axis and plant functional group, where solid trendlines indicate slopes that are different from zero ( $p < 0.05$ ) and dashed trendlines indicate slopes that are not different from zero ( $p > 0.05$ ). Error ribbons represent the upper and lower 95% confidence intervals of each fitted trendline.

**1517** 4.3.2  $C_i:C_a$

**1518** Model selection indicated that 4-day daily VPD was the timescale that conferred

**1519** the best model fit for leaf  $C_i:C_a$  (AICc = -793.49; Table S1; Fig. S2).

**1520** Model results revealed that increasing VPD generally decreased leaf  $C_i:C_a$

**1521** ( $p < 0.001$ ; Table 4.3; Fig. 4.3a). There was no effect of soil moisture ( $p =$

**1522** 0.843; Table 4.3; Fig. 4.3b) or soil nitrogen availability ( $p = 0.544$ ; Table 4.3;

**1523** Fig. 4.3c) on leaf  $C_i:C_a$ . A strong plant functional group effect ( $p < 0.001$ ; Table

**1524** 4.3) indicated that C<sub>4</sub> nonlegumes had lower leaf  $C_i:C_a$  than C<sub>3</sub> legumes and C<sub>3</sub>

**1525** nonlegumes (Tukey:  $p < 0.001$  in both cases), with no difference between C<sub>3</sub>

**1526** legumes and C<sub>3</sub> nonlegumes (Tukey:  $p = 0.865$ ).

**Table 4.3.** Effects of soil moisture, soil nitrogen availability, and plant functional group on leaf  $C_i:C_a$ \*

	df	Coefficient	$\chi^2$	p
Intercept	-	1.32E+00	-	-
Vapor pressure deficit ( $VPD_4$ )	1	-4.53E-01	11.211	<b>&lt;0.001</b>
Soil moisture ( $SM_{90}$ )	1	-1.71E-01	0.039	0.843
Soil N (N)	1	-3.33E-03	0.369	0.544
PFT	2	-	227.005	<b>&lt;0.001</b>
$SM_{90}^*N$	1	need this	2.361	0.124
$VPD_4^*PFT$	2	-	0.927	0.629
$SM_{90}^*PFT$	2	-	0.817	0.664
$N^*PFT$	2	-	4.085	0.130
$SM_{90}^*N^*PFT$	2	-	3.677	0.159

**1527** \*Significance determined using Type II Wald  $\chi^2$  tests ( $\alpha = 0.05$ ). *P*-values less  
**1528** than 0.05 are in bold and *p*-values where  $0.05 < p < 0.1$  are italicized. Leaf  $C_i:C_a$   
**1529** was not transformed prior to model fitting, so model coefficients are reported  
**1530** on the response scale. Model coefficients are only included for continuous fixed  
**1531** effects.

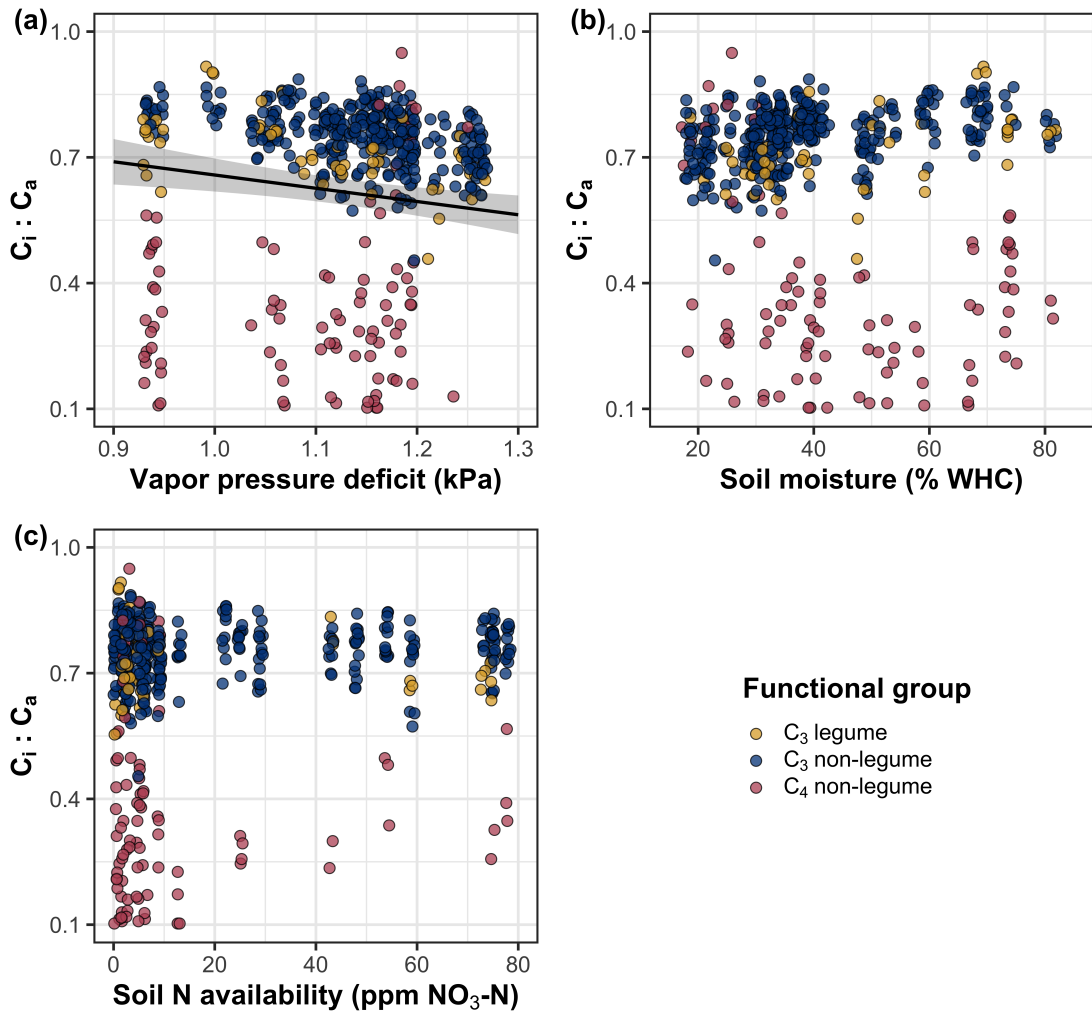


**Figure 4.3.** Effects of 4-day mean vapor pressure deficit (a), 90-day soil moisture (per water holding capacity; b), and soil nitrogen availability (c) on leaf  $C_i:C_a$ . Shading and trendlines are as explained in Figure 4.3. Points are jittered for visibility. Variably colored trendlines are only included if there is an interaction between the x-axis and plant functional group, where solid trendlines indicate slopes that are different from zero ( $p < 0.05$ ) and dashed trendlines indicate slopes that are not different from zero ( $p < 0.05$ ). Error ribbons represent the upper and lower 95% confidence intervals of each fitted trendline.

**1532** 4.3.3 *Leaf nitrogen content*

**1533** An interaction between leaf  $C_i:C_a$  and plant functional group ( $p < 0.001$ ;  
**1534** Table 4.4) revealed that the negative effect of increasing leaf  $C_i:C_a$  on  $N_{area}$  ( $p <$   
**1535** 0.001; Table 4.4) was driven by a negative effect of increasing leaf  $C_i:C_a$  on  $N_{area}$   
**1536** in C<sub>3</sub> nonlegumes (Tukey:  $p < 0.001$ ) and C<sub>3</sub> legumes (Tukey:  $p = 0.002$ ), with no  
**1537** observable effect in C<sub>4</sub> nonlegumes (Tukey:  $p = 0.795$ ; Fig. 4.4a). An interaction  
**1538** between soil nitrogen availability and plant functional group ( $p = 0.041$ ; Table  
**1539** 4.4) indicated that the positive effect of increasing soil nitrogen ( $p = 0.007$ ; Table  
**1540** 4.4) was only apparent in C<sub>3</sub> legumes (Tukey:  $p < 0.001$ ; Table 4.4; Fig. 4.4d),  
**1541** with no observable effect in C<sub>3</sub> nonlegumes (Tukey:  $p = 0.449$ ) or C<sub>4</sub> nonlegumes  
**1542** (Tukey:  $p = 0.680$ ). Increasing soil moisture increased  $N_{area}$  ( $p=0.010$ , Table  
**1543** 4.4). A plant functional group effect ( $p < 0.001$ ; Table 4.4) indicated that C<sub>4</sub>  
**1544** nonlegumes had lower  $N_{area}$  compared to C<sub>3</sub> legumes (Tukey:  $p < 0.001$ ) and C<sub>3</sub>  
**1545** nonlegumes (Tukey:  $p < 0.001$ ), while C<sub>3</sub> legumes had lower  $N_{area}$  compared to  
**1546** C<sub>3</sub> nonlegumes (Tukey:  $p = 0.030$ ).

**1547** A marginal interaction between soil nitrogen availability and soil moisture  
**1548** ( $p = 0.097$ ; Table 4.4) indicated that the positive effect of increasing soil nitrogen  
**1549** on  $N_{mass}$  ( $p < 0.001$ ; Table 4.4; Fig. 4.4e) was only apparent when soil moisture  
**1550** was less than 50% of the maximum water holding capacity (Tukey:  $p < 0.05$  in  
**1551** all cases). There was no effect of leaf  $C_i:C_a$  on  $N_{mass}$  ( $p = 0.447$ ; Table 4.4; Fig.  
**1552** 4.4b), but a positive effect of increasing soil moisture on  $N_{mass}$ . A plant functional  
**1553** group effect ( $p < 0.001$ ; Table 4.4) indicated that C<sub>4</sub> nonlegumes had lower  $N_{mass}$   
**1554** compared to C<sub>3</sub> legumes (Tukey:  $p=0.003$ ) and C<sub>3</sub> nonlegumes (Tukey:  $p =$   
**1555** 0.011), while  $N_{mass}$  did not differ between C<sub>3</sub> legumes and C<sub>3</sub> nonlegumes (Tukey:

**1556**  $p = 0.231$ ).

**1557** Variance in  $M_{\text{area}}$  was driven by a three-way interaction between soil ni-  
**1558** trogen availability, soil moisture, and plant functional group ( $p = 0.018$ ; Table  
**1559** 4.4). This interaction indicated that increasing soil moisture increased the posi-  
**1560** tive effect of increasing soil nitrogen availability on  $M_{\text{area}}$  in C<sub>3</sub> legumes (Tukey:  
**1561**  $p = 0.030$ ) but did not modify the negative effect of increasing soil nitrogen on  
**1562**  $M_{\text{area}}$  in C<sub>4</sub> nonlegumes (Tukey:  $p = 0.511$ ) or C<sub>3</sub> nonlegumes (Tukey:  $p > 0.999$ ).  
**1563** There was otherwise no effect of soil moisture on  $M_{\text{area}}$  ( $p = 0.696$ ; Table 4.4).  
**1564** An interaction between leaf  $C_i:C_a$  and plant functional group ( $p < 0.001$ ; Table  
**1565** 4.4; Fig. 4.4c) indicated that negative effect of increasing leaf  $C_i:C_a$  on  $M_{\text{area}}$  ( $p$   
**1566**  $< 0.001$ ; Table 4.4) was driven by a negative effect of increasing leaf  $C_i:C_a$  on  
**1567**  $M_{\text{area}}$  in C<sub>3</sub> legumes and C<sub>3</sub> nonlegumes (Tukey:  $p < 0.001$  in both cases), with  
**1568** no effect in C<sub>4</sub> nonlegumes (Tukey:  $p = 0.343$ ; Fig. 4.4c).

**Table 4.4.** Effects of soil nitrogen fertilization, inoculation, and CO<sub>2</sub> treatments on  $N_{\text{area}}$ ,  $N_{\text{mass}}$ , and  $M_{\text{area}}$ 

	df	$N_{\text{area}}$			$N_{\text{mass}}$			$M_{\text{area}}$		
		Coefficient	$\chi^2$	p	Coefficient	$\chi^2$	p	Coefficient	$\chi^2$	p
(Intercept)	-	2.41E+00	-	-	6.28E-02	-	-	6.90E+00	-	-
$C_i:C_a$	1	-2.32E+00	7.386	<b>0.007</b>	8.04E-01	0.578	0.447	-3.13E+00	15.913	<0.001
Soil N (N)	1	1.26E-02	6.070	<b>0.014</b>	1.12E-02	90.940	<0.001	-2.66E-02	43.529	<0.001
Soil moisture (SM <sub>90</sub> )	1	5.60E-01	6.717	<b>0.010</b>	7.81E-01	11.205	<0.001	-2.53E-01	0.153	0.696
PFT	1	-	52.277	<0.001	-	17.184	<0.001	-	7.289	<b>0.026</b>
SM <sub>90</sub> *N	1	5.44E-02	0.444	0.505	-1.91E-02	2.749	0.097	8.16E-02	1.690	0.194
$C_i:C_a$ *PFT	1	-	25.631	<0.001	-	4.864	0.078	-	34.683	<0.001
N*PFT	1	-	6.389	<b>0.041</b>	-	1.219	0.544	-	19.949	<0.001
SM <sub>90</sub> *PFT	1	-	3.548	0.170	-	0.911	0.634	-	3.293	0.193
SM <sub>90</sub> *N*PFT	1	-	3.520	0.172	-	0.092	0.955	-	7.987	<b>0.018</b>

<sup>9</sup>  
**1569** \*Significance determined using Type II Wald  $\chi^2$  tests ( $\alpha = 0.05$ ). P-values less than 0.05 are in bold and p-values  
**1570** where  $0.05 < p < 0.1$  are italicized. Coefficients are reported on the natural-log scale and are only included for  
**1571** continuous fixed effects.

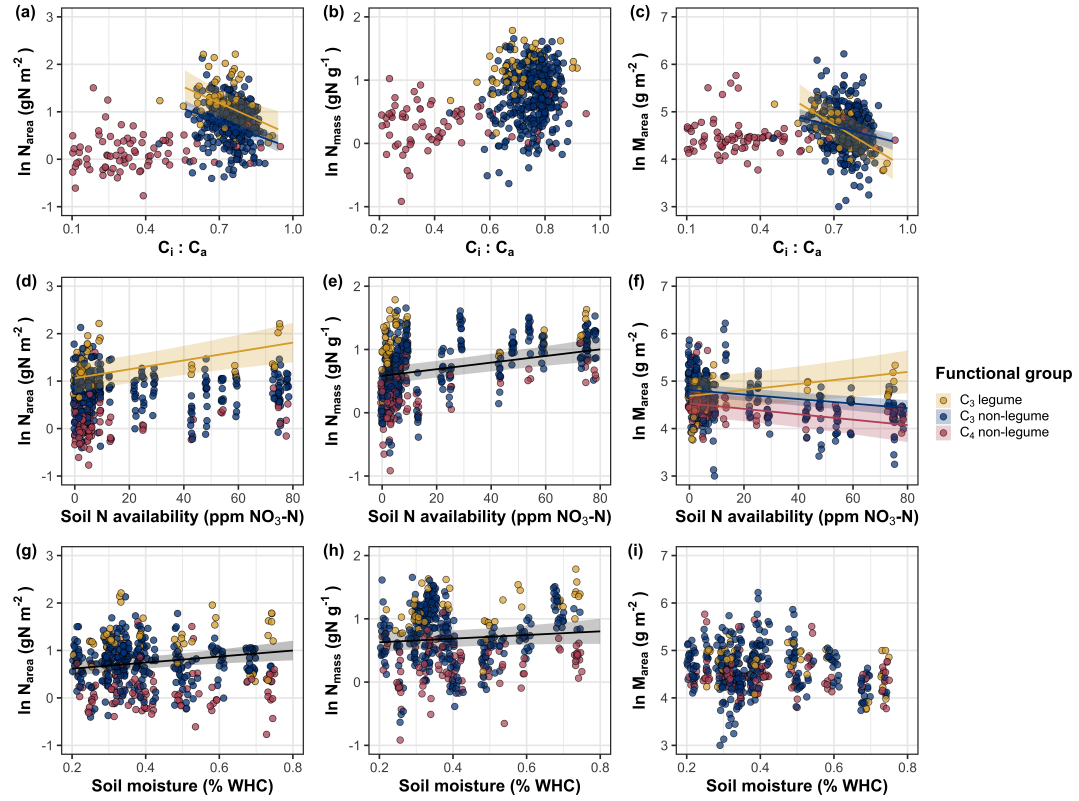


**Figure 4.4.** Effects of leaf  $C_i:C_a$  (a-c), soil nitrogen availability (d-f), and soil moisture (g-i) on leaf nitrogen content per unit leaf area (a, d, g), leaf nitrogen content per unit leaf biomass (b, e, h), and leaf mass per area (c, f, i). Yellow points and trendlines indicate  $C_3$  legumes, blue points and trendlines indicate  $C_3$  nonlegumes, and red points and trendlines indicate  $C_4$  nonlegumes. Points are jittered for visibility. Variably colored trendlines are only included if there is an interaction between plant functional group and the x-axis. Black solid trendlines denote bivariate slopes that are different from zero ( $p < 0.05$ ) where there is no apparent interaction between plant functional group and the x-axis.

**1572** 4.3.4 *Structural equation model*

**1573** The piecewise structural equation model explained 89%, 56%, 77%, 82%, and 37%  
**1574** of variance in  $N_{\text{area}}$ ,  $N_{\text{mass}}$ ,  $M_{\text{area}}$ , leaf  $C_i:C_a$ , and  $\beta$ , respectively (Table 4.5; Fig.  
**1575** 4.5). Variance in  $N_{\text{area}}$  was driven by a positive effect of increasing  $N_{\text{mass}}$  and  
**1576**  $M_{\text{area}}$  ( $p < 0.001$  in both cases; Table 4.5; Fig. 4.5). Model results indicated that  
**1577** an indirect negative effect of  $C_i:C_a$  on  $N_{\text{area}}$  was driven by a strong reduction in  
**1578**  $M_{\text{area}}$  with increasing leaf  $C_i:C_a$  ( $p < 0.001$ ; Table 4.5) paired with no effect of  
**1579** increasing  $C_i:C_a$  on  $N_{\text{mass}}$  ( $p = 0.111$ ; Table 4.5). However, there was a strong  
**1580** negative effect of increasing  $M_{\text{area}}$  on  $N_{\text{mass}}$  ( $p < 0.001$ ; Table 4.5; Fig. 4.5).  
**1581** Leaf  $C_i:C_a$  increased with increasing  $\beta$  ( $p < 0.001$ ; Table 4.5) and decreased with  
**1582** increasing VPD ( $p < 0.001$ ; Table 4.5; Fig. 4.5). Variance in  $\beta$  was driven by a  
**1583** negative effect of increasing soil nitrogen availability ( $p < 0.001$ ; Table 4.5) and  
**1584** was generally higher in C3 species ( $p < 0.001$ ; Table 4.5; Fig. 4.5). However,  
**1585**  $\beta$  did not change with soil moisture ( $p = 0.904$ ; Table 4.5) or with ability to  
**1586** acquire nitrogen via symbiotic nitrogen fixation ( $p = 0.495$ ; Table 4.5). Finally,  
**1587** soil nitrogen availability was positively associated with increasing soil moisture ( $p$   
**1588** = 0.002; Table 4.5; Fig. 4.5).

**Table 4.5.** Structural equation model results investigating direct effects of climatic and soil resource availability on  $N_{\text{area}}$ ,  $N_{\text{mass}}$ ,  $M_{\text{area}}$ , leaf  $C_i:C_a$ , and  $\beta$ 

Predictor	Coefficient	<i>p</i>
$N_{\text{area}} (R^2_c = 0.89)$		
$M_{\text{area}}$	0.758	<b>&lt;0.001</b>
$N_{\text{mass}}$	0.781	<b>&lt;0.001</b>
$N_{\text{mass}} (R^2_c = 0.56)$		
Leaf $C_i:C_a$	0.092	0.111
$M_{\text{area}}$	-0.311	<b>&lt;0.001</b>
$M_{\text{area}} (R^2_c = 0.77)$		
Leaf $C_i:C_a$	-0.237	<b>&lt;0.001</b>
Leaf $C_i:C_a (R^2_c) = 0.82$		
$\beta$	0.309	<b>&lt;0.001</b>
$\text{VPD}_4$	-0.110	<b>&lt;0.001</b>
$\beta (R^2_c = 0.37)$		
Soil N	-0.213	<b>&lt;0.001</b>
$\text{SM}_{90}$	-0.006	0.904
Photo. pathway	0.446	<b>&lt;0.001</b>
N-fixing ability	-0.056	0.495
Soil N ( $R^2_c = 0.35$ )		
$\text{SM}_{90}$	-0.154	<b>0.002</b>

1589 \*Reported coefficients are standardized across the structural equation model.  $P$ -  
 1590 values less than 0.05 are noted in bold. Positive coefficients for photosynthetic  
 1591 pathway indicate generally larger values in C<sub>3</sub> species, while positive coefficients  
 1592 for N-fixing ability indicate generally larger values in N-fixing species. Key:  $N_{\text{area}}$   
 1593 = leaf nitrogen content per unit leaf area,  $M_{\text{area}}$  = leaf mass per unit leaf dry  
 1594 biomass,  $N_{\text{mass}}$  = leaf nitrogen content per unit leaf dry biomass,  $\beta$  = cost of  
 1595 acquiring nitrogen relative to water,  $\text{VPD}_4$  = 4-day mean vapor pressure deficit,  
 1596  $\text{SM}_{90}$  = 90-day mean soil moisture,  $R^2_c$  = conditional R<sup>2</sup> value

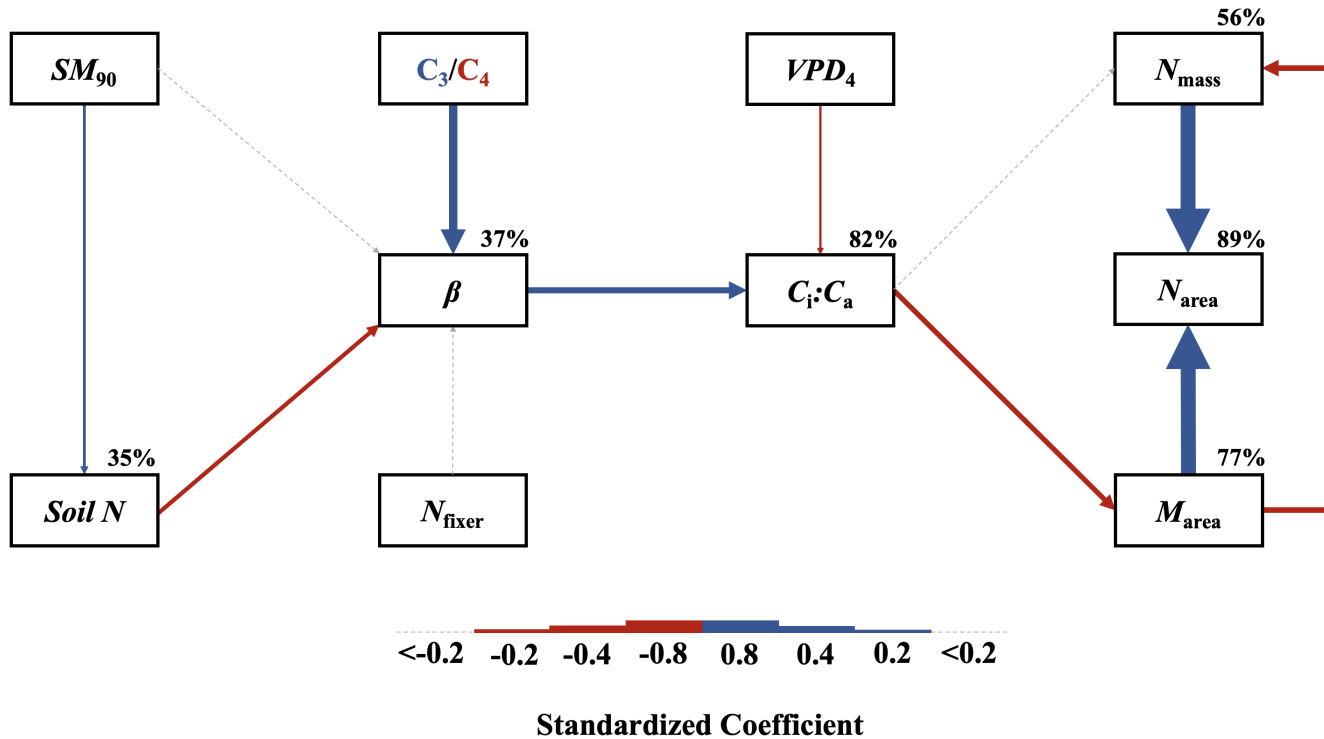


**Figure 4.5.** Structural equation model results exploring drivers of  $N_{area}$ . Boxes indicate measured edaphic factors, climatic factors, and leaf traits. Solid arrows indicate bivariate relationships where  $p < 0.05$ , while dashed arrows indicate relationships where  $p > 0.05$ . Positive model coefficients are indicated through blue arrows, negative model coefficients are indicated through red arrows, and insignificant coefficients ( $p > 0.05$ ) are indicated through gray dashed arrows. Arrow thickness scales with the standardized model coefficient of each bivariate relationship. A positive coefficient for photosynthetic pathway indicates larger values in  $C_3$  species, while a positive coefficient for  $N_{fixer}$  indicates larger values in N-fixing species. Standardized model coefficients and associated  $p$ -values are reported in Table 4.5, with conditional R<sup>2</sup> values for each response variable reported on the top right of each box.

**1597** 4.4 Discussion

**1598** In this study, we quantified direct and indirect effects of soil resource availability,  
**1599** climate, leaf  $C_i:C_a$ , and  $\beta$  on  $N_{\text{area}}$  and components of  $N_{\text{area}}$  ( $N_{\text{mass}}$  and  $M_{\text{area}}$ ) in  
**1600** 520 individuals spanning across a soil resource availability and climate gradient  
**1601** in Texas, USA. We found consistent support for patterns expected from photo-  
**1602** synthetic least-cost theory, a result driven by a strong direct negative relationship  
**1603** between the relative costs to acquire nitrogen versus water ( $\beta$ ) on  $N_{\text{area}}$  as me-  
**1604** diated through changes in the leaf  $C_i:C_a$  ratio. In further support of patterns  
**1605** expected from theory, increasing soil nitrogen availability had a strong negative  
**1606** effect on  $\beta$ , resulting in an indirect stimulation in  $N_{\text{area}}$ . Increasing VPD also  
**1607** indirectly increased  $N_{\text{area}}$  through a direct negative effect of increasing VPD on  
**1608** leaf  $C_i:C_a$ . Interestingly, a strong positive association between soil moisture and  
**1609**  $N_{\text{area}}$  was driven by positive covariance between soil moisture and soil nitrogen  
**1610** availability and was not associated with a direct effect of soil moisture on  $\beta$ .  
**1611** Overall, results provide strong and consistent support for patterns expected from  
**1612** photosynthetic least-cost theory, showing that both soil resource availability and  
**1613** climate drive variance in  $N_{\text{area}}$  through changes in leaf  $C_i:C_a$ .

**1614** 4.4.1 *Negative effects of leaf  $C_i:C_a$  on  $N_{\text{area}}$  are driven by reductions in  $M_{\text{area}}$ ,*  
**1615** *not  $N_{\text{mass}}$*

**1616** A strong negative effect of increasing leaf  $C_i:C_a$  on  $N_{\text{area}}$  was detected in both  
**1617** the linear mixed effect and piecewise structural equation models. The negative  
**1618** response of  $N_{\text{area}}$  to increasing leaf  $C_i:C_a$  is consistent with previous environmental  
**1619** gradient (Dong et al. 2017; Querejeta et al. 2022) and manipulation experiments

1620 (Perkowski et al. n.d.), showing strong support for the nitrogen-water use tradeoffs  
1621 expected from photosynthetic least cost theory (Wright et al. 2003; Prentice et al.  
1622 2014). Negative effects of increasing leaf  $C_i:C_a$  on  $N_{\text{area}}$  were driven by a strong  
1623 negative effect of increasing  $C_i:C_a$  on  $M_{\text{area}}$ , with no apparent effect of leaf  $C_i:C_a$   
1624 on  $N_{\text{mass}}$ , suggesting that changes in  $N_{\text{area}}$  were driven by changes in leaf structure  
1625 and not leaf chemistry. Interestingly, increasing  $M_{\text{area}}$  was negatively associated  
1626 with  $N_{\text{mass}}$ , indicating that an increase in  $N_{\text{mass}}$  was associated with larger, thinner  
1627 leaves (i.e. lower  $M_{\text{area}}$ ). These results are consistent with patterns reported  
1628 from previous studies indicating that variance in  $N_{\text{area}}$  is driven by changes in  
1629  $M_{\text{area}}$  across environmental gradients, and that part of this response is due to  
1630 negative covariance between  $M_{\text{area}}$  and  $N_{\text{mass}}$  associated with tradeoffs between  
1631 leaf longevity and leaf productivity (Wright et al. 2004; Dong et al. 2017; Dong  
1632 et al. 2022; Querejeta et al. 2022; Wang et al. 2023).

1633 The negative relationship between leaf  $C_i:C_a$  and  $M_{\text{area}}$  could be also re-  
1634 sponse that allows leaves to maximize productivity in shorter-lived leaves. Trade-  
1635 offs between leaf longevity and leaf productivity are commonly observed and are  
1636 included in a continuum of coordinated leaf traits that position individuals along  
1637 a fast- or slow-growing leaf economics spectrum (Wright et al. 2003; Onoda et al.  
1638 2004; Onoda et al. 2017; Reich 2014; Wang et al. 2023). Negative relationships  
1639 between  $C_i:C_a$  and  $M_{\text{area}}$  indicate that increased stomatal conductance and re-  
1640 duced water use efficiency were associated with thinner, larger leaves (i.e., lower  
1641  $M_{\text{area}}$ ). These patterns, combined with the negative relationship between  $M_{\text{area}}$   
1642 and  $N_{\text{mass}}$  mentioned above, likely allowed individuals to maximize light intercep-  
1643 tion and productivity by exploiting high light environments, though this may come

1644 at the expense of increased water loss and decreased water-use efficiency. This  
1645 strategy may be especially advantageous for fast-growing species in open canopy  
1646 systems. In this study, C<sub>3</sub> legumes and C<sub>3</sub> nonlegumes dominated the dataset  
1647 (78% of total sampling effort), of which 22% (17% of total sampling effort) were  
1648 classified as annual species with short growing seasons. We observed no effect of  
1649 leaf C<sub>i</sub>:C<sub>a</sub> on N<sub>area</sub> or M<sub>area</sub> in C<sub>4</sub> nonlegumes, which made up 22% of the sampling  
1650 effort and were generally classified as warm season graminoid species with slower  
1651 growth rates and longer growing seasons. These patterns indicate that stronger  
1652 tradeoffs between nitrogen and water use may be more apparent in fast-growing  
1653 species with high demand for building and maintaining productive leaf tissues.

1654 4.4.2 *Soil nitrogen availability increases N<sub>area</sub> through changes in the cost to*  
1655 *acquire nitrogen*

1656 The null effect of soil nitrogen availability on N<sub>area</sub> was driven by positive  
1657 and negative respective effects of increasing soil nitrogen availability on N<sub>mass</sub> and  
1658 M<sub>area</sub> that were equal in magnitude. The null response of N<sub>area</sub> to soil nitrogen  
1659 availability occurred alongside a negative effect of increasing soil nitrogen availabil-  
1660 ity on  $\beta$ , which, paired with the negative relationship between leaf C<sub>i</sub>:C<sub>a</sub> and N<sub>area</sub>,  
1661 suggests a general positive effect of increasing soil nitrogen availability on N<sub>area</sub>,  
1662 but only when mediated through changes in  $\beta$ . This result is consistent with our  
1663 hypotheses and patterns expected from photosynthetic least-cost theory. These  
1664 results suggest that positive direct effects of increasing soil nitrogen availability  
1665 on N<sub>area</sub> are not ubiquitous across environmental gradients. Instead, as predicted  
1666 by our hypotheses and patterns expected from theory, positive responses of N<sub>area</sub>

1667 to increasing soil nitrogen availability are a deterministic acclimation response to  
1668 shifts in climate-related demand to build and maintain photosynthetic enzymes,  
1669 which allows plants to optimize photosynthetic processes and resource use to a  
1670 given environment (Paillassa et al. 2020; Peng et al. 2021; Dong et al. 2022;  
1671 Westerband et al. 2023).

1672 4.4.3 *Soil moisture increases  $N_{\text{area}}$  by facilitating increases in soil nitrogen  
1673 availability*

1674 Increasing soil moisture generally had no effect on  $N_{\text{area}}$ , a response that was as-  
1675 sociated with a null effect of soil moisture on  $\beta$ . These results contrast patterns  
1676 expected from theory, where increasing soil moisture is expected to indirectly de-  
1677 crease  $N_{\text{area}}$  through an increase in  $\beta$  due to a reduction in costs associated with  
1678 water acquisition and use (Wright et al. 2003; Prentice et al. 2014; Lavergne  
1679 et al. 2020). Interestingly, structural equation model results revealed a strong  
1680 positive association between soil moisture and soil nitrogen availability, indicat-  
1681 ing an indirect positive effect of increasing soil moisture on  $N_{\text{area}}$  mediated by the  
1682 negative effect of increasing soil nitrogen availability on  $\beta$ . In Texan grasslands,  
1683 productivity and nutrient uptake are often co-limited by precipitation and nutrient  
1684 availability (Yahdjian et al. 2011; Wang et al. 2017). Thus, increases in soil mois-  
1685 ture may have facilitated more favorable and productive environments for soil  
1686 microbial communities, thereby stimulating the accumulation of plant-available  
1687 nitrogen substrate through increased ammonification or nitrification rates (Reich-  
1688 man et al. 1966; Stark and Firestone 1995; Paul et al. 2003). Alternatively, soil  
1689 moisture may have facilitated greater nitrogen mobility through soil solution. As  
1690 discussed above, the positive indirect response of  $N_{\text{area}}$  to increasing soil nitrogen  
1691 availability as mediated through reductions in  $\beta$  follow patterns expected from

**1692** theory.

**1693** 4.4.4 *Indirect effects of climate on  $N_{\text{area}}$  are mediated through changes in leaf*  
**1694**  $C_i:C_a$  *and  $\beta$*

**1695** In support of our hypothesis and patterns expected from theory, increasing VPD  
**1696** indirectly increased  $N_{\text{area}}$ , mediated through the negative effect of increasing VPD  
**1697** on leaf  $C_i:C_a$ . These responses are consistent with previous work noting strong  
**1698** reductions in stomatal conductance with increasing VPD (Oren et al. 1999; Novick  
**1699** et al. 2016; Sulman et al. 2016; Grossiord et al. 2020; López et al. 2021), a  
**1700** response that allows plants to minimize water loss as a result of high atmospheric  
**1701** water demand. Results also support findings from previous experiments across  
**1702** environmental gradients, where increasing VPD generally increases  $N_{\text{area}}$  at lower  
**1703** stomatal conductance across environmental gradients (Dong et al. 2017; Dong  
**1704** et al. 2022; Paillassa et al. 2020; Westerband et al. 2023).

**1705** 4.4.5 *Species identity traits modify effects of the environment on  $\beta$ , leaf  $C_i:C_a$ ,*  
**1706** *and  $N_{\text{area}}$*

**1707** N-fixing species generally had higher  $N_{\text{area}}$  values on average compared to non-  
**1708** fixing species, a pattern driven by a stronger stimulation in  $N_{\text{mass}}$  in N-fixing  
**1709** species coupled with no change in  $M_{\text{area}}$  between species with different N-fixation  
**1710** ability. We found no evidence to suggest that N-fixing species had different  $\beta$  or  
**1711** leaf  $C_i:C_a$  values compared to non-fixing species across the environmental gradient.  
**1712** These results follow patterns from previous environmental gradient experiments  
**1713** that investigate variance in leaf nitrogen allocation in N-fixing species (Adams  
**1714** et al. 2016; Dong et al. 2017; Dong et al. 2020), and that increases in  $N_{\text{mass}}$   
**1715** and  $N_{\text{area}}$  in N-fixing species are not necessarily correlated to increases in water

1716 use efficiency or reductions in leaf  $C_i:C_a$  (Adams et al. 2016). While our results  
1717 are consistent with results from previous environmental gradient experiments,  
1718 they do not necessarily support our hypothesis or patterns expected from theory,  
1719 which predicts that stimulations in  $N_{area}$  by N-fixing species should be driven  
1720 by a reduction in  $\beta$  relative to non-fixing species, and that this response should  
1721 decrease stomatal conductance and leaf  $C_i:C_a$ .

1722 C<sub>4</sub> species generally had lower  $\beta$ , leaf  $C_i:C_a$ , and  $N_{area}$  than C<sub>3</sub> species.  
1723 Reduced  $\beta$  and leaf  $C_i:C_a$  values in C<sub>4</sub> species follow our hypothesis, a pattern  
1724 that could be the result of either reduced costs of nitrogen acquisition and use or  
1725 increased costs of water acquisition and use or both (Wright et al. 2003, Prentice  
1726 et al. 2014). Results also indicate that  $\beta$  in C<sub>4</sub> nonlegumes was unresponsive to  
1727 changes in soil nitrogen availability despite an apparent negative effect of increas-  
1728 ing soil nitrogen availability on  $\beta$  in C<sub>3</sub> legumes and C<sub>3</sub> nonlegumes. Combined  
1729 with a general null response of  $\beta$  to soil moisture regardless of plant functional  
1730 group, these patterns imply that reduced  $\beta$  values in C<sub>4</sub> species may be the re-  
1731 sult of lower costs of nitrogen acquisition and use relative to C<sub>3</sub> species. While  
1732 lower  $\beta$  values in C<sub>4</sub> species provides a possible explanation for why C<sub>4</sub> species  
1733 often have lower leaf  $C_i:C_a$  and greater water use efficiency, theory predicts that  
1734 this response should cause C<sub>4</sub> species to have greater  $N_{area}$  values compared to  
1735 C<sub>3</sub> species, though C<sub>4</sub> species commonly exhibit lower  $N_{area}$  and higher nitrogen  
1736 use efficiency than C<sub>3</sub> species (Schmitt and Edwards 1981; Sage and Pearcy 1987;  
1737 Ghannoum et al. 2011). We speculate that lowered costs of nitrogen acquisition  
1738 and use in C<sub>4</sub> species could be driven by more efficient Rubisco carboxylation effi-  
1739 ciency in C<sub>4</sub> species associated with CO<sub>2</sub> concentrating mechanisms that eliminate

1740 photorespiration (Ghannoum et al. 2011), which could reduce or eliminate the  
1741 need to sacrifice inefficient nitrogen use for efficient water use to achieve optimal  
1742 photosynthesis rates.

1743 4.4.6 *Next steps for optimality model development*

1744 Optimality models for both C<sub>3</sub> and C<sub>4</sub> species have been developed using principles  
1745 from photosynthetic least-cost theory (Prentice et al. 2014; Wang et al. 2017;  
1746 Smith et al. 2019; Stocker et al. 2020; Scott and Smith 2022). In both C<sub>3</sub> and  
1747 C<sub>4</sub> model variants,  $\beta$  values are held constant using global datasets of leaf  $\delta^{13}\text{C}$   
1748 (Wang et al. 2017; Cornwell et al. 2018). Specifically, the C<sub>3</sub> optimality model  
1749 initially assumed a constant  $\beta$  value of 240 (Wang et al. 2017), later corrected to  
1750 146 (Stocker et al. 2020), while the C<sub>4</sub> optimality model assumes a constant  $\beta$   
1751 value of 166 (Scott and Smith 2022). Our results, which build on findings from  
1752 Paillassa et al. (2020), demonstrate high variability in calculated  $\beta$  values across  
1753 environmental gradients. Specifically,  $\beta$  values in C<sub>3</sub> species ranged from 1.7 to  
1754 188.0 (mean: 30.2; median: 23.1; standard deviation: 25.4), while ranged from 0.1  
1755 to 110.6 in C<sub>4</sub> species (mean: 7.2; median: 0.7; standard deviation: 18.6). Mean  
1756  $\beta$  values in both C<sub>3</sub> and C<sub>4</sub> species were consistently lower than values currently  
1757 implemented in optimality models, though this was likely the result of increased  
1758 water limitation across our sites relative to global averages. Regardless, the high  
1759 degree of  $\beta$  variability across this environmental gradient, together with findings  
1760 from Lavergne et al. (2020) and Paillassa et al. (2020), suggests that the use of  
1761 constant  $\beta$  values may contribute to erroneous errors when conducting optimality  
1762 model simulations. We therefore build on suggestions from Wang et al. (2017),  
1763 recommending future photosynthetic least-cost model developments to consider

**1764** the use of dynamic  $\beta$  values.

**1765** 4.4.7 *Conclusions*

**1766** To summarize, variability in  $N_{\text{area}}$  across an environmental gradient in Texan  
**1767** grasslands was driven by indirect effects of climate and soil resource availability  
**1768** mediated. Results from this experiment provide strong and consistent support  
**1769** for patterns expected from photosynthetic least-cost theory, demonstrating that  
**1770** negative relationships between  $C_i:C_a$  and  $N_{\text{area}}$  unify expected effects of climatic  
**1771** and edaphic characteristics on  $N_{\text{area}}$  across environmental gradients. Our results  
**1772** also demonstrate a need to consider the dynamic nature of the relative cost of  
**1773** nitrogen versus water uptake ( $\beta$ ) across environmental gradients in optimality  
**1774** models that leverage principles of photosynthetic least-cost theory.

1775

## Chapter 5

1776 Optimal resource investment to photosynthetic capacity maximizes  
1777 nutrient allocation to whole plant growth under elevated CO<sub>2</sub>

1778 5.1 Introduction

1779 Terrestrial ecosystems are regulated by complex carbon and nitrogen cy-  
1780 cles. As a result, terrestrial biosphere models, which are beginning to include  
1781 coupled carbon and nitrogen cycles (Shi et al. 2016; Davies-Barnard et al. 2020;  
1782 Braghieri et al. 2022), must accurately represent these cycles under different  
1783 environmental scenarios to reliably simulate carbon and nitrogen atmosphere-  
1784 biosphere fluxes (Hungate et al. 2003; Prentice et al. 2015). While the inclusion  
1785 of coupled carbon and nitrogen cycles tends to reduce model uncertainty (Arora  
1786 et al. 2020), large uncertainty in role of soil nitrogen availability and nitrogen ac-  
1787 quisition strategy on leaf and whole plant acclimation responses to CO<sub>2</sub> remains  
1788 (Smith and Dukes 2013; Terrer et al. 2018; Smith and Keenan 2020). This source  
1789 of uncertainty likely contributes to the widespread divergence in future carbon  
1790 and nitrogen flux simulations across terrestrial biosphere models (Friedlingstein  
1791 et al. 2014; Zaehle et al. 2014; Meyerholt et al. 2020).

1792 Plants grown under elevated CO<sub>2</sub> generally have less leaf nitrogen content  
1793 than those grown under ambient CO<sub>2</sub>, a response that often corresponds with  
1794 reductions in photosynthetic capacity and stomatal conductance at the leaf-level  
1795 and biomass stimulation over time at the whole plant level (Curtis 1996; Drake  
1796 et al. 1997; Ainsworth et al. 2002; Makino 2003; Morgan et al. 2004; Ainsworth  
1797 and Long 2005; Ainsworth and Rogers 2007; Smith and Dukes 2013; Poorter et al.  
1798 2022). As net primary productivity is generally limited by nitrogen availability

**1799** (Vitousek and Howarth 1991; LeBauer and Treseder 2008; Fay et al. 2015), and  
**1800** soil nitrogen availability is often positively correlated with leaf nitrogen content  
**1801** and photosynthetic capacity (Field and Mooney 1986; Evans and Seemann 1989;  
**1802** Evans 1989; Walker et al. 2014; Firn et al. 2019; Liang et al. 2020), some  
**1803** have hypothesized that leaf and whole plant acclimation responses to CO<sub>2</sub> are  
**1804** constrained by soil nitrogen availability. The progressive nitrogen limitation hy-  
**1805** pothesis predicts that elevated CO<sub>2</sub> will increase plant nitrogen demand, which  
**1806** will increase plant nitrogen uptake and progressively deplete soil nitrogen if soil  
**1807** nitrogen supply does not exceed plant nitrogen demand (Luo et al. 2004). The  
**1808** hypothesis predicts that this response should result in strong acute stimulations in  
**1809** whole plant growth and primary productivity that diminish over time as nitrogen  
**1810** becomes more limiting. Assuming a positive relationship between soil nitrogen  
**1811** availability, leaf nitrogen content, and photosynthetic capacity, this hypothesis  
**1812** also implies that progressive reductions in soil nitrogen availability should be the  
**1813** mechanism that drives the downregulation in leaf nitrogen content and photosyn-  
**1814** thetic capacity under elevated CO<sub>2</sub>. This hypothesis has received some support  
**1815** from free air CO<sub>2</sub> enrichment experiments (Reich et al. 2006; Norby et al. 2010),  
**1816** although is not consistently observed across experiments (Finzi et al. 2006; Moore  
**1817** et al. 2006; Liang et al. 2016).

**1818** While possible that progressive nitrogen limitation may determine leaf and  
**1819** whole plant acclimation responses to CO<sub>2</sub>, growing evidence indicates that leaf ni-  
**1820** trogen and photosynthetic capacity are more strongly determined through above-  
**1821** ground growing conditions than by soil resource availability (Dong et al. 2017;  
**1822** Dong et al. 2020; Dong et al. 2022; Smith et al. 2019; Smith and Keenan 2020;

1823 Paillassa et al. 2020; Peng et al. 2021; Querejeta et al. 2022; Westerband et al.  
1824 2023), and satellite-derived chlorophyll fluorescence data indicate that increasing  
1825 atmospheric CO<sub>2</sub> may decrease leaf and canopy demand for nitrogen (Dong et al.  
1826 2022). Together, results from these studies suggest that the downregulation in  
1827 leaf nitrogen content and photosynthetic capacity due to increasing CO<sub>2</sub> may not  
1828 be as tightly linked to progressive nitrogen limitation as previously hypothesized.

1829 A unification of optimal coordination and photosynthetic least-cost the-  
1830 ories predicts that leaves acclimate to elevated CO<sub>2</sub> by downregulating nitrogen  
1831 allocation to Ribulose-1,5-bisphosphate (RuBP) carboxylase/oxygenase (Rubisco)  
1832 to optimize resource use efficiencies at the leaf level, which allows for greater re-  
1833 source allocation to whole plant growth (Drake et al. 1997; Wright et al. 2003;  
1834 Prentice et al. 2014; Smith et al. 2019). The theory predicts that the downregu-  
1835 lation in nitrogen allocation to Rubisco results in a stronger downregulation in the  
1836 maximum rate of Rubisco carboxylation ( $V_{cmax}$ ) than the maximum rate of RuBP  
1837 regeneration ( $J_{max}$ ), which maximizes photosynthetic efficiency by allowing net  
1838 photosynthesis rates to be equally co-limited by Rubisco carboxylation and RuBP  
1839 regeneration (Chen et al. 1993; Maire et al. 2012). This acclimation response  
1840 allows plants to make more efficient use of available light while avoiding overin-  
1841 vestment in Rubisco, which has high nitrogen and energetic costs of building and  
1842 maintaining (Evans 1989; Evans and Clarke 2019). Instead, additional acquired  
1843 resources not needed to optimize leaf photosynthesis are allocated to the mainte-  
1844 nance of structures that support whole plant growth (e.g., total leaf area, whole  
1845 plant biomass, etc.) or to allocation processes not related to leaf photosynthesis  
1846 or growth, such as plant defense mechanisms or leaf structural tissue. Regardless,

1847 optimized resource allocation at the leaf level should allow for greater resource  
1848 allocation to whole plant growth. The theory indicates that leaf acclimation re-  
1849 sponses to CO<sub>2</sub> should be independent of changes in soil nitrogen availability.  
1850 While this leaf acclimation response maximizes nitrogen allocation to structures  
1851 that support whole plant growth, the theory suggests that the positive effect of  
1852 elevated CO<sub>2</sub> on whole plant growth may be further stimulated by soil nitrogen  
1853 availability through a reduction in the cost of acquiring nitrogen (Bae et al. 2015;  
1854 Perkowski et al. 2021; Lu et al. 2022).

1855 Plants acquire nitrogen by allocating photosynthetically derived carbon be-  
1856 lowground in exchange for nitrogen through different nitrogen acquisition strate-  
1857 gies. These nitrogen acquisition strategies can include direct uptake pathways  
1858 such as mass flow or diffusion (Barber 1962), symbioses with mycorrhizal fungi or  
1859 symbiotic nitrogen-fixing bacteria (Vance and Heichel 1991; Marschner and Dell  
1860 1994; Smith and Read 2008; Udvardi and Poole 2013), or through the release  
1861 of root exudates that prime free-living soil microbial communities (Phillips et al.  
1862 2011; Wen et al. 2022). Plants cannot acquire nitrogen without first allocating  
1863 carbon belowground, which implies an inherent carbon cost to the plant for acquir-  
1864 ing nitrogen regardless of nitrogen acquisition strategy. Carbon costs to acquire  
1865 nitrogen often vary in species with different nitrogen acquisition strategies and  
1866 are dependent on external environmental factors such as atmospheric CO<sub>2</sub>, light  
1867 availability, and soil nitrogen availability (Brzostek et al. 2014; Terrer et al. 2016;  
1868 Terrer et al. 2018; Allen et al. 2020; Perkowski et al. 2021; Lu et al. 2022), which  
1869 suggests that acquisition strategy may be an important factor in determining ef-  
1870 fects of soil nitrogen availability on leaf and whole plant acclimation responses to

1871 elevated CO<sub>2</sub>.

1872 A recent meta-analysis using data across 20 grassland and forest CO<sub>2</sub> en-  
1873 richment experiments suggested that species which acquire nitrogen from sym-  
1874 biotic nitrogen-fixing bacteria had reduced costs of nitrogen acquisition under  
1875 elevated CO<sub>2</sub> (Terrer et al. 2018). Findings from this meta-analysis indicated  
1876 that reductions in costs of nitrogen acquisition in species that form associations  
1877 with symbiotic nitrogen-fixing bacteria under elevated CO<sub>2</sub> may drive stronger  
1878 stimulations in whole plant growth and downregulations in  $V_{cmax}$  than species that  
1879 associate with arbuscular mycorrhizal fungi (Smith and Keenan 2020), which gen-  
1880 erally have higher costs of nitrogen acquisition under elevated CO<sub>2</sub> (Terrer et al.  
1881 2018). However, plant investments in symbiotic nitrogen fixation generally de-  
1882 cline with increasing nitrogen availability (Dovrat et al. 2018; Perkowski et al.  
1883 2021), a response that has been previously inferred to be the result of a shift in  
1884 the dominant mode of nitrogen acquisition to direct uptake pathways as costs of  
1885 direct uptake decrease with increasing soil nitrogen availability (Rastetter et al.  
1886 2001; Perkowski et al. 2021). Thus, effects of symbiotic nitrogen fixation on plant  
1887 acclimation responses to CO<sub>2</sub> should decline with increasing soil nitrogen avail-  
1888 ability, although manipulative experiments that directly test these patterns are  
1889 rare.

1890 Here, I conducted a 7-week growth chamber experiment using *Glycine max*  
1891 L. (Merr.) to examine the effects of soil nitrogen fertilization and inoculation with  
1892 symbiotic nitrogen-fixing bacteria on leaf and whole plant acclimation responses  
1893 to elevated CO<sub>2</sub>. Following patterns expected from theory, I hypothesized that in-  
1894 dividual leaves should acclimate to elevated CO<sub>2</sub> by more strongly downregulating

1895  $V_{cmax}$  relative to  $J_{max}$ , allowing leaf photosynthesis to approach optimal coordi-  
1896 nation. I expected this response to correspond with a stronger downregulation in  
1897 leaf nitrogen content than  $V_{cmax}$  and  $J_{max}$ , which would increase the fraction of  
1898 leaf nitrogen content allocated to photosynthesis and photosynthetic nitrogen use  
1899 efficiency. At the whole-plant level, I hypothesized that plants would acclimate  
1900 to elevated CO<sub>2</sub> by stimulating whole plant growth and productivity, a response  
1901 that would be driven by a strong positive response of total leaf area and above-  
1902 ground biomass to elevated CO<sub>2</sub>. I predicted that leaf acclimation responses to  
1903 elevated CO<sub>2</sub> would be independent of soil nitrogen fertilization and inoculation  
1904 with symbiotic nitrogen-fixing bacteria; however, I expected that increasing soil  
1905 nitrogen fertilization would increase the positive effect of elevated CO<sub>2</sub> on mea-  
1906 sures of whole plant growth due to a stronger reduction in the cost of acquiring  
1907 nitrogen under elevated CO<sub>2</sub> with increasing fertilization. I also expected stronger  
1908 stimulations in whole plant growth due to inoculation, but that this effect would  
1909 only be apparent under low fertilization due to a reduction in root nodulation  
1910 with increasing fertilization.

1911 5.2 Methods

1912 5.2.1 *Seed treatments and experimental design*

1913 *Glycine max* L. (Merr) seeds were planted in 144 6-liter surface sterilized  
1914 pots (NS-600, Nursery Supplies, Orange, CA, USA) containing a steam-sterilized  
1915 70:30 v:v mix of Sphagnum peat moss (Premier Horticulture, Quakertown, PA,  
1916 USA) to sand (Pavestone, subsidiary of Quikrete Companies, Atlanta, GA, USA).  
1917 Before planting, all *G. max* seeds were surface sterilized in 2% sodium hypochlorite

1918 for 3 minutes, followed by three separate 3-minute washes with ultrapure water  
1919 (MilliQ 7000; MilliporeSigma, Burlington, MA USA). A subset of surface steril-  
1920 ized seeds were inoculated with *Bradyrhizobium japonicum* (Verdesian N-Dure™  
1921 Soybean, Cary, NC, USA) in a slurry following manufacturer recommendations  
1922 (3.12 g inoculant and 241 g deionized water per 1 kg seed).

1923 Seventy-two pots were randomly planted with surface-sterilized seeds inoc-  
1924 ulated with *B. japonicum*, while the remaining 72 pots were planted with surface-  
1925 sterilized uninoculated seeds. Thirty-six pots within each inoculation treatment  
1926 were randomly placed in one of two atmospheric CO<sub>2</sub> treatments (ambient and  
1927 1000 μmol mol<sup>-1</sup> CO<sub>2</sub>). Pots within each unique inoculation-by-CO<sub>2</sub> treatment  
1928 combination randomly received one of nine soil nitrogen fertilization treatments  
1929 equivalent to 0, 35, 70, 105, 140, 210, 280, 350, or 630 ppm N. Nitrogen fertil-  
1930 ization treatments were created using a modified Hoagland solution (Hoagland  
1931 and Arnon 1950) designed to keep concentrations of other macronutrients and  
1932 micronutrients equivalent across treatments (Table S1). Pots received the same  
1933 fertilization treatment throughout the entire duration experiment, which were ap-  
1934 plied twice per week in 150 mL doses as topical agents to the soil surface through-  
1935 out the duration of the experiment. This experimental design yielded a fully  
1936 factorial experiment with four replicates per unique fertilization-by-inoculation-  
1937 by-CO<sub>2</sub> combination.

1938 5.2.2 *Growth chamber conditions*

1939 Upon experiment initiation, pots were randomly placed in one of six Per-  
1940 cival LED-41L2 growth chambers (Percival Scientific Inc., Perry, IA, USA) over

1941 two experimental iterations due to chamber space limitation. Two iterations were  
1942 conducted such that one iteration included all elevated CO<sub>2</sub> pots and the second  
1943 iteration included all ambient CO<sub>2</sub> pots. Average ( $\pm$  SD) CO<sub>2</sub> concentrations  
1944 across chambers throughout the experiment were  $439 \pm 5 \mu\text{mol mol}^{-1}$  for the  
1945 ambient CO<sub>2</sub> treatment and  $989 \pm 4 \mu\text{mol mol}^{-1}$  for the elevated CO<sub>2</sub> treatment.

1946 Daytime growing conditions were simulated using a 16-hour photoperiod,  
1947 with incoming light radiation set to chamber maximum (mean  $\pm$  SD:  $1240 \pm 32$   
1948  $\mu\text{mol m}^{-2} \text{s}^{-1}$  across chambers), air temperature set to 25°C, and relative humid-  
1949 ity set to 50%. The remaining 8 hours simulated nighttime growing conditions,  
1950 with incoming light radiation set to 0  $\mu\text{mol m}^{-2} \text{s}^{-1}$ , chamber temperature set  
1951 to 17°C, and relative humidity set to 50%. Transitions between daytime and  
1952 nighttime growing conditions were simulated by ramping incoming light radiation  
1953 in 45-minute increments and temperature in 90-minute increments over a 3-hour  
1954 period (Table S2).

1955 Including the two, 3-hour ramping periods, pots grew under average ( $\pm$   
1956 SD) daytime light intensity of  $1049 \pm 27 \mu\text{mol m}^{-2} \text{s}^{-1}$ . In the elevated CO<sub>2</sub>  
1957 iteration, pots grew under  $24.0 \pm 0.2^\circ\text{C}$  during the day,  $16.4 \pm 0.8^\circ\text{C}$  during the  
1958 night, and  $51.6 \pm 0.4\%$  relative humidity. In the ambient CO<sub>2</sub> iteration, pots grew  
1959 under  $23.9 \pm 0.2^\circ\text{C}$  during the day,  $16.0 \pm 1.4^\circ\text{C}$  during the night, and  $50.3 \pm 0.2\%$   
1960 relative humidity. We accounted for climatic differences across the six chambers  
1961 by shuffling the same group of pots daily throughout the growth chambers. This  
1962 process was done by iteratively moving the group of pots on the top rack of a  
1963 chamber to the bottom rack of the same chamber, while simultaneously moving  
1964 the group of pots on the bottom rack of a chamber to the top rack of the adjacent

1965 chamber. I moved pots within and across chambers every day throughout the  
1966 course of each experiment iteration.

1967 5.2.3 *Leaf gas exchange measurements*

1968 Gas exchange measurements were collected for all individuals on the sev-  
1969 enth week of development. All gas exchange measurements were collected on  
1970 the center leaf of the most recent fully expanded trifoliate leaf set. Specifi-  
1971 cally, I measured net photosynthesis ( $A_{\text{net}}$ ;  $\mu\text{mol m}^{-2} \text{s}^{-1}$ ), stomatal conductance  
1972 ( $g_{\text{sw}}$ ;  $\text{mol m}^{-2} \text{s}^{-1}$ ), and intercellular CO<sub>2</sub> ( $C_i$ ;  $\mu\text{mol mol}^{-1}$ ) concentrations across  
1973 a range of atmospheric CO<sub>2</sub> concentrations (i.e., an  $A_{\text{net}}/C_i$  curve) using the  
1974 Dynamic Assimilation Technique™. The Dynamic Assimilation Technique™ has  
1975 been shown to correspond well with traditional steady-state CO<sub>2</sub> response curves  
1976 in *G. max* (Saathoff and Welles 2021).  $A_{\text{net}}/C_i$  curves were generated along a  
1977 reference CO<sub>2</sub> ramp down from 420  $\mu\text{mol mol}^{-1}$  CO<sub>2</sub> to 20  $\mu\text{mol mol}^{-1}$  CO<sub>2</sub>, fol-  
1978 lowed by a ramp up from 420  $\mu\text{mol mol}^{-1}$  CO<sub>2</sub> to 1620  $\mu\text{mol mol}^{-1}$  CO<sub>2</sub> after  
1979 a 90-second wait period at 420  $\mu\text{mol mol}^{-1}$  CO<sub>2</sub>. The ramp rate for each curve  
1980 was set to 200  $\mu\text{mol mol}^{-1} \text{min}^{-1}$ , logging every five seconds, which generated 96  
1981 data points per response curve. All  $A_{\text{net}}/C_i$  curves were generated after  $A_{\text{net}}$  and  
1982  $g_{\text{sw}}$  stabilized in a LI-6800 cuvette set to a 500  $\text{mol s}^{-1}$ , 10,000 rpm mixing fan  
1983 speed, 1.5 kPa vapor pressure deficit, 25°C leaf temperature, 2000  $\mu\text{mol m}^{-2} \text{s}^{-1}$   
1984 incoming light radiation, and initial reference CO<sub>2</sub> set to 420  $\mu\text{mol mol}^{-1}$ .

1985 With the same focal leaf used to generate  $A_{\text{net}}/C_i$  curves, I measured dark  
1986 respiration ( $R_{\text{d25}}$ ;  $\mu\text{mol m}^{-2} \text{s}^{-1}$ ) following at least a 30-minute period of darkness.  
1987 Measurements were collected on a 5-second log interval for 60 seconds after stabi-

1988 lizing in a LI-6800 cuvette set to a  $500 \text{ mol s}^{-1}$ , 10,000 rpm mixing fan speed, 1.5  
1989 kPa vapor pressure deficit, 25°C leaf temperature, and  $420 \mu\text{mol mol}^{-1}$  reference  
1990 CO<sub>2</sub> concentration (for both CO<sup>2</sup> concentrations), with incoming light radiation  
1991 set to  $0 \mu\text{mol m}^{-2} \text{ s}^{-1}$ . A single dark respiration value was determined for each  
1992 focal leaf by calculating the mean dark respiration value (i.e. the absolute value  
1993 of  $A_{\text{net}}$  during the logging period) across the logging interval.

1994 5.2.4 *Leaf trait measurements*

1995 The focal leaf used to generate  $A_{\text{net}}/C_i$  curves and dark respiration was  
1996 harvested immediately following gas exchange measurements. Images of each focal  
1997 leaf were curated using a flat-bed scanner to determine wet leaf area using the  
1998 'LeafArea' R package (Katabuchi 2015), which automates leaf area calculations  
1999 using ImageJ software (Schneider et al. 2012). Each leaf was dried at 65°C for  
2000 at least 48 hours, and subsequently weighed and ground until homogenized. Leaf  
2001 mass per area ( $M_{\text{area}}$ ; g m<sup>-2</sup>) was calculated as the ratio of dry leaf biomass  
2002 to fresh leaf area. Using subsamples of ground and homogenized leaf tissue, I  
2003 measured leaf nitrogen content ( $N_{\text{mass}}$ ; gN g<sup>-1</sup>) through elemental combustion  
2004 analysis (Costech-4010, Costech, Inc., Valencia, CA, USA). Leaf nitrogen content  
2005 per unit leaf area ( $N_{\text{area}}$ ; gN m<sup>-2</sup>) was calculated by multiplying  $N_{\text{mass}}$  and  $M_{\text{area}}$ .

2006 I extracted chlorophyll content from a second leaf in the same trifoliolate  
2007 leaf set as the focal leaf used to generate  $A_{\text{net}}/C_i$  curves. Prior to chlorophyll  
2008 extraction, I used a cork borer to punch between 3 and 5 0.6 cm<sup>2</sup> disks from the  
2009 leaf. Separate images of each punched leaf and set of leaf disks were curated using  
2010 a flat-bed scanner to determine wet leaf area, again quantified using the 'LeafArea'

2011 R package (Katabuchi 2015). The punched leaf was dried and weighed after at  
2012 least 65°C in the drying oven to determine  $M_{\text{area}}$  of the chlorophyll leaf.  
  
2013 Leaf disks were shuttled into a test tube containing 10mL dimethyl sul-  
2014 foxide, vortexed, and incubated at 65degreeC for 120 minutes (Barnes et al.  
2015 1992). Incubated test tubes were vortexed again before loaded in 150  $\mu\text{L}$  trip-  
2016 licate aliquots to a 96-well plate. Dimethyl sulfoxide was also loaded in a 150  
2017  $\mu\text{L}$  triplicate aliquot as a blank. Absorbance measurements at 649.1 nm ( $A_{649.1}$ )  
2018 and 665.1 nm ( $A_{665.1}$ ) were read in each well using a plate reader (Biotek Synergy  
2019 H1; Biotek Instruments, Winooski, VT USA) (Wellburn 1994), with triplicates  
2020 subsequently averaged and corrected by the mean of the blank absorbance value.  
2021 Blank-corrected absorbance values were used to estimate  $Chl_a$  ( $\mu\text{g mL}^{-1}$ ) and  
2022  $Chl_b$  ( $\mu\text{g mL}^{-1}$ ) following equations from Wellburn (1994):

$$Chl_a = 12.47A_{665.1} - 3.62A_{649.1} \quad (5.1)$$

2023 and

$$Chl_b = 25.06A_{665.1} - 6.50A_{649.1} \quad (5.2)$$

2024  $Chl_a$  and  $Chl_b$  were converted to mmol  $\text{mL}^{-1}$  using the molar mass of chlorophyll a  
2025 (893.51 g  $\text{mol}^{-1}$ ) and the molar mass of chlorophyll b (907.47 g  $\text{mol}^{-1}$ ), then added  
2026 together to calculate total chlorophyll content in the dimethyl sulfoxide extractant  
2027 (mmol  $\text{mL}^{-1}$ ). Total chlorophyll content was multiplied by the volume of the  
2028 dimethyl sulfoxide extractant (10 mL) and converted to area-based chlorophyll  
2029 content by dividing by the total area of the leaf disks ( $Chl_{\text{area}}$ ; mmol  $\text{m}^{-2}$ ). Mass-  
2030 based chlorophyll content ( $Chl_{\text{mass}}$ ; mmol  $\text{g}^{-1}$ ) was calculated by dividing  $Chl_{\text{area}}$

**2031** by the leaf mass per area of the punched leaf.

**2032** 5.2.5 *A/C<sub>i</sub> curve fitting and parameter estimation*

**2033** I fit  $A_{\text{net}}/C_i$  curves of each individual using the ‘fitaci’ function in the  
**2034** ‘plantecophys’ R package (Duursma 2015). This function estimates the maxi-  
**2035** mum rate of Rubisco carboxylation ( $V_{\text{cmax}}$ ;  $\mu\text{mol m}^{-2} \text{s}^{-1}$ ) and maximum rate  
**2036** of electron transport for RuBP regeneration ( $J_{\text{max}}$ ;  $\mu\text{mol m}^{-2} \text{s}^{-1}$ ) based on the  
**2037** Farquhar biochemical model of C<sub>3</sub> photosynthesis (Farquhar et al. 1980). Triose  
**2038** phosphate utilization (TPU) limitation was included in all curve fits, and all curve  
**2039** fits included measured dark respiration values. As  $A_{\text{net}}/C_i$  curves were generated  
**2040** using a common leaf temperature, curves were fit using Michaelis-Menten coeffi-  
**2041** cients for Rubisco affinity to CO<sub>2</sub> ( $K_c$ ;  $\mu\text{mol mol}^{-1}$ ) and O<sub>2</sub> ( $K_o$ ;  $\mu\text{mol mol}^{-1}$ ), and  
**2042** the CO<sub>2</sub> compensation point ( $\Gamma^*$ ;  $\mu\text{mol mol}^{-1}$ ) reported in Bernacchi et al. (2001).  
**2043** Specifically,  $K_c$  was set to 404.9  $\mu\text{mol mol}^{-1}$ ,  $K_o$  was set to 278.4  $\mu\text{mol mol}^{-1}$ , and  
**2044**  $\Gamma^*$  was set to 42.75  $\mu\text{mol mol}^{-1}$ . The use of a common leaf temperature across  
**2045** curves and dark respiration measurements also eliminated the need to manually  
**2046** temperature standardize rate estimates. For clarity, I reference  $V_{\text{cmax}}$ ,  $J_{\text{max}}$ , and  
**2047**  $R_d$  estimates throughout the rest of the paper as  $V_{\text{cmax}25}$ ,  $J_{\text{max}25}$ , and  $R_{d25}$ .

**2048** 5.2.6 Stomatal limitation

**2049** I quantified the extent by which stomatal conductance limited photosynthe-  
**2050** sis (l; unitless) following equations originally described in Farquhar and Sharkey  
**2051** (1982). Stomatal limitation was calculated as:

$$l = 1 - \frac{A_{net}}{A_{mod}} \quad (5.3)$$

**2052** where  $A_{mod}$  represents the photosynthetic rate where  $C_i = C_a$ .  $A_{mod}$  was calcu-

**2053** lated as:

$$A_{mod} = V_{cmax25} - \frac{420 - \Gamma^*}{420 + K_m} - R_{d25} \quad (5.4)$$

**2054**  $K_m$  is the Michaelis-Menten coefficient for Rubisco-limited photosynthesis, calcu-

**2055** lated as:

$$K_m = K_c \cdot \left(1 + \frac{O_i}{K_o}\right) \quad (5.5)$$

**2056** where  $O_i$  refers to leaf intercellular  $O_2$  concentrations, set to  $210 \mu\text{mol mol}^{-1}$ .

**2057** 5.2.7 *Proportion of leaf nitrogen allocated to photosynthesis and structure*

**2058** I used equations from Niinemets and Tenhunen (1997) to estimate the

**2059** proportion of leaf N content allocated to Rubisco bioenergetics, and light harvest-

**2060** ing proteins. The proportion of leaf N allocated to Rubisco ( $\rho_{rub}$ ;  $\text{gN gN}^{-1}$ ) was

**2061** calculated as a function of  $V_{cmax25}$  and  $N_{area}$ :

$$\rho_{rubisco} = \frac{V_{cmax25} N_r}{V_{cr} N_{area}} \quad (5.6)$$

**2062** where  $N_r$  is the amount of nitrogen in Rubisco, set to  $0.16 \text{ gN (gN in Rubisco)}^{-1}$

**2063** and  $V_{cr}$  is the maximum rate of RuBP carboxylation per unit Rubisco protein,

**2064** set to  $20.5 \mu\text{mol CO}_2 (\text{g Rubisco})^{-1}$ . The proportion of leaf nitrogen allocated to

**2065** bioenergetics ( $\rho_{bioe}$ ;  $\text{gN gN}^{-1}$ ) was similarly calculated as a function of  $J_{max25}$  and

**2066**  $N_{\text{area}}$ :

$$\rho_{\text{bioe}} = \frac{J_{\text{max}25} N_b}{J_{\text{mc}} N_{\text{area}}} \quad (5.7)$$

**2067** where  $N_b$  is the amount of nitrogen in cytochrome f, set to 0.12407 gN ( $\mu\text{mol}$  cytochrome f) $^{-1}$  assuming a constant 1: 1: 1.2 cytochrome f: ferredoxin NADP reductase: coupling factor molar ratio (Evans and Seemann 1989; Niinemets and Tenhunen 1997), and  $J_{\text{mc}}$  is the capacity of electron transport per cytochrome f, set to 156  $\mu\text{mol}$  electron ( $\mu\text{mol}$  cytochrome f) $^{-1}\text{s}^{-1}$ .

**2072** The proportion of leaf nitrogen allocated to light harvesting proteins was  
**2073** calculated as a function of  $Chl_{\text{mass}}$  and  $N_{\text{mass}}$ :

$$\rho_{\text{light}} = \frac{Chl_{\text{mass}}}{N_{\text{mass}} c_b} \quad (5.8)$$

**2074** where  $c_b$  is the stoichiometry of the light-harvesting chlorophyll complexes of photosystem II, set to 2.75 mmol chlorophyll (gN in chlorophyll) $^{-1}$ . We used the  $N_{\text{mass}}$  value of the focal leaf used to generate  $A_{\text{net}}/C_i$  curves instead of the leaf used to extract chlorophyll content, as the two leaves are from the same trifoliolate leaf set and are highly correlated with each other (Figure SX).

**2079** The proportion of leaf nitrogen content allocated to photosynthetic tissue  
**2080** ( $\rho_{\text{photo}}$ ; gN gN $^{-1}$ ) was estimated as the sum of  $\rho_{\text{rubisco}}$ ,  $\rho_{\text{bioe}}$ , and  $\rho_{\text{light}}$ .

**2081** Finally, the proportion of leaf N content allocated to structural tissue ( $\rho_{\text{str}}$ ;  
**2082** gN gN $^{-1}$ ) was estimated as:

$$\rho_{\text{structure}} = \frac{N_{\text{cw}}}{N_{\text{area}}} \quad (5.9)$$

2083 where  $N_{cw}$  is the leaf N content allocated to cell walls ( $\text{gN m}^{-2}$ ), calculated as a  
2084 function of  $M_{area}$  using an empirical equation from Onoda et al. (2017):

$$N_{cw} = 0.000355 * M_{area}^{1.39} \quad (5.10)$$

2085 5.2.8 *Whole plant traits*

2086 Seven weeks after experiment initiation and immediately following gas ex-  
2087 change measurements, I harvested all experimental individuals and separated  
2088 biomass of each experimental individual into major organ types (leaves, stems,  
2089 roots, and nodules when present). Fresh leaf area of all harvested leaves was mea-  
2090 sured using an LI-3100C (Li-COR Biosciences, Lincoln, Nebraska, USA). Total  
2091 fresh leaf area ( $\text{cm}^2$ ) was calculated as the sum of all leaf areas, including the focal  
2092 leaf used to collect gas exchange data and the focal leaf used to extract chlorophyll  
2093 content. All harvested material was dried in an oven set to 65°C for at least 48  
2094 hours, weighed, and ground to homogeneity. Leaves and nodules were manually  
2095 ground either with a mortar and pestle, while stems and roots were ground using  
2096 a Wiley mill (E3300 Mini Mill; Eberbach Corp., MI, USA). Total dry biomass (g)  
2097 was calculated as the sum of dry leaf (including focal leaf for both the  $A_{net}/C_i$   
2098 curve and leaf used to extract chlorophyll content), stem, root, and root nodule  
2099 biomass. I quantified carbon and nitrogen content of each respective organ type  
2100 through elemental combustion (Costech-4010, Costech, Inc., Valencia, CA, USA)  
2101 using subsamples of ground and homogenized organ tissue.

2102 Following the approach explained in the first experimental chapter, I calcu-  
2103 lated structural carbon costs to acquire nitrogen as the ratio of total belowground

**2104** carbon biomass to whole plant nitrogen biomass ( $N_{\text{cost}}$ ; gC gN<sup>-1</sup>). Belowground  
**2105** carbon biomass ( $C_{\text{bg}}$ ; gC) was calculated as the sum of root carbon biomass  
**2106** and root nodule carbon biomass. Root carbon biomass and root nodule carbon  
**2107** biomass was calculated as the product of the organ biomass and the respective  
**2108** organ carbon content. Whole plant nitrogen biomass ( $N_{\text{wp}}$ ; gN) was similarly  
**2109** calculated as the sum of total leaf, stem, root, and root nodule nitrogen biomass,  
**2110** including the focal leaf used for  $A_{\text{net}}/C_i$  curve and chlorophyll extractions. Leaf,  
**2111** stem, root, and root nodule nitrogen biomass was calculated as the product of  
**2112** the organ biomass and the respective organ nitrogen content. This calculation  
**2113** only quantifies plant structural carbon costs to acquire nitrogen and does not  
**2114** include any additional costs of nitrogen acquisition associated with respiration,  
**2115** root exudation, or root turnover. An explicit explanation of the limitations for  
**2116** interpreting this calculation can be found in Perkowski et al. (2021) and Terrer  
**2117** et al. (2018).

**2118** Finally, plant investments in nitrogen fixation were calculated as the ra-  
**2119** tio of root nodule biomass to root biomass, where increasing values indicate an  
**2120** increase in plant investments to nitrogen fixation (Dovrat et al. 2018; Dovrat  
**2121** et al. 2020; Perkowski et al. 2021). I also calculated the percent of leaf nitrogen  
**2122** acquired from the atmosphere (% $N_{\text{dfa}}$ ) using leaf  $\delta^{15}\text{N}$  and the following equation  
**2123** from Andrews et al. (2011):

$$\%N_{\text{dfa}} = \frac{\delta^{15}N_{\text{reference}} - \delta^{15}N_{\text{sample}}}{\delta^{15}N_{\text{reference}} - B} \quad (5.11)$$

**2124** where  $\delta^{15}\text{N}_{\text{reference}}$  refers to a reference plant that exclusively acquires nitrogen via

2125 direct uptake,  $\delta^{15}\text{N}_{\text{sample}}$  refers to an individual's leaf  $\delta^{15}\text{N}$ , and B refers to individuals  
2126 that are entirely reliant on nitrogen fixation. Within each unique nitrogen  
2127 fertilization treatment-by-CO<sub>2</sub> treatment combination, I calculated the mean leaf  
2128  $\delta^{15}\text{N}$  for individuals growing in the non-inoculated treatment for  $\delta^{15}\text{N}_{\text{reference}}$ . Any  
2129 individuals with visual confirmation of root nodule formation or nodule initiation  
2130 were omitted from the calculation of  $\delta^{15}\text{N}_{\text{reference}}$ . Following recommendations  
2131 from Andrews et al. (2011) I calculated B within each CO<sub>2</sub> treatment using  
2132 the mean leaf  $\delta^{15}\text{N}$  of inoculated individuals that received 0 ppm N. I did not  
2133 calculate B within each unique soil nitrogen-by-CO<sub>2</sub> treatment combination, as  
2134 previous studies suggest decreased reliance on nitrogen fixation with increasing  
2135 soil nitrogen availability (Perkowski et al. 2021). This approach for estimating  
2136 nitrogen fixation standardizes values such that approaching 1 indicates increasing  
2137 reliance on nitrogen fixation.

2138 5.2.9 *Statistical analyses*

2139 Any uninoculated pots that had substantial root nodule formation (nodule  
2140 biomass: root biomass values greater than 0.05 g g<sup>-1</sup>) were removed from analyses.  
2141 This was because they were assumed to have been colonized by symbiotic nitrogen-  
2142 fixing bacteria from outside sources. This decision resulted in the removal of  
2143 sixteen pots from our analysis: two pots in the elevated CO<sub>2</sub> treatment that  
2144 received 35 ppm N, three pots in the elevated CO<sub>2</sub> treatment that received 70  
2145 ppm N, one pot in the elevated CO<sub>2</sub> treatment that received 210 ppm N, two pots  
2146 in the elevated CO<sub>2</sub> treatment that received 280 ppm N, two pots in the ambient  
2147 CO<sub>2</sub> treatment that received 0 ppm N, three pots in the ambient CO<sub>2</sub> treatment

2148 that received 70 ppm N, two pots in the ambient CO<sub>2</sub> treatment that received  
2149 105 ppm N, and one pot in the ambient CO<sub>2</sub> treatment that received 280 ppm N.

2150 I built a series of linear mixed effects models to investigate the impacts of  
2151 CO<sub>2</sub> concentration, soil nitrogen fertilization, and inoculation with *B. japonicum*  
2152 on *G. max* gas exchange, tradeoffs between nitrogen and water use, whole plant  
2153 growth, and investment in nitrogen fixation. All models included CO<sub>2</sub> treatment  
2154 as a categorical fixed effect, inoculation treatment as a categorical fixed effect,  
2155 soil nitrogen fertilization as a continuous fixed effect, with interaction terms be-  
2156 tween all three fixed effects. All models also accounted for climatic difference  
2157 between chambers across experiment iterations by including a random intercept  
2158 term that nested starting chamber rack by CO<sub>2</sub> treatment. Models with this  
2159 independent variable structure were created for each of the following dependent  
2160 variables:  $N_{\text{area}}$ ,  $M_{\text{area}}$ ,  $N_{\text{mass}}$ ,  $Chl_{\text{area}}$ ,  $V_{\text{cmax25}}$ ,  $J_{\text{max25}}$ ,  $J_{\text{max25}}:V_{\text{cmax25}}$ ,  $R_{\text{d25}}$ ,  $g_{\text{sw}}$ ,  
2161 stomatal limitation,  $\rho_{\text{rubisco}}$ ,  $\rho_{\text{bioe}}$ ,  $\rho_{\text{light}}$ ,  $\rho_{\text{photo}}$ ,  $\rho_{\text{structure}}$ ,  $N_{\text{cost}}$ ,  $C_{\text{bg}}$ ,  $N_{\text{wp}}$ , total  
2162 biomass, total leaf area, nodule biomass, and the ratio of nodule biomass to root  
2163 biomass.

2164 I used Shapiro-Wilk tests of normality to determine whether linear mixed  
2165 effects models satisfied residual normality assumptions. If residual normality as-  
2166 sumptions were not met (Shapiro-Wilk:  $p < 0.05$ ), then models were fit using  
2167 dependent variables that were natural log transformed. All residual normality  
2168 assumptions that did not originally satisfy residual normality assumptions were  
2169 met with either a natural log or square root data transformation (Shapiro-Wilk:  
2170  $p > 0.05$  in all cases). Specifically, models for  $N_{\text{area}}$ ,  $N_{\text{mass}}$ ,  $Chl_{\text{area}}$ ,  $V_{\text{cmax25}}$ ,  
2171  $J_{\text{max25}}$ ,  $J_{\text{max25}}:V_{\text{cmax25}}$ ,  $g_{\text{sw}}$ , stomatal limitation,  $\rho_{\text{rubisco}}$ ,  $\rho_{\text{bioe}}$ ,  $\rho_{\text{light}}$ ,  $\rho_{\text{photo}}$ , and to-

**2172** tal leaf area satisfied residual normality assumptions without data transformation.  
**2173** Models for  $M_{\text{area}}$ ,  $\rho_{\text{structure}}$ ,  $N_{\text{cost}}$ ,  $C_{\text{bg}}$ ,  $N_{\text{wp}}$ , and total biomass satisfied residual  
**2174** normality assumptions with a natural log data transformation, while models for  
**2175** nodule biomass and nodule biomass: root biomass satisfied residual normality  
**2176** assumptions with a square root data transformation.

**2177** In all statistical models, I used the 'lmer' function in the 'lme4' R package  
**2178** (Bates et al. 2015) to fit each model and the 'Anova' function in the 'car' R  
**2179** package (Fox and Weisberg 2019) to calculate Type II Wald's  $\chi^2$  and determine  
**2180** the significance ( $\alpha = 0.05$ ) of each fixed effect coefficient. I used the 'emmeans'  
**2181** R package (Lenth 2019) to conduct post-hoc comparisons using Tukey's tests,  
**2182** where degrees of freedom were approximated using the Kenward-Roger approach  
**2183** (Kenward and Roger 1997). All analyses and plots were conducted in R version  
**2184** 4.2.0 (R Core Team 2021).

## **2185** 5.3 Results

### **2186** 5.3.1 Leaf nitrogen and chlorophyll content

**2187** Elevated CO<sub>2</sub> reduced  $N_{\text{area}}$ ,  $N_{\text{mass}}$ , and  $Chl_{\text{area}}$  by 29%, 50%, and 31%,  
**2188** respectively, and stimulated  $M_{\text{area}}$  by 44% ( $p < 0.001$  in all cases; Table 5.1). An  
**2189** interaction between fertilization and CO<sub>2</sub> (CO<sub>2</sub>-by-fertilization interaction:  $p_{N_{\text{area}}}$   
**2190** = 0.017,  $p_{N_{\text{mass}}} < 0.001$ ,  $p_{M_{\text{area}}} = 0.006$ ,  $p_{Chl_{\text{area}}} = 0.083$ ; Table 5.1) indicated  
**2191** that the general positive effect of increasing fertilization on  $N_{\text{area}}$ ,  $N_{\text{mass}}$ , and  
**2192**  $Chl_{\text{area}}$  ( $p < 0.001$  in all cases; Table 5.1) was generally stronger under ambient  
**2193** CO<sub>2</sub> (Tukey <sub>$N_{\text{area}}$</sub> :  $p = 0.026$ ; Tukey <sub>$N_{\text{mass}}$</sub> :  $p < 0.001$ ; Tukey <sub>$M_{\text{area}}$</sub> :  $p = 0.009$ ;  
**2194** Tukey <sub>$Chl_{\text{area}}$</sub> :  $p = 0.065$ ; Table 5.1; Figs. 5.1a-d). This pattern resulted in a

2195 stronger reduction in  $N_{\text{area}}$ ,  $N_{\text{mass}}$ , and  $Chl_{\text{area}}$  as well as a stronger stimulation  
2196 in  $M_{\text{area}}$  under elevated CO<sub>2</sub> with increasing fertilization. An additional interac-  
2197 tion between inoculation and CO<sub>2</sub> on  $N_{\text{area}}$  (CO<sub>2</sub>-by-inoculation interaction:  $p =$   
2198 0.030; Table 5.1) indicated that the general positive effect of inoculation on  $N_{\text{area}}$   
2199 ( $p < 0.001$ ; Table 5.1) was stronger under elevated CO<sub>2</sub> (45% increase; Tukey:  $p$   
2200  $< 0.001$ ) than under ambient CO<sub>2</sub> (18% increase; Tukey:  $p < 0.001$ ), a result that  
2201 increased the reduction in  $N_{\text{area}}$  in inoculated pots under elevated CO<sub>2</sub>. Inocula-  
2202 tion treatment did not modify the downregulation in  $N_{\text{mass}}$  (CO<sub>2</sub>-by-inoculation  
2203 interaction:  $p = 0.148$ ; Table 5.1) and  $Chl_{\text{area}}$  ( $p = 0.147$ ; Table 5.1) or the stimu-  
2204 lation in  $M_{\text{area}}$  ( $p = 0.866$ ; Table 5.1) under elevated CO<sub>2</sub>. However, interactions  
2205 between fertilization and inoculation on  $N_{\text{area}}$  (fertilization-by-inoculation inter-  
2206 action:  $p < 0.001$ ; Table 5.1; Fig. 5.1a),  $N_{\text{mass}}$  ( $p = 0.001$ ; Table 5.1; Fig. 5.1b),  
2207  $M_{\text{area}}$  ( $p = 0.025$ ; Table 5.1; Fig. 5.1c), and  $Chl_{\text{area}}$  ( $p < 0.001$ ; Table 5.1; Fig.  
2208 5.1d) indicated that the general positive effect of increasing fertilization on each  
2209 trait was stronger in uninoculated pots (Tukey <sub>$N_{\text{area}}$</sub> :  $p < 0.001$ ; Tukey <sub>$N_{\text{mass}}$</sub> :  $p =$   
2210 0.001; Tukey <sub>$M_{\text{area}}$</sub> :  $p = 0.031$ ; Tukey <sub>$Chl_{\text{area}}$</sub> :  $p < 0.001$ ).

**Table 5.1.** Effects of soil nitrogen fertilization, inoculation, and CO<sub>2</sub> treatments on  $N_{\text{area}}$ ,  $N_{\text{mass}}$ ,  $M_{\text{area}}$ , and  $Chl_{\text{area}}$ 

	$N_{\text{area}}$			$N_{\text{mass}}$			$M_{\text{area}}^a$			
	df	Coefficient	$\chi^2$	p	Coefficient	$\chi^2$	p	Coefficient	$\chi^2$	p
(Intercept)	-	1.10E+00	-	-	3.05E-02	-	-	3.64E+00	-	-
CO <sub>2</sub>	1	-5.67E-01	155.908	<0.001	-1.80E-02	272.362	<0.001	3.04E-01	151.319	<0.001
Inoculation (I)	1	6.21E-01	86.029	<0.001	7.54E-03	15.576	<0.001	1.81E-01	19.158	<0.001
Fertilization (N)	1	3.06E-03	316.408	<0.001	5.78E-05	106.659	<0.001	3.10E-04	21.440	<0.001
CO <sub>2</sub> *I	1	2.63E-01	4.729	<b>0.030</b>	3.96E-03	2.025	0.155	-3.37E-02	0.029	0.866
CO <sub>2</sub> *N	1	-3.68E-04	5.723	<b>0.017</b>	-2.85E-05	22.542	<0.001	2.80E-04	7.619	<b>0.006</b>
I*N	1	-1.36E-03	43.381	<0.001	-2.00E-05	11.137	<b>0.001</b>	-3.36E-04	5.022	<b>0.025</b>
CO <sub>2</sub> *I*N	1	-3.23E-04	0.489	0.484	-2.59E-06	0.041	0.839	1.15E-04	0.208	0.649

	$Chl_{\text{area}}$			
	df	Coefficient	$\chi^2$	p
(Intercept)	-	2.13E-02	-	-
CO <sub>2</sub>	1	-1.33E-02	69.233	<0.001
Inoculation (I)	1	1.24E-01	136.341	<0.001
Fertilization (N)	1	3.35E-04	163.111	<0.001
CO <sub>2</sub> *I	1	-3.18E-02	2.102	0.147
CO <sub>2</sub> *N	1	-8.79E-05	2.999	<i>0.083</i>
I*N	1	-2.65E-04	75.769	<0.001
CO <sub>2</sub> *I*N	1	7.68E-05	2.144	0.147

2211 \*Significance determined using Type II Wald  $\chi^2$  tests ( $\alpha = 0.05$ ).  $P$ -values  $< 0.05$  are in bold, while  $p$ -values between  
 2212 0.05 and 0.1 are italicized. A superscript “a” is included after trait labels to indicate if models were fit with natural  
 2213 log transformed response variables. Key: df = degrees of freedom,  $N_{\text{area}}$  = leaf nitrogen content per unit leaf area,  
 2214  $N_{\text{mass}}$  = leaf nitrogen content,  $M_{\text{area}}$  = leaf mass per unit leaf area.

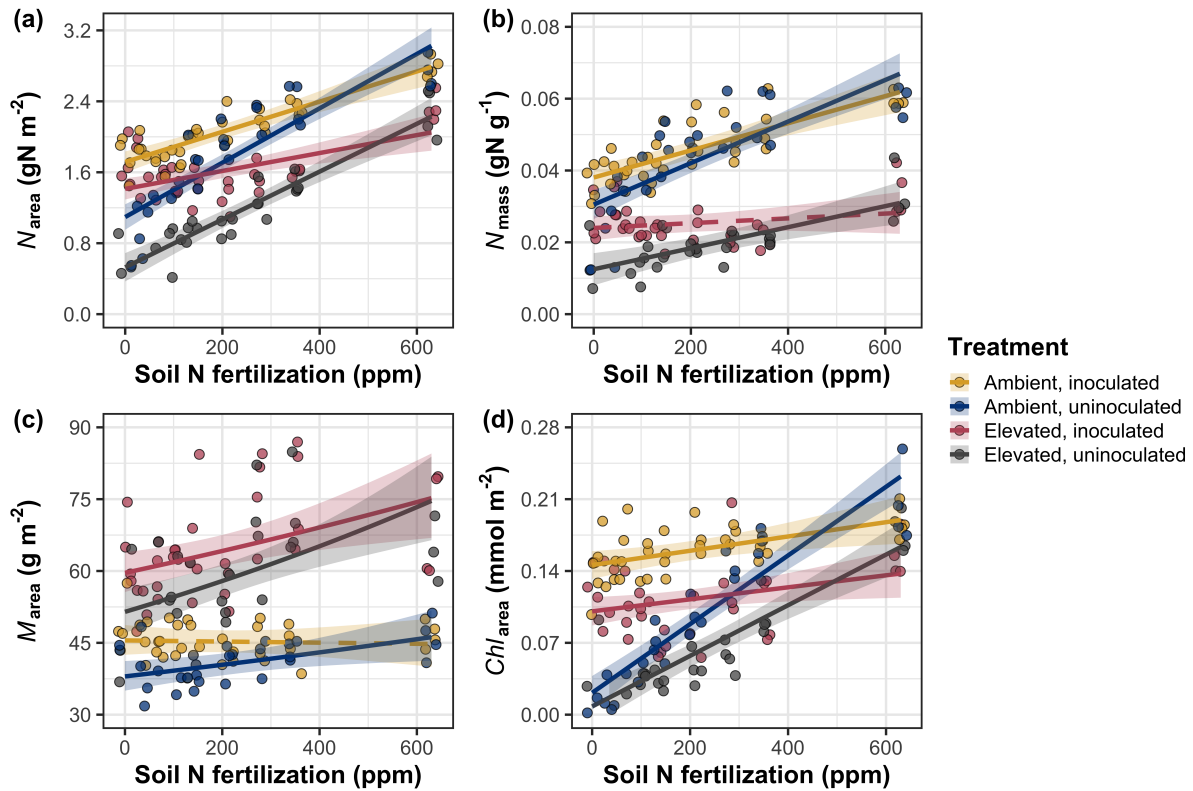


**Figure 5.1.** Effects of  $\text{CO}_2$ , fertilization, and inoculation on leaf nitrogen per unit leaf area (a), leaf nitrogen content (b), leaf mass per unit leaf area (c), and chlorophyll content per unit leaf area (d). Soil nitrogen fertilization is represented on the x-axis in all panels. Yellow points and trendlines indicate inoculated individuals grown under ambient  $\text{CO}_2$ , blue points and trendlines indicate uninoculated individuals grown under ambient  $\text{CO}_2$ , red points and trendlines indicate inoculated individuals grown under elevated  $\text{CO}_2$ , and grey points indicate uninoculated individuals grown under elevated  $\text{CO}_2$ . Solid trendlines indicate regression slopes that are different from zero ( $p < 0.05$ ), while dashed trendlines indicate slopes that are not distinguishable from zero ( $p > 0.05$ ).

**2215** 5.3.2 *Leaf biochemistry and stomatal conductance*

**2216** Elevated CO<sub>2</sub> resulted in plants with 16% lower  $V_{cmax25}$  ( $p < 0.001$ ; Table  
**2217** 5.2) and 10% lower  $J_{max25}$  ( $p = 0.014$ ; Table 5.2) as compared to those grown under  
**2218** ambient CO<sub>2</sub>. However, CO<sub>2</sub> concentration did not influence  $R_{d25}$  ( $p = 0.613$ ;  
**2219** Table 5.2). A relatively stronger downregulation in  $V_{cmax25}$  than  $J_{max25}$  resulted  
**2220** in an 8% stimulation in  $J_{max25}:V_{cmax25}$  under elevated CO<sub>2</sub> ( $p < 0.001$ ; Table 5.2;  
**2221** Fig. 2E). The downregulatory effect of CO<sub>2</sub> on  $V_{cmax25}$  and  $J_{max25}$  was not modified  
**2222** across the fertilization gradient (CO<sub>2</sub>-by-fertilization interaction:  $p = 0.185$ ,  $p =$   
**2223** 0.389 for  $V_{cmax25}$  and  $J_{max25}$ , respectively; Table 5.2; Fig. 5.2a-b) or between  
**2224** inoculation treatments (CO<sub>2</sub>-by-inoculation interaction:  $p = 0.799$  and  $p = 0.714$   
**2225** for  $V_{cmax25}$  and  $J_{max25}$ , respectively; Table 5.2). However, a strong interaction  
**2226** between fertilization and inoculation (fertilization-by-inoculation interaction:  $p \leq$   
**2227** 0.001 in all cases; Table 5.2) indicated that the general positive effect of increasing  
**2228** fertilization on  $V_{cmax25}$  ( $p < 0.001$ ; Table 5.2),  $J_{max25}$  ( $p < 0.001$ ; Table 5.2), and  
**2229**  $R_{d25}$  ( $p = 0.015$ ; Table 2) was only observed in uninoculated pots (Tukey:  $p$   
**2230**  $\leq 0.001$  in all cases), as there was no apparent effect of fertilization on  $V_{cmax25}$   
**2231** (Tukey:  $p = 0.456$ ),  $J_{max25}$  (Tukey:  $p = 0.180$ ), or  $R_{d25}$  (Tukey:  $p = 0.443$ ) in  
**2232** inoculated pots (Figs. 5.2a-d). A relatively stronger positive effect of increasing  
**2233** fertilization on  $V_{cmax25}$  than  $J_{max25}$  resulted in a general reduction in  $J_{max25}:V_{cmax25}$   
**2234** with increasing fertilization ( $p < 0.001$ ), though this pattern was only seen in  
**2235** uninoculated pots (Tukey:  $p = 0.003$ ) and not inoculated plants (Tukey:  $p >$   
**2236** 0.05).

**2237** Elevated CO<sub>2</sub> reduced stomatal conductance by 20% ( $p < 0.001$ ; Table  
**2238** 5.2; Fig. 5.2e) compared to ambient CO<sub>2</sub>, but this downregulation did not influ-

ence stomatal limitation of photosynthesis ( $p = 0.355$ ; Table 5.2; Fig. 5.2f). As with  $V_{cmax25}$  and  $J_{max25}$ , the downregulation of stomatal conductance due to elevated CO<sub>2</sub> was not modified across the fertilization gradient (CO<sub>2</sub>-by-fertilization interaction:  $p = 0.141$ ; Table 5.2) or between inoculation treatments (CO<sub>2</sub>-by-inoculation interaction:  $p = 0.179$ ; Table 5.2). Fertilization also did not modify the general null effect of CO<sub>2</sub> on stomatal limitation (CO<sub>2</sub>-by-fertilization interaction:  $p = 0.554$ ; Table 5.2), although an interaction between CO<sub>2</sub> and inoculation (CO<sub>2</sub>-by-inoculation interaction:  $p = 0.043$ ; Table 5.2) indicated that inoculation increased stomatal limitation under ambient CO<sub>2</sub> (Tukey:  $p = 0.021$ ), but not under elevated CO<sub>2</sub> (Tukey:  $p > 0.999$ ). An interaction between inoculation and fertilization on stomatal conductance (fertilization-by-inoculation interaction:  $p < 0.001$ ; Table 5.2) indicated that increasing fertilization increased stomatal conductance in uninoculated pots (Tukey:  $p = 0.003$ ) but decreased stomatal conductance in inoculated pots (Tukey:  $p = 0.021$ ). The similar in magnitude, but opposite direction, trend in the effect of increasing fertilization on stomatal conductance between inoculation treatments likely drove a null general response of stomatal conductance to increasing fertilization ( $p = 0.642$ ; Table 5.2).

**Table 5.2.** Effects of soil nitrogen fertilization, inoculation, and CO<sub>2</sub> on leaf biochemistry

	<i>V<sub>cmax25</sub></i>			<i>J<sub>max25</sub></i>			<i>R<sub>d25</sub></i>			
	df	Coefficient	$\chi^2$	p	Coefficient	$\chi^2$	p	Coefficient	$\chi^2$	p
(Intercept)	-	4.36E+01	-	-	8.30E+01	-	-	1.69E+00	-	-
CO <sub>2</sub>	1	-7.05E+00	18.039	<0.001	-9.11E+00	6.042	<b>0.014</b>	4.53E-01	0.256	0.613
Inoculation (I)	1	5.87E+01	98.579	<0.001	9.62E+01	85.064	<0.001	1.04E+00	3.094	0.079
Fertilization (N)	1	1.32E-01	37.053	<0.001	2.09E-01	25.356	<0.001	2.86E-03	5.965	<b>0.015</b>
CO <sub>2</sub> *I	1	-4.65E+00	0.065	0.799	7.84E-01	0.667	0.414	-5.71E-01	2.563	0.109
CO <sub>2</sub> *N	1	-3.58E-02	1.758	0.185	-4.33E-02	0.742	0.389	-1.55E-03	2.675	0.102
I*N	1	-1.35E-01	60.394	<0.001	-2.30E-01	57.410	<0.001	-2.84E-03	12.083	<b>0.001</b>
CO <sub>2</sub> *I*N	1	2.73E-02	0.748	0.387	3.46E-02	0.377	0.539	7.21E-04	0.244	0.622

	<i>J<sub>max25</sub>:V<sub>cmax25</sub></i>			<i>g<sub>sw</sub></i>			Stomatal limitation			
	df	Coefficient	$\chi^2$	p	Coefficient	$\chi^2$	p	Coefficient	$\chi^2$	p
(Intercept)	-	1.92E+00	-	-	1.95E-01	-	-	2.12E-01	-	-
CO <sub>2</sub>	1	5.71E-02	92.010	<0.001	-6.23E-02	9.718	<b>0.002</b>	3.91E-02	0.856	0.355
Inoculation (I)	1	-1.79E-01	27.768	<0.001	1.30E-01	22.351	<0.001	7.87E-02	4.582	<b>0.032</b>
Fertilization (N)	1	-4.61E-04	28.147	<0.001	2.50E-04	0.066	0.797	2.60E-04	32.218	<0.001
CO <sub>2</sub> *I	1	8.94E-02	2.916	0.088	6.69E-02	1.810	0.179	-7.84E-02	4.093	<b>0.043</b>
CO <sub>2</sub> *N	1	2.35E-04	3.210	0.073	-8.50E-05	2.165	0.141	-1.24E-04	0.350	0.554
I*N	1	3.27E-04	9.607	<b>0.002</b>	-3.09E-04	14.696	<0.001	-1.67E-04	2.547	0.110
CO <sub>2</sub> *I*N	1	-1.66E-04	1.102	0.294	-8.89E-05	0.234	0.629	1.67E-04	2.231	0.135

134

2256 \*Significance determined using Type II Wald  $\chi^2$  tests ( $\alpha = 0.05$ ). *P*-values  $< 0.05$  are in bold, while *p*-values between  
 2257 0.05 and 0.1 are italicized. Key: *V<sub>cmax25</sub>* = maximum rate of Rubisco carboxylation at 25°C; *J<sub>max25</sub>* = maximum rate  
 2258 of electron transport for RuBP regeneration at 25°C, *R<sub>d25</sub>* = dark respiration at 25°C; *J<sub>max25</sub>:V<sub>cmax25</sub>* = the ratio of  
 2259 *J<sub>max25</sub>* to *V<sub>cmax25</sub>*; *g<sub>sw</sub>* = stomatal conductance.

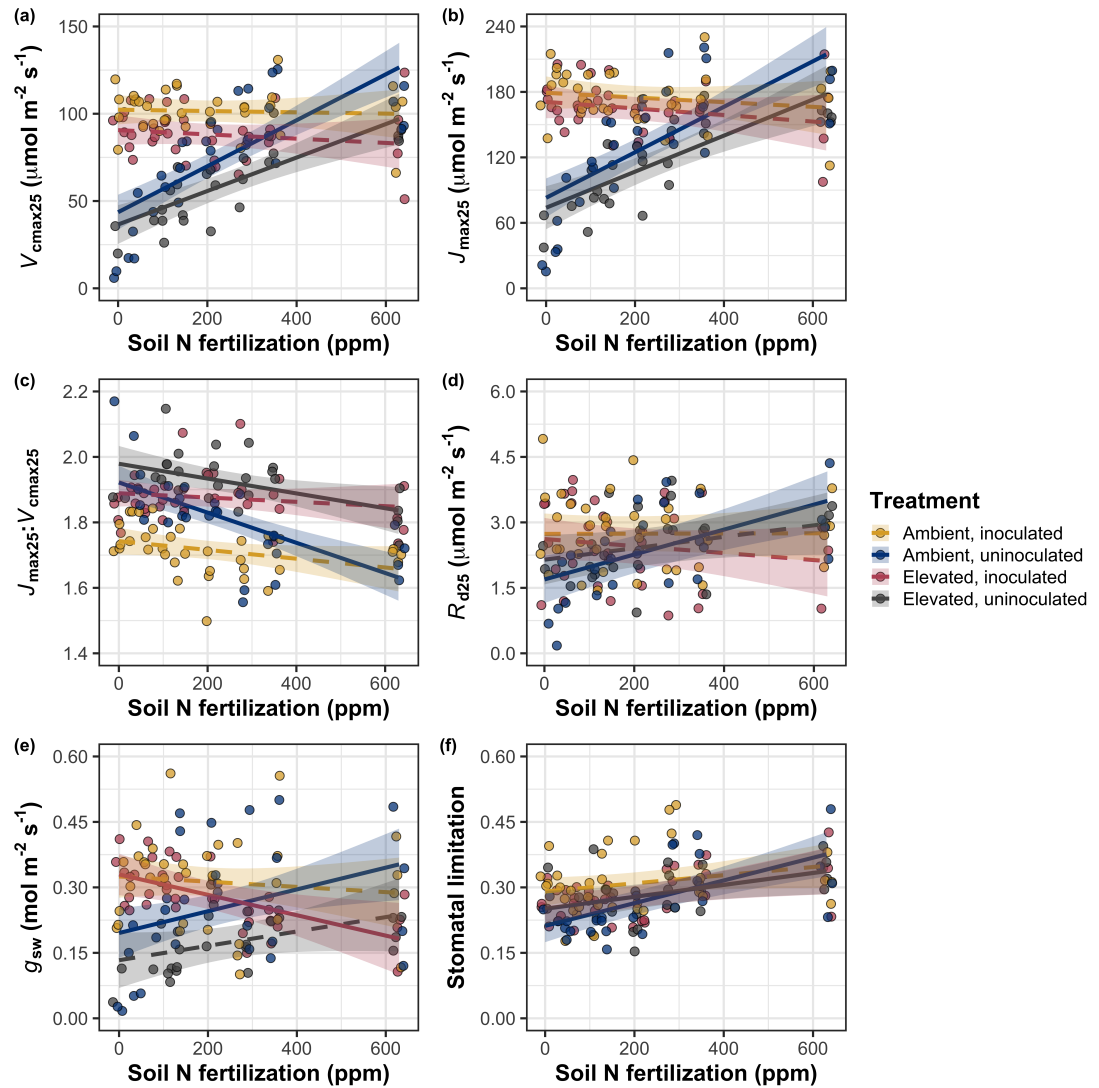


**Figure 5.2.** Effects of CO<sub>2</sub>, fertilization, and inoculation on maximum rate of Rubisco carboxylation (a), the maximum rate of RuBP regeneration (b), and the ratio of the maximum rate of RuBP regeneration to the maximum rate of Rubisco carboxylation leaf mass per unit leaf area (c), dark respiration (d), stomatal conductance (e), and stomatal limitation (f). Soil nitrogen fertilization is represented on the x-axis in all panels. Colored points and trendlines are as explained in Figure 1.

**2260** 5.3.3 *Leaf nitrogen allocation*

**2261** A relatively stronger downregulation in  $N_{\text{area}}$  than  $V_{\text{cmax}25}$  or  $J_{\text{max}25}$  resulted  
**2262** in an 20% and 29% respective stimulation in  $\rho_{\text{rubisco}}$  and  $\rho_{\text{bioe}}$  under elevated CO<sub>2</sub>  
**2263** ( $p < 0.001$  in both cases; Table 5.3). There was no apparent CO<sub>2</sub> effect on  $\rho_{\text{light}}$   
**2264** ( $p = 0.700$ ; Table 5.3), but the strong stimulation in  $\rho_{\text{rubisco}}$  and  $\rho_{\text{bioe}}$  resulted  
**2265** in a 21% stimulation of  $\rho_{\text{photo}}$  under elevated CO<sub>2</sub> ( $p < 0.001$ ; Table 5.3; Fig.  
**2266** 5.3a). The stimulation of  $\rho_{\text{rubisco}}$ ,  $\rho_{\text{bioe}}$ , and  $\rho_{\text{photo}}$  due to elevated CO<sub>2</sub> was not  
**2267** modified across the fertilization gradient (CO<sub>2</sub>-by-fertilization interaction:  $p_{\text{rubisco}}$   
**2268** = 0.269,  $p_{\text{bioe}} = 0.298$ ,  $p_{\text{photo}} = 0.281$ ; Table 5.3). A marginal interaction between  
**2269** inoculation and CO<sub>2</sub> on  $\rho_{\text{rubisco}}$  and  $\rho_{\text{photo}}$  (CO<sub>2</sub>-by-inoculation interaction:  $p_{\text{rubisco}}$   
**2270** = 0.057,  $p_{\text{photo}} = 0.057$ ; Table 5.3) indicated that the general positive effect of  
**2271** inoculation on  $\rho_{\text{rubisco}}$  and  $\rho_{\text{photo}}$  ( $p < 0.001$  in both cases; Table 5.3) was only  
**2272** apparent under ambient CO<sub>2</sub> (Tukey:  $p < 0.001$  in both cases), with no apparent  
**2273** effect of inoculation under elevated CO<sub>2</sub> (Tukey<sub>rubisco</sub>:  $p = 0.200$ ; Tukey<sub>photo</sub>:  $p$   
**2274** = 0.147). Inoculation did not modify the stimulation of  $\rho_{\text{bioe}}$  under elevated CO<sub>2</sub>  
**2275** (CO<sub>2</sub>-by-inoculation interaction:  $p = 0.122$ ; Table 5.3) or the null effect of CO<sub>2</sub> on  
**2276**  $\rho_{\text{bioe}}$  (CO<sub>2</sub>-by-inoculation interaction:  $p = 0.298$ ; Table 5.3). Strong interactions  
**2277** between fertilization and inoculation on  $\rho_{\text{rubisco}}$ ,  $\rho_{\text{bioe}}$ , and  $\rho_{\text{photo}}$  (fertilization-  
**2278** by-inoculation interaction:  $p < 0.001$  in all cases; Table 5.3) indicated that the  
**2279** general negative effect of increasing fertilization ( $p < 0.001$  in all cases; Table  
**2280** 5.3) was only observed in inoculated pots (Tukey:  $p < 0.001$  in all cases), with  
**2281** no apparent effect of fertilization on  $\rho_{\text{rubisco}}$  (Tukey:  $p = 0.612$ ),  $\rho_{\text{bioe}}$  (Tukey:  
**2282**  $p = 0.544$ ), or  $\rho_{\text{photo}}$  (Tukey:  $p = 0.521$ ; Fig 5.3a) in uninoculated pots. An  
**2283** additional interaction between fertilization and inoculation on  $\rho_{\text{light}}$  (fertilization-

**2284** by-inoculation interaction:  $p < 0.001$ ; Table 5.3) indicated a negative effect of  
**2285** increasing fertilization on  $\rho_{\text{light}}$  in inoculated pots (Tukey:  $p = 0.041$ ), but a  
**2286** positive effect of increasing fertilization in uninoculated pots (Tukey:  $p < 0.001$ ).

**2287** The stimulation in  $M_{\text{area}}$  resulted in an 133% stimulation of  $\rho_{\text{structure}}$  under  
**2288** elevated CO<sub>2</sub> ( $p < 0.001$ ; Table 5.3; Fig 5.3b). An interaction between fertiliza-  
**2289** tion and CO<sub>2</sub> (CO<sub>2</sub>-by-fertilization interaction:  $p = 0.039$ ; Table 5.3) indicated  
**2290** that the general negative effect of increasing fertilization ( $p < 0.001$ ; Table 5.3) on  
**2291**  $\rho_{\text{structure}}$  was marginally stronger under ambient CO<sub>2</sub> (Tukey:  $p = 0.055$ ), resulting  
**2292** in a stronger stimulation in  $\rho_{\text{structure}}$  under elevated CO<sub>2</sub> with increasing fertiliza-  
**2293** tion. A marginal interaction between inoculation and CO<sub>2</sub> (CO<sub>2</sub>-by-inoculation  
**2294** interaction:  $p = 0.057$ ; Table 5.3) indicated that the general positive effect of  
**2295** inoculation on  $\rho_{\text{structure}}$  ( $p < 0.001$ ; Table 5.3) was only observed under elevated  
**2296** CO<sub>2</sub> (Tukey:  $p < 0.001$ ), with no apparent inoculation effect observed under am-  
**2297** bient CO<sub>2</sub> (Tukey:  $p = 0.513$ ). Finally, an interaction between fertilization and  
**2298** inoculation (fertilization-by-inoculation interaction:  $p < 0.001$ ; Table 5.3) indi-  
**2299** cated that, while increasing fertilization generally increased  $\rho_{\text{structure}}$  ( $p < 0.001$ ;  
**2300** Table 5.3), this response was generally stronger in uninoculated pots (Tukey:  $p$   
**2301** = 0.001; Fig. 5.3b).

**Table 5.3.** Effects of soil N availability, soil pH, species, and  $N_{\text{area}}$  on leaf nitrogen allocation

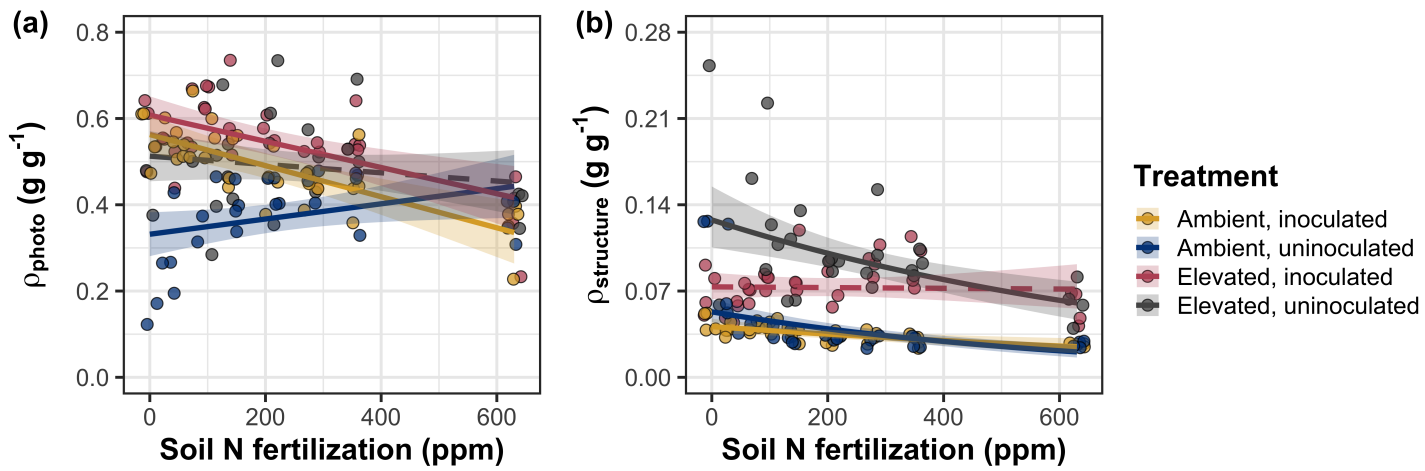
		$\rho_{\text{rubisco}}$		$\rho_{\text{bioe}}$		$\rho_{\text{light}}$				
	df	Coefficient	$\chi^2$	p	Coefficient	$\chi^2$	p	Coefficient	$\chi^2$	p
(Intercept)	-	2.70E-01	-	-	5.26E-02	-	-	8.48E-03	-	-
$\text{CO}_2$	1	1.42E-01	23.510	<b>&lt;0.001</b>	3.00E-02	53.899	<b>&lt;0.001</b>	2.03E-03	0.149	0.700
Inoculation (I)	1	1.83E-01	23.475	<b>&lt;0.001</b>	2.80E-02	13.860	<b>&lt;0.001</b>	2.04E-02	147.234	<b>&lt;0.001</b>
Fertilization (N)	1	1.35E-04	16.609	<b>&lt;0.001</b>	1.22E-05	26.827	<b>&lt;0.001</b>	3.22E-05	19.378	<b>&lt;0.001</b>
$\text{CO}_2*I$	1	-1.07E-01	3.629	<i>0.057</i>	-1.67E-02	2.390	0.122	-5.33E-03	0.684	0.408
$\text{CO}_2*N$	1	-2.16E-04	1.223	0.269	-3.59E-05	1.085	0.298	-7.01E-06	0.351	0.553
$I*N$	1	-4.26E-04	20.045	<b>&lt;0.001</b>	-6.87E-05	15.458	<b>&lt;0.001</b>	-4.37E-05	64.042	<b>&lt;0.001</b>
$\text{CO}_2*I*N$	1	2.50E-04	3.327	<i>0.068</i>	4.08E-05	2.651	0.103	1.74E-05	3.735	<i>0.053</i>

		$\rho_{\text{photo}}$		$\rho_{\text{structure}}^a$				
	df	Coefficient	$\chi^2$	p	Coefficient	$\chi^2$	p	
(Intercept)	-	3.32E-01	-	-	-2.93E+00	-	-	
$\text{CO}_2$	1	1.81E-01	27.651	<b>&lt;0.001</b>	8.77E-01	229.571	<b>&lt;0.001</b>	
Inoculation (I)	1	2.31E-01	26.238	<b>&lt;0.001</b>	-2.55E-01	13.872	<b>&lt;0.001</b>	
Fertilization (N)	1	1.76E-04	15.899	<b>&lt;0.001</b>	-1.51E-03	38.128	<b>&lt;0.001</b>	
$\text{CO}_2*I$	1	-1.36E-01	3.671	<i>0.055</i>	-2.99E-01	3.622	<i>0.057</i>	
$\text{CO}_2*N$	1	-2.72E-04	1.163	0.281	3.14E-04	4.266	<b>0.039</b>	
$I*N$	1	-5.37E-04	21.355	<b>&lt;0.001</b>	7.00E-04	11.025	<b>0.001</b>	
$\text{CO}_2*I*N$	1	3.29E-04	4.009	<b>0.045</b>	4.52E-04	0.669	0.413	

138

2302 \*Significance determined using Type II Wald  $\chi^2$  tests ( $\alpha = 0.05$ ).  $P$ -values  $< 0.05$  are in bold, while  $p$ -values  
 2303 between 0.05 and 0.1 are italicized. A superscript “a” is included after trait labels to indicate if models were fit with  
 2304 natural log transformed response variables. Key: df=degrees of freedom,  $\rho_{\text{rubisco}}$  = proportion of leaf N allocated  
 2305 to photosynthesis,  $\rho_{\text{bioe}}$  = proportion of leaf N allocated to bioenergetics,  $\rho_{\text{light}}$  = proportion of leaf N allocated to  
 2306 light harvesting proteins,  $\rho_{\text{photo}}$  = proportion of leaf N allocated to photosynthesis,  $\rho_{\text{structure}}$  = proportion of leaf N  
 2307 allocated to cell wall structural tissue



**Figure 5.3.** Effects of  $\text{CO}_2$ , fertilization, and inoculation on the relative fraction of leaf nitrogen allocated to photosynthesis (a) and the fraction of leaf nitrogen allocated to structure (b). Soil nitrogen fertilization is represented on the x-axis in both panels. Colored points and trendlines are as explained in Figure 1.

**2308** 5.3.4 *Whole plant traits*

**2309** Total leaf area was 51% greater and total biomass was 102% greater under  
**2310** elevated CO<sub>2</sub> ( $p < 0.001$  in both cases; Table 5.4), a pattern that was enhanced  
**2311** by fertilization (CO<sub>2</sub>-by-fertilization interaction:  $p < 0.001$  in both cases; Table  
**2312** 5.4; Figs. 5.4a-b) but was not modified across inoculation treatments (CO<sub>2</sub>-by-  
**2313** inoculation interaction:  $p_{total\_leaf\_area} = 0.151$ ,  $p_{total\_biomass} = 0.472$ ; Table 5.4).  
**2314** Specifically, the general positive effect of increasing fertilization on total leaf area  
**2315** and whole plant biomass ( $p < 0.001$  in both cases; Table 5.4) was stronger under  
**2316** elevated CO<sub>2</sub> (Tukey:  $p < 0.001$  in both cases). The general positive effect of  
**2317** increasing fertilization on total leaf area was modified by inoculation treatment  
**2318** (fertilization-by-inoculation interaction:  $p < 0.001$  in both cases; Table 5.4), in-  
**2319** dicating a stronger positive effect of increasing fertilization in uninoculated pots  
**2320** (Tukey:  $p_{total\_leaf\_area} = 0.002$ ,  $p_{total\_biomass} = 0.001$ , Fig. 5.4a).

**2321** A 62% stimulation in  $N_{cost}$  under elevated CO<sub>2</sub> was modified through a  
**2322** strong three-way interaction between CO<sub>2</sub>, fertilization, and inoculation (CO<sub>2</sub>-  
**2323** by-inoculation-by-fertilization interaction:  $p < 0.001$ ; Table 5.4; Fig. 5.4). This  
**2324** interaction revealed a general negative effect of increasing fertilization on  $N_{cost}$   
**2325** ( $p < 0.001$ ; Table 5.4) that was observed in all treatment combinations (Tukey:  
**2326**  $p < 0.001$  in all cases) except for inoculated pots grown under elevated CO<sub>2</sub>  
**2327** (Tukey:  $p = 0.779$ ; Fig. 5.4c). This response also resulted in generally stronger  
**2328** negative effects of increasing fertilization on  $N_{cost}$  in uninoculated pots grown  
**2329** under elevated CO<sub>2</sub> than uninoculated pots grown under ambient CO<sub>2</sub> (Tukey:  
**2330**  $p = 0.001$ ) and inoculated pots grown under either ambient CO<sub>2</sub> (Tukey:  $p <$   
**2331** 0.001) or elevated CO<sub>2</sub> (Tukey:  $p < 0.001$ ), while uninoculated pots grown under

**2332** ambient CO<sub>2</sub> had generally stronger negative effects of increasing fertilization on  
**2333**  $N_{\text{cost}}$  than inoculated pots grown under elevated CO<sub>2</sub> (Tukey:  $p = 0.002$ ), but  
**2334** not inoculated pots grown under ambient CO<sub>2</sub> (Tukey:  $p = 0.216$ ; Fig. 5.4).  
**2335** The general reduction in  $N_{\text{cost}}$  with increasing fertilization and in uninoculated  
**2336** pots were driven by a stronger positive effect of increasing fertilization on  $N_{\text{wp}}$   
**2337** (denominator of  $N_{\text{cost}}$ ) than  $C_{\text{bg}}$  (numerator of  $N_{\text{cost}}$ ), while the general stimulation  
**2338** in  $N_{\text{cost}}$  under elevated CO<sub>2</sub> was driven by a stronger positive effect of elevated  
**2339** CO<sub>2</sub> on  $C_{\text{bg}}$  than  $N_{\text{wp}}$  (Table 5.4).

**Table 5.4.** Effects of soil N availability, soil pH, species, and  $N_{\text{area}}$  on total leaf area, whole plant biomass, and carbon costs to acquire nitrogen

	Total leaf area			Total biomass			$N_{\text{cost}}$			
	df	Coefficient	$\chi^2$	p	Coefficient	$\chi^2$	p	Coefficient	$\chi^2$	p
(Intercept)	-	8.78E+01	-	-	9.96E-01	-	-	8.67E+00	-	-
$\text{CO}_2$	1	3.36E+01	69.291	<b>&lt;0.001</b>	5.07E-01	131.477	<b>&lt;0.001</b>	8.75E+00	88.189	<b>&lt;0.001</b>
Inoculation (I)	1	1.88E+02	35.715	<b>&lt;0.001</b>	7.96E-01	34.264	<b>&lt;0.001</b>	-1.68E+00	136.343	<b>&lt;0.001</b>
Fertilization (N)	1	9.35E-01	274.199	<b>&lt;0.001</b>	3.14E-03	269.046	<b>&lt;0.001</b>	-8.50E-03	80.501	<b>&lt;0.001</b>
$\text{CO}_2 * \text{I}$	1	6.44E+01	2.064	0.151	-7.69E-02	0.518	0.472	-8.38E+00	85.237	<b>&lt;0.001</b>
$\text{CO}_2 * \text{N}$	1	5.05E-01	18.655	<b>&lt;0.001</b>	1.61E-03	16.877	<b>&lt;0.001</b>	-9.17E-03	1.050	0.306
$\text{I} * \text{N}$	1	-3.84E-01	10.804	<b>0.001</b>	-1.45E-03	15.779	<b>&lt;0.001</b>	4.20E-03	46.489	<b>&lt;0.001</b>
$\text{CO}_2 * \text{I} * \text{N}$	1	-2.97E-03	<0.001	0.990	-1.14E-04	0.023	0.880	1.32E-02	18.125	<b>&lt;0.001</b>

	$C_{\text{bg}}$			$N_{\text{wp}}$			
	df	Coefficient	$\chi^2$	p	Coefficient	$\chi^2$	p
(Intercept)	-	-1.70E+00	-	-	1.24E-01	-	-
$\text{CO}_2$	1	9.21E-01	84.134	<b>&lt;0.001</b>	-3.41E-03	23.890	<b>&lt;0.001</b>
Inoculation (I)	1	1.18E+00	41.030	<b>&lt;0.001</b>	1.68E-01	134.460	<b>&lt;0.001</b>
N fertilization (N)	1	3.38E-03	152.248	<b>&lt;0.001</b>	6.69E-04	529.021	<b>&lt;0.001</b>
$\text{CO}_2 * \text{I}$	1	-6.18E-01	8.965	<b>0.003</b>	3.68E-02	1.190	0.275
$\text{CO}_2 * \text{N}$	1	-3.66E-05	1.188	0.276	1.58E-04	5.915	<b>0.015</b>
$\text{I} * \text{N}$	1	-2.22E-03	22.648	<b>&lt;0.001</b>	-3.20E-04	55.562	<b>&lt;0.001</b>
$\text{CO}_2 * \text{I} * \text{N}$	1	8.09E-04	1.109	0.292	-7.54E-05	0.620	0.431

142

2340 \*Significance determined using Type II Wald  $\chi^2$  tests ( $\alpha = 0.05$ ). P-values  $< 0.05$  are in bold, while p-values between  
 2341 0.05 and 0.1 are italicized. Key: df = degrees of freedom;  $N_{\text{cost}}$  = structural carbon cost to acquire nitrogen;  $C_{\text{bg}}$  =  
 2342 belowground carbon biomass;  $N_{\text{wp}}$  = whole plant nitrogen biomass

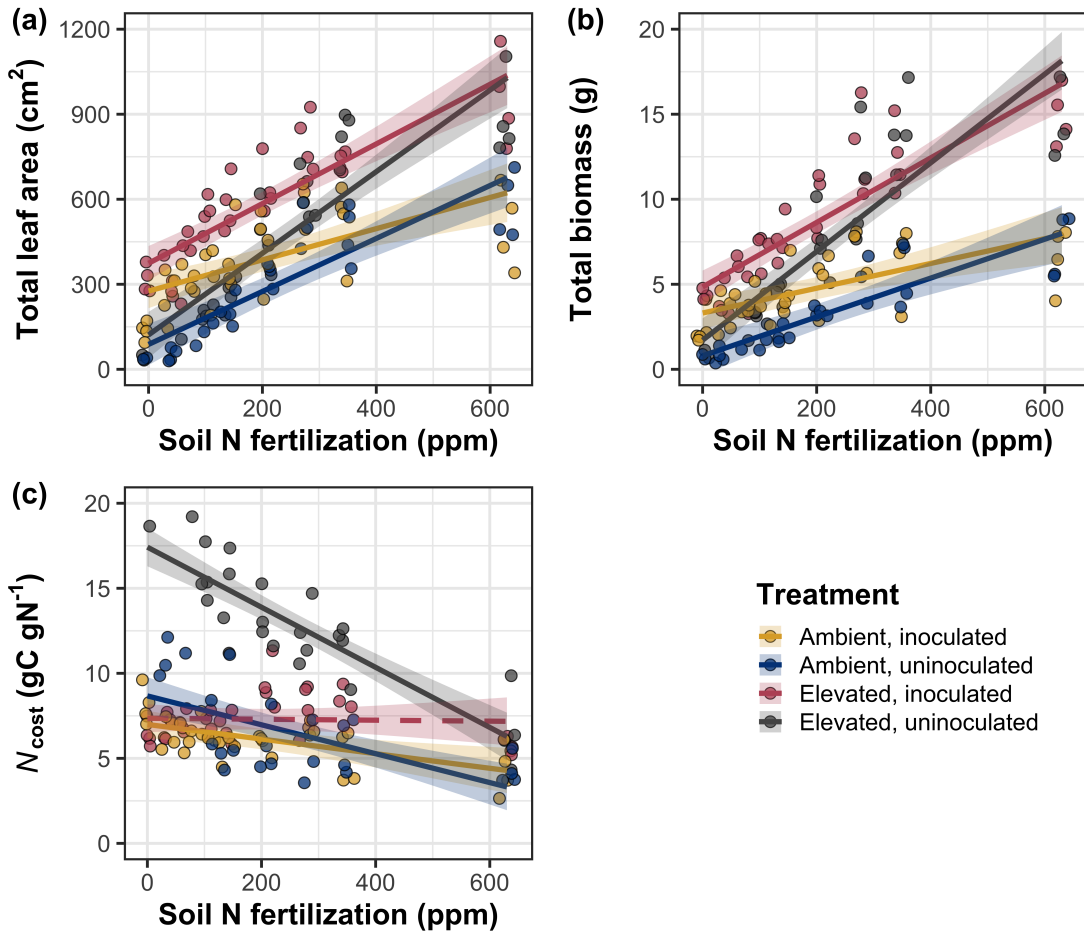


**Figure 5.4.** Effects of  $\text{CO}_2$ , fertilization, and inoculation on total leaf area (a), total biomass (b), and structural carbon costs to acquire nitrogen (c). Soil nitrogen fertilization is represented continuously on the x-axis in all panels. Colored points and trendlines are as explained in Figure 1.

**2343** 5.3.5 *Nitrogen fixation*

**2344** Nodule biomass was stimulated by 30% under elevated CO<sub>2</sub> ( $p < 0.001$ ;  
**2345** Table 5.5), a pattern that was modified across the fertilization gradient (CO<sub>2</sub>-  
**2346** by-fertilization interaction:  $p = 0.479$ ; Table 5.5), but not between inoculation  
**2347** treatments (CO<sub>2</sub>-by-inoculation interaction:  $p = 0.404$ ; Table 5.5). Specifically,  
**2348** the general negative effect of increasing fertilization on nodule biomass ( $p < 0.001$ ;  
**2349** Table 5.5) was stronger under elevated CO<sub>2</sub> than ambient CO<sub>2</sub> (Tukey:  $p <$   
**2350** 0.001; Fig. 5.5a), which reduced the stimulation in nodule biomass under elevated  
**2351** CO<sub>2</sub> with increasing fertilization. A strong interaction between fertilization and  
**2352** inoculation (fertilization-by-inoculation interaction:  $p < 0.001$ ; Table 5.5) was  
**2353** driven by a stronger negative effect of increasing fertilization in inoculated pots  
**2354** (Tukey:  $p < 0.001$ ; Fig. 5.5a).

**2355** There was no effect of CO<sub>2</sub> on nodule: root biomass ( $p = 0.767$ ; Table  
**2356** 5.5), although an interaction between CO<sub>2</sub> and inoculation (CO<sub>2</sub>-by-inoculation  
**2357** interaction:  $p < 0.001$ ; Table 5.5) indicated that the general positive effect of in-  
**2358** oculation on nodule: root biomass ( $p < 0.001$ ; Table 5.5) was stronger under am-  
**2359** bient CO<sub>2</sub> (3129% increase; Tukey:  $p < 0.001$ ) than elevated CO<sub>2</sub> (379% increase;  
**2360** Tukey:  $p < 0.001$ ; Fig. 5.5b). The null effect of CO<sub>2</sub> on nodule: root biomass  
**2361** was consistently observed across the fertilization gradient ( $p = 0.183$ ; Table 5.5;  
**2362** Fig. 5.5b). An interaction between fertilization and inoculation (fertilization-by-  
**2363** inoculation interaction:  $p < 0.001$ ; Table 5.5) indicated that the general negative  
**2364** effect of increasing fertilization on nodule: root biomass ( $p < 0.001$ ; Table 5.5)  
**2365** was stronger in inoculated pots (Tukey:  $p < 0.001$ ; Fig. 5.5b).

**2366** There was no effect of CO<sub>2</sub> on %N<sub>dfa</sub> ( $p = 0.472$ ; Table 5.5), a pattern

**2367** that was not modified by inoculation ( $\text{CO}_2$ -by-inoculation interaction:  $p = 0.156$ ;  
**2368** Table 5.5) or fertilization ( $\text{CO}_2$ -by-fertilization interaction:  $p = 0.099$ ; Table 5.5).  
**2369** An interaction between fertilization and inoculation (fertilization-by-inoculation  
**2370** interaction:  $p < 0.001$ ; Table 5.5) indicated that the general negative effect of  
**2371** increasing fertilization on  $\%N_{\text{dfa}}$  ( $p < 0.001$ ; Table 5.5) was only observed in  
**2372** inoculated pots (Tukey:  $p < 0.001$ ), with no apparent effect of fertilization on  
**2373**  $\%N_{\text{dfa}}$  in uninoculated pots (Tukey:  $p = 0.651$ ; Table 5.5; Fig. 5.5c).

**Table 5.5.** Effects of soil N availability, soil pH, species, and  $N_{\text{area}}$  on root nodule biomass and plant investments in symbiotic nitrogen fixation

	Root nodule biomass <sup>b</sup>			Root nodule: root biomass <sup>b</sup>			% $N_{\text{dfa}}^b$			
	df	Coefficient	$\chi^2$	p	Coefficient	$\chi^2$	p	Coefficient	$\chi^2$	p
(Intercept)	-	9.41E-03	-	-	1.33E-02	-	-	7.48E-01	-	-
CO <sub>2</sub>	1	1.20E-01	19.258	<b>&lt;0.001</b>	9.94E-02	0.087	0.768	-1.00E-01	0.518	0.472
Inoculation (I)	1	5.74E-01	755.020	<b>&lt;0.001</b>	5.40E-01	903.691	<b>&lt;0.001</b>	9.01E+00	955.570	<b>&lt;0.001</b>
Fertilization (N)	1	7.71E-06	84.376	<b>&lt;0.001</b>	-5.99E-06	258.099	<b>&lt;0.001</b>	3.64E-04	292.938	<b>&lt;0.001</b>
CO <sub>2</sub> *I	1	-4.68E-02	0.950	0.330	-1.38E-01	20.614	<b>&lt;0.001</b>	-1.44E-01	2.010	0.156
CO <sub>2</sub> *N	1	-1.59E-04	2.106	0.147	-1.73E-04	1.773	0.183	-6.21E-05	2.716	0.099
I*N	1	-5.82E-04	44.622	<b>&lt;0.001</b>	-7.45E-04	133.918	<b>&lt;0.001</b>	-1.58E-02	231.290	<b>&lt;0.001</b>
CO <sub>2</sub> *I*N	1	7.26E-05	0.196	0.658	1.76E-04	2.359	0.125	2.77E-03	2.119	0.145

**2374** \*Significance determined using Type II Wald  $\chi^2$  tests ( $\alpha = 0.05$ ). P-values  $< 0.05$  are in bold, while p-values between  
**2375** 0.05 and 0.1 are italicized. Superscript letters indicate model coefficients fit to square-root (<sup>b</sup>) transformed data.  
**2376** Key: df = degrees of freedom % $N_{\text{dfa}}$  = percent nitrogen fixed from the atmosphere.

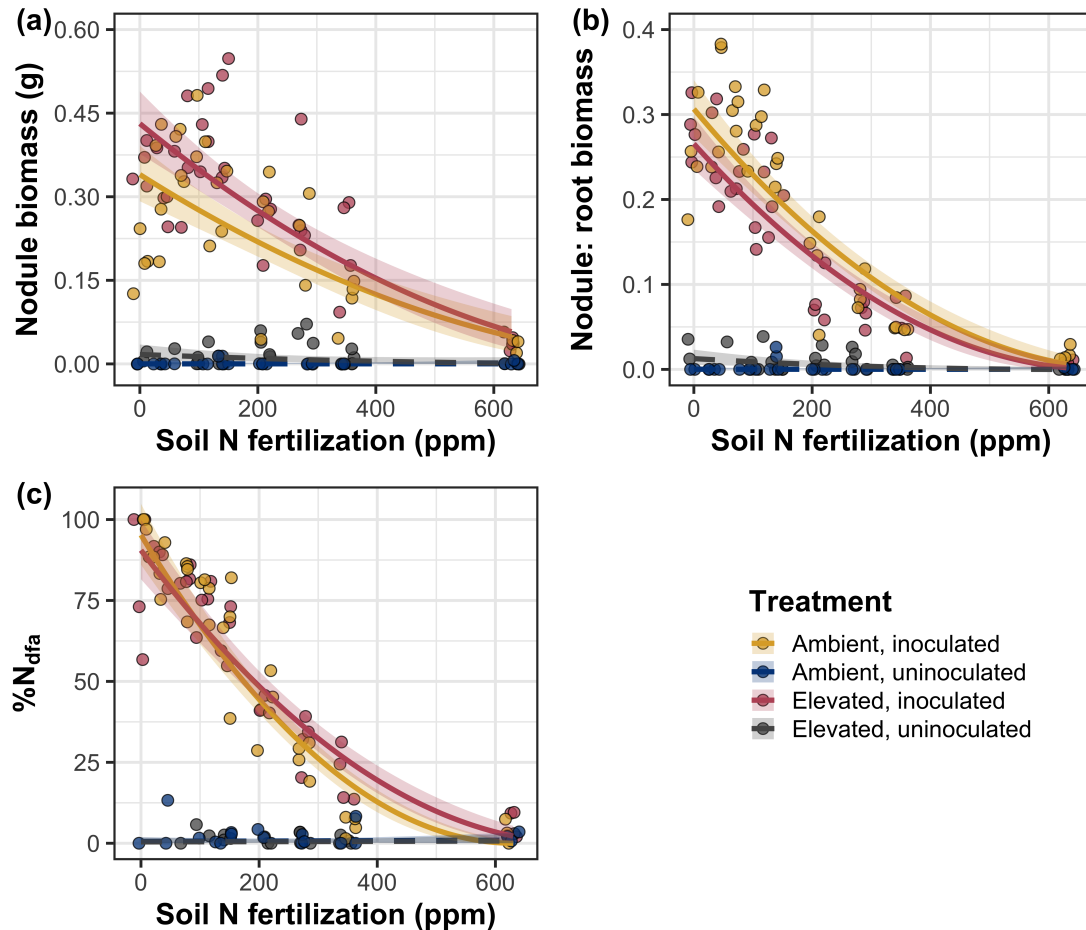


**Figure 5.5.** Effects of  $\text{CO}_2$ , fertilization, and inoculation on nodule biomass (a), nodule: root biomass (b), and percent nitrogen fixed from the atmosphere (c). Soil nitrogen fertilization is represented on the x-axis. Yellow points and trendlines indicate inoculated individuals grown under ambient  $\text{CO}_2$ , blue points and trendlines indicate uninoculated individuals grown under ambient  $\text{CO}_2$ , red points and trendlines indicate inoculated individuals grown under elevated  $\text{CO}_2$ , and grey points indicate uninoculated individuals grown under elevated  $\text{CO}_2$ . Solid trendlines indicate slopes that are different from zero ( $p < 0.05$ ), while dashed trendlines indicate slopes that are not different from zero ( $p > 0.05$ ). Curvilinear trendlines occur as a result of back-transforming models where response variables received either a natural log or square root transformation prior to fitting.

**2377** 5.4 Discussion

**2378** In this study, I determined leaf and whole plant acclimation responses of  
**2379** 7-week *G. max* seedlings grown under two CO<sub>2</sub> concentrations, two inoculation  
**2380** treatments, and nine soil nitrogen fertilization treatments in a full-factorial growth  
**2381** chamber experiment. In support of my hypotheses and patterns expected from  
**2382** theory, elevated CO<sub>2</sub> reduced  $N_{\text{area}}$ ,  $V_{\text{cmax25}}$ , and  $J_{\text{max25}}$ . The relatively stronger  
**2383** downregulation in  $V_{\text{cmax25}}$  than  $J_{\text{max25}}$  under elevated CO<sub>2</sub> resulted in a stimulation  
**2384** in  $J_{\text{max25}}:V_{\text{cmax25}}$  under elevated CO<sub>2</sub>. The downregulation of  $V_{\text{cmax25}}$  and  $J_{\text{max25}}$   
**2385** under elevated CO<sub>2</sub> was similar across fertilization and inoculation treatments,  
**2386** indicating that the CO<sub>2</sub> responses were not due to nitrogen limitation. Interest-  
**2387** ingly, results indicate that elevated CO<sub>2</sub> increased the fraction of leaf nitrogen  
**2388** allocated to photosynthesis and structure, leading to a stimulation in nitrogen  
**2389** use efficiency under elevated CO<sub>2</sub> despite the apparent downregulation in  $N_{\text{area}}$ ,  
**2390**  $V_{\text{cmax25}}$ , and  $J_{\text{max25}}$ . The downregulation in leaf photosynthetic processes under  
**2391** elevated CO<sub>2</sub> also corresponded with a strong stimulation in total leaf area and to-  
**2392** tal biomass. Strong stimulations in whole plant growth due to elevated CO<sub>2</sub> were  
**2393** generally enhanced with increasing fertilization and were negatively related to  
**2394** structural carbon costs to acquire nitrogen. Inoculation generally did not modify  
**2395** whole plant responses to elevated CO<sub>2</sub> across the fertilization gradient, likely due  
**2396** to a strong reduction in root nodulation with increasing fertilization. However,  
**2397** strong positive effects of inoculation on whole plant growth were observed under  
**2398** low fertilization, consistent with our hypothesis. Overall, observed leaf and whole  
**2399** plant acclimation responses to CO<sub>2</sub> support hypotheses and patterns expected  
**2400** from photosynthetic least-cost theory, showing that leaf acclimation responses to

2401 CO<sub>2</sub> were decoupled from soil nitrogen availability and ability to acquire nitro-  
2402 gen via symbiotic nitrogen fixation. Instead, leaf and whole plant acclimation  
2403 responses to CO<sub>2</sub> were driven by optimal resource investment to photosynthetic  
2404 capacity, where optimal resource investment at the leaf level maximized nitrogen  
2405 allocation to structures that support whole plant growth.

2406 5.4.1 *Soil nitrogen fertilization has divergent effects on leaf and whole plant*  
2407 *acclimation responses to CO<sub>2</sub>*

2408 Elevated CO<sub>2</sub> reduced  $N_{\text{area}}$ ,  $V_{\text{cmax25}}$ ,  $J_{\text{max25}}$ , and stomatal conductance by  
2409 29%, 16%, 10%, and 20%, respectively (Table 5.2). The larger downregulation in  
2410  $V_{\text{cmax25}}$  than  $J_{\text{max25}}$  led to an 8% stimulation in  $J_{\text{max25}}:V_{\text{cmax25}}$  (Table 5.2), while  
2411 the larger downregulation in  $N_{\text{area}}$  than  $V_{\text{cmax25}}$  resulted in a 21% stimulation  
2412 in the fraction of leaf nitrogen allocated to photosynthesis under elevated CO<sub>2</sub>.  
2413 These acclimation responses are directionally consistent with previous studies that  
2414 have investigated or reviewed leaf acclimation responses to CO<sub>2</sub> (Drake et al.  
2415 1997; Makino et al. 1997; Ainsworth et al. 2002; Ainsworth and Long 2005;  
2416 Ainsworth and Rogers 2007; Smith and Dukes 2013; Smith and Keenan 2020;  
2417 Poorter et al. 2022), and follow patterns expected from photosynthetic least-cost  
2418 theory (Wright et al. 2003; Prentice et al. 2014; Smith et al. 2019; Smith and  
2419 Keenan 2020). Together, the stimulation in  $J_{\text{max25}}:V_{\text{cmax25}}$  and the fraction of leaf  
2420 nitrogen allocated to photosynthesis, and nitrogen use efficiency under elevated  
2421 CO<sub>2</sub> provide strong support for the idea that leaves were downregulating  $V_{\text{cmax25}}$   
2422 in response to elevated CO<sub>2</sub> in order to optimally coordinate photosynthesis such  
2423 that net photosynthesis rates approached becoming equally co-limited by Rubisco

**2424** carboxylation and RuBP regeneration (Chen et al. 1993; Maire et al. 2012).

**2425** Increasing fertilization and inoculation induced strong positive effects on  
**2426**  $N_{\text{area}}$  (Fig. 1a),  $V_{\text{cmax}25}$  (Fig. 5.2a),  $J_{\text{max}25}$  (Fig. 5.2b). The general positive  
**2427** response of  $N_{\text{area}}$  to increasing fertilization and in inoculated pots was enhanced  
**2428** under ambient CO<sub>2</sub>, which, paired with the general downregulation in  $N_{\text{area}}$  un-  
**2429** der elevated CO<sub>2</sub>, resulted in a stronger downregulation of  $N_{\text{area}}$  under elevated  
**2430** CO<sub>2</sub> with increasing fertilization and in inoculated pots (Fig. 5.1a). These pat-  
**2431** terns suggest that  $N_{\text{area}}$  responses to CO<sub>2</sub> were at least partially dependent on  
**2432** soil nitrogen fertilization and nitrogen acquisition strategy. However, the general  
**2433** stimulation in the fraction of leaf nitrogen allocated to Rubisco, bioenergetics,  
**2434** or photosynthesis under elevated CO<sub>2</sub> was not modified across the fertilization  
**2435** gradient and was only marginally enhanced in inoculated pots. These patterns  
**2436** suggest that the increased downregulation of Narea under elevated CO<sub>2</sub> with in-  
**2437** creasing fertilization was not associated with a change in relative investment to  
**2438** photosynthetic tissue. Instead, a stronger downregulation in the fraction of leaf  
**2439** nitrogen allocated to structure under ambient CO<sub>2</sub> resulted in a stronger stim-  
**2440** ulation in  $\rho_{\text{structure}}$  under elevated CO<sub>2</sub> with increasing fertilization (Fig. 5.3b),  
**2441** indicating that fertilization shifted relative investment in leaf structural tissue un-  
**2442** der elevated CO<sub>2</sub>. These results, combined with a stimulation in PNUE (Fig. SX)  
**2443** and iWUE (Fig. SX) under elevated CO<sub>2</sub> that was independent of fertilization  
**2444** or inoculation treatment, provide additional support for the hypothesis that leaf  
**2445** acclimation photosynthetic responses to CO<sub>2</sub> were independent of fertilization;  
**2446** though fertilization may contribute to changes in leaf morphology under elevated  
**2447** CO<sub>2</sub> through shifts in  $M_{\text{area}}$  (Onoda et al. 2017; Wang et al. 2017; Dong et al.

**2448** 2022).

**2449** The downregulation in  $N_{\text{area}}$ ,  $V_{\text{cmax}25}$ , and  $J_{\text{max}25}$  under elevated CO<sub>2</sub> cor-  
**2450** responded with a respective 62% and 100% stimulation in total leaf area (Fig.  
**2451** 5.4a) and total biomass (Fig. 5.4b). The stimulation in total leaf area and total  
**2452** biomass under elevated CO<sub>2</sub> also corresponded with generally higher structural  
**2453** carbon costs to acquire nitrogen (Fig. 5.4c), a pattern driven by a stimulation  
**2454** in belowground carbon biomass and reduction in whole plant nitrogen biomass.  
**2455** Alone, this result suggests that elevated CO<sub>2</sub> reduces plant nitrogen uptake effi-  
**2456** ciency, which does not explain why plants grown under elevated CO<sub>2</sub> generally had  
**2457** higher biomass and total leaf area. However, a strong negative effect of increasing  
**2458** fertilization on structural carbon costs to acquire nitrogen, which were generally  
**2459** similar between CO<sub>2</sub> concentrations, was driven by a stronger increase in whole  
**2460** plant nitrogen biomass than belowground carbon biomass. Thus, increases in the  
**2461** positive response of whole plant growth and total leaf area under elevated CO<sub>2</sub>  
**2462** with increasing fertilization were likely driven by an increase in nitrogen uptake  
**2463** efficiency, allowing plants to satisfy any increase in whole plant nitrogen demand  
**2464** associated with increased CO<sub>2</sub>.

**2465** Interestingly, these results indicate that the general stimulation in total  
**2466** leaf area and whole plant growth under elevated CO<sub>2</sub> was not modified by inoc-  
**2467** ulation despite an apparent general negative effect of inoculation on  $N_{\text{cost}}$ . This  
**2468** response could have been due to strong negative effect of increasing fertilization on  
**2469** nodulation (Fig. 5.5), which may have caused the strong increase in the positive  
**2470** effect of elevated CO<sub>2</sub> on whole plant growth with increasing fertilization to mask  
**2471** any increase in the positive effect of elevated CO<sub>2</sub> on whole plant growth due to

**2472** inoculation. Reductions in nodulation with increasing fertilization are commonly  
**2473** observed patterns that have been inferred to be a response that allows species  
**2474** optimize nitrogen uptake efficiency as costs to acquire nitrogen via direct uptake  
**2475** become more similar (Fig. 5.4c) (Gibson and Harper 1985; Rastetter et al. 2001).  
**2476** In this study, pairwise comparisons indicated strong positive effects of inocula-  
**2477** tion on total leaf area and total biomass (158% increase in total leaf area, 119%  
**2478** increase in total biomass) under elevated CO<sub>2</sub> at 0 ppm N, but no observable  
**2479** inoculation effect on total leaf area or total biomass under elevated CO<sub>2</sub> at 350  
**2480** ppm N or 630 ppm N. While these responses did not generally differ from those  
**2481** observed under ambient CO<sub>2</sub>, they do confirm the hypothesis that positive effects  
**2482** of inoculation on whole plant growth responses to elevated CO<sub>2</sub> would decrease  
**2483** with increasing fertilization.

**2484** Combined, results reported here suggest that soil nitrogen availability has  
**2485** a divergent role in modifying leaf and whole plant acclimation responses to CO<sub>2</sub>.  
**2486** Leaf acclimation responses were generally decoupled from fertilization, while whole  
**2487** plant acclimation responses relied heavily on an increase in nitrogen uptake ef-  
**2488** ficiency and consequent reduction in costs of acquiring nitrogen associated with  
**2489** increasing fertilization. However, whole plant responses to CO<sub>2</sub> indicated that  
**2490** fertilization may play a more important role in determining whole plant acclima-  
**2491** tion responses to CO<sub>2</sub> than nitrogen acquisition strategy, although these patterns  
**2492** were likely driven by reductions in nodulation with increasing fertilization. These  
**2493** results suggest that plants acclimate to CO<sub>2</sub> in nitrogen-limited systems by mini-  
**2494** mizing the number of optimally coordinated leaves, and that the downregulation  
**2495** in leaf nitrogen content under elevated CO<sub>2</sub> is not a direct response to changes in

**2496** soil nitrogen availability as previously implied.

**2497** 5.4.2 *Implications for future model development*

**2498** Many terrestrial biosphere models predict photosynthetic capacity through  
**2499** plant functional group-specific linear regressions between  $N_{\text{area}}$  and  $V_{\text{cmax}}$  (Rogers  
**2500** 2014; Rogers et al. 2017), which assumes that leaf nitrogen-photosynthesis rela-  
**2501** tionships are constant across growing environments. Our results build on previ-  
**2502** ous work suggesting that leaf nitrogen-photosynthesis relationships dynamically  
**2503** change across growing environments (Luo et al. 2021; Dong et al. 2022). Specif-  
**2504** ically, results from this experiment indicate that  $\text{CO}_2$  concentration increased  
**2505** the fraction of leaf nitrogen content allocated to photosynthesis, while a general  
**2506** negative effect of increasing fertilization on the fraction of leaf nitrogen content  
**2507** allocated to photosynthesis was dependent on inoculation treatment. Similar in-  
**2508** creases in  $N_{\text{area}}$ ,  $V_{\text{cmax}25}$ , and  $J_{\text{max}25}$  with increasing fertilization resulted in no  
**2509** change in the fraction of leaf nitrogen allocated to photosynthesis in uninoculated  
**2510** pots, while larger increases in  $N_{\text{area}}$  than  $V_{\text{cmax}25}$  and  $J_{\text{max}25}$  with increasing fertil-  
**2511** ization decreased the fraction of leaf nitrogen allocated to photosynthesis in inoc-  
**2512** ulated pots (Fig. 5.3a). As inoculated pots were able to access less finite supply of  
**2513** nitrogen across the fertilization gradient, these patterns suggest that constant leaf  
**2514** nitrogen-photosynthesis relationships may only apply in environments where ni-  
**2515** trogen is limiting and will likely change with increasing  $\text{CO}_2$  concentrations. Thus,  
**2516** terrestrial biosphere models that parameterize photosynthetic capacity through  
**2517** linear relationships between  $N_{\text{area}}$  and  $V_{\text{cmax}}$  (Rogers 2014; Rogers et al. 2017)  
**2518** may be overestimating photosynthetic capacity in systems where nitrogen is not

2519 as limiting and may contribute to erroneous model simulations under future CO<sub>2</sub>  
2520 concentrations.

2521 These results also demonstrate that optimal resource investment to photo-  
2522 tosynthetic capacity defines leaf acclimation responses to elevated CO<sub>2</sub>, and that  
2523 these responses were independent of fertilization or inoculation treatment. Cur-  
2524 rent approaches for simulating photosynthetic responses to CO<sub>2</sub> generally invoke  
2525 patterns expected from progressive nitrogen limitation, where the downregulation  
2526 in  $N_{\text{area}}$ , and therefore photosynthetic capacity, due to elevated CO<sub>2</sub> are com-  
2527 monly a function of progressive reductions in soil nitrogen availability. Results  
2528 reported here contradict this formulation, suggesting that the leaf acclimation re-  
2529 sponse is driven by optimal resource investment to photosynthetic capacity and  
2530 is independent of soil resource supply. Optimality models that leverage prin-  
2531 ciples from optimal coordination and photosynthetic least-cost theories (Wang  
2532 et al. 2017; Stocker et al. 2020; Scott and Smith 2022) are capable of capturing  
2533 such acclimation responses to CO<sub>2</sub> (Smith and Keenan 2020), suggesting that the  
2534 implementation of these models may improve the simulation of photosynthetic  
2535 processes in terrestrial biosphere models under increasing CO<sub>2</sub> concentrations.

2536 5.4.3 *Study limitations and future directions*

2537 There are two study limitations that must be addressed to contextualize  
2538 patterns observed in this study. First, restricting the volume of belowground  
2539 substrate via a potted experiment does not adequately replicate belowground en-  
2540 vironments of natural systems, and therefore may modify effects of soil resource  
2541 availability and inoculation on plant nitrogen uptake, particularly if pot size limits

2542 whole plant growth (Poorter et al. 2012). I attempted to minimize the extent of  
2543 pot size limitation experienced in the first experimental chapters while account-  
2544 ing for the expected stimulation in whole plant growth under elevated CO<sub>2</sub> by  
2545 using 6-liter pots. Despite attempts to minimize growth limitation imposed by  
2546 pot volume, fertilization and CO<sub>2</sub> treatments increased the biomass: pot volume  
2547 ratio such that all treatment combinations to exceed 1 g L<sup>-1</sup> biomass: pot volume  
2548 under high fertilization. The 1 g L<sup>-1</sup> biomass: pot volume recommendation from  
2549 Poorter et al. (2012) was designated to avoid growth limitation imposed by pot  
2550 volume. However, if pot size limitation indeed limited whole plant growth, then  
2551 structural carbon costs to acquire nitrogen, belowground carbon biomass, whole  
2552 plant nitrogen biomass, and whole plant biomass should each exhibit strong sat-  
2553 uration points with increasing fertilization, which was not observed here. Addi-  
2554 tionally, a second set of photosynthetic measurements from one week prior to the  
2555 harvest (6 weeks post-germination) revealed ... As pot limitation is expected  
2556 to decrease net photosynthesis, and focal leaves were of similar ages between the  
2557 sixth and seventh week, one might expect growth limitation induced by constricted  
2558 pot volume to result in a dampened effect of inoculation and fertilization on net  
2559 photosynthesis,  $V_{cmax}$ , and  $J_{max25}$ . Analyses from the sixth week of development  
2560 revealed ... Additionally, analyses revealed a stronger/weaker downregulation in  
2561  $V_{cmax25}$  and  $J_{max25}$  on week 7, though disentangling the causality of this response  
2562 (i.e. whether due to pot size limitation or simply a stronger acclimation response)  
2563 would be difficult.

2564 Second, this study evaluated leaf and whole plant responses to CO<sub>2</sub> in 7-  
2565 week seedlings. Given the long-term scale of the progressive nitrogen limitation

2566 hypothesis, patterns observed here should be validated in longer-term nitrogen  
2567 manipulation experiments. Previous work in free air CO<sub>2</sub> enrichment experiments  
2568 show some support for patterns expected from the progressive nitrogen limitation  
2569 hypothesis (Reich et al. 2006; Norby et al. 2010), although results are not consis-  
2570 tent across experimental sites (Finzi et al. 2006; Moore et al. 2006; Liang et al.  
2571 2016). We found some support for patterns expected by the progressive nitrogen  
2572 limitation hypothesis, namely an increase in plant nitrogen uptake under elevated  
2573 CO<sub>2</sub> (Luo et al. 2004), though leaf acclimation responses to CO<sub>2</sub> were strongly  
2574 indicative of optimal resource investment to photosynthetic capacity as expected  
2575 from photosynthetic least-cost theory (Prentice et al. 2014; Smith et al. 2019;  
2576 Smith and Keenan 2020).

2577 5.4.4 *Conclusions*

2578 This study provides strong evidence suggesting that leaf acclimation re-  
2579 sponds to elevated CO<sub>2</sub> did not vary with soil nitrogen fertilization or ability  
2580 to acquire nitrogen through symbiotic nitrogen fixation. However, whole plant  
2581 acclimation responses to CO<sub>2</sub> were dependent on fertilization, where increasing  
2582 fertilization increased the positive effect of whole plant growth under elevated  
2583 CO<sub>2</sub>. Results also indicate that fertilization played a relatively more important  
2584 role in modifying whole plant responses to CO<sub>2</sub>, perhaps due to a reduction in  
2585 nodulation across the fertilization gradient. These patterns strongly support the  
2586 hypothesis that leaf and whole plant acclimation responses are driven by opti-  
2587 mal resource investment to photosynthetic capacity, and that leaf acclimation  
2588 responses to CO<sub>2</sub> were not modified by changes in soil nitrogen availability. Ad-

2589 ditionally, strong interactions between fertilization and inoculation on leaf and  
2590 whole plant traits indicated positive effects of fertilization on leaf and whole plant  
2591 traits in uninoculated pots, but null effects of fertilization on leaf and whole plant  
2592 traits in inoculated pots. These results build on previous work suggesting that  
2593 constant leaf nitrogen-photosynthesis relationships are dynamic and change across  
2594 growing environments, calling the use of constant relationships by terrestrial bio-  
2595 sphere models into question.

2596

## Chapter 6

2597

### Conclusions

2598 The experiments included in this dissertation were designed to test mechanisms  
2599 that drive patterns expected from photosynthetic least-cost theory across various  
2600 edaphic and climatic gradients. Specifically, I evaluate the context dependency  
2601 of carbon costs to acquire nitrogen across soil nitrogen availability and how vari-  
2602 ance in carbon costs to acquire nitrogen scales to influence leaf and whole plant  
2603 acclimation responses to changing environments.

2604 In the first experimental chapter, I quantified carbon costs to acquire ni-  
2605 trogen in a species capable of forming associations with symbiotic nitrogen-fixing  
2606 bacteria (*Glycine max*) and a species not capable of forming such associations  
2607 (*Gossypium hirsutum*) grown under four soil nitrogen fertilization treatments and  
2608 four light availability treatments in a full factorial greenhouse experiment. I found  
2609 that increasing light availability increased carbon costs to acquire nitrogen in both  
2610 species due to a larger increase in belowground carbon biomass than whole plant  
2611 nitrogen biomass. These patterns were observed in both species. I also found  
2612 that increasing fertilization decreased carbon costs to acquire nitrogen due to a  
2613 larger increase in whole plant nitrogen biomass than belowground carbon biomass.  
2614 While these patterns were observed in both species, carbon costs to acquire nitro-  
2615 gen in *G. max* were less responsive to increasing fertilization than *G. hirsutum*,  
2616 providing some support for my second hypothesis. Root nodulation data indicated  
2617 that *G. max* shifted relative carbon allocation from nitrogen fixation to direct up-  
2618 take with increasing fertilization, which may explain the reduced responsiveness

**2619** of *G. max* carbon costs to acquire nitrogen across the fertilization gradient.

**2620** Despite evidence that reductions in the response of *G. max* carbon costs  
**2621** to acquire nitrogen to increasing fertilization may have been driven by shifts away  
**2622** from nitrogen fixation with increasing fertilization, I urge caution in assigning  
**2623** causality to the differential response of carbon costs to acquire nitrogen between  
**2624** species. This is because *G. max* and *G. hirsutum* are not phylogenetically related  
**2625** and have different life histories. Specifically, *G. max* is a herbaceous annual species,  
**2626** while *G. hirsutum* is a woody perennial species. Differences in life history between  
**2627** the two species limit my ability to assess whether reductions in the negative effect  
**2628** of increasing fertilization on carbon costs to acquire nitrogen in *G. max* were  
**2629** driven by shifts to direct uptake with increasing fertilization. However, these  
**2630** patterns were later confirmed in the fourth experimental chapter, where I quantify  
**2631** similar weaker negative effects of increasing fertilization on carbon costs to acquire  
**2632** nitrogen in *G. max* that were inoculated with symbiotic nitrogen-fixing bacteria  
**2633** compared to *G. max* that were left uninoculated across a similar soil nitrogen  
**2634** fertilization gradient.

**2635** In the second experimental chapter, I assessed whether changes in soil  
**2636** nitrogen availability or soil pH drove changes in nitrogen-water use tradeoffs pre-  
**2637** dicted by photosynthetic least-cost theory. I measured leaf traits of mature upper  
**2638** canopy deciduous trees growing in a nine-year nitrogen-by-sulfur field manipula-  
**2639** tion experiment, where experimental sulfur additions were added with intent to  
**2640** acidify plots. Following patterns expected from the theory, increasing soil nitrogen  
**2641** availability was associated with increased leaf nitrogen content, but not net pho-  
**2642** tosynthesis, resulting in an increase in photosynthetic nitrogen use efficiency. In

**2643** further support of theory, increasing soil nitrogen availability exhibited slight, but  
**2644** nonsignificant, decreases in leaf  $C_i:C_a$  and increases in measures of photosynthetic  
**2645** capacity. Perhaps the strongest evidence for the theory was a strong negative  
**2646** relationship between leaf nitrogen content and leaf  $C_i:C_a$ , of which increased with  
**2647** increasing soil nitrogen availability through a stronger increase in leaf nitrogen  
**2648** content than leaf  $C_i:C_a$ .

**2649** I found no effect of soil pH on nitrogen-water use tradeoffs aside from a  
**2650** marginal reduction in net photosynthesis rates that marginally reduced photosyn-  
**2651** thetic nitrogen use efficiency with increasing soil pH. Directionally, reductions in  
**2652** photosynthetic nitrogen use efficiency with increasing soil pH were as expected per  
**2653** theory; however, this response was driven by no change in leaf nitrogen content  
**2654** and a reduction in net photosynthesis. Theory predicts that these tradeoffs should  
**2655** be driven by no change in net photosynthesis and an increase in leaf nitrogen con-  
**2656** tent. Regardless, the general null leaf response to changing soil pH may have  
**2657** been due to experimental treatments directly increased soil nitrogen availability  
**2658** and affected soil pH in opposite patterns, suggesting that soil nitrogen availability  
**2659** may be more important in dictating nitrogen-water use tradeoffs than soil pH per  
**2660** se.

**2661** In the third experimental chapter, I quantified variance in leaf nitrogen  
**2662** content across a precipitation and soil resource availability gradient in Texan  
**2663** grasslands. Specifically, I measured area-based leaf nitrogen content, components  
**2664** of area-based leaf nitrogen content (leaf mass per unit leaf area, leaf nitrogen per  
**2665** unit dry biomass), leaf  $C_i:C_a$ , and the unit cost of acquiring nitrogen relative to  
**2666** water in 520 individuals comprising 57 species. I found that variance in area-

**2667** based leaf nitrogen content was positively associated with increasing soil nitrogen  
**2668** availability, soil moisture, vapor pressure deficit, and was negatively related to  
**2669** increasing leaf  $C_i:C_a$ . Following patterns expected from theory, a path analysis  
**2670** revealed that the positive soil nitrogen-leaf nitrogen relationship was driven by a  
**2671** positive relationship between soil nitrogen availability and the unit cost of acquir-  
**2672** ing and using nitrogen relative to water, a positive relationship between the unit  
**2673** cost of acquiring and using nitrogen relative to water, and negative relationship  
**2674** between leaf  $C_i:C_a$  and leaf mass per unit leaf area. Interestingly, there was no  
**2675** effect of  $C_i:C_a$  on leaf nitrogen content per unit dry biomass, indicating that vari-  
**2676** ance in area-based leaf nitrogen content across the environmental gradient was  
**2677** driven by a change in leaf morphology and not leaf chemistry.

**2678** In the fourth experimental chapter, I quantified leaf and whole plant accli-  
**2679** mation responses in *G. max* grown under two atmospheric CO<sub>2</sub> levels, with and  
**2680** without inoculation with *Bradyrhizobium japonicum*, and across nine nitrogen fer-  
**2681** tilization treatments in a full factorial growth chamber experiment. I found strong  
**2682** evidence that leaf nitrogen content,  $V_{cmax}$ , and  $J_{max}$  were each downregulated un-  
**2683** der elevated CO<sub>2</sub>. A stronger downregulation in  $V_{cmax}$  than  $J_{max}$  and stronger  
**2684** downregulation in leaf nitrogen content than  $V_{cmax}$  or  $J_{max}$  provided strong sup-  
**2685** port suggesting that leaves were acclimating to elevated CO<sub>2</sub> by optimizing leaf  
**2686** photosynthetic resource use efficiency to achieve optimal coordination. In striking  
**2687** support of my hypotheses, I find strong evidence suggesting that leaf acclimation  
**2688** responses to elevated CO<sub>2</sub> were decoupled from soil nitrogen fertilization and in-  
**2689** oculation treatment, despite apparent strong increases in leaf nitrogen content,  
**2690**  $V_{cmax}$ , and  $J_{max}$  with increasing fertilization and in inoculated pots. These find-

2691 ings contrast the current formulation of photosynthetic processes in terrestrial  
2692 biosphere models, where many models simulate downregulations in leaf nitrogen  
2693 content under elevated CO<sub>2</sub> schemes as a function of progressive nitrogen limita-  
2694 tion.

2695 There are currently two iterations of optimality models that employ the  
2696 use of patterns expected from photosynthetic least-cost theory, one for C<sub>3</sub> species  
2697 (Wang et al. 2017; Smith et al. 2019; Stocker et al. 2020) and one more recently  
2698 developed for C<sub>4</sub> species (Scott and Smith 2022). In both model variants, costs to  
2699 acquire and use nitrogen relative to water are held constant using a global dataset  
2700 of δ<sup>13</sup>C (Cornwell et al. 2018). The C<sub>3</sub> optimality model initially assumed a  
2701 constant cost to acquire and use nitrogen relative to water value of 240 (Wang et al.  
2702 2017), later corrected to 146 (Stocker et al. 2020), while the C<sub>4</sub> optimality model  
2703 assumes a constant value of 166 (Scott and Smith 2022). Throughout experiments,  
2704 I show strong evidence suggesting that costs to acquire and use nitrogen are  
2705 dynamic and vary predictably across environmental gradients, and that changes  
2706 in these costs yield predictable changes in leaf nitrogen-water use tradeoffs and  
2707 acclimation responses to changing environments. Thus, optimality models that  
2708 hold unit costs of resource use constant may contribute to erroneous errors in  
2709 model simulations. Future iterations of optimality models that leverage patterns  
2710 expected from photosynthetic least-cost theory should consider development of  
2711 explicit schemes for dynamically calculating costs to acquire and use nitrogen  
2712 relative to water, or be coupled with previously established plant nitrogen uptake  
2713 models (e.g., FUN) (Fisher et al. 2010; Brzostek et al. 2014; Allen et al. 2020).

2714 First principles of photosynthetic least-cost theory suggest that plants can

2715 optimize photosynthesis rates by sacrificing inefficient use of a relatively more  
2716 abundant (and less costly to acquire) resource for more efficient use of a relatively  
2717 less abundant (and more costly to acquire) resource. I show strong support for  
2718 these patterns across experiments, where increasing soil nitrogen fertilization gen-  
2719 erally decreased the cost of acquiring nitrogen relative to water, a pattern that  
2720 scaled to influence leaf nitrogen-water use tradeoffs. These findings provide im-  
2721 portant empirical validation of photosynthetic least-cost theory needed to further  
2722 develop optimality models and eventually implement in terrestrial biosphere model  
2723 products. Many current terrestrial biosphere model products do not include ro-  
2724 bust frameworks for simulating acclimation responses to changing environmental  
2725 conditions, and empirical findings shown here provide some support that optimal-  
2726 ity models that leverage photosynthetic least-cost theory predictions may improve  
2727 the ability of terrestrial biosphere models to accurately simulate photosynthetic  
2728 processes. Future work should leverage data collected from these experiments,  
2729 particularly the environmental gradient experiment across Texan grasslands, to  
2730 conduct model-data comparisons to evaluate optimality model performance.

2731       Many terrestrial biosphere models predict photosynthetic capacity through  
2732 plant functional group-specific linear regressions between area-based leaf nitrogen  
2733 content and  $V_{cmax}$  (Rogers 2014; Rogers et al. 2017), which assumes that leaf  
2734 nitrogen-photosynthesis relationships are constant across growing environments.  
2735 I found constant leaf nitrogen-photosynthesis relationships with increasing soil ni-  
2736 trogen availability in the nitrogen-by-sulfur field manipulation experiment. How-  
2737 ever, results from the CO<sub>2</sub>-by-nitrogen-by-inoculation manipulation experiment  
2738 indicated that leaf nitrogen-photosynthesis responses to soil nitrogen availability

2739 were dependent on whether nitrogen was limiting. Specifically, similar increases in  
2740 area-based leaf nitrogen content,  $V_{\text{cmax}25}$ , and  $J_{\text{max}25}$  with increasing fertilization  
2741 resulted in no change in the fraction of leaf nitrogen allocated to photosynthesis in  
2742 uninoculated pots, while larger increases in area-based leaf nitrogen content than  
2743  $V_{\text{cmax}25}$  and  $J_{\text{max}25}$  with increasing fertilization decreased the fraction of leaf nitro-  
2744 gen allocated to photosynthesis in inoculated pots. As inoculated pots were able  
2745 to access less finite supply of nitrogen across the fertilization gradient, these pat-  
2746 terns suggest that constant leaf nitrogen-photosynthesis relationships may only  
2747 apply in environments where nitrogen is limiting. Further investigation is cer-  
2748 tainly warranted regarding the effect of soil nitrogen availability in modifying leaf  
2749 nitrogen-photosynthesis relationships, but findings from these experiments suggest  
2750 that representing photosynthetic processes through positive relationships between  
2751 soil nitrogen availability, leaf nitrogen, and photosynthetic capacity are likely con-  
2752 tributing to erroneous errors in model simulations and may be an explanation for  
2753 the high degree of divergence between carbon and nutrient flux simulations across  
2754 terrestrial biosphere model products (Friedlingstein et al. 2014; Davies-Barnard  
2755 et al. 2020).

2756 The experiments included in this dissertation have provided a strong foun-  
2757 dation for me to continue growing as a plant physiological ecologist. I envision  
2758 five primary avenues for future research that build on the work presented here,  
2759 which are briefly summarized below:

2760 1. Manipulative and environmental gradient experiments included in this dis-  
2761 sertation were designed to provide empirical data needed to test photosyn-  
2762 thetic least-cost theory assumptions. While these results show promising

- 2763 patterns for patterns expected from photosynthetic least-cost theory, they  
2764 do not necessarily address whether these patterns follow those simulated by  
2765 optimality models that leverage photosynthetic least-cost principles. Thus,  
2766 a clear future direction of this research could be to conduct model-data  
2767 comparisons using data collected here (or similar experiments) to compare  
2768 against optimality model simulations.
- 2769 2. Experiments included in this dissertation explicitly quantify effects of sym-  
2770 biotic nitrogen fixation on carbon costs to acquire nitrogen, nitrogen-water  
2771 use tradeoffs, and leaf nitrogen-photosynthesis relationships. However, car-  
2772 bon costs to acquire nitrogen also vary in species that associate with dif-  
2773 ferent mycorrhizal types (Brzostek et al. 2014; Terrer et al. 2018), and  
2774 dominant mycorrhizal type in an ecosystem may dictate net biogeochemical  
2775 cycle dynamics (Phillips et al. 2013). Thus, future work should consider  
2776 conducting similar experiments while manipulating mycorrhizal association  
2777 to comprehensively understand how microbial symbioses modify leaf and  
2778 whole plant acclimation responses to changing environments. This avenue  
2779 of research would be particularly useful in forested ecosystems, as previous  
2780 work suggests that dominant mycorrhizal type in hardwood forests dictate  
2781 net biogeochemical cycle dynamics
- 2782 3. Recent work indicates a high degree of variance in symbiotic nitrogen fixa-  
2783 tion rates across terrestrial biosphere models (Davies-Barnard et al. 2020;  
2784 Meyerholt et al. 2016), perhaps due to nitrogen fixation rates that are im-  
2785 plemented across terrestrial biosphere models as a function of temperature  
2786 (Houlton et al. 2008). While energetic costs of nitrogen fixation are cer-

2787 tainly temperature dependent, I show that structural costs of nitrogen fix-  
2788 ation are driven by shifts in soil resource availability. The light-by-nitrogen  
2789 greenhouse experiment was recently published in *Journal of Experimental*  
2790 *Botany*, and a reviewer encouraged future work to include a model-data  
2791 comparison comparing carbon costs to acquire nitrogen measured in the  
2792 experiment to carbon costs to acquire nitrogen simulated by the FUN bio-  
2793 geochemical model (Fisher et al. 2010; Brzostek et al. 2014; Allen et al.  
2794 2020). Conveniently, FUN calculates carbon costs to acquire nitrogen follow-  
2795 ing the same calculation used in the first and fourth experimental chapter,  
2796 and doing this would be a useful next step toward understanding why ni-  
2797 trogen fixation simulations in terrestrial biosphere models might deviate to  
2798 such a large degree between products.

2799 4. Carbon costs to acquire nitrogen relative to water were quantified at the  
2800 leaf level as a function of  $\delta^{13}\text{C}$  and vapor pressure deficit, while structural  
2801 carbon costs to acquire nitrogen were quantified at the whole plant level  
2802 as the ratio of belowground carbon allocation per unit whole plant nitro-  
2803 gen biomass. As increasing soil nitrogen availability decreases both leaf and  
2804 whole plant estimates of costs to acquire and use nitrogen, one might expect  
2805 leaf and whole plant carbon cost to acquire nitrogen estimates to covary. Fu-  
2806 ture work should consider investigating if leaf and whole plant estimates of  
2807 carbon costs to acquire nitrogen covary and evaluate whether environmental  
2808 conditions (or species acquisition strategy) modifies any of this possible co-  
2809 variance. Strong covariance between leaf and whole plant costs of nitrogen  
2810 acquisition could be a possible avenue to implement frameworks for allowing

2811 costs of nitrogen acquisition to vary in optimality models, as the FUN model  
2812 calculates carbon costs of nitrogen acquisition at the whole plant level.

2813 5. While experiments included in this dissertation target effects of soil nitrogen  
2814 availability on carbon costs to acquire nitrogen and associated leaf nitrogen-  
2815 water use tradeoffs, photosynthetic least-cost theory predicts that costs of  
2816 nutrient use, not just nitrogen, relative to water are substitutable. Recent  
2817 iterations of the FUN biogeochemical cycle includes the carbon and nitro-  
2818 gen cost of acquiring and using phosphorus, which similarly varies in species  
2819 with different nutrient acquisition strategies (Allen et al. 2020). The im-  
2820 plementation of this model in a terrestrial biosphere model (E3SM) was  
2821 recently shown to improve model performance of ecosystem nutrient lim-  
2822 itation (Braghiere et al. 2022). As phosphorus commonly co-limits leaf  
2823 photosynthesis and primary productivity, extending experiments reported  
2824 here to investigate carbon and nitrogen costs of phosphorus use may be a  
2825 useful next step in understanding extensions and limitations of photosyn-  
2826 thetic least-cost theory.

2827 I conclude this dissertation with a brief word of thanks to all who have  
2828 shaped me into the plant physiological ecologist that I am today. Specifically,  
2829 I am thankful for the incredible mentorship of my advisor and committee chair,  
2830 Dr. Nick Smith, who provided invaluable insight for each of these experimental  
2831 chapters, and for my committee members for their helpful advise and support  
2832 throughout these experiments. I am excited to continue growing as a plant phys-  
2833 iological ecologist, look forward to continuing to understand nutrient acquisition  
2834 and allocation responses to global change, and am excited to help mentor future

**2835** generations of young researchers.

**2836**

**References**

- 2837** Abrams, M. D. and S. A. Mostoller (1995). Gas exchange, leaf structure and  
**2838** nitrogen in contrasting successional tree species growing in open and under-  
**2839** story sites during a drought. *Tree Physiology* 15(6), 361–370.
- 2840** Adams, M. A., T. L. Turnbull, J. I. Sprent, and N. Buchmann (2016). Legumes  
**2841** are different: Leaf nitrogen, photosynthesis, and water use efficiency. *Pro-  
**2842** ceedings of the National Academy of Sciences of the United States of Amer-  
**2843** ica* 113(15), 4098–4103.
- 2844** Ainsworth, E. A., P. A. Davey, C. J. Bernacchi, O. C. Dermody, E. A. Heaton,  
**2845** D. J. Moore, P. B. Morgan, S. L. Naidu, H. S. Y. Ra, X. G. Zhu, P. S. Curtis,  
**2846** and S. P. Long (2002). A meta-analysis of elevated [CO<sub>2</sub>] effects on soybean  
**2847** (*Glycine max*) physiology, growth and yield. *Global Change Biology* 8(8),  
**2848** 695–709.
- 2849** Ainsworth, E. A. and S. P. Long (2005). What have we learned from 15 years of  
**2850** free-air CO<sub>2</sub> enrichment (FACE)? A meta-analytic review of the responses  
**2851** of photosynthesis, canopy properties and plant production to rising CO<sub>2</sub>.  
**2852** *New Phytologist* 165(2), 351–372.
- 2853** Ainsworth, E. A. and A. Rogers (2007). The response of photosynthesis and  
**2854** stomatal conductance to rising [CO<sub>2</sub>]: mechanisms and environmental in-  
**2855** teractions. *Plant, Cell and Environment* 30(3), 258–270.
- 2856** Allen, K., J. B. Fisher, R. P. Phillips, J. S. Powers, and E. R. Brzostek (2020).  
**2857** Modeling the carbon cost of plant nitrogen and phosphorus uptake across  
**2858** temperate and tropical forests. *Frontiers in Forests and Global Change* 3,

- 2859 1–12.
- 2860 Allison, S. D., C. I. Czimczik, and K. K. Treseder (2008). Microbial activity  
2861 and soil respiration under nitrogen addition in Alaskan boreal forest. *Global  
2862 Change Biology* 14(5), 1156–1168.
- 2863 Andersen, M. K., H. Hauggaard-Nielsen, P. Ambus, and E. S. Jensen (2005).  
2864 Biomass production, symbiotic nitrogen fixation and inorganic N use in dual  
2865 and tri-component annual intercrops. *Plant and Soil* 266(1-2), 273–287.
- 2866 Andrews, M., E. K. James, J. I. Sprent, R. M. Boddey, E. Gross, and F. B. dos  
2867 Reis (2011). Nitrogen fixation in legumes and actinorhizal plants in natural  
2868 ecosystems: Values obtained using  $^{15}\text{N}$  natural abundance. *Plant Ecology  
2869 and Diversity* 4(2-3), 117–130.
- 2870 Arndal, M. F., A. Tolver, K. S. Larsen, C. Beier, and I. K. Schmidt (2018). Fine  
2871 root growth and vertical distribution in response to elevated CO<sub>2</sub>, warming  
2872 and drought in a mixed heathland–grassland. *Ecosystems* 21(1), 15–30.
- 2873 Arnone, J. A. (1997). Indices of plant N availability in an alpine grassland under  
2874 elevated atmospheric CO<sub>2</sub>. *Plant and Soil* 190(1), 61–66.
- 2875 Arora, V. K., A. Katavouta, R. G. Williams, C. D. Jones, V. Brovkin,  
2876 P. Friedlingstein, J. Schwinger, L. Bopp, O. Boucher, P. Cadule, M. A.  
2877 Chamberlain, J. R. Christian, C. Delire, R. A. Fisher, T. Hajima, T. Ilyina,  
2878 E. Joetzjer, M. Kawamiya, C. D. Koven, J. P. Krasting, R. M. Law, D. M.  
2879 Lawrence, A. Lenton, K. Lindsay, J. Pongratz, T. Raddatz, R. Séférian,  
2880 K. Tachiiri, J. F. Tjiputra, A. Wiltshire, T. Wu, and T. Ziehn (2020).  
2881 Carbon-concentration and carbon-climate feedbacks in CMIP6 models and  
2882 their comparison to CMIP5 models. *Biogeosciences* 17(16), 4173–4222.

- 2883 Bae, K., T. J. Fahey, R. D. Yanai, and M. Fisk (2015). Soil nitrogen availability affects belowground carbon allocation and soil respiration in northern  
2884 hardwood forests of New Hampshire. *Ecosystems* 18(7), 1179–1191.
- 2885
- 2886 Barber, S. A. (1962). A diffusion and mass-flow concept of soil nutrient availability. *Soil Science* 93(1), 39–49.
- 2887
- 2888 Barnes, J. D., L. Balaguer, E. Manrique, S. Elvira, and A. W. Davison (1992).  
2889 A reappraisal of the use of DMSO for the extraction and determination  
2890 of chlorophylls a and b in lichens and higher plants. *Environmental and  
2891 Experimental Botany* 32(2), 85–100.
- 2892 Bates, D., M. Mächler, B. Bolker, and S. Walker (2015). Fitting linear mixed-  
2893 effects models using lme4. *Journal of Statistical Software* 67(1), 1–48.
- 2894 Beaudette, D., J. Skovlin, S. Roeker, and A. Brown (2022). soilDB: Soil  
2895 Database Interface.
- 2896 Bengtson, P., J. Barker, and S. J. Grayston (2012). Evidence of a strong cou-  
2897 pling between root exudation, C and N availability, and stimulated SOM  
2898 decomposition caused by rhizosphere priming effects. *Ecology and Evolu-  
2899 tion* 2(8), 1843–1852.
- 2900 Bernacchi, C. J., E. L. Singsaas, C. Pimentel, A. R. Portis, and S. P. Long  
2901 (2001). Improved temperature response functions for models of Rubisco-  
2902 limited photosynthesis. *Plant, Cell and Environment* 24(2), 253–259.
- 2903 Bialic-Murphy, L., N. G. Smith, P. Voothuluru, R. M. McElderry, M. D.  
2904 Roche, S. T. Cassidy, S. N. Kivlin, and S. Kalisz (2021). Invasion-induced  
2905 root–fungal disruptions alter plant water and nitrogen economies. *Ecology*

- 2906** *Letters* 24(6), 1145–1156.
- 2907** Bloom, A. J., F. S. Chapin, and H. A. Mooney (1985). Resource limitation  
**2908** in plants - an economic analogy. *Annual Review of Ecology and Systemat-*  
**2909** *ics* 16(1), 363–392.
- 2910** Bloomfield, K. J., B. D. Stocker, T. F. Keenan, and I. C. Prentice (2023).  
**2911** Environmental controls on the light use efficiency of terrestrial gross primary  
**2912** production. *Global Change Biology* 29(4), 0–2.
- 2913** Bonan, G. B., M. D. Hartman, W. J. Parton, and W. R. Wieder (2013). Eval-  
**2914** uating litter decomposition in earth system models with long-term litter  
**2915** bag experiments: an example using the Community Land Model version 4  
**2916** (CLM4). *Global Change Biology* 19(3), 957–974.
- 2917** Bonan, G. B., P. J. Lawrence, K. W. Oleson, S. Levis, M. Jung, M. Reich-  
**2918** stein, D. M. Lawrence, and S. C. Swenson (2011). Improving canopy pro-  
**2919** cesses in the Community Land Model version 4 (CLM4) using global flux  
**2920** fields empirically inferred from FLUXNET data. *Journal of Geophysical Re-*  
**2921** *search* 116(G2), G02014.
- 2922** Booth, B. B. B., C. D. Jones, M. Collins, I. J. Totterdell, P. M. Cox, S. Sitch,  
**2923** C. Huntingford, R. A. Betts, G. R. Harris, and J. Lloyd (2012). High sen-  
**2924** sitivity of future global warming to land carbon cycle processes. *Environ-*  
**2925** *mental Research Letters* 7(2), 024002.
- 2926** Borer, E. T., W. S. Harpole, P. B. Adler, E. M. Lind, J. L. Orrock, E. W.  
**2927** Seabloom, and M. D. Smith (2014). Finding generality in ecology: A model  
**2928** for globally distributed experiments. *Methods in Ecology and Evolution* 5(1),  
**2929** 65–73.

- 2930 Braghieri, R. K., J. B. Fisher, K. Allen, E. Brzostek, M. Shi, X. Yang, D. M.  
2931 Ricciuto, R. A. Fisher, Q. Zhu, and R. P. Phillips (2022). Modeling global  
2932 carbon costs of plant nitrogen and phosphorus acquisition. *Journal of Ad-*  
2933 *vances in Modeling Earth Systems* 14(8), 1–23.
- 2934 Brix, H. (1971). Effects of nitrogen fertilization on photosynthesis and respi-  
2935 ration in Douglas-fir. *Forest Science* 17(4), 407–414.
- 2936 Brzostek, E. R., J. B. Fisher, and R. P. Phillips (2014). Modeling the carbon  
2937 cost of plant nitrogen acquisition: Mycorrhizal trade-offs and multipath  
2938 resistance uptake improve predictions of retranslocation. *Journal of Geo-*  
2939 *physical Research: Biogeosciences* 119, 1684–1697.
- 2940 Bubier, J. L., R. Smith, S. Juutinen, T. R. Moore, R. Minocha, S. Long, and  
2941 S. Minocha (2011). Effects of nutrient addition on leaf chemistry, morphol-  
2942 ogy, and photosynthetic capacity of three bog shrubs. *Oecologia* 167(2),  
2943 355–368.
- 2944 Cernusak, L. A., N. Ubierna, K. Winter, J. A. M. Holtum, J. D. Marshall, and  
2945 G. D. Farquhar (2013). Environmental and physiological determinants of  
2946 carbon isotope discrimination in terrestrial plants. *New Phytologist* 200(4),  
2947 950–965.
- 2948 Chen, J.-L., J. F. Reynolds, P. C. Harley, and J. D. Tenhunen (1993). Coor-  
2949 dination theory of leaf nitrogen distribution in a canopy. *Oecologia* 93(1),  
2950 63–69.
- 2951 Clark, D. B., L. M. Mercado, S. Sitch, C. D. Jones, N. Gedney, M. J. Best,  
2952 M. Pryor, G. G. Rooney, R. L. H. Essery, E. Blyth, O. Boucher, R. J.  
2953 Harding, C. Huntingford, and P. M. Cox (2011). The Joint UK Land Envi-

- 2954 ronment Simulator (JULES), model description. Part 2: Carbon fluxes and  
2955 vegetation dynamics. *Geoscientific Model Development* 4(3), 701–722.
- 2956 Cornwell, W. K., J. H. C. Cornelissen, K. Amatangelo, E. Dorrepaal, V. T.  
2957 Eviner, O. Godoy, S. E. Hobbie, B. Hoorens, H. Kurokawa, N. Pérez-  
2958 Harguindeguy, H. M. Quested, L. S. Santiago, D. A. Wardle, I. J. Wright,  
2959 R. Aerts, S. D. Allison, P. van Bodegom, V. Brovkin, A. Chatain, T. V.  
2960 Callaghan, S. Díaz, E. Garnier, D. E. Gurvich, E. Kazakou, J. A. Klein,  
2961 J. Read, P. B. Reich, N. A. Soudzilovskaia, M. V. Vaieretti, and M. Westoby  
2962 (2008). Plant species traits are the predominant control on litter decompo-  
2963 sition rates within biomes worldwide. *Ecology Letters* 11(10), 1065–1071.
- 2964 Cornwell, W. K., I. J. Wright, J. Turner, V. Maire, M. M. Barbour, L. A.  
2965 Cernusak, T. E. Dawson, D. S. Ellsworth, G. D. Farquhar, H. Griffiths,  
2966 C. Keitel, A. Knohl, P. B. Reich, D. G. Williams, R. Bhaskar, J. H. C. Cor-  
2967 nelissen, A. Richards, S. Schmidt, F. Valladares, C. Körner, E.-D. Schulze,  
2968 N. Buchmann, and L. S. Santiago (2018). Climate and soils together regulate  
2969 photosynthetic carbon isotope discrimination within C<sub>3</sub> plants worldwide.  
2970 *Global Ecology and Biogeography* 27(9), 1056–1067.
- 2971 Cramer, W. and I. C. Prentice (1988). Simulation of regional soil moisture  
2972 deficits on a European scale. *Norsk Geografisk Tidsskrift - Norwegian Jour-*  
2973 *nal of Geography* 42(2-3), 149–151.
- 2974 Curtis, P. S. (1996). A meta-analysis of leaf gas exchange and nitrogen in trees  
2975 grown under elevated carbon dioxide. *Plant, Cell and Environment* 19(2),  
2976 127–137.
- 2977 Daly, C., M. Halbleib, J. I. Smith, W. P. Gibson, M. K. Doggett, G. H. Taylor,

- 2978** J. Curtis, and P. P. Pasteris (2008). Physiographically sensitive mapping  
**2979** of climatological temperature and precipitation across the conterminous  
**2980** United States. *International Journal of Climatology* 28(15), 2031–2064.
- 2981** Davies-Barnard, T., J. Meyerholt, S. Zaehle, P. Friedlingstein, V. Brovkin,  
**2982** Y. Fan, R. A. Fisher, C. D. Jones, H. Lee, D. Peano, B. Smith, D. Wårlind,  
**2983** and A. J. Wiltshire (2020). Nitrogen cycling in CMIP6 land surface models:  
**2984** progress and limitations. *Biogeosciences* 17(20), 5129–5148.
- 2985** Davis, T. W., I. C. Prentice, B. D. Stocker, R. T. Thomas, R. J. Whitley,  
**2986** H. Wang, B. J. Evans, A. V. Gallego-Sala, M. T. Sykes, and W. Cramer  
**2987** (2017). Simple process-led algorithms for simulating habitats (SPLASH  
**2988** v.1.0): robust indices of radiation, evapotranspiration and plant-available  
**2989** moisture. *Geoscientific Model Development* 10, 689–708.
- 2990** Delaire, M., E. Frak, M. Sigogne, B. Adam, F. Beaujard, and X. Le Roux  
**2991** (2005). Sudden increase in atmospheric CO<sub>2</sub> concentration reveals strong  
**2992** coupling between shoot carbon uptake and root nutrient uptake in young  
**2993** walnut trees. *Tree Physiology* 25(2), 229–235.
- 2994** Doane, T. A. and W. R. Horwáth (2003). Spectrophotometric determination of  
**2995** nitrate with a single reagent. *Analytical Letters* 36(12), 2713–2722.
- 2996** Dong, N., I. C. Prentice, B. J. Evans, S. Caddy-Retalic, A. J. Lowe, and I. J.  
**2997** Wright (2017). Leaf nitrogen from first principles: field evidence for adaptive  
**2998** variation with climate. *Biogeosciences* 14(2), 481–495.
- 2999** Dong, N., I. C. Prentice, I. J. Wright, B. J. Evans, H. F. Togashi, S. Caddy-  
**3000** Retalic, F. A. McInerney, B. Sparrow, E. Leitch, and A. J. Lowe (2020).  
**3001** Components of leaf-trait variation along environmental gradients. *New Phy-*

- 3002** *tologist* 228(1), 82–94.
- 3003** Dong, N., I. C. Prentice, I. J. Wright, H. Wang, O. K. Atkin, K. J. Bloomfield,
- 3004** T. F. Domingues, S. M. Gleason, V. Maire, Y. Onoda, H. Poorter, and N. G.
- 3005** Smith (2022). Leaf nitrogen from the perspective of optimal plant function.
- 3006** *Journal of Ecology* 110(11), 2585–2602.
- 3007** Dong, N., I. J. Wright, J. M. Chen, X. Luo, H. Wang, T. F. Keenan, N. G.
- 3008** Smith, and I. C. Prentice (2022). Rising CO<sub>2</sub> and warming reduce global
- 3009** canopy demand for nitrogen. *New Phytologist* 235(5), 1692–1700.
- 3010** Dovrat, G., H. Bakhshian, T. Masci, and E. Sheffer (2020). The nitrogen eco-
- 3011** nomic spectrum of legume stoichiometry and fixation strategy. *New Phytol-*
- 3012** *ogist* 227(2), 365–375.
- 3013** Dovrat, G., T. Masci, H. Bakhshian, E. Mayzlish Gati, S. Golan, and E. Shef-
- 3014** fer (2018). Drought-adapted plants dramatically downregulate dinitrogen
- 3015** fixation: Evidences from Mediterranean legume shrubs. *Journal of Ecol-*
- 3016** *ogy* 106(4), 1534–1544.
- 3017** Drake, B. G., M. A. Gonzàlez-Meler, and S. P. Long (1997). More efficient
- 3018** plants: a consequence of rising atmospheric CO<sub>2</sub>? *Annual Review of Plant*
- 3019** *Biology* 48, 609–639.
- 3020** Duursma, R. A. (2015). Plantecophys - An R package for analyzing and mod-
- 3021** eling leaf gas exchange data. *PLOS ONE* 10(11), e0143346.
- 3022** Eastman, B. A., M. B. Adams, E. R. Brzostek, M. B. Burnham, J. E. Carrara,
- 3023** C. Kelly, B. E. McNeil, C. A. Walter, and W. T. Peterjohn (2021). Altered
- 3024** plant carbon partitioning enhanced forest ecosystem carbon storage after 25

- 3025** years of nitrogen additions. *New Phytologist* 230(4), 1435–1448.
- 3026** Ellsworth, D. S. and P. B. Reich (1996). Photosynthesis and leaf nitrogen in five
- 3027** Amazonian tree species during early secondary succession. *Ecology* 77(2),
- 3028** 581–594.
- 3029** Espelta, J. M., P. Cortés, M. Mangirón, and J. Retana (2005). Differences
- 3030** in biomass partitioning, leaf nitrogen content, and water use efficiency  $\delta^{13}$
- 3031** result in similar performance of seedlings of two Mediterranean oaks with
- 3032** contrasting leaf habit. *Ecoscience* 12(4), 447–454.
- 3033** Evans, J. R. (1989). Photosynthesis and nitrogen relationships in leaves of C<sub>3</sub>
- 3034** plants. *Oecologia* 78(1), 9–19.
- 3035** Evans, J. R. and V. C. Clarke (2019). The nitrogen cost of photosynthesis.
- 3036** *Journal of Experimental Botany* 70(1), 7–15.
- 3037** Evans, J. R. and H. Poorter (2001). Photosynthetic acclimation of plants to
- 3038** growth irradiance: the relative importance of specific leaf area and nitrogen
- 3039** partitioning in maximizing carbon gain. *Plant, Cell and Environment* 24(8),
- 3040** 755–767.
- 3041** Evans, J. R. and J. R. Seemann (1989). The allocation of protein nitrogen in
- 3042** the photosynthetic apparatus: costs, consequences, and control. *Photosyn-*
- 3043** *thesis* 8, 183–205.
- 3044** Exbrayat, J.-F., A. A. Bloom, P. Falloon, A. Ito, T. L. Smallman, and
- 3045** M. Williams (2018). Reliability ensemble averaging of 21<sup>st</sup> century projec-
- 3046** tions of terrestrial net primary productivity reduces global and regional
- 3047** uncertainties. *Earth System Dynamics* 9(1), 153–165.

- 3048** Farquhar, G. D., J. R. Ehleringer, and K. T. Hubick (1989). Carbon isotope  
**3049** discrimination and photosynthesis. *Annual Review of Plant Physiology and*  
**3050** *Plant Molecular Biology* 40(1), 503–537.
- 3051** Farquhar, G. D. and T. D. Sharkey (1982). Stomatal conductance and photo-  
**3052** synthesis. *Annual Review of Plant Physiology* 33(1), 317–345.
- 3053** Farquhar, G. D., S. von Caemmerer, and J. A. Berry (1980). A biochemical  
**3054** model of photosynthetic CO<sub>2</sub> assimilation in leaves of C<sub>3</sub> species.  
**3055** *Planta* 149(1), 78–90.
- 3056** Fay, P. A., S. M. Prober, W. S. Harpole, J. M. H. Knops, J. D. Bakker, E. T.  
**3057** Borer, E. M. Lind, A. S. MacDougall, E. W. Seabloom, P. D. Wragg, P. B.  
**3058** Adler, D. M. Blumenthal, Y. M. Buckley, C. Chu, E. E. Cleland, S. L.  
**3059** Collins, K. F. Davies, G. Du, X. Feng, J. Firn, D. S. Gruner, N. Hagenah,  
**3060** Y. Hautier, R. W. Heckman, V. L. Jin, K. P. Kirkman, J. A. Klein, L. M.  
**3061** Ladwig, Q. Li, R. L. McCulley, B. A. Melbourne, C. E. Mitchell, J. L. Moore,  
**3062** J. W. Morgan, A. C. Risch, M. Schütz, C. J. Stevens, D. A. Wedin, and  
**3063** L. H. Yang (2015). Grassland productivity limited by multiple nutrients.  
**3064** *Nature Plants* 1(7), 15080.
- 3065** Feng, X. (1999). Trends in intrinsic water-use efficiency of natural trees for the  
**3066** past 100-200 years: A response to atmospheric CO<sub>2</sub> concentration. *Geochim-  
3067* *ica et Cosmochimica Acta* 63(13-14), 1891–1903.
- 3068** Field, C. B. and H. A. Mooney (1986). The photosynthesis-nitrogen relationship  
**3069** in wild plants. In T. J. Givnish (Ed.), *On the Economy of Plant Form and*  
**3070** *Function*, pp. 25–55. Cambridge: Cambridge University Press.
- 3071** Finzi, A. C., D. J. P. Moore, E. H. DeLucia, J. Lichter, K. S. Hofmockel, R. B.

- 3072 Jackson, H. S. Kim, R. Matamala, H. R. McCarthy, R. Oren, J. S. Pippen,  
3073 and W. H. Schlesinger (2006). Progressive nitrogen limitation of ecosystem  
3074 processes under elevated CO<sub>2</sub> in a warm-temperate forest. *Ecology* 87(1),  
3075 15–25.
- 3076 Firn, J., J. M. McGree, E. Harvey, H. Flores Moreno, M. Schutz, Y. M. Buckley,  
3077 E. T. Borer, E. W. Seabloom, K. J. La Pierre, A. M. MacDougall, S. M.  
3078 Prober, C. J. Stevens, L. L. Sullivan, E. Porter, E. Ladouceur, C. Allen,  
3079 K. H. Moromizato, J. W. Morgan, W. S. Harpole, Y. Hautier, N. Eisen-  
3080 hauer, J. P. Wright, P. B. Adler, C. A. Arnillas, J. D. Bakker, L. Biederman,  
3081 A. A. D. Broadbent, C. S. Brown, M. N. Bugalho, M. C. Caldeira, E. E. Cle-  
3082 land, A. Ebeling, P. A. Fay, N. Hagenah, A. R. Kleinhesselink, R. Mitchell,  
3083 J. L. Moore, C. Nogueira, P. L. Peri, C. Roscher, M. D. Smith, P. D. Wragg,  
3084 and A. C. Risch (2019). Leaf nutrients, not specific leaf area, are consistent  
3085 indicators of elevated nutrient inputs. *Nature Ecology and Evolution* 3(3),  
3086 400–406.
- 3087 Fisher, J. B., S. Sitch, Y. Malhi, R. A. Fisher, C. Huntingford, and S.-Y. Tan  
3088 (2010). Carbon cost of plant nitrogen acquisition: A mechanistic, globally  
3089 applicable model of plant nitrogen uptake, retranslocation, and fixation.  
3090 *Global Biogeochemical Cycles* 24(1), 1–17.
- 3091 Fox, J. and S. Weisberg (2019). *An R companion to applied regression* (Third  
3092 edit ed.). Thousand Oaks, California: Sage.
- 3093 Franklin, O., R. E. McMurtrie, C. M. Iversen, K. Y. Crous, A. C. Finzi, D. Tis-  
3094 sue, D. S. Ellsworth, R. Oren, and R. J. Norby (2009). Forest fine-root  
3095 production and nitrogen use under elevated CO<sub>2</sub>: contrasting responses

- 3096** in evergreen and deciduous trees explained by a common principle. *Global  
3097 Change Biology* 15(1), 132–144.
- 3098** Friedlingstein, P., M. Meinshausen, V. K. Arora, C. D. Jones, A. Anav, S. K.  
**3099** Liddicoat, and R. Knutti (2014). Uncertainties in CMIP5 climate projections  
**3100** due to carbon cycle feedbacks. *Journal of Climate* 27(2), 511–526.
- 3101** Friel, C. A. and M. L. Friesen (2019). Legumes modulate allocation to rhizobial  
**3102** nitrogen fixation in response to factorial light and nitrogen manipulation.  
**3103** *Frontiers in Plant Science* 10, 1316.
- 3104** Fujikake, H., A. Yamazaki, N. Ohtake, K. Sueoshi, S. Matsuhashi, T. Ito,  
**3105** C. Mizuniwa, T. Kume, S. Hoshimoto, N.-S. Ishioka, S. Watanabe, A. Osa,  
**3106** T. Sekine, H. Uchida, A. Tsuji, and T. Ohyama (2003). Quick and reversible  
**3107** inhibition of soybean root nodule growth by nitrate involves a decrease in  
**3108** sucrose supply to nodules. *Journal of Experimental Botany* 54(386), 1379–  
**3109** 1388.
- 3110** Ghannoum, O., J. R. Evans, and S. von Caemmerer (2011). Nitrogen and water  
**3111** use efficiency of C<sub>4</sub> plants. In A. S. Raghavendra and R. F. Sage (Eds.), *C<sub>4</sub>  
3112 Photosynthesis and Related CO<sub>2</sub> Concentrating Mechanisms*, Chapter 8, pp.  
**3113** 129–146. Springer.
- 3114** Ghimire, B., W. J. Riley, C. D. Koven, J. Kattge, A. Rogers, P. B. Reich, and  
**3115** I. J. Wright (2017). A global trait-based approach to estimate leaf nitrogen  
**3116** functional allocation from observations:. *Ecological Applications* 27(5),  
**3117** 1421–1434.
- 3118** Giardina, C. P., M. D. Coleman, J. E. Hancock, J. S. King, E. A. Lilleskov,  
**3119** W. M. Loya, K. S. Pregitzer, M. G. Ryan, and C. C. Trettin (2005). The

- 3120** response of belowground carbon allocation in forests to global change. In  
**3121** D. Binkley and O. Manyailo (Eds.), *Tree Species Effects on Soils: Implica-*  
**3122** *tions for Global Change* (Volume 55 ed.), Chapter Chapter 7, pp. 119–154.  
**3123** Berlin/Heidelberg: Springer-Verlag.
- 3124** Gibson, A. H. and J. E. Harper (1985). Nitrate effect on nodulation of soybean  
**3125** by *Bradyrhizobium japonicum*. *Crop Science* 25(3), 497–501.
- 3126** Gill, A. L. and A. C. Finzi (2016). Belowground carbon flux links biogeochemical  
**3127** cycles and resource-use efficiency at the global scale. *Ecology Letters* 19(12),  
**3128** 1419–1428.
- 3129** Goll, D. S., V. Brovkin, B. R. Parida, C. H. Reick, J. Kattge, P. B. Reich, P. M.  
**3130** van Bodegom, and Ü. Niinemets (2012). Nutrient limitation reduces land  
**3131** carbon uptake in simulations with a model of combined carbon, nitrogen  
**3132** and phosphorus cycling. *Biogeosciences Discussions* 9(3), 3173–3232.
- 3133** Gregory, L. M., A. M. McClain, D. M. Kramer, J. D. Pardo, K. E. Smith, O. L.  
**3134** Tessmer, B. J. Walker, L. G. Ziccardi, and T. D. Sharkey (2021, oct). The  
**3135** triose phosphate utilization limitation of photosynthetic rate: Out of global  
**3136** models but important for leaf models. *Plant, Cell and Environment* 44(10),  
**3137** 3223–3226.
- 3138** Grossiord, C., T. N. Buckley, L. A. Cernusak, K. A. Novick, B. Poulter, R. T. W.  
**3139** Siegwolf, J. S. Sperry, and N. G. McDowell (2020). Plant responses to rising  
**3140** vapor pressure deficit. *New Phytologist* 226(6), 1550–1566.
- 3141** Guerrieri, R., M. Mencuccini, L. J. Sheppard, M. Saurer, M. P. Perks, P. Levy,  
**3142** M. A. Sutton, M. Borghetti, and J. Grace (2011). The legacy of enhanced  
**3143** N and S deposition as revealed by the combined analysis of  $\delta^{13}\text{C}$ ,  $\delta^{18}\text{O}$  and

- 3144**  $\delta^{15}\text{N}$  in tree rings. *Global Change Biology* 17(5), 1946–1962.
- 3145** Gulmon, S. L. and C. C. Chu (1981). The effects of light and nitrogen on photo-
- 3146** synthesis, leaf characteristics, and dry matter allocation in the chaparral
- 3147** shrub, *Diplacus aurantiacus*. *Oecologia* 49(2), 207–212.
- 3148** Gutschick, V. P. (1981). Evolved strategies in nitrogen acquisition by plants.
- 3149** *The American Naturalist* 118(5), 607–637.
- 3150** Hallik, L., Ü. Niinemets, and I. J. Wright (2009). Are species shade and drought
- 3151** tolerance reflected in leaf-level structural and functional differentiation in
- 3152** Northern Hemisphere temperate woody flora? *New Phytologist* 184(1), 257–
- 3153** 274.
- 3154** Harrison, M. T., E. J. Edwards, G. D. Farquhar, A. B. Nicotra, and J. R.
- 3155** Evans (2009). Nitrogen in cell walls of sclerophyllous leaves accounts for
- 3156** little of the variation in photosynthetic nitrogen-use efficiency. *Plant, Cell*
- 3157** and *Environment* 32(3), 259–270.
- 3158** Harrison, S. P., W. Cramer, O. Franklin, I. C. Prentice, H. Wang,
- 3159** Å. Brännström, H. de Boer, U. Dieckmann, J. Joshi, T. F. Keenan,
- 3160** A. Lavergne, S. Manzoni, G. Mengoli, C. Morfopoulos, J. Peñuelas,
- 3161** S. Pietsch, K. T. Rebel, Y. Ryu, N. G. Smith, B. D. Stocker, and I. J.
- 3162** Wright (2021). Eco-evolutionary optimality as a means to improve vegeta-
- 3163** tion and land-surface models. *New Phytologist* 231(6), 2125–2141.
- 3164** Henneron, L., P. Kardol, D. A. Wardle, C. Cros, and S. Fontaine (2020). Rhizo-
- 3165** sphere control of soil nitrogen cycling: a key component of plant economic
- 3166** strategies. *New Phytologist* 228(4), 1269–1282.

- 3167** Hijmans, R. J. (2022). *terra: Spatial Data Analysis*.
- 3168** Hikosaka, K. and A. Shigeno (2009). The role of Rubisco and cell walls in the  
**3169** interspecific variation in photosynthetic capacity. *Oecologia* 160(3), 443–  
**3170** 451.
- 3171** Hoagland, D. R. and D. I. Arnon (1950). The water culture method for growing  
**3172** plants without soil. *California Agricultural Experiment Station: 347* 347(2),  
**3173** 1–32.
- 3174** Hobbie, E. A. (2006). Carbon allocation to ectomycorrhizal fungi correlates  
**3175** with belowground allocation in culture studies. *Ecology* 87(3), 563–569.
- 3176** Hobbie, E. A. and J. E. Hobbie (2008). Natural abundance of  $^{15}\text{N}$  in nitrogen-  
**3177** limited forests and tundra can estimate nitrogen cycling through mycorrhizal  
**3178** fungi: a review. *Ecosystems* 11(5), 815–830.
- 3179** Hoek, T. A., K. Axelrod, T. Biancalani, E. A. Yurtsev, J. Liu, and J. Gore  
**3180** (2016). Resource availability modulates the cooperative and competitive na-  
**3181** nature of a microbial cross-feeding mutualism. *PLOS Biology* 14(8), e1002540.
- 3182** Höglberg, M. N., M. J. I. Briones, S. G. Keel, D. B. Metcalfe, C. Campbell, A. J.  
**3183** Midwood, B. Thornton, V. Hurry, S. Linder, T. Näsholm, and P. Höglberg  
**3184** (2010). Quantification of effects of season and nitrogen supply on tree below-  
**3185** ground carbon transfer to ectomycorrhizal fungi and other soil organisms in  
**3186** a boreal pine forest. *New Phytologist* 187(2), 485–493.
- 3187** Höglberg, P., M. N. Höglberg, S. G. Göttlicher, N. R. Betson, S. G. Keel, D. B.  
**3188** Metcalfe, C. Campbell, A. Schindlbacher, V. Hurry, T. Lundmark, S. Linder,  
**3189** and T. Näsholm (2008). High temporal resolution tracing of photosynthate

- 3190 carbon from the tree canopy to forest soil microorganisms. *New Phytologist* 177(1), 220–228.
- 3192 Houlton, B. Z., Y.-P. Wang, P. M. Vitousek, and C. B. Field (2008). A uni-  
3193 fying framework for dinitrogen fixation in the terrestrial biosphere. *Nature* 454(7202), 327–330.
- 3195 Huber, M. L., R. A. Perkins, A. Laesecke, D. G. Friend, J. V. Sengers, M. J.  
3196 Assael, I. N. Metaxa, E. Vogel, R. Mareš, and K. Miyagawa (2009). New  
3197 international formulation for the viscosity of H<sub>2</sub>O. *Journal of Physical and*  
3198 *Chemical Reference Data* 38(2), 101–125.
- 3199 Hungate, B. A., J. S. Dukes, M. R. Shaw, Y. Luo, and C. B. Field (2003).  
3200 Nitrogen and climate change. *Science* 302(5650), 1512–1513.
- 3201 IPCC (2021). *Climate Change 2021: The Physical Science Basis. Contribution*  
3202 *of Working Group I to the Sixth Assessment Report of the Intergovernmental*  
3203 *Panel on Climate Change*, Volume In Press. Cambridge, United Kingdom  
3204 and New York, NY, USA: Cambridge University Press.
- 3205 Johnson, N. C., J. H. Graham, and F. A. Smith (1997). Functioning of mycor-  
3206 rhizal associations along the mutualism-parasitism continuum. *New Phytol-*  
3207 *ogist* 135(4), 575–585.
- 3208 Kachurina, O. M., H. Zhang, W. R. Raun, and E. G. Krenzer (2000). Simul-  
3209 taneous determination of soil aluminum, ammonium- and nitrate- nitrogen  
3210 using 1 M potassium chloride. *Communications in Soil Science and Plant*  
3211 *Analysis* 31(7-8), 893–903.
- 3212 Kaiser, C., M. R. Kilburn, P. L. Clode, L. Fuchslueger, M. Koranda, J. B. Cliff,

- 3213** Z. M. Solaiman, and D. V. Murphy (2015). Exploring the transfer of recent  
**3214** plant photosynthates to soil microbes: mycorrhizal pathway vs direct root  
**3215** exudation. *New Phytologist* 205(4), 1537–1551.
- 3216** Katabuchi, M. (2015). LeafArea: An R package for rapid digital analysis of leaf  
**3217** area. *Ecological Research* 30(6), 1073–1077.
- 3218** Kattge, J. and W. Knorr (2007). Temperature acclimation in a biochemical  
**3219** model of photosynthesis: a reanalysis of data from 36 species. *Plant, Cell*  
**3220** and *Environment* 30(9), 1176–1190.
- 3221** Kattge, J., W. Knorr, T. Raddatz, and C. Wirth (2009). Quantifying photosyn-  
**3222** thetic capacity and its relationship to leaf nitrogen content for global-scale  
**3223** terrestrial biosphere models. *Global Change Biology* 15(4), 976–991.
- 3224** Kayler, Z., A. Gessler, and N. Buchmann (2010). What is the speed of link  
**3225** between aboveground and belowground processes? *New Phytologist* 187(4),  
**3226** 885–888.
- 3227** Kayler, Z., C. Keitel, K. Jansen, and A. Gessler (2017). Experimental evidence  
**3228** of two mechanisms coupling leaf-level C assimilation to rhizosphere CO<sub>2</sub>  
**3229** release. *Environmental and Experimental Botany* 135, 21–26.
- 3230** Keeling, C. D., W. G. Mook, and P. P. Tans (1979, jan). Recent trends in the  
**3231** <sup>13</sup>C:<sup>12</sup>C ratio of atmospheric carbon dioxide. *Nature* 277(5692), 121–123.
- 3232** Keeney, D. R. and D. W. Nelson (1983). Nitrogen—Inorganic Forms. In A. L.  
**3233** Page (Ed.), *Methods of Soil Analysis* (2nd ed.), Chapter 33, pp. 643–698.  
**3234** Madison, WI, USA: ASA and SSSA.
- 3235** Kenward, M. G. and J. H. Roger (1997). Small sample inference for fixed effects

- 3236** from restricted maximum likelihood. *Biometrics* 53(3), 983.
- 3237** Knapp, A. K., M. L. Avolio, C. Beier, C. J. W. Carroll, S. L. Collins, J. S.
- 3238** Dukes, L. H. Fraser, R. J. Griffin-Nolan, D. L. Hoover, A. Jentsch, M. E.
- 3239** Loik, R. P. Phillips, A. K. Post, O. E. Sala, I. J. Slette, L. Yahdjian, and
- 3240** M. D. Smith (2017). Pushing precipitation to the extremes in distributed
- 3241** experiments: recommendations for simulating wet and dry years. *Global*
- 3242** *Change Biology* 23(5), 1774–1782.
- 3243** Knorr, W. (2000). Annual and interannual CO<sub>2</sub> exchanges of the
- 3244** terrestrial biosphere: process-based simulations and uncertainties. *Global*
- 3245** *Ecology and Biogeography* 9(3), 225–252.
- 3246** Knorr, W. and M. Heimann (2001). Uncertainties in global terrestrial biosphere
- 3247** modeling: 1. A comprehensive sensitivity analysis with a new photosynthesis
- 3248** and energy balance scheme. *Global Biogeochemical Cycles* 15(1), 207–225.
- 3249** Kulmatiski, A., P. B. Adler, J. M. Stark, and A. T. Tredennick (2017). Water
- 3250** and nitrogen uptake are better associated with resource availability than
- 3251** root biomass. *Ecosphere* 8(3), e01738.
- 3252** Lavergne, A., D. Sandoval, V. J. Hare, H. Graven, and I. C. Prentice (2020).
- 3253** Impacts of soil water stress on the acclimated stomatal limitation of pho-
- 3254** tosynthesis: Insights from stable carbon isotope data. *Global Change Biol-*
- 3255** *ogy* 26(12), 7158–7172.
- 3256** Lawrence, D. M., R. A. Fisher, C. D. Koven, K. W. Oleson, S. C. Swen-
- 3257** son, G. B. Bonan, N. Collier, B. Ghimire, L. Kampenhout, D. Kennedy,
- 3258** E. Kluzek, P. J. Lawrence, F. Li, H. Li, D. L. Lombardozzi, W. J. Riley,
- 3259** W. J. Sacks, M. Shi, M. Vertenstein, W. R. Wieder, C. Xu, A. A. Ali,

- 3260** A. M. Badger, G. Bisht, M. Broeke, M. A. Brunke, S. P. Burns, J. Buzan,  
**3261** M. Clark, A. Craig, K. M. Dahlin, B. Drewniak, J. B. Fisher, M. Flanner,  
**3262** A. M. Fox, P. Gentine, F. M. Hoffman, G. Keppel-Aleks, R. Knox, S. Ku-  
**3263** mar, J. Lenaerts, L. R. Leung, W. H. Lipscomb, Y. Lu, A. Pandey, J. D.  
**3264** Pelletier, J. Perket, J. T. Randerson, D. M. Ricciuto, B. M. Sanderson,  
**3265** A. Slater, Z. M. Subin, J. Tang, R. Q. Thomas, M. Val Martin, and X. Zeng  
**3266** (2019). The Community Land Model Version 5: description of new features,  
**3267** benchmarking, and impact of forcing uncertainty. *Journal of Advances in*  
**3268** *Modeling Earth Systems* 11(12), 4245–4287.
- 3269** LeBauer, D. S. and K. K. Treseder (2008). Nitrogen limitation of net primary  
**3270** productivity. *Ecology* 89(2), 371–379.
- 3271** Lefcheck, J. S. (2016). piecewiseSEM: Piecewise structural equation modelling  
**3272** in r for ecology, evolution, and systematics. *Methods in Ecology and Evolu-*  
**3273** *tion* 7(5), 573–579.
- 3274** Lenth, R. (2019). emmeans: estimated marginal means, aka least-squares  
**3275** means.
- 3276** Li, W., H. Zhang, G. Huang, R. Liu, H. Wu, C. Zhao, and N. G. McDowell  
**3277** (2020). Effects of nitrogen enrichment on tree carbon allocation: A global  
**3278** synthesis. *Global Ecology and Biogeography* 29(3), 573–589.
- 3279** Liang, J., X. Qi, L. Souza, and Y. Luo (2016). Processes regulating progressive  
**3280** nitrogen limitation under elevated carbon dioxide: a meta-analysis. *Bioge-  
osciences* 13(9), 2689–2699.
- 3282** Liang, X., T. Zhang, X. Lu, D. S. Ellsworth, H. BassiriRad, C. You, D. Wang,  
**3283** P. He, Q. Deng, H. Liu, J. Mo, and Q. Ye (2020). Global response patterns of

- 3284 plant photosynthesis to nitrogen addition: A meta-analysis. *Global Change*  
3285 *Biology* 26(6), 3585–3600.
- 3286 López, J., D. A. Way, and W. Sadok (2021). Systemic effects of rising atmo-  
3287 spheric vapor pressure deficit on plant physiology and productivity. *Global*  
3288 *Change Biology* 27(9), 1704–1720.
- 3289 Lu, J., J. Yang, C. Keitel, L. Yin, P. Wang, W. Cheng, and F. A. Dijkstra  
3290 (2022). Belowground carbon efficiency for nitrogen and phosphorus acqui-  
3291 sition varies between *Lolium perenne* and *Trifolium repens* and depends on  
3292 phosphorus fertilization. *Frontiers in Plant Science* 13, 1–9.
- 3293 Luo, X., T. F. Keenan, J. M. Chen, H. Croft, I. C. Prentice, N. G. Smith,  
3294 A. P. Walker, H. Wang, R. Wang, C. Xu, and Y. Zhang (2021). Global  
3295 variation in the fraction of leaf nitrogen allocated to photosynthesis. *Nature*  
3296 *Communications* 12(1), 4866.
- 3297 Luo, Y., W. S. Currie, J. S. Dukes, A. C. Finzi, U. A. Hartwig, B. A. Hungate,  
3298 R. E. McMurtrie, R. Oren, W. J. Parton, D. E. Pataki, R. M. Shaw, D. R.  
3299 Zak, and C. B. Field (2004). Progressive nitrogen limitation of ecosystem  
3300 responses to rising atmospheric carbon dioxide. *BioScience* 54(8), 731–739.
- 3301 Maire, V., P. Martre, J. Kattge, F. Gastal, G. Esser, S. Fontaine, and J.-F.  
3302 Soussana (2012). The coordination of leaf photosynthesis links C and N  
3303 fluxes in C<sub>3</sub> plant species. *PLoS ONE* 7(6), e38345.
- 3304 Makino, A. (2003). Rubisco and nitrogen relationships in rice: leaf photosyn-  
3305 thesis and plant growth. *Soil Science and Plant Nutrition* 49(3), 319–327.
- 3306 Makino, A., M. Harada, T. Sato, H. Nakano, and T. Mae (1997). Growth and N

- 3307** Allocation in Rice Plants under CO<sub>2</sub> Enrichment. *Plant Physiology* 115(1),  
**3308** 199–203.
- 3309** Markham, J. H. and C. Zekveld (2007). Nitrogen fixation makes biomass al-  
**3310** location to roots independent of soil nitrogen supply. *Canadian Journal of*  
**3311** *Botany* (9), 787–793.
- 3312** Marschner, H. and B. Dell (1994). Nutrient uptake in mycorrhizal symbiosis.  
**3313** *Plant and Soil* 159(1), 89–102.
- 3314** Matamala, R. and W. H. Schlesinger (2000). Effects of elevated atmospheric  
**3315** CO<sub>2</sub> on fine root production and activity in an intact temperate forest  
**3316** ecosystem. *Global Change Biology* 6(8), 967–979.
- 3317** Medlyn, B. E., E. Dreyer, D. S. Ellsworth, M. Forstreuter, P. C. Harley,  
**3318** M. U. F. Kirschbaum, X. Le Roux, P. Montpied, J. Strassmeyer, A. Wal-  
**3319** croft, K. Wang, and D. Loustau (2002). Temperature response of parameters  
**3320** of a biochemically based model of photosynthesis. II. A review of experimen-  
**3321** tal data. *Plant, Cell and Environment* 25(9), 1167–1179.
- 3322** Menge, D. N. L., S. A. Levin, and L. O. Hedin (2008). Evolutionary tradeoffs can  
**3323** select against nitrogen fixation and thereby maintain nitrogen limitation.  
**3324** *Proceedings of the National Academy of Sciences* 105(5), 1573–1578.
- 3325** Menne, M. J., I. Durre, R. S. Vose, B. E. Gleason, and T. G. Houston (2012).  
**3326** An overview of the global historical climatology network-daily database.  
**3327** *Journal of Atmospheric and Oceanic Technology* 29(7), 897–910.
- 3328** Meyerholt, J., K. Sickel, and S. Zaehle (2020). Ensemble projections elucidate  
**3329** effects of uncertainty in terrestrial nitrogen limitation on future carbon up-

- 3330** take. *Global Change Biology* 26(7), 3978–3996.
- 3331** Meyerholt, J., S. Zaehle, and M. J. Smith (2016). Variability of projected ter-
- 3332** restrial biosphere responses to elevated levels of atmospheric CO<sub>2</sub> due to
- 3333** uncertainty in biological nitrogen fixation. *Biogeosciences* 13(5), 1491–1518.
- 3334** Minocha, R., S. Long, A. H. Magill, J. D. Aber, and W. H. McDowell (2000).
- 3335** Foliar free polyamine and inorganic ion content in relation to soil and soil
- 3336** solution chemistry in two fertilized forest stands at the Harvard Forest,
- 3337** Massachusetts. *Plant and Soil* 222(1-2), 119–137.
- 3338** Moore, D. J., S. Aref, R. M. Ho, J. S. Pippen, J. G. Hamilton, and E. H. De
- 3339** Lucia (2006). Annual basal area increment and growth duration of Pinus
- 3340** taeda in response to eight years of free-air carbon dioxide enrichment. *Global*
- 3341** *Change Biology* 12(8), 1367–1377.
- 3342** Morgan, J. A., D. E. Pataki, C. Körner, H. Clark, S. J. Del Gross, J. M.
- 3343** Grünzweig, A. K. Knapp, A. R. Mosier, P. C. D. Newton, P. A. Niklaus,
- 3344** J. B. Nippert, R. S. Nowak, W. J. Parton, H. W. Polley, and M. R. Shaw
- 3345** (2004). Water relations in grassland and desert ecosystems exposed to ele-
- 3346** vated atmospheric CO<sub>2</sub>. *Oecologia* 140(1), 11–25.
- 3347** Muñoz, N., X. Qi, M. W. Li, M. Xie, Y. Gao, M. Y. Cheung, F. L. Wong, and
- 3348** H.-M. Lam (2016). Improvement in nitrogen fixation capacity could be part
- 3349** of the domestication process in soybean. *Heredity* 117(2), 84–93.
- 3350** Nadelhoffer, K. J. and J. W. Raich (1992). Fine root production estimates and
- 3351** belowground carbon allocation in forest ecosystems. *Ecology* 73(4), 1139–
- 3352** 1147.

- 3353 Niinemets, Ü. and J. D. Tenhunen (1997). A model separating leaf structural  
3354 and physiological effects on carbon gain along light gradients for the shade-  
3355 tolerant species *Acer saccharum*. *Plant, Cell and Environment* 20(7), 845–  
3356 866.
- 3357 Norby, R. J., J. Ledford, C. D. Reilly, N. E. Miller, and E. G. O'Neill  
3358 (2004). Fine-root production dominates response of a deciduous forest to  
3359 atmospheric CO<sub>2</sub> enrichment. *Proceedings of the National Academy of Sci-  
3360 ences* 101(26), 9689–9693.
- 3361 Norby, R. J., J. M. Warren, C. M. Iversen, B. E. Medlyn, and R. E. Mc-  
3362 Murtrie (2010). CO<sub>2</sub> enhancement of forest productivity constrained by  
3363 limited nitrogen availability. *Proceedings of the National Academy of Sci-  
3364 ences* 107(45), 19368–19373.
- 3365 Novick, K. A., D. L. Ficklin, P. C. Stoy, C. A. Williams, G. Bohrer, A. C.  
3366 Oishi, S. A. Papuga, P. D. Blanken, A. Noormets, B. N. Sulman, R. L.  
3367 Scott, L. Wang, and R. P. Phillips (2016). The increasing importance of  
3368 atmospheric demand for ecosystem water and carbon fluxes. *Nature Climate  
3369 Change* 6(11), 1023–1027.
- 3370 Noyce, G. L., M. L. Kirwan, R. L. Rich, and J. P. Megonigal (2019). Asyn-  
3371 chronous nitrogen supply and demand produce nonlinear plant allocation re-  
3372 sponds to warming and elevated CO<sub>2</sub>. *Proceedings of the National Academy  
3373 of Sciences* 116(43), 21623–21628.
- 3374 Onoda, Y., K. Hikosaka, and T. Hirose (2004). Allocation of nitrogen to  
3375 cell walls decreases photosynthetic nitrogen-use efficiency. *Functional Ecol-  
3376 ogy* 18(3), 419–425.

- 3377** Onoda, Y., I. J. Wright, J. R. Evans, K. Hikosaka, K. Kitajima, Ü. Niinemets,  
**3378** H. Poorter, T. Tosens, and M. Westoby (2017). Physiological and structural  
**3379** trade-offs underlying the leaf economics spectrum. *New Phytologist* 214(4),  
**3380** 1447–1463.
- 3381** Oren, R., J. S. Sperry, G. G. Katul, D. E. Pataki, B. E. Ewers, N. Phillips,  
**3382** and K. V. R. Schäfer (1999). Survey and synthesis of intra- and interspecific  
**3383** variation in stomatal sensitivity to vapor pressure deficit. *Plant, Cell and*  
**3384** *Environment* 22(12), 1515–1526.
- 3385** Oreskes, N., K. Shrader-Frechette, and K. Belitz (1994). Verification, vali-  
**3386** dation, and confirmation of numerical models in the Earth sciences. *Sci-  
ence* 263(5147), 641–646.
- 3388** Paillassa, J., I. J. Wright, I. C. Prentice, S. Pepin, N. G. Smith, G. Ethier,  
**3389** A. C. Westerband, L. J. Lamarque, H. Wang, W. K. Cornwell, and V. Maire  
**3390** (2020). When and where soil is important to modify the carbon and water  
**3391** economy of leaves. *New Phytologist* 228(1), 121–135.
- 3392** Parvin, S., S. Uddin, S. Tausz Posch, R. Armstrong, and M. Tausz (2020). Car-  
**3393** bon sink strength of nodules but not other organs modulates photosynthesis  
**3394** of faba bean (*Vicia faba*) grown under elevated [CO<sub>2</sub>] and different water  
**3395** supply. *New Phytologist* 227(1), 132–145.
- 3396** Paul, K. I., P. J. Polglase, A. M. O'Connell, J. C. Carlyle, P. J. Smethurst, and  
**3397** P. K. Khanna (2003). Defining the relation between soil water content and  
**3398** net nitrogen mineralization. *European Journal of Soil Science* 54(1), 39–48.
- 3399** Peng, Y., K. J. Bloomfield, L. A. Cernusak, T. F. Domingues, and I. C. Pre-  
**3400** nance (2021). Global climate and nutrient controls of photosynthetic capacity.

- 3401** *Communications Biology* 4(1), 462.
- 3402** Perkowski, E. A., E. F. Waring, and N. G. Smith (2021). Root mass carbon  
**3403** costs to acquire nitrogen are determined by nitrogen and light availability  
**3404** in two species with different nitrogen acquisition strategies. *Journal of*  
**3405** *Experimental Botany* 72(15), 5766–5776.
- 3406** Phillips, R. P., E. R. Brzostek, and M. G. Midgley (2013). The mycorrhizal-  
**3407** associated nutrient economy: a new framework for predicting carbon-  
**3408** nutrient couplings in temperate forests. *New Phytologist* 199(1), 41–51.
- 3409** Phillips, R. P., A. C. Finzi, and E. S. Bernhardt (2011). Enhanced root ex-  
**3410** udation induces microbial feedbacks to N cycling in a pine forest under  
**3411** long-term CO<sub>2</sub> fumigation. *Ecology Letters* 14(2), 187–194.
- 3412** Pinheiro, J. and D. Bates (2022). nlme: linear and nonlinear mixed effects  
**3413** models.
- 3414** Poggio, L., L. M. De Sousa, N. H. Batjes, G. B. M. Heuvelink, B. Kempen,  
**3415** E. Ribeiro, and D. Rossiter (2021). SoilGrids 2.0: Producing soil information  
**3416** for the globe with quantified spatial uncertainty. *Soil* 7(1), 217–240.
- 3417** Pons, T. L. and R. W. Pearcy (1994). Nitrogen reallocation and photosynthetic  
**3418** acclimation in response to partial shading in soybean plants. *Physiologia*  
**3419** *Plantarum* 92(4), 636–644.
- 3420** Poorter, H., J. Bühler, D. Van Dusschoten, J. Climent, and J. A. Postma (2012).  
**3421** Pot size matters: A meta-analysis of the effects of rooting volume on plant  
**3422** growth. *Functional Plant Biology* 39(11), 839–850.
- 3423** Poorter, H., O. Knopf, I. J. Wright, A. A. Temme, S. W. Hogewoning, A. Graf,

- 3424** L. A. Cernusak, and T. L. Pons (2022). A meta-analysis of responses of C<sub>3</sub>  
**3425** plants to atmospheric CO<sub>2</sub>: dose-response curves for 85 traits ranging from  
**3426** the molecular to the whole-plant level. *New Phytologist* 233(4), 1560–1596.
- 3427** Prentice, I. C., N. Dong, S. M. Gleason, V. Maire, and I. J. Wright (2014).  
**3428** Balancing the costs of carbon gain and water transport: testing a new theo-  
**3429** retical framework for plant functional ecology. *Ecology Letters* 17(1), 82–91.
- 3430** Prentice, I. C., X. Liang, B. E. Medlyn, and Y.-P. Wang (2015). Reliable, ro-  
**3431** bust and realistic: The three R's of next-generation land-surface modelling.  
**3432** *Atmospheric Chemistry and Physics* 15, 5987–6005.
- 3433** Priestley, C. H. B. and R. J. Taylor (1972). On the Assessment of Surface  
**3434** Heat Flux and Evaporation Using Large-Scale Parameters. *Monthly Weather  
Review* 100(2), 81–92.
- 3436** Querejeta, J. I., I. Prieto, C. Armas, F. Casanoves, J. S. Diémé, M. Diouf,  
**3437** H. Yossi, B. Kaya, F. I. Pugnaire, and G. M. Rusch (2022). Higher leaf  
**3438** nitrogen content is linked to tighter stomatal regulation of transpiration  
**3439** and more efficient water use across dryland trees. *New Phytologist* 235(4),  
**3440** 1351–1364.
- 3441** R Core Team (2021). R: A language and environment for statistical computing.
- 3442** Raich, J. W., D. A. Clark, L. Schwendenmann, and T. E. Wood (2014). Above-  
**3443** ground tree growth varies with belowground carbon allocation in a tropical  
**3444** rainforest environment. *PLoS ONE* 9(6), e100275.
- 3445** Rastetter, E. B., P. M. Vitousek, C. B. Field, G. R. Shaver, D. Herbert, and  
**3446** G. I. Ågren (2001). Resource optimization and symbiotic nitrogen fixation.

- 3447** *Ecosystems* 4(4), 369–388.
- 3448** Reich, P. B. (2014). The world-wide 'fast-slow' plant economics spectrum: a  
**3449** traits manifesto. *Journal of Ecology* 102(2), 275–301.
- 3450** Reich, P. B., S. E. Hobbie, T. Lee, D. S. Ellsworth, J. B. West, D. Tilman,  
**3451** J. M. H. Knops, S. Naeem, and J. Trost (2006). Nitrogen limitation con-  
**3452** strains sustainability of ecosystem response to CO<sub>2</sub>. *Nature* 440(7086), 922–  
**3453** 925.
- 3454** Reichman, G. A., D. L. Grunes, and F. G. Viets (1966). Effect of soil moisture  
**3455** on ammonification and nitrification in two Northern Plains soils. *Soil Science  
Society of America Journal* 30(3), 363–366.
- 3457** Rhine, E. D., R. L. Mulvaney, E. J. Pratt, and G. K. Sims (1998). Improving  
**3458** the Berthelot reaction for determining ammonium in soil extracts and water.  
**3459** *Soil Science Society of America Journal* 62(2), 473.
- 3460** Rogers, A. (2014). The use and misuse of  $V_{\text{cmax}}$  in Earth System Models. *Pho-*  
**3461** *tosynthesis Research* 119(1-2), 15–29.
- 3462** Rogers, A., B. E. Medlyn, J. S. Dukes, G. B. Bonan, S. Caemmerer, M. C.  
**3463** Dietze, J. Kattge, A. D. B. Leakey, L. M. Mercado, Ü. Niinemets, I. C.  
**3464** Prentice, S. P. Serbin, S. Sitch, D. A. Way, and S. Zaehle (2017). A roadmap  
**3465** for improving the representation of photosynthesis in Earth system models.  
**3466** *New Phytologist* 213(1), 22–42.
- 3467** Saathoff, A. J. and J. Welles (2021). Gas exchange measurements in the un-  
**3468** steady state. *Plant Cell and Environment* 44(11), 3509–3523.
- 3469** Sage, R. F. and R. W. Pearcy (1987). The nitrogen use efficiency of C<sub>3</sub> and C<sub>4</sub>

- 3470 plants: I. Leaf nitrogen, growth, and biomass partitioning in *Chenopodium*  
3471 *album* (L.) and *Amaranthus retroflexus* (L.). *Plant Physiology* 84(3), 954–  
3472 958.
- 3473 Saleh, A. M., M. Abdel-Mawgoud, A. R. Hassan, T. H. Habeeb, R. S. Yehia,  
3474 and H. AbdElgawad (2020). Global metabolic changes induced by arbuscular  
3475 mycorrhizal fungi in oregano plants grown under ambient and elevated levels  
3476 of atmospheric CO<sub>2</sub>. *Plant Physiology and Biochemistry* 151, 255–263.
- 3477 Saxton, K. E. and W. J. Rawls (2006). Soil water characteristic estimates by  
3478 texture and organic matter for hydrologic solutions. *Soil Science Society of  
3479 America Journal* 70(5), 1569–1578.
- 3480 Schaefer, K., C. R. Schwalm, C. Williams, M. A. Arain, A. Barr, J. M. Chen,  
3481 K. J. Davis, D. Dimitrov, T. W. Hilton, D. Y. Hollinger, E. Humphreys,  
3482 B. Poulter, B. M. Racza, A. D. Richardson, A. Sahoo, P. Thornton, R. Var-  
3483 gas, H. Verbeeck, R. Anderson, I. Baker, T. A. Black, P. Bolstad, J. Chen,  
3484 P. S. Curtis, A. R. Desai, M. C. Dietze, D. Dragoni, C. M. Gough, R. F.  
3485 Grant, L. Gu, A. K. Jain, C. Kucharik, B. E. Law, S. Liu, E. Lokipitiya,  
3486 H. A. Margolis, R. Matamala, J. H. McCaughey, R. Monson, J. W. Munger,  
3487 W. Oechel, C. Peng, D. T. Price, D. Ricciuto, W. J. Riley, N. Roulet,  
3488 H. Tian, C. Tonitto, M. Torn, E. Weng, and X. Zhou (2012). A model-  
3489 data comparison of gross primary productivity: Results from the North  
3490 American Carbon Program site synthesis. *Journal of Geophysical Research:  
3491 Biogeosciences* 117(G3), G03010.
- 3492 Schmitt, M. R. and G. E. Edwards (1981). Photosynthetic capacity and nitrogen  
3493 use efficiency of maize, wheat, and rice: A comparison between C<sub>3</sub> and C<sub>4</sub>

- 3494** photosynthesis. *Journal of Experimental Botany* 32(3), 459–466.
- 3495** Schneider, C. A., W. S. Rasband, and K. W. Eliceiri (2012). NIH Image to
- 3496** ImageJ: 25 years of image analysis. *Nature Methods* 9(7), 671–675.
- 3497** Scott, H. G. and N. G. Smith (2022). A Model of C<sub>4</sub> photosynthetic acclima-
- 3498** tion based on least-cost optimality theory suitable for Earth system model
- 3499** incorporation. *Journal of Advances in Modeling Earth Systems* 14(3), 1–16.
- 3500** Shi, M., J. B. Fisher, E. R. Brzostek, and R. P. Phillips (2016). Carbon cost
- 3501** of plant nitrogen acquisition: Global carbon cycle impact from an improved
- 3502** plant nitrogen cycle in the Community Land Model. *Global Change Biol-*
- 3503** *ogy* 22(3), 1299–1314.
- 3504** Shi, M., J. B. Fisher, R. P. Phillips, and E. R. Brzostek (2019). Neglecting
- 3505** plant–microbe symbioses leads to underestimation of modeled climate im-
- 3506** pacts. *Biogeosciences* 16(2), 457–465.
- 3507** Smith, B., D. Wärldin, A. Arneth, T. Hickler, P. Leadley, J. Siltberg, and
- 3508** S. Zaehle (2014). Implications of incorporating N cycling and N limitations
- 3509** on primary production in an individual-based dynamic vegetation model.
- 3510** *Biogeosciences* 11(7), 2027–2054.
- 3511** Smith, N. G. and J. S. Dukes (2013). Plant respiration and photosynthesis in
- 3512** global-scale models: incorporating acclimation to temperature and CO<sub>2</sub>.
- 3513** *Global Change Biology* 19(1), 45–63.
- 3514** Smith, N. G. and T. F. Keenan (2020). Mechanisms underlying leaf photosyn-
- 3515** thetic acclimation to warming and elevated CO<sub>2</sub> as inferred from least-cost
- 3516** optimality theory. *Global Change Biology* 26(9), 5202–5216.

- 3517 Smith, N. G., T. F. Keenan, I. C. Prentice, H. Wang, I. J. Wright, Ü. Niinemets,  
3518 K. Y. Crous, T. F. Domingues, R. Guerrieri, F. oko Ishida, J. Kattge, E. L.  
3519 Kruger, V. Maire, A. Rogers, S. P. Serbin, L. Tarvainen, H. F. Togashi,  
3520 P. A. Townsend, M. Wang, L. K. Weerasinghe, and S.-X. Zhou (2019).  
3521 Global photosynthetic capacity is optimized to the environment. *Ecology  
Letters* 22(3), 506–517.
- 3522
- 3523 Smith, N. G., D. L. Lombardozzi, A. Tawfik, G. B. Bonan, and J. S. Dukes  
3524 (2017). Biophysical consequences of photosynthetic temperature acclimation  
3525 for climate. *Journal of Advances in Modeling Earth Systems* 9(1), 536–547.
- 3526 Smith, N. G., S. L. Malyshev, E. Shevliakova, J. Kattge, and J. S. Dukes  
3527 (2016). Foliar temperature acclimation reduces simulated carbon sensitivity  
3528 to climate. *Nature Climate Change* 6(4), 407–411.
- 3529 Smith, S. E. and D. J. Read (2008). *Mycorrhizal Symbiosis*. Academic Press.
- 3530 Soil Survey Staff (2022). Web Soil Survey.
- 3531 Soudzilovskaia, N. A., J. C. Douma, A. A. Akhmetzhanova, P. M. van Bode-  
3532 gom, W. K. Cornwell, E. J. Moens, K. K. Treseder, and J. H. C. Cornelissen  
3533 (2015). Global patterns of plant root colonization intensity by mycorrhizal  
3534 fungi explained by climate and soil chemistry. *Global Ecology and Biogeog-  
3535 raphy* 24(3), 371–382.
- 3536 Stark, J. M. and M. K. Firestone (1995). Mechanisms for soil moisture ef-  
3537 fects on activity of nitrifying bacteria. *Applied and Environmental Microbi-  
3538 ology* 61(1), 218–221.
- 3539 Stocker, B. D., H. Wang, N. G. Smith, S. P. Harrison, T. F. Keenan, D. San-

- 3540 doval, T. Davis, and I. C. Prentice (2020). P-model v1.0: An optimality-based light use efficiency model for simulating ecosystem gross primary production. *Geoscientific Model Development* 13(3), 1545–1581.
- 3541
- 3542
- 3543 Stocker, B. D., J. Zscheischler, T. F. Keenan, I. C. Prentice, J. Peñuelas, and S. I. Seneviratne (2018). Quantifying soil moisture impacts on light use efficiency across biomes. *New Phytologist* 218(4), 1430–1449.
- 3544
- 3545
- 3546 Sulman, B. N., D. T. Roman, K. Yi, L. Wang, R. P. Phillips, and K. A. Novick (2016). High atmospheric demand for water can limit forest carbon uptake and transpiration as severely as dry soil. *Geophysical Research Letters* 43(18), 9686–9695.
- 3547
- 3548
- 3549
- 3550 Sulman, B. N., E. Shevliakova, E. R. Brzostek, S. N. Kivlin, S. L. Malyshev, D. N. L. Menge, and X. Zhang (2019). Diverse mycorrhizal associations enhance terrestrial C storage in a global model. *Global Biogeochemical Cycles* 33(4), 501–523.
- 3551
- 3552
- 3553
- 3554 Sweet, S. K., D. W. Wolfe, A. DeGaetano, and R. Benner (2017). Anatomy of the 2016 drought in the Northeastern United States: Implications for agriculture and water resources in humid climates. *Agricultural and Forest Meteorology* 247, 571–581.
- 3555
- 3556
- 3557
- 3558 Taylor, B. N. and D. N. L. Menge (2018). Light regulates tropical symbiotic nitrogen fixation more strongly than soil nitrogen. *Nature Plants* 4(9), 655–661.
- 3559
- 3560
- 3561 Terrer, C., S. Vicca, B. A. Hungate, R. P. Phillips, and I. C. Prentice (2016). Mycorrhizal association as a primary control of the CO<sub>2</sub> fertilization effect. *Science* 353(6294), 72–74.
- 3562
- 3563

- 3564 Terrer, C., S. Vicca, B. D. Stocker, B. A. Hungate, R. P. Phillips, P. B. Reich,  
3565 A. C. Finzi, and I. C. Prentice (2018). Ecosystem responses to elevated CO<sub>2</sub>  
3566 governed by plant–soil interactions and the cost of nitrogen acquisition. *New  
3567 Phytologist* 217(2), 507–522.
- 3568 Thieurmel, B. and A. Elmarhraoui (2019). suncalc: Compute sun position,  
3569 sunlight phases, moon position, and lunar phase.
- 3570 Thomas, R. Q., E. N. J. Brookshire, and S. Gerber (2015). Nitrogen limita-  
3571 tion on land: how can it occur in Earth system models? *Global Change  
3572 Biology* 21(5), 1777–1793.
- 3573 Thomas, R. Q., S. Zaehle, P. H. Templer, and C. L. Goodale (2013). Global pat-  
3574 terns of nitrogen limitation: confronting two global biogeochemical models  
3575 with observations. *Global Change Biology* 19(10), 2986–2998.
- 3576 Thornton, P. E., J.-F. Lamarque, N. A. Rosenbloom, and N. M. Mahowald  
3577 (2007). Influence of carbon-nitrogen cycle coupling on land model response  
3578 to CO<sub>2</sub> fertilization and climate variability. *Global Biogeochemical Cy-  
3579 cles* 21(4), GB4018.
- 3580 Tingey, D. T., D. L. Phillips, and M. G. Johnson (2000). Elevated CO<sub>2</sub> and  
3581 conifer roots: effects on growth, life span and turnover. *New Phytolo-  
3582 gist* 147(1), 87–103.
- 3583 Udvardi, M. and P. S. Poole (2013). Transport and metabolism in legume-  
3584 rhizobia symbioses. *Annual Review of Plant Biology* 64, 781–805.
- 3585 USDA NRCS (2022). The PLANTS Database.
- 3586 Uselman, S. M., R. G. Qualls, and R. B. Thomas (2000). Effects of increased

- 3587 atmospheric CO<sub>2</sub>, temperature, and soil N availability on root exudation  
3588 of dissolved organic carbon by an N-fixing tree (*Robinia pseudoacacia* L.).  
3589 *Plant and Soil* 222, 191–202.
- 3590 van Diepen, L. T. A., E. A. Lilleskov, K. S. Pregitzer, and R. M. Miller (2007).  
3591 Decline of arbuscular mycorrhizal fungi in northern hardwood forests ex-  
3592 posed to chronic nitrogen additions. *New Phytologist* 176(1), 175–183.
- 3593 Vance, C. P. and G. H. Heichel (1991). Carbon in N<sub>2</sub> fixation: Limitation or  
3594 exquisite adaptation. *Annual Review of Plant Physiology and Plant Molec-*  
3595 *ular Biology* 42(1), 373–392.
- 3596 Viet, H. D., J.-H. Kwak, K.-S. Lee, S.-S. Lim, M. Matsushima, S. X. Chang,  
3597 K.-H. Lee, and W.-J. Choi (2013). Foliar chemistry and tree ring δ<sup>13</sup>C of  
3598 *Pinus densiflora* in relation to tree growth along a soil pH gradient. *Plant*  
3599 *and Soil* 363(1-2), 101–112.
- 3600 Vitousek, P. M., K. Cassman, C. C. Cleveland, T. Crews, C. B. Field, N. B.  
3601 Grimm, R. W. Howarth, R. Marino, L. Martinelli, E. B. Rastetter, and  
3602 J. I. Sprent (2002). Towards an ecological understanding of biological nitro-  
3603 gen fixation. In *The Nitrogen Cycle at Regional to Global Scales*, pp. 1–45.  
3604 Springer Netherlands.
- 3605 Vitousek, P. M. and R. W. Howarth (1991). Nitrogen limitation on land and in  
3606 the sea: How can it occur? *Biogeochemistry* 13(2), 87–115.
- 3607 Vitousek, P. M., S. Porder, B. Z. Houlton, and O. A. Chadwick (2010).  
3608 Terrestrial phosphorus limitation: mechanisms, implications, and nitro-  
3609 gen–phosphorus interactions. *Ecological Applications* 20(1), 5–15.

- 3610** Walker, A. P., A. P. Beckerman, L. Gu, J. Kattge, L. A. Cernusak, T. F.  
**3611** Domingues, J. C. Scales, G. Wohlfahrt, S. D. Wullschleger, and F. I. Woodward (2014). The relationship of leaf photosynthetic traits -  $V_{cmax}$  and  $J_{max}$  - to leaf nitrogen, leaf phosphorus, and specific leaf area: a meta-analysis and modeling study. *Ecology and Evolution* 4(16), 3218–3235.
- 3615** Walker, A. P., A. L. Johnson, A. Rogers, J. Anderson, R. A. Bridges, R. A.  
**3616** Fisher, D. Lu, D. M. Ricciuto, S. P. Serbin, and M. Ye (2021). Multi-hypothesis comparison of Farquhar and Collatz photosynthesis models reveals the unexpected influence of empirical assumptions at leaf and global scales. *Global Change Biology* 27(4), 804–822.
- 3620** Wang, H., I. C. Prentice, T. F. Keenan, T. W. Davis, I. J. Wright, W. K.  
**3621** Cornwell, B. J. Evans, and C. Peng (2017). Towards a universal model for  
**3622** carbon dioxide uptake by plants. *Nature Plants* 3(9), 734–741.
- 3623** Wang, H., I. C. Prentice, I. J. Wright, D. I. Warton, S. Qiao, X. Xu, J. Zhou,  
**3624** Kikuzawa, and N. C. Stenseth (2023). Leaf economics fundamentals explained by optimality principles. *Science Advances* 9(3), eadd566.
- 3626** Wang, J., J. M. Knops, C. E. Brassil, and C. Mu (2017). Increased productivity  
**3627** in wet years drives a decline in ecosystem stability with nitrogen additions  
**3628** in arid grasslands. *Ecology* 98(7), 1779–1786.
- 3629** Wang, W., Y. Wang, G. Hoch, Z. Wang, and J. Gu (2018). Linkage of root mor-  
**3630** phology to anatomy with increasing nitrogen availability in six temperate  
**3631** tree species. *Plant and Soil* 425(1-2), 189–200.
- 3632** Weatherburn, M. W. (1967). Phenol-hypochlorite reaction for determination of  
**3633** ammonia. *Analytical Chemistry* 39(8), 971–974.

- 3634** Wellburn, A. R. (1994). The spectral determination of chlorophylls a and b, as  
**3635** well as total carotenoids, using various solvents with spectrophotometers of  
**3636** different resolution. *Journal of Plant Physiology* 144(3), 307–313.
- 3637** Wen, Z., P. J. White, J. Shen, and H. Lambers (2022). Linking root exuda-  
**3638** tion to belowground economic traits for resource acquisition. *New Phytolo-*  
**3639** *gist* 233(4), 1620–1635.
- 3640** Westerband, A. C., I. J. Wright, V. Maire, J. Paillassa, I. C. Prentice, O. K.  
**3641** Atkin, K. J. Bloomfield, L. A. Cernusak, N. Dong, S. M. Gleason, C. Guil-  
**3642** herme Pereira, H. Lambers, M. R. Leishman, Y. Malhi, and R. H. Nolan  
**3643** (2023). Coordination of photosynthetic traits across soil and climate gradi-  
**3644** ents. *Global Change Biology* 29(3), 1–29.
- 3645** Wieder, W. R., C. C. Cleveland, W. K. Smith, and K. Todd-Brown (2015).  
**3646** Future productivity and carbon storage limited by terrestrial nutrient avail-  
**3647** ability. *Nature Geoscience* 8(6), 441–444.
- 3648** Wieder, W. R., D. M. Lawrence, R. A. Fisher, G. B. Bonan, S. J. Cheng, C. L.  
**3649** Goodale, A. S. Grandy, C. D. Koven, D. L. Lombardozzi, K. W. Oleson,  
**3650** and R. Q. Thomas (2019). Beyond static benchmarking: using experimental  
**3651** manipulations to evaluate land model assumptions. *Global Biogeochemical*  
**3652** *Cycles* 33(10), 1289–1309.
- 3653** Wright, I. J., P. B. Reich, and M. Westoby (2003). Least-cost input mixtures  
**3654** of water and nitrogen for photosynthesis. *The American Naturalist* 161(1),  
**3655** 98–111.
- 3656** Wright, I. J., P. B. Reich, M. Westoby, D. D. Ackerly, Z. Baruch, F. Bongers,  
**3657** J. Cavender-Bares, T. Chapin, J. H. C. Cornelissen, M. Diemer, J. Flexas,

- 3658** E. Garnier, P. K. Groom, J. Gulias, K. Hikosaka, B. B. Lamont, T. Lee,  
**3659** W. Lee, C. Lusk, J. J. Midgley, M.-L. Navas, Ü. Niinemets, J. Oleksyn,  
**3660** N. Osada, H. Poorter, P. Poot, L. Prior, V. I. Pyankov, C. Roumet, S. C.  
**3661** Thomas, M. G. Tjoelker, E. J. Veneklaas, and R. Villar (2004). The world-  
**3662** wide leaf economics spectrum. *Nature* 428(6985), 821–827.
- 3663** Xu-Ri and I. C. Prentice (2017). Modelling the demand for new nitrogen fixation  
**3664** by terrestrial ecosystems. *Biogeosciences* 14(7), 2003–2017.
- 3665** Yahdjian, L., L. A. Gherardi, and O. E. Sala (2011). Nitrogen limitation in  
**3666** arid-subhumid ecosystems: A meta-analysis of fertilization studies. *Journal*  
**3667** of Arid Environments 75(8), 675–680.
- 3668** Zaehle, S., B. E. Medlyn, M. G. De Kauwe, A. P. Walker, M. C. Dietze, T. Hick-  
**3669** ler, Y. Luo, Y. P. Wang, B. El-Masri, P. Thornton, A. Jain, S. Wang,  
**3670** D. Warlind, E. Weng, W. Parton, C. M. Iversen, A. Gallet-Budynek, H. Mc-  
**3671** carthy, A. C. Finzi, P. J. Hanson, I. C. Prentice, R. Oren, and R. J. Norby  
**3672** (2014). Evaluation of 11 terrestrial carbon-nitrogen cycle models against  
**3673** observations from two temperate Free-Air CO<sub>2</sub> Enrichment studies. *New*  
**3674** *Phytologist* 202(3), 803–822.
- 3675** Zaehle, S., S. Sitch, B. Smith, and F. Hatterman (2005). Effects of parame-  
**3676** ter uncertainties on the modeling of terrestrial biosphere dynamics. *Global*  
**3677** *Biogeochemical Cycles* 19(3), GB3020.
- 3678** Zhu, Q., W. J. Riley, J. Tang, N. Collier, F. M. Hoffman, X. Yang, and G. Bisht  
**3679** (2019). Representing nitrogen, phosphorus, and carbon interactions in the  
**3680** E3SM land model: development and global benchmarking. *Journal of Ad-*  
**3681** *vances in Modeling Earth Systems* 11(7), 2238–2258.

- 3682** Ziegler, C., M. E. Dusenge, B. Nyirambangutse, E. Zibera, G. Wallin, and  
**3683** J. Uddling (2020). Contrasting dependencies of photosynthetic capacity on  
**3684** leaf nitrogen in early- and late-successional tropical montane tree species.  
**3685** *Frontiers in Plant Science* 11, 1–12.
- 3686** Ziehn, T., J. Kattge, W. Knorr, and M. Scholze (2011). Improving the pre-  
**3687** dictability of global CO<sub>2</sub> assimilation rates under climate change. *Geophys-  
3688* *ical Research Letters* 38(10), L10404.

3689      **Appendix A: Supplemental material for "Structural carbon costs to**  
 3690      **acquire nitrogen are determined by nitrogen and light availability in**  
 3691      **two species with different nitrogen acquisition strategies"**

**Table A1.** Summary table containing volumes of compounds used to create modified Hoagland's solutions for each soil nitrogen fertilization treatment. All volumes are expressed as milliliters per liter (mL/L)

Compound	0 ppm N	70 ppm N	210 ppm N	630 ppm N
1 M NH <sub>4</sub> H <sub>2</sub> PO <sub>4</sub>	0	0.33	1	1
2 M KNO <sub>3</sub>	0	0.67	2	2
2 M Ca(NO <sub>3</sub> ) <sub>2</sub>	0	0.67	2	2
1 M NH <sub>4</sub> NO <sub>3</sub>	0	0.33	1	0
8 M NH <sub>4</sub> NO <sub>3</sub>	0	0	0	2
1 M KH <sub>2</sub> PO <sub>4</sub>	1	0.67	0	0
1 M KCl	4	1.33	0	0
1 M CaCO <sub>3</sub>	4	3	0	0
2 M MgSO <sub>4</sub>	1	1	1	1
10% Fe-EDTA	1	1	1	1
Trace Elements	1	1	1	1

**Table A2.** Analysis of variance results exploring species-specific effects of light availability, nitrogen fertilization, and their interactions on the ratio of whole plant biomass to pot volume

	df	Biomass:pot volume		
		Coefficient	$\chi^2$	p
<i>G. hirsutum</i>				
Intercept		0.740	-	-
Light (L)	1	-4.23E-03	189.581	<b>&lt;0.001</b>
Nitrogen (N)	1	7.86E-04	17.927	<b>&lt;0.001</b>
L*N	1	-6.61E-06	4.709	<b>0.030</b>
<i>G. max</i>				
Intercept		-0.233	-	-
Light (L)	1	-1.12E-02	69.500	<b>&lt;0.001</b>
Nitrogen (N)	1	8.29E-04	40.297	<b>&lt;0.001</b>
L*N	1	-8.51E-06	5.548	<b>0.019</b>

**3692** \*Significance determined using Wald's  $\chi^2$  tests ( $P = 0.05$ ).  $P$ -values  $< 0.05$  are  
**3693** in bold and  $p$ -values between 0.05 and 0.1 are italicized. Negative coefficients  
**3694** for light treatments indicate a positive effect of increasing light availability on  
**3695** all response variables, as light availability is treated as percent shade cover in all  
**3696** linear mixed-effects models.

**Table A3.** Slopes of the regression line describing the relationship between each dependent variable and nitrogen fertilization at each light level\*

Shade cover	Slope
<i>G. hirsutum</i>	
0%	<b>8.29E-04<sup>a</sup></b>
30%	<b>5.74E-04<sup>a</sup></b>
50%	<b>4.03E-04<sup>a</sup></b>
80%	1.48E-04 <sup>a</sup>
<i>G. max</i>	
0%	<b>7.86E-04</b>
30%	<b>5.87E-04</b>
50%	<b>4.55E-04</b>
80%	<i>2.57E-05</i>

3697 \*Slopes represent estimated marginal mean slopes from linear mixed-effects models described in the Methods. Slopes  
3698 were calculated using the ‘emmeans’ R package (Lenth 2019). Superscripts indicate slopes fit to natural-log (<sup>a</sup>) or  
3699 square root (<sup>b</sup>) transformed data. Slopes statistically different from zero (Tukey:  $p < 0.05$ ) are indicated in bold.  
3700 Marginally significant slopes (Tukey:  $0.05 < p < 0.1$ ) are italicized.

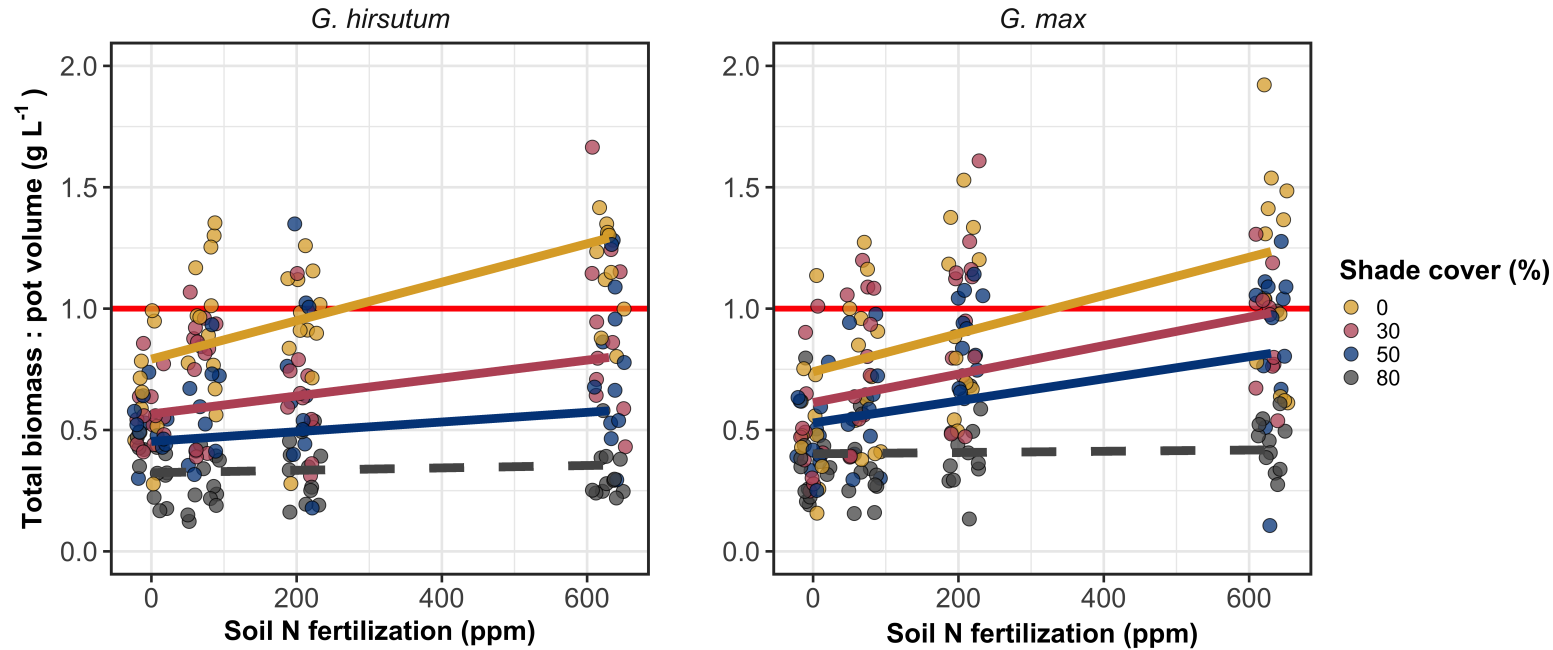


**Figure A1.** Effects of shade cover and nitrogen fertilization on the ratio of plant biomass to rooting volume in *G. hirsutum* (left panel) and *G. max* (right panel). The red horizontal line indicates the recommended  $1 \text{ g L}^{-1}$  threshold for BVR recommended by Poorter et al. (2012) to avoid pot size-induced growth limitation. Nitrogen fertilization treatments are represented on the x-axis. Shade cover treatments are represented through colored points and trendlines. Trendlines were created by back-transforming marginal mean slopes and intercepts from species-specific linear mixed-effects models. These values were calculated using the 'emtrends' and 'emmmeans' functions in the 'emmmeans' R package (Lenth 2019). Points are jittered for visibility. Yellow points and trendlines represent the 0% shade cover treatment, blue points and trendlines represent the 30% shade cover treatment, green points and trendlines represent the 50% shade cover treatment, and purple points and trendlines represent the 80% shade cover treatment. Solid trendlines indicate slopes that are significantly different from zero (Tukey:  $p < 0.05$ ), while dashed trendlines indicate slopes that are not statistically different from zero.

**3701      Appendix B: Supplemental material for "Soil nitrogen availability**  
**3702      modifies leaf nitrogen economies in mature temperate deciduous**  
**3703      forests: a direct test of photosynthetic least-cost theory"**

**Table B1.** Sample sizes of each species, abbreviated by their USDA NRCS PLANTS database code, within each plot at each site

	ACRU	ACSA	FAGR	FRAM	QURU	$N_{\text{plot}}$
Bald Hill						
+N; +S	0	6	1	0	1	8
+N; -S	1	2	2	0	1	6
-N; +S	2	2	0	0	2	6
-N; -S	2	3	3	0	2	10
Carter Creek						
+N; +S	0	6	1	2	0	9
+N; -S	0	4	0	2	0	6
-N; +S	0	5	1	4	0	10
-N; -S	0	7	0	0	0	7
Mount Pleasant						
+N; +S	3	2	1	0	3	9
+N; -S	0	5	4	1	0	10
-N; +S	1	2	4	0	0	7
-N; -S	3	3	1	2	1	10
$N_{\text{spp}}$	12	47	18	11	10	98

**3704** \*Plots within each site are represented based on nitrogen and sulfur addition  
**3705** status. The final column on the right depicts total sample size per plot in each  
**3706** site ( $N_{\text{plot}}$ ) and the final row on the bottom represents cumulative species sample  
**3707** size across all plots and all sites ( $N_{\text{spp}}$ ). Key: ACRU = *A. rubrum*; ACSA = *A.*  
**3708** *saccharum*; FAGR = *F. grandifolia*; FRAM = *F. americana*; QURU = *Q. rubra*

**Table B2.** Analysis of variance results exploring the linear effect of leaf temperature on net photosynthesis rate and stomatal conductance measured at 400  $\mu\text{mol mol}^{-1}$  CO<sub>2</sub>

		$A_{\text{net}}$		$g_s$	
	df	$\chi^2$	p	$\chi^2$	p
Leaf temperature	1	1.287	0.257	1.716	0.190

**3709** Results detail linear mixed effects model where temperature was regressed against  
**3710** net photosynthesis or stomatal conductance, with site and species designated as  
**3711** random intercept terms. Significance was determined using Type II Wald  $\chi^2$   
**3712** tests ( $\alpha = 0.05$ ). Key:  $A_{\text{net}}$  = net photosynthesis rate at 400  $\mu\text{mol mol}^{-1}$  CO<sub>2</sub>;  
**3713**  $g_s$ =stomatal conductance measured at 400  $\mu\text{mol mol}^{-1}$  CO<sub>2</sub>

**Table B3.** Second order log-polynomial regression coefficients that described the effect of leaf temperature on net photosynthesis and stomatal conductance measured at 400  $\mu\text{mol mol}^{-1}$  CO<sub>2</sub>

	a	b	c
$A_{\text{net}}$	9.422	-0.573	0.010
$g_s$	-0.170	-0.186	0.003

**3714** Net photosynthesis and stomatal conductance values were fit to the log-polynomial  
**3715** equation  $\log(y) = a + bx + cx^2$ , where x is leaf temperature. Key:  $A_{\text{net}}$  = net  
**3716** photosynthesis rate at 400  $\mu\text{mol mol}^{-1}$  CO<sub>2</sub>;  $g_s$  = stomatal conductance measured  
**3717** at 400  $\mu\text{mol mol}^{-1}$  CO<sub>2</sub>

**Table B4.** Mean, standard error, and 95% confidence interval ranges of soil nitrogen availability estimates across all measured plots. All units are expressed as  $\mu\text{g N g}^{-1}$  resin  $\text{d}^{-1}$

Site	Treatment	Mean	SE	Lower 95% CI	Upper 95% CI
Bald Hill	Ammonium sulfate	27.11	6.14	15.08	39.13
Bald Hill	Control	14.41	5.02	4.56	24.26
Bald Hill	Sodium nitrate	20.65	3.15	14.46	26.83
Bald Hill	Sulfur	6.33	2.19	2.04	10.62
Carter Creek	Ammonium sulfate	26.94	5.36	16.43	37.44
Carter Creek	Control	19.87	1.92	16.10	23.64
Carter Creek	Sodium nitrate	15.51	4.16	7.36	23.65
Carter Creek	Sulfur	5.50	1.40	2.75	8.25
Mount Pleasant	Ammonium sulfate	8.02	2.31	3.49	12.56
Mount Pleasant	Control	2.00	0.57	0.89	3.11
Mount Pleasant	Sodium nitrate	2.52	0.68	1.19	3.85
Mount Pleasant	Sulfur	2.42	0.39	1.66	3.17

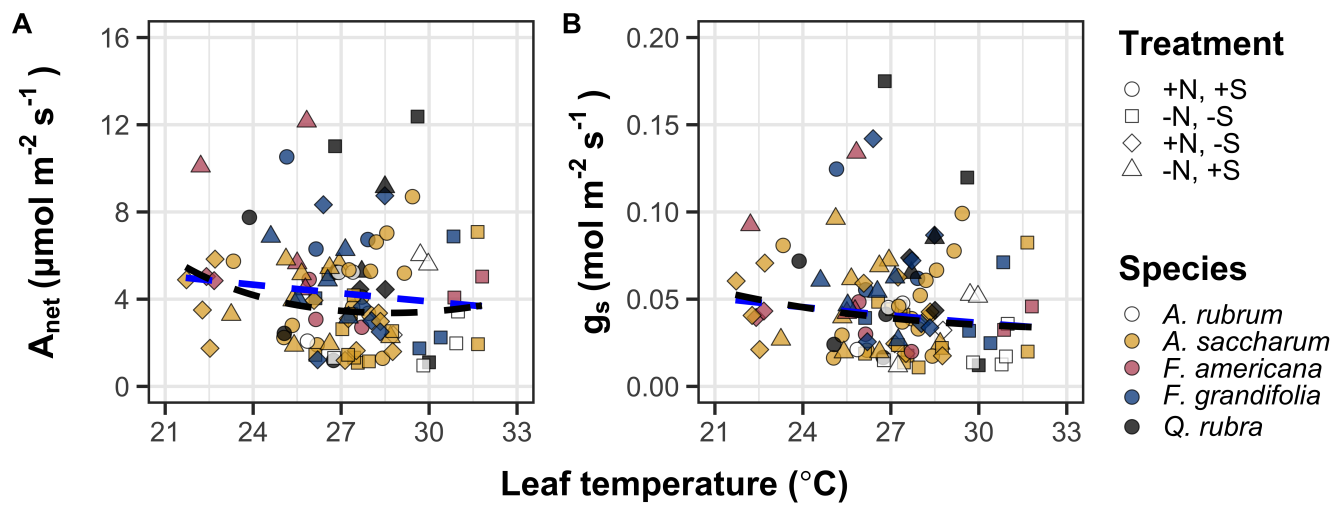


**Figure B1.** Effects of leaf temperature on net photosynthesis rate (panel A) and stomatal conductance (panel B) values when measured at  $400 \mu\text{mol mol}^{-1} \text{CO}_2$ . Leaf temperature is represented continuously on the x-axis, while species are represented as colored points. Colored points and shapes are as explained in Figure 3.1. The dashed blue trendline describes the linear relationship between leaf temperature and each response variable, while the dashed black trendline describes the same relationship with a log-polynomial regression equation.

**3718 Appendix C: Supplemental material for "The relative cost of resource  
3719 use for photosynthesis drives variance in leaf nitrogen content across a  
3720 climate and soil resource availability gradient"**

**3721** C.1 Calculations for soil water holding capacity

**3722** Water holding capacity ( $\theta_{WHC}$ ; mm) was calculated as a function of the  
**3723** volumetric soil water storage at field capacity ( $W_{FC}$ ; m<sup>3</sup> m<sup>-3</sup>), and the volumetric  
**3724** soil water storage at wilting point ( $W_{PWP}$ ; m<sup>3</sup> m<sup>-3</sup>):

$$\theta_{WHC} = (W_{FC} - W_{PWP})(1 - f_{gravel}) * \min(z_{bedrock}, z_{max}) \quad (\text{C4.1})$$

**3725** where  $f_{gravel}$  (%) is the fraction of gravel content in soil,  $z_{bedrock}$  (mm) is the  
**3726** distance to bedrock, and  $z_{max}$  (mm) is the maximum allowable distance to bedrock,  
**3727** set to 2000mm.  $W_{FC}$  is calculated as:

$$\theta_{FC} = k_{fc} + (1.283 * (k_{fc})^2 - 0.374 * k_{fc} - 0.015) \quad (\text{C4.2})$$

**3728** where

$$\begin{aligned} k_{fc} = & -0.251 * f_{sand} + 0.195 * f_{clay} + 0.011 * f_{OM} \\ & + 0.006 * (f_{sand} * f_{OM}) - 0.027 * (f_{clay} \\ & * f_{OM}) + 0.452 * (f_{sand} * f_{clay}) + 0.299 \end{aligned} \quad (\text{C4.3})$$

**3729**  $W_{PWP}$  is calculated as:

$$W_{PWP} = k_{pwp} + (0.14 * k_{pwp} - 0.02) \quad (\text{C4.4})$$

**3730** where

$$\begin{aligned} k_{pwp} = & -0.024 * f_{sand} + 0.487 * f_{clay} + 0.006 * f_{OM} \\ & + 0.005 * (f_{sand} * f_{OM}) - 0.013 * (f_{clay} \\ & * f_{OM}) + 0.068 * (f_{sand} * f_{clay}) + 0.031 \end{aligned} \quad (\text{C4.5})$$

**3731** In Equations C4.4 and C4.5,  $f_{sand}$  (%) is the fraction of sand content in soil (%),  
**3732**  $f_{clay}$  (%) is the fraction of clay content in soil (%), and  $f_{OM}$  is the fraction of  
**3733** organic matter in soil (%). Organic matter in the soil was calculated in this study  
**3734** by converting soil organic carbon data extracted from SoilGrids 2.0 to soil organic  
**3735** matter using the van Bemmelen factor (1.724 conversion factor).

**Table C1.** List of sampled species and their plant functional group assignment

Symbol	Species	Photo. pathway	Growth duration	Growth habit	N-fixer?	Plant functional group	Number sampled
ACAN11	<i>Acaciella angustissima</i>	c3	perennial	forb	yes	c3_legume	3
AMAR2	<i>Ambrosia artemisiifolia</i>	c3	annual	forb	no	c3_nonlegume	25
AMPS	<i>Ambrosia psilostachya</i>	c3	perennial	forb	no	c3_nonlegume	32
ARAL3	<i>Argemone albiflora</i>	c3	annual	forb	no	c3_nonlegume	3
ARPU9	<i>Aristida purpurea</i>	c4	perennial	graminoid	no	c4_nonlegume	2
ASAS	<i>Asclepias asperula</i>	c3	perennial	forb	no	c3_nonlegume	3
ASLA4	<i>Asclepias latifolia</i>	c3	perennial	forb	no	c3_nonlegume	3
ASSY	<i>Asclepias syriaca</i>	c3	perennial	forb	no	c3_nonlegume	18
BASA	<i>Baccharis salicina</i>	c3	perennial	shrub	no	c3_nonlegume	3
BOIS	<i>Bothriochloa ischaemum</i>	c4	perennial	graminoid	no	c4_nonlegume	6
BOSA	<i>Bothriochloa saccharoides</i>	c4	perennial	graminoid	no	c4_nonlegume	6
CAAM2	<i>Callicarpa americana</i>	c3	perennial	shrub	no	c3_nonlegume	3
CAPL3	<i>Carex planostachys</i>	c4	perennial	graminoid	no	c4_nonlegume	3
CAREX	<i>Carex</i> spp.	c4	perennial	graminoid	no	c4_nonlegume	16
CHFE3	<i>Chamaesyce fendleri</i>	c3	perennial	forb	no	c3_nonlegume	2
CHPI8	<i>Chrysopsis pilosa</i>	c3	annual	forb	no	c3_nonlegume	3
COCO13	<i>Conoclinium coelestinum</i>	c3	perennial	forb	no	c3_nonlegume	3
COER	<i>Commelina erecta</i>	c3	perennial	forb	no	c3_nonlegume	3
CRGLL	<i>Croton glandulosus</i>	c3	annual	forb	no	c3_nonlegume	22
CYDA	<i>Cynodon dactylon</i>	c4	perennial	graminoid	no	c4_nonlegume	15
DATE3	<i>Dasyllirion texanum</i>	c3	perennial	shrub	no	c3_nonlegume	3
DIAN	<i>Dichanthium annulatum</i>	c4	perennial	graminoid	no	c4_nonlegume	8
ENPE4	<i>Engelmannia peristenia</i>	c3	perennial	forb	no	c3_nonlegume	6
EUMA8	<i>Euphorbia marginata</i>	c3	annual	forb	no	c3_nonlegume	6
GAPU	<i>Gaillardia pulchella</i>	c3	annual	forb	no	c3_nonlegume	16
GLGO	<i>Glandularia gooddingii</i>	c3	perennial	forb	no	c3_nonlegume	2
HEAN3	<i>Helianthus annuus</i>	c3	annual	forb	no	c3_nonlegume	6

**Table C2.** List of sampled species and their plant functional group assignment (cont.)

Symbol	Species	Photo. pathway	Growth duration	Growth habit	N-fixer?	Plant functional group	Number sampled
HECA8	<i>Heterotheca canescens</i>	c3	perennial	forb	no	c3_nonlegume	2
HETE3	<i>Heliotropium tenellum</i>	c3	annual	forb	no	c3_nonlegume	3
IVAX	<i>Iva axillaris</i>	c3	perennial	forb	no	c3_nonlegume	4
LIAT	<i>Lilaeopsis attenuata</i>	c3	perennial	forb	no	c3_nonlegume	3
LIPU	<i>Liatris punctata</i>	c3	perennial	forb	no	c3_nonlegume	3
LOPE	<i>Lolium perenne</i>	c3	perennial	graminoid	no	c3_nonlegume	9
MIQU2	<i>Mimosa quadrivalvis</i>	c3	perennial	forb	yes	c3_legume	15
NALE3	<i>Nassella leucotricha</i>	c3	perennial	graminoid	no	c3_nonlegume	19
OECU2	<i>Oenothera curtiflora</i>	c3	annual	forb	no	c3_nonlegume	3
OENOT	<i>Oenothera</i> spp.	c3	annual	forb	no	c3_nonlegume	1
PAVI2	<i>Panicum virgatum</i>	c4	perennial	graminoid	no	c4_nonlegume	12
PRGL2	<i>Prosopis glandulosa</i>	c3	perennial	shrub	yes	c3_legume	33
QUHA3	<i>Quercus harvardii</i>	c3	perennial	shrub	no	c3_nonlegume	3
QUMO	<i>Quercus mohriana</i>	c3	perennial	shrub	no	c3_nonlegume	1
RACO3	<i>Ratibida columnifera</i>	c3	perennial	forb	no	c3_nonlegume	40
RHAM	<i>Rhamnus</i> spp.	c3	perennial	shrub	yes	c3_legume	1
RHSET	<i>Rhynchosia senna</i>	c3	perennial	forb	yes	c3_legume	1
RUHI2	<i>Rudbeckia hirta</i>	c3	perennial	forb	no	c3_nonlegume	3
RUNU	<i>Ruellia nudiflora</i>	c3	perennial	forb	no	c3_nonlegume	15
RUTR	<i>Rubus trivialis</i>	c3	perennial	vine	no	c3_nonlegume	3
SAFA2	<i>Salvia farinacea</i>	c3	perennial	forb	no	c3_nonlegume	7
SCHIZ4	<i>Schizachyrium</i> spp.	c4	perennial	graminoid	no	c4_nonlegume	8
SCSC	<i>Schizachyrium scoparium</i>	c4	perennial	graminoid	no	c4_nonlegume	3
SODI	<i>Solanum dimidiatum</i>	c3	perennial	forb	no	c3_nonlegume	1
SOEL	<i>Solanum elaeagnifolium</i>	c3	perennial	forb	no	c3_nonlegume	53
SOHA	<i>Sorghum halapense</i>	c4	perennial	graminoid	no	c4_nonlegume	38
STTE3	<i>Stillingia texana</i>	c3	perennial	forb	no	c3_nonlegume	3

**Table C3.** List of sampled species and their plant functional group assignment (cont.)

Symbol	Species	Photo. pathway	Growth duration	Growth habit	N-fixer?	Plant functional group	Number sampled
VEOC	<i>Verbesina occidentalis</i>	c3	perennial	forb	no	c3_nonlegume	3
VEST	<i>Verbena stricta</i>	c3	perennial	forb	no	c3_nonlegume	3
WEAC	<i>Wedelia acapulcensis</i>	c3	perennial	shrub	no	c3_nonlegume	6

**Table C4.** Model selection results for soil moisture, air temperature, and vapor pressure deficit. Soil moisture was used in a bivariate regression against  $\beta$ , while vapor pressure deficit was used in bivariate regressions against leaf  $C_i:C_a$ \*

Day	Soil moisture		VPD	
	AICc	RMSE	AICc	RMSE
1	1431.77	0.8400	-772.71	0.0853
2	1431.76	0.8400	-775.47	0.0849
3	1431.78	0.8400	-770.86	0.0854
4	1431.79	0.8401	<b>-793.49</b>	<b>0.0839</b>
5	1431.79	0.8401	-771.66	0.0853
6	1431.78	0.8401	-771.66	0.0853
7	1431.78	0.8401	-771.05	0.0854
8	1431.76	0.8401	-770.94	0.0854
9	1431.75	0.8401	-770.11	0.0854
10	1431.74	0.8401	-770.08	0.0855
15	1431.54	0.8401	-768.64	0.0856
20	1431.40	0.8401	-769.77	0.0855
30	1431.23	0.8400	-772.18	0.0853
60	1429.84	0.8391	-779.06	0.0848
90	<b>1429.14</b>	<b>0.8385</b>	-773.99	0.0852

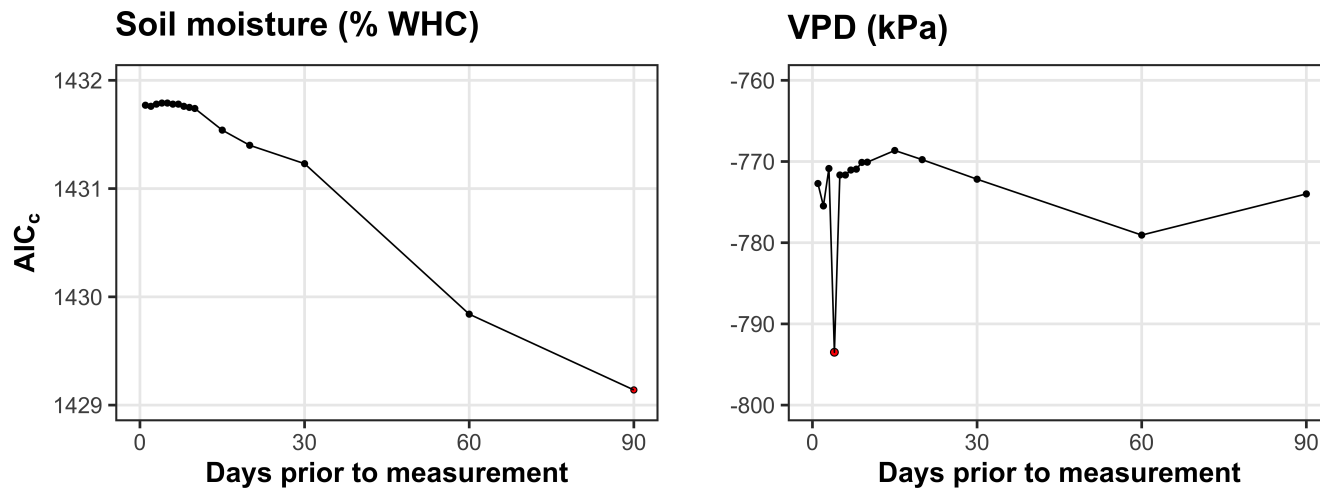


**Figure C2.** Model selection results exploring relevant timescales for soil moisture (left panel) and vapor pressure deficit (right panel). The x-axis indicates the number of days before each site visit and the y-axis notes the corrected Akaike Information Criterion value. The timescale with the lowest AIC<sub>c</sub> value, and therefore most relevant timescale to include in statistical models, is noted as a red point.

**3736 Appendix D: Supplemental material for "Optimal resource investment  
 3737 to photosynthetic capacity maximizes nutrient allocation to whole  
 3738 plant growth under elevated CO<sub>2</sub>"**

**Table D1.** Summary table containing volumes of compounds used to create modified Hoagland's solutions for each soil nitrogen fertilization treatment. All volumes are expressed as milliliters per liter (mL/L)

Compound	0 ppm N	35 ppm N	70 ppm N	105 ppm N	140 ppm N
1 M NH <sub>4</sub> H <sub>2</sub> PO <sub>4</sub>	0	0.165	0.33	0.5	0.67
2 M KNO <sub>3</sub>	0	0.335	0.67	1	1.33
2 M Ca(NO <sub>3</sub> ) <sub>2</sub>	0	0.335	0.67	1	1.33
1 M NH <sub>4</sub> NO <sub>3</sub>	0	0.165	0.33	0.5	0.67
8 M NH <sub>4</sub> NO <sub>3</sub>	0	0	0	0	0
1 M KH <sub>2</sub> PO <sub>4</sub>	1	0.85	0.67	0.5	0.33
1 M KCl	3	2.45	2	1.5	1
1 M CaCO <sub>3</sub>	4	3.33	2.67	2	1.33
2 M MgSO <sub>4</sub>	1	1	1	1	1
10% Fe-EDTA	1	1	1	1	1
Trace elements	1	1	1	1	1

Compound	210 ppm N	280 ppm N	350 ppm N	630 ppm N
1 M NH <sub>4</sub> H <sub>2</sub> PO <sub>4</sub>	1	1	1	1
2 M KNO <sub>3</sub>	2	2	2	2
2 M Ca(NO <sub>3</sub> ) <sub>2</sub>	2	2	2	2
1 M NH <sub>4</sub> NO <sub>3</sub>	1	3.5	0	0
8 M NH <sub>4</sub> NO <sub>3</sub>	0	0	0.75	2
1 M KH <sub>2</sub> PO <sub>4</sub>	0	0	0	0
1 M KCl	0	0	0	0
1 M CaCO <sub>3</sub>	0	0	0	0
2 M MgSO <sub>4</sub>	1	1	1	1
10% Fe-EDTA	1	1	1	1
Trace elements	1	1	1	1

**Table D2.** Summary of the daily growth chamber growing condition program

Time	Air temperature (°C)	Light (%)
09:00	21	25
09:45		50
10:30	25	75
11:15		100
22:45	21	75
23:30		50
00:15	17	25
01:00		0

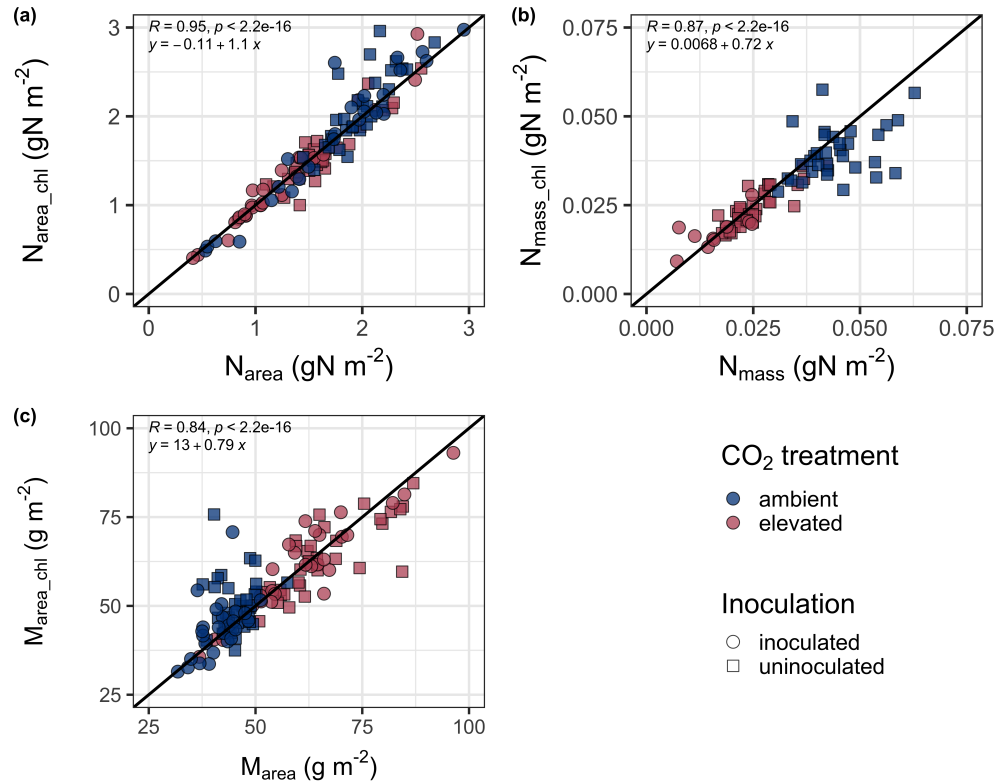


**Figure D1.** Relationships between area-based leaf nitrogen content (a), mass-based leaf nitrogen content (b), and leaf mass per unit leaf area (c) measured on the focal leaf used to generate  $A_{net}/C_i$  curves and leaf nitrogen content measured on the leaf used for chlorophyll extractions. Blue points refer to leaves grown under ambient CO<sub>2</sub> and red points refer leaves grown under elevated CO<sub>2</sub>. Square points indicate uninoculated pots and circular points indicate inoculated pots. Pearson's correlation, associated  $p$ -values, and the line of the regression line that described each bivariate are included in the top left corner of each plot. The solid black line visualizes the trend given a 1:1 bivariate relationship.

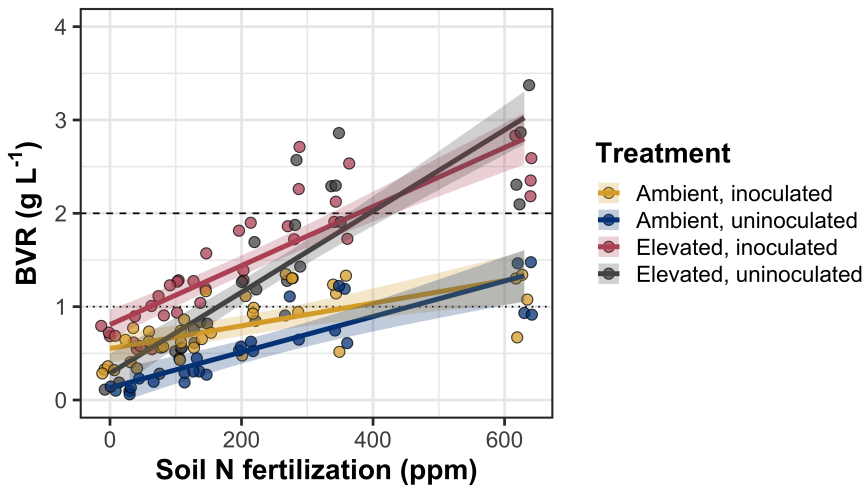


**Figure D2.** Effects of CO<sub>2</sub>, fertilization, and inoculation on the ratio of whole plant biomass to pot volume. Soil nitrogen fertilization is represented on the x-axis in all panels. Yellow points and trendlines indicate inoculated individuals grown under ambient CO<sub>2</sub>, blue points and trendlines indicate uninoculated individuals grown under ambient CO<sub>2</sub>, red points and trendlines indicate inoculated individuals grown under elevated CO<sub>2</sub>, and grey points indicate uninoculated individuals grown under elevated CO<sub>2</sub>. Solid trendlines indicate regression slopes that are different from zero ( $p < 0.05$ ), while dashed trendlines indicate slopes that are not distinguishable from zero ( $p > 0.05$ ). The dotted horizontal line indicates the point where biomass:pot volume exceeds 1  $\text{g L}^{-1}$ , and the dashed line indicates the point where biomass:pot volume exceeds 2  $\text{g L}^{-1}$ .